

# **Synthesis and Self-Assembly of Novel ABC Miktoarm Star Terpolymers**

DISSERTATION

zur Erlangung des akademisches Grades eines  
Doktors der Naturwissenschaften (Dr. rer. nat.)  
im Fach Chemie  
an der Bayreuther Graduiertenschule  
für Mathematik und Naturwissenschaften  
der Universität Bayreuth

vorgelegt von

**Andreas Hanisch**

Geboren in Kulmbach

Bayreuth, 2013



Die vorliegende Arbeit wurde in der Zeit von Juli 2008 bis Januar 2013 in Bayreuth am Lehrstuhl Makromolekulare Chemie II unter Betreuung von Herrn Prof. Dr. Axel H. E. Müller angefertigt.

Vollständiger Abdruck der von der Bayreuther Graduiertenschule für Mathematik und Naturwissenschaften der Universität Bayreuth genehmigten Dissertation zur Erlangung des akademischen Grades eines Doktors der Naturwissenschaften (Dr. rer. nat.).

Dissertation eingereicht am:	25.01.2013
Zulassung durch die Promotionskommission:	13.02.2013
Wissenschaftliches Kolloquium:	26.04.2013

Amtierender Dekan: Prof. Dr. Beate Lohnert

Prüfungsausschuss:

Prof. Dr. Axel H. E. Müller (Erstgutachter)

Prof. Dr. Stephan Förster (Zweitgutachter)

Prof. Dr. Matthias Karg (Vorsitz)

Prof. Dr. Karlheinz Seifert



*"Life is like riding a bicycle.  
To keep your balance you must keep moving."*

Albert Einstein



***Meiner Familie***  
***Greta und Oskar***



---



---

**Table of Contents**

<b>Summary</b>	<b>1</b>
<b>Zusammenfassung</b>	<b>3</b>
<b>Glossary</b>	<b>7</b>
<b>1 – Introduction</b>	<b>9</b>
1.1 Solution Based Self-Assembly in Polymer Systems	9
1.1.1 General Aspects of Self-Assembly	9
1.1.2 Multicompartment Structures from Ternary Systems	10
1.1.2.1 Linear Triblock Terpolymers and Directed Self-Assembly	12
1.1.2.2 Miktoarm Star Terpolymers	16
1.2 Miktoarm Star Polymers	19
1.2.1 Synthesis	19
1.2.1.1 ABC Miktoarm Star Terpolymers as Model Systems	19
1.2.1.2 Other Miktoarm Star Polymer Systems	26
1.2.2 Self-Assembly in Bulk	27
1.2.3 Application of ABC Miktoarm Star Terpolymers for Functional Materials	29
1.3 Synthetic Strategies in Polymer Science	31
1.3.1 DPE Chemistry in Anionic Polymerization	31
1.3.2 Click Chemistry	32
1.4 Aim of this Thesis	34
1.5 References	35
<b>2 – Overview of the thesis</b>	<b>41</b>
2.1 Modular Synthesis of Miktoarm Star Terpolymers	42
2.2 Counterion-Mediated Hierarchical Self-Assembly of an ABC Miktoarm Star Terpolymer Containing a Poly( <i>N</i> -methyl-2-vinylpyridinium iodide) Segment	45
2.3 Application of the Triiodide-Directed Self-Assembly to other ABC and ABA' Miktoarm Star Polymers with a Poly( <i>N</i> -methyl-2-vinylpyridinium iodide) Segment	47
2.4 Individual Contributions to Joint Publications	51
<b>3 – A Modular Route for the Synthesis of ABC Miktoarm Star Terpolymers <i>via</i> a New Alkyne-Substituted Diphenylethylene Derivative</b>	<b>53</b>
3.1 Introduction	54
3.2 Experimental Section	57
3.3 Results and Discussion	60
3.3.1 Synthesis of 1-[(4-( <i>tert</i> -Butyldimethylsilyl)ethynyl)-phenyl]-1-phenylethylene (click-DPE)	60
3.3.2 Synthesis of Alkyne Mid-Functionalized Diblock Copolymers	61
3.3.3 Hydrolysis of the Alkyne Mid-Functionalized Diblock Copolymers	64
3.3.4 Synthesis of $\omega$ -Azido Homopolymers	66

3.3.5	Synthesis of Miktoarm Star Terpolymers <i>via</i> Click Chemistry	67
3.4	Conclusions	74
3.5	References	76
3.6	Supporting Information	78
3.6.1	Additional Experimental Section	78
3.6.2	Additional Figures	82
3.6.3	Test Polymerization with P2VP and Click-DPE	86
3.6.4	Characterization of $\omega$ -Azido Homopolymers	88
3.6.5	Click Reaction with $\omega$ -Azido-Functionalized Poly( <i>tert</i> -butyl methacrylate)	91
3.6.6	References	92
<b>4 – Counterion-Mediated Hierarchical Self-Assembly of an ABC Miktoarm Star Terpolymer</b>		<b>93</b>
4.1	Introduction	94
4.2	Results and Discussion	97
4.2.1	Synthesis and Characterization of the PB-P2VP-PtBMA Miktoarm Star Terpolymer	97
4.2.2	Self-Assembly Behavior of $\mu$ -BVqT	98
4.2.2.1	Hierarchical Superstructure Formation	100
4.2.2.2	Importance of the Nature of the Counterion	102
4.2.3	Structural Characterization of “Woodlouse” Aggregates	105
4.3	Conclusions	109
4.4	Experimental Section	111
4.5	References	116
4.6	Supporting Information	119
4.6.1	Additional Experimental Section	119
4.6.2	Synthesis and Characterization of PB- <i>arm</i> -P2VP- <i>arm</i> -PtBMA Miktoarm Star Terpolymer	121
4.6.3	Self-Assembly of $\mu$ -BVqT	123
4.6.3.1	Intermediate Structures of “Woodlouse” Aggregates	124
4.6.3.2	Importance of the Nature of the Counterion	127
4.6.3.3	Structural Characterization of “Woodlouse” Aggregates	129
4.6.4	References	131
<b>5 – Hierarchical Self-Assembly of Miktoarm Star Polymer Systems Containing a Polycationic Segment: A General Concept</b>		<b>133</b>
5.1	Introduction	135
5.2	Experimental Part	138
5.3	Results and Discussion	142
5.3.1	Miktoarm Star Ter- and Copolymer Synthesis	142
5.3.2	Hierarchical Self-Assembly of Miktoarm Star Polymers of Different Composition and Chemistry	144
5.3.2.1	Hydrophilic/Hydrophobic Balance	144
5.3.2.2	Effect of a High- $T_g$ Core-Forming Block	150
5.4	Conclusions	158
5.5	References	160

---

---

5.6	Supporting Information	163
5.6.1	Additional Experimental Section	163
5.6.2	Miktoarm Star Ter- and Copolymer Synthesis	164
5.6.3	Hierarchical Self-Assembly of Miktoarm Star Terpolymers of Different Composition and Chemistry	166
5.6.3.1	Hydrophilic/Hydrophobic Balance	166
5.6.3.2	Effect of a High- $T_g$ Core-Forming Block	168
5.6.4	References	170
<b>6</b>	<b>– Appendix</b>	<b>171</b>
6.1	Triiodide-Directed Self-Assembly: Polycation Nature and Reversibility	171
6.2	References	173
	<b>List of Publications</b>	<b>175</b>
	<b>Danksagung</b>	<b>177</b>



## Summary

A novel synthesis for ABC miktoarm star terpolymers and their self-assembly into complex superstructures in aqueous solution are described within this thesis. To this aim a modular route for such materials was developed, combining anionic polymerization and copper-catalyzed azide-alkyne cycloaddition. At the example of ABC miktoarm star terpolymers and an ABA' miktoarm star copolymer containing a poly(*N*-methyl-2-vinylpyridinium iodide) (P2VPq) segment, the counterion-mediated superstructure-formation of complex shaped aggregates was thoroughly investigated.

The key compound of the combinatorial synthesis is the newly synthesized 4-alkyne-substituted diphenylethylene derivative 1-[(4-(*tert*-butyldimethylsilyl)ethynyl)phenyl]-1-phenylethylene ("click-DPE"). This was applied in sequential anionic polymerization to prepare well-defined alkyne mid-functional diblock copolymers composed of polybutadiene (PB) as first and poly(*tert*-butyl methacrylate) (PtBMA), poly(2-vinylpyridine) (P2VP), or poly(*N,N*-dimethylaminoethyl methacrylate) (PDMAEMA) as second block. The alkyne-midfunctional diblock copolymers were afterwards conjugated with azido-functional polystyrenes (PS), poly(ethylene oxide) (PEO), PtBMA and PDMAEMA to successfully obtain different novel ABC miktoarm star terpolymers with narrow molecular weight distributions.

For an ABC miktoarm star terpolymer consisting of arms of PB, PtBMA and P2VP it was demonstrated that after quaternization with methyl iodide (yielding  $\mu$ -BVqT) and dialysis to water the nature of the counterion allows for manipulation of the obtained structures. The miktoarm star architecture together with iodide as counterion is essential for this directed self-assembly. Transformation of iodide to triiodide, *via* the addition of iodine before dialysis to water, decreases the hydrophilicity of the P2VPq corona and therefore induces the directed self-assembly of spherical micelles with a PB/PtBMA core, into cylinders, superstructures thereof and finally barrel-shaped aggregates of up to 1  $\mu$ m with an internal lamellar fine structure. Based on their appearance in transmission electron micrographs these were termed "woodlouse" aggregates. The compact particles consist of alternating lamellae of a partially demixed PB/PtBMA phase and a swollen P2VPq phase.

The general applicability of this counterion-mediated hierarchical self-assembly was furthermore demonstrated by using two other miktoarm star systems. For three ABC miktoarm star terpolymers of different composition, consisting of PB, PS and P2VPq segments ( $\mu$ -BVqS), a dependence of the morphology on the fraction of the hydrophilic block was determined, in analogy to diblock copolymers. For long P2VPq blocks stacked lamellar/disk-like structures evolve from micellar building units. In contrast, a short P2VPq segment yields multilamellar vesicles *via* fusion of vesicular primary building blocks. The vesicle walls are supposed to consist of a lamellar structure with the PB phase in the centre, shielded from the P2VPq corona by thin PS layers. At the example of one  $\mu$ -BVqS miktoarm star terpolymer the successful formation of nanohybrids containing gold nanoparticles within the P2VPq phase is demonstrated.

In the second system the low- $T_g$  PB segment was replaced by a second PS block of different length ( $\mu$ -SVqS'). Even though vesicles serve as initial building units, the triiodide-induced superstructure formation leads to anisotropic aggregation of deformed vesicles, rather than to the fusion into multilamellar vesicles. This is attributed to the two glassy PS core blocks which minimize the dynamics during self-assembly and allow only minor rearrangement of the aggregated structures. Similar to the "woodlouse" aggregates from  $\mu$ -BVqT, lamellar structured particles of elongated shape were obtained from  $\mu$ -SVqS', despite vesicles serving as primary building units. Consequently, the presented triiodide-directed self-assembly into complex superstructures is not restricted to miktoarm star polymers containing a low- $T_g$  segment, as the rearrangement processes take place during the dialysis process, where the organic co-solvent enables sufficient mobility of the core-forming blocks.

Besides the introduction of a novel synthetic approach for the construction of miktoarm star terpolymers and the synthetic advance of the alkyne-functionalized DPE, the presented triiodide-mediated superstructure formation represents an interesting concept for directed self-assembly processes.

## Zusammenfassung

Die vorliegende Arbeit verknüpft eine neuartige Synthesemethode für ABC-Miktoarmstern-Terpolymere mit der Untersuchung ihrer Selbstanordnung zu Überstrukturen in wässriger Lösung. Hierfür wurde ein modularer synthetischer Ansatz entwickelt, der auf anionischer Polymerisation und der kupfer-katalysierten Azid-Alkin-Cycloaddition beruht. Die durch das Gegenion gesteuerte Überstrukturbildung von ABC-Miktoarmstern-Terpolymeren und einem ABA' Miktoarmstern-Copolymer mit einem Poly(*N*-methyl-2-vinylpyridiniumiodid)-Segment in komplex strukturierte Aggregate wurden detailliert untersucht.

Das neuartige 4-Alkin-substituierte Diphenylethylenderivat 1-[(4-(*tert*-Butyldimethylsilyl)ethynyl)phenyl]-1-phenylethylene („click-DPE“) ist die Kernverbindung der kombinatorischen Sternsynthese. Diese wurde erstmals in der sequentiellen, lebenden anionischen Polymerisation eingesetzt, um wohldefinierte Diblock-Copolymere mit einer Alkinfunktion an der Grenze zwischen den zwei Blöcken zu synthetisieren. Hierbei stellt Polybutadien (PB) den ersten Block dar und Poly(*tert*-Butylmethacrylat) (PtBMA), Poly(2-Vinylpyridin) (P2VP) oder Poly(*N,N*-Dimethylaminoethylmethacrylat) (PDMAEMA) den zweiten Block. Schließlich wurde erfolgreich der modulare Ansatz durch Konjugation mit Azid-funktionalisiertem Polystyrol (PS), Polyethylenoxid (PEO), PtBMA und PDMAEMA demonstriert und Miktoarmstern-Terpolymere mit enger Molekulargewichtsverteilung erhalten.

Am Beispiel eines ABC-Miktoarmstern-Terpolymers mit einem PB-, PtBMA- und P2VP-Block wurde gezeigt, dass nach Quaternisierung mit Methyljodid und anschließender Dialyse gegen Wasser, über die Beschaffenheit des Gegenions die Lösungsstruktur gesteuert werden konnte. Hierbei ist neben der Polymerarchitektur die Anwesenheit von Iod als Gegenion die Grundvoraussetzung für die hierarchische Überstrukturbildung. Die durch Iodzugabe vor Dialyse kontrollierbare Ausbildung von Triiodid führt zu einer Verringerung der Wasserlöslichkeit der quaternisierten Poly(2-Vinylpyridin)-Korona (P2VPq). Um die ungünstige Wechselwirkung mit dem wässrigen Medium zu verringern, ordnen sich Kugelmizellen mit einem PB/PtBMA-Kern zu Zylindermizellen um, welche wiederum Überstrukturen ausbilden und sich schließlich zu bis zu 1  $\mu\text{m}$  großen, fassförmigen Ag-

gregaten umlagern. Aufgrund ihrer Erscheinung in elektronenmikroskopischen Aufnahmen wurde für diese der Begriff „woodlouse“ („Kellerassel“) eingeführt. Die Aggregate sind nicht hohl und bestehen aus PB/PtBMA Lamellen, die über eine teilweise gequollene P2VPq Phase miteinander verbunden und dadurch stabilisiert werden. Die PB/PtBMA Lamellen besitzen dabei eine teilweise entmischte innere Struktur.

Dieses Konzept wurde erfolgreich auf zwei weitere Mikroarmstern-Systeme angewandt. Für eine Serie von ABC-Mikroarmstern-Terpolymeren aus PS, PB und P2VPq ( $\mu$ -BVqS) wurde eine Abhängigkeit der Mizellform vom hydrophilen Anteil beobachtet; analog zu Diblock-Copolymeren. Einerseits wurden für lange P2VPq-Blöcke Aggregate aus gestapelten Lamellen/Scheiben erhalten, die aus Kugelmizellen als Grundbausteinen entstanden sind; andererseits wurde für kurze P2VPq Blöcke die Ausbildung multilamellarer Vesikel durch Fusion unilamellarer Vesikel beobachtet. Anders als durch die Polymerarchitektur erwartet, konnte für die Vesikelwand keine Kompartimentalisierung beobachtet werden, sondern es wird eine lamellare Zusammensetzung mit einem PB Kern angenommen, die durch eine dünne PS-Schicht vor der P2VPq-Korona geschützt wird. Für einen der  $\mu$ -BVqS-Mikroarmsterne wurde erfolgreich eine Nanohybridstruktur mit Goldnanopartikeln gebildet.

Für ein zweites Polymersystem wurde das elastische PB-Segment durch einen weiteren glasartigen PS-Block mit unterschiedlicher Länge ersetzt ( $\mu$ -SVqS'). Obwohl mit Iodid als Gegenion Vesikel erhalten wurden, bildeten sich bei der Triiodid-induzierten Überstrukturbildung anisotrope Aggregate aus deformierten Vesikeln. Die Abwesenheit von multilamellaren Vesikeln wird dabei auf die reduzierte Dynamik der kernbildenden, glasartigen PS-Blöcke zurückgeführt. Ähnlich zu den „woodlouse“ Partikeln von  $\mu$ -BVqT, wurden somit für  $\mu$ -SVqS' längliche Aggregate mit einer lamellaren Struktur erhalten, jedoch über Vesikel als Grundbausteine. Somit ist dieses über das Triiodid-Ion beeinflussbare Konzept der gesteuerten Selbstaggregation nicht nur auf Mikroarmstern Systeme mit einem elastischen Block beschränkt, da die Umordnungsprozesse während des Dialyse stattfinden, wo das anfangs vorhandene organische Lösungsmittel eine ausreichende Mobilität der den Mizellkern bildenden Blöcke zur Folge hat.

Neben einer neuen Synthesestrategie für Mikroarmstern-Terpolymere, basierend auf einem vielseitigen Alkin-substituierten DPE Derivat, konnte somit die durch das Triiodid-Ion induzierte Überstrukturbildung als neuartiges Konzept für gesteuerte Selbstanordnungsprozesse in wässrigen Lösungen aufgezeigt werden.



## Glossary

2VP	2-vinylpyridine
AAO	anodic aluminium oxide
ATRP	atom transfer radical polymerization
CoQ10	coenzyme Q10
CRP	controlled radical polymerization
cryo-TEM	cryogenic transmission electron microscopy
CuAAC	copper-assisted azide-alkyne cycloaddition
DNA	deoxyribonucleic acid
DPE	1,1-diphenylethylene
DVB	divinylbenzene
$f_w$	volume fraction of water
IPEC	interpolyelectrolyte complex
MCM	multicompartment micelles
NRC	nitroxide radical coupling
SET-LRP	single electron transfer living radical polymerization
PAA	poly(acrylic acid)
PB	polybutadiene
PBLL	poly( $\epsilon$ - <i>tert</i> -butyloxycarbonyl-L-lysine)
PCEMA	poly(2-cinnamoyloxyethyl methacrylate)
PDMAEA	poly( <i>N,N</i> -dimethylaminoethyl acrylate)
PDMAEMA	poly( <i>N,N</i> -dimethylaminoethyl methacrylate)
PEO	poly(ethylene oxide)
PEE	polyethylethylene
PI	polyisoprene
PISC	poly((sulfamate-carboxylate)isoprene)
PMA	poly(methyl acrylate)
PMAA	poly(methacrylic acid)
PMCL	poly( $\gamma$ -methyl- $\epsilon$ -caprolactone)
<i>Pn</i> Bu	poly( <i>n</i> -butyl acrylate)
PNiPAAm	poly( <i>N</i> -isopropylacrylamide)
PS	polystyrene
PSGA	poly(succinated glyceryl monomethacrylate)
<i>Pt</i> BA	poly( <i>tert</i> -butyl acrylate)
<i>Pt</i> BMA	poly( <i>tert</i> -butyl methacrylate)
PVBFP	poly(pentafluorophenyl 4-vinylbenzyl ether)
P2VP	poly(2-vinylpyridine)
P2VPq	poly( <i>N</i> -methyl-2-vinylpyridinium)
ROP	ring-opening polymerization
TEM	transmission electron microscopy
THF	tetrahydrofuran
TPPBr	triphenylphosphonium bromide
$\Delta G_{agg.}$	Gibbs free energy of micelle formation
$\Delta H_{agg.}$	enthalpy of micelle formation
$\Delta S_{agg.}$	entropy of micelle formation



# 1 – Introduction

## 1.1 Solution Based Self-Assembly in Polymer Systems

### 1.1.1 General Aspects of Self-Assembly

*Self-assembly* describes the well-defined organization of one species or a set of identical molecular building units into highly ordered aggregates by non covalent interactions. Here, the complexity and diversity achieved in nature displays an impressive prototype for such structures at diverse length scales.<sup>1-3</sup> Examples of biological structures of different dimensions, built up with the concept of self-assembly include *e.g.* DNA,<sup>4</sup> viruses<sup>5</sup> or spider silk.<sup>6</sup> The engineering of natural building units resembles a remarkable pathway for the programmed construction of nanoscale objects in a bottom-up approach.<sup>7</sup> An outstanding example is DNA-origami, which is based on the combination of a long scaffold strand of virus-DNA with small, designed staple strands of adequate base-sequence to obtain directed folding into diverse two-dimensional<sup>8</sup> or three-dimensional structures.<sup>9</sup>

Despite the synthetic advances in polymer chemistry, achieving such a distinct complexity with polymer systems has not been reached. Nevertheless, it represents a desirable paradigm for the construction of complex functional structures of different dimension in analogy to systems in nature (Figure 1-1A).<sup>10</sup> In the case of block copolymers as most simplified polymeric system two chemically different blocks are covalently linked together. If the polymer now is exposed to a solvent selective for only one block, the individual molecules have to self-organize to shield the solvophobic block. The gain in free energy ( $\Delta H_{\text{agg.}} < 0$ ) for minimizing the unfavorable interaction between the solvent and the insoluble block overcomes the loss of entropy ( $\Delta S_{\text{agg.}} > 0$ ), leading to an overall negative Gibbs free energy  $\Delta G_{\text{agg.}}$ .

$$\Delta G_{\text{agg.}} = \Delta H_{\text{agg.}} - T\Delta S_{\text{agg.}} < 0$$

Depending on the fraction of the stabilizing block the polymers assemble into spherical micelles, cylindrical micelles or vesicles (Figure 1-1-B).<sup>11-14</sup> Despite the structural simplicity of these aggregates the tailored synthesis of block copolymers enables constructing functional material. These micellar structures can serve as nanocarriers<sup>15,16</sup> or

nanoreactors,<sup>17-19</sup> or as scaffold for *e.g.* hybrid materials.<sup>20-22</sup> Vesicles (or also called polymersomes) resemble the synthetic analogues of liposomes and are therefore of interest for biological applications.<sup>23-25</sup> Even though this thesis deals with the self-assembly in solution it should be mentioned that the same principles also apply for the bulk state, provided that the thermodynamic incompatibility of the two blocks is sufficiently high. The covalent linkage prevents phase separation on the macroscale and therefore forces the polymer to align in nanoscopic structures, *i.e.* spherical, cylindrical, gyroid or (perforated) lamellar morphologies.<sup>26,27</sup>

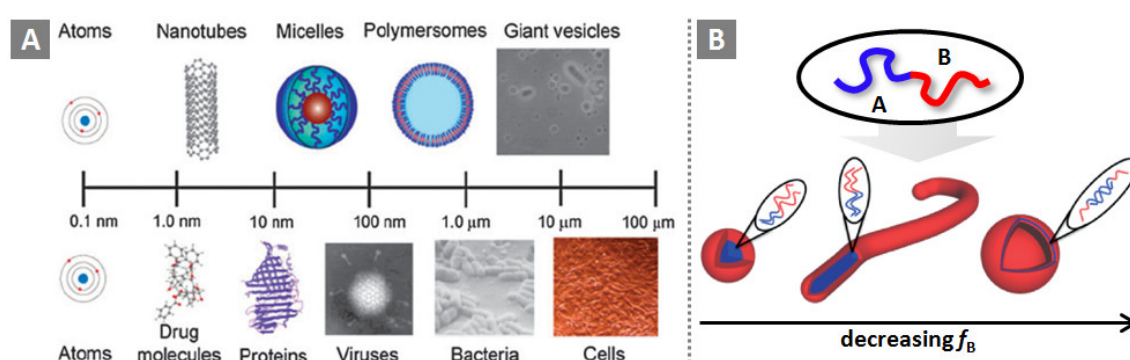


**Figure 1-1.** (A) Length scales of molecular self-assembled structures in synthetic and biological systems with increasing complexity.<sup>10</sup> (B) Schematic representation of the structures of AB diblock copolymers in a solvent selective for the B block. Depending on the volume fraction of the soluble block,  $f_B$ , the polymer self assembles into spherical micelles, cylindrical micelles or vesicles.<sup>11</sup>

### 1.1.2 Multicompartment Structures from Ternary Systems

Extending the functionality of block copolymer systems with a third chemically differing block can be accomplished in two manners. The linear attachment leads to triblock terpolymers, whereas by nonlinear conjunction of the third block miktoarm star terpolymers (from the greek word μικτός for mixed) are achieved.<sup>28</sup> The synthesis of the latter will be discussed in chapter 1.2. In contrast to diblock copolymers different block-selective solvents are possible for these ternary systems, which induce either a compartmentalization of the core or the corona.<sup>29</sup> In the following a short overview of possible structures at the example of spherical micelles is given. If linear terpolymers are exposed to a solvent selective for the end-blocks micelles with an either mixed, patchy or Janus-type corona are obtained (Figure 1-2A).<sup>30</sup> However, accessing the region of exclusively Janus-type micelles from ABC triblock terpolymers in endblock-selective solvents

is challenging and mostly leads to mixtures with patchy micelles.<sup>30,31</sup> Additionally, in solvents selective for the middle and one end-block core-shell-corona structures will be obtained (Figure 1-2B).<sup>32</sup> In contrast to their linear analogues the influence of block sequence is eliminated for miktoarm star terpolymers as a consequence of the polymer architecture. Hence core-shell-corona structures are not possible and for the corona-compartmentalized structures Janus-type micelles are rather unfavored due to the sterical frustration of the two soluble blocks.

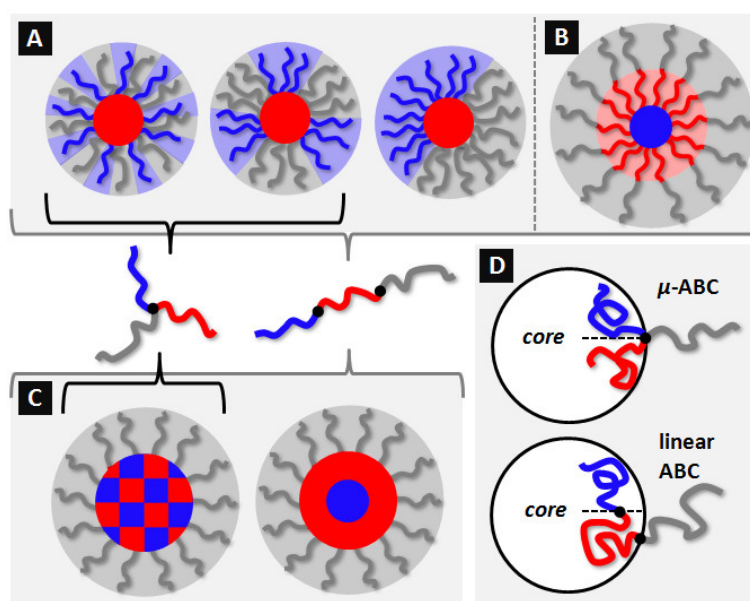


**Figure 1-2.** Overview of corona- (A, B) and core-compartmentalized structures (C) obtained from ABC miktoarm star terpolymers and linear ABC terpolymers. The structures depicted are micelles with a mixed, patchy or Janus-type corona (A, from left to right), core-shell-corona micelles (B) for solvents selective for the end-blocks of linear terpolymers and multicompartment or “onion”-like micelles (C, from left to right). (D) shows a schematic illustration of the chain packing for ABC miktoarm star and linear terpolymers to obtain multicompartment micelles.

On the other hand, solvents selective for only one block lead to a compartmentalization of the micellar core (Figure 1-2C). Inspired by biological systems, in 1999 Ringsdorf introduced the concept of multicompartment micelles (MCM’s) for synthetic polymer systems.<sup>33</sup> Separated compartments within the core would allow for storage of two different payloads within one micelle, while simultaneously maintaining access to the surrounding medium. When triblock terpolymers self-assemble in solvents selective for one end block, the interfacial energies between each of the individual core-forming blocks and the corona-forming block determine whether micelles with simple concentric compartments (“onion”-like structures, right-hand structure in Figure 1-2C)<sup>34</sup> or micelles

with non-concentric nano-structured cores (multicompartment micelles, left-hand structure in Figure 1-2C) are obtained.<sup>35</sup> However, attributed to their frustrated architecture, miktoarm star terpolymers are inherently forced to self-assemble in structures with compartmentalized cores upon dissolution in a solvent selective for one block, disregarding different pairs of interfacial energies (Figure 1-2D). The first example for visualization of the individual core-segments of multicompartment micelles and worms was given by Hillmyer, Lodge and co-workers in 2004 for a miktoarm star terpolymer with highly incompatible segments, poly(ethylene)-*arm*-poly(ethylene oxide)-*arm*-poly(perfluoropropylene oxide),  $\mu$ -EOF.<sup>36,37</sup> In cryo-TEM the perfluorinated segments were *in-situ* detectable owing to their increased electron density. In contrast to this miktoarm system, for linear terpolymers, besides special chemical composition, interpolyelectrolyte complexation, the use of additives, solvent mixtures or adequate assembly pathways have to be applied to guide the sequentially connected blocks towards multi-compartmentalized structures. In the following two sections I will first give an overview of the directed self-assembly of linear triblock terpolymers into multicompartment structures (1.1.2.1) and then highlight the well-defined morphologies obtained by different miktoarm star terpolymer systems (1.1.2.2).

### 1.1.2.1 Linear Triblock Terpolymers and Directed Self-Assembly

In the field of linear triblock terpolymers Laschewsky *et al.* presented the first successful *in-situ* visualization of the multicompartment character in 2005 for a poly(4-methyl-4-(4-vinylbenzyl)morpholin-4-ium chloride)-*block*-polystyrene-*block*-poly(pentafluorophenyl 4-vinylbenzyl ether) (PVBM-*b*-PS-*b*-PVBFP) system by cryo-TEM.<sup>38</sup> After dialysis to water the terpolymer assembled into micelles with a core consisting of spherical domains (~3 nm in diameter) of the pentafluorophenyl group within a hydrocarbon matrix formed by both the polystyrene block and the aromatic moiety of the fluorinated block (Figure 1-3A). Therefore segregation within the PVBFP block took place. They extended this polymer design to other terpolymers based on acrylate-type monomers to obtain spherical compartmentalized structures.<sup>39-41</sup> Besides systems with a solvophilic endblock, also systems with a solvophilic midblock were shown to self-assemble into multicompartment structures.<sup>40-42</sup> Even though simulations of triblock systems in mid-

block selective solvents predict multicore micelles, where the two chemically different cores are separated by the solvophilic block,<sup>43</sup> the presence of multicompart ment micelles here might be attributed to the short lengths of the solvophobic blocks and their chemical nature. Interestingly, instead of using triblock terpolymers, most recently, Langlois and co-workers followed another approach utilizing a statistical terpolymer based on biocompatible poly(3-hydroxyalkanoates).<sup>44</sup> Again, the segregation is induced by the hydrophilic, lipophilic and fluorophilic character of the attached sidechains. Nanoprecipitation in water forced to polymer to form micelles (18 and 79 nm in diameter for two different systems) with distinct fluorinated subdomains in the core.

Another possibility to induce phase segregation within the core is based on segments carrying charged functions. As a consequence of the charge neutrality of poly((sulfamate-carboxylate)isoprene) at low pH, poly((sulfamate-carboxylate)isoprene)-*block*-polystyrene-*block*-poly(ethylene oxide) (PISC-*b*-PS-*b*-PEO) was reported to yield micelles with a “raspberry”-like PISC core with spherical PS domains under acidic conditions.<sup>45</sup> The remaining isoprene units within the PISC domain and the formation of hydrogen-bonds with PEO are supposed to further reduce its water solubility and additionally the transition into micelles with a mixed PISC/PEO corona was demonstrated at increased pH. Schacher *et al.* showed for zwitterionic polybutadiene-*block*-poly(*N*-methyl-2-vinylpyridinium)-*block*-poly(methacrylic acid) (PB-*b*-P2VPq-*b*-PMAA) that in aqueous media patchy intermicellar IPEC domains of P2VPq/PMAA are formed on the PB core.<sup>46</sup> Surprisingly, the non-quaternized and non-hydrolyzed precursor polymer also formed multicompart ment micelles with a “sphere on sphere” morphology in acetone as selective solvent for the poly(*tert*-butyl methacrylate) block.<sup>47</sup> Due to the strong incompatibility between PB and P2VP, the system is assumed to aim surface minimization of the PB/P2VP interface.

Apart from the spherical multicompart ment micelles discussed so far, Fang *et al.* demonstrated the hierarchical self-assembly of pre-formed corona-compartmentalized micelles into one-dimensional core-compartmentalized structures upon reducing the solvent quality.<sup>48</sup> Depending on the corona structure (patchy or Janus-type) of the micelles from poly(4-*tert*-butoxystyrene)-*block*-polybutadiene-*block*-poly(*tert*-butyl methacrylate) with a perfluoro-modified midblock insoluble in dioxane, the dialysis into etha-

nol induces stacking of these subunits into linear or branched structures with a core consisting of alternating fluorinated and poly(4-*tert*-butoxystyrene) domains. Similarly, preformed corona-compartmentalized micelles from bis-hydrophilic poly(ethylene oxide)-*block*-poly(*n*-butyl acrylate)-*block*-poly(*N*-isopropylacrylamide) terpolymers (PEO-*b*-PnBu-*b*-PNiPAAm) underwent aggregation into chain-like structures at temperatures above the cloud point of the thermoresponsive PNiPAAm block.<sup>30</sup> Repeated heating cycles improved the coronal chain segregation and induced the anisotropic stacking for the systems, where the degree of polymerization of the PNiPAAm block was higher than that of the hydrophilic PEO. In another terpolymer system studied by Liu and co-workers, solvent mixtures being selective for one end block and only marginally solubilizing the other endblock were applied. Ageing of the solutions led to a transition of spherical micelles to cylinders, crossed cylinders and finally double and triple helices.<sup>49</sup> Even though for the endblock with decreased solubility no phase segregation occurred, minimization of its unfavorable surface with the surrounding medium induced the formation of helical superstructures. Based on this results they achieved structural reorganization into segmented wormlike structures for a poly(*tert*-butyl acrylate)-*block*-poly(2-cinnamoyloxyethyl methacrylate)-*block*-poly(*N,N*-dimethylaminoethyl methacrylate) (PtBA-*b*-PCEMA-*b*-PDMAEMA) triblock.<sup>50</sup> By dissolution in methanol wormlike micelles with a PCEMA core and a corona from PtBA and PDMAEMA were formed. Again, addition of a nonsolvent (water) induced time-dependent morphological transition due to shielding of the coronal PtBA segments of decreased solubility. For low water contents ( $f_w = 2.9\%$ , "less soluble" condition for PtBA) "wriggled" structures were obtained, whereas at water contents leading to a complete insolubility of PtBA ( $f_w = 10.7\%$ ), distinct rearrangement processes into multicompartiment cylinders with a segmented core of PCEMA and PtBA occurred (Figure 1-3B).

Wooley, Pochan and coworkers conducted intensive studies on the self-assembly of poly(acrylic acid)-*block*-poly(methyl acrylate)-*block*-polystyrene (PAA-*b*-PMA-*b*-PS) triblock terpolymers. Using diamines as additives they manipulated the micellar morphologies to obtain spherical micelles, cylinders, toroids, disk-like micelles and stacks of discs in THF/water mixtures.<sup>51-56</sup> The key aspect was the control of the interfacial curvature precisely adjustable *via* the polymer composition (respective volume fractions),

water content (collapse/swelling of the hydrophobic/hydrophilic moieties) and nature and amount of the diamine-based counterion (coronal volume restraint). On basis of these parameters they were able to kinetically control the aggregation of spherical micelles into nano-structured cylindrical micelles with disk-like micelles as intermediates.<sup>57</sup> In addition, Dupont and Liu successfully demonstrated (–)-sparteine to be a suitable diamine additive in directing the self-assembly of another triblock terpolymer system with a carboxyl-containing terminal block (poly(*tert*-butyl acrylate)-*block*-poly(2-cinnamoyloxyethyl methacrylate)-*block*-poly(succinated glyceryl monomethacrylate), PtBA-*b*-PCEMA-*b*-PSGMA).<sup>58</sup> The diamine-induced collapse of the PSGMA segment induced the formation of “hamburger” and segmented wormlike micelles in distinct solvent mixtures.

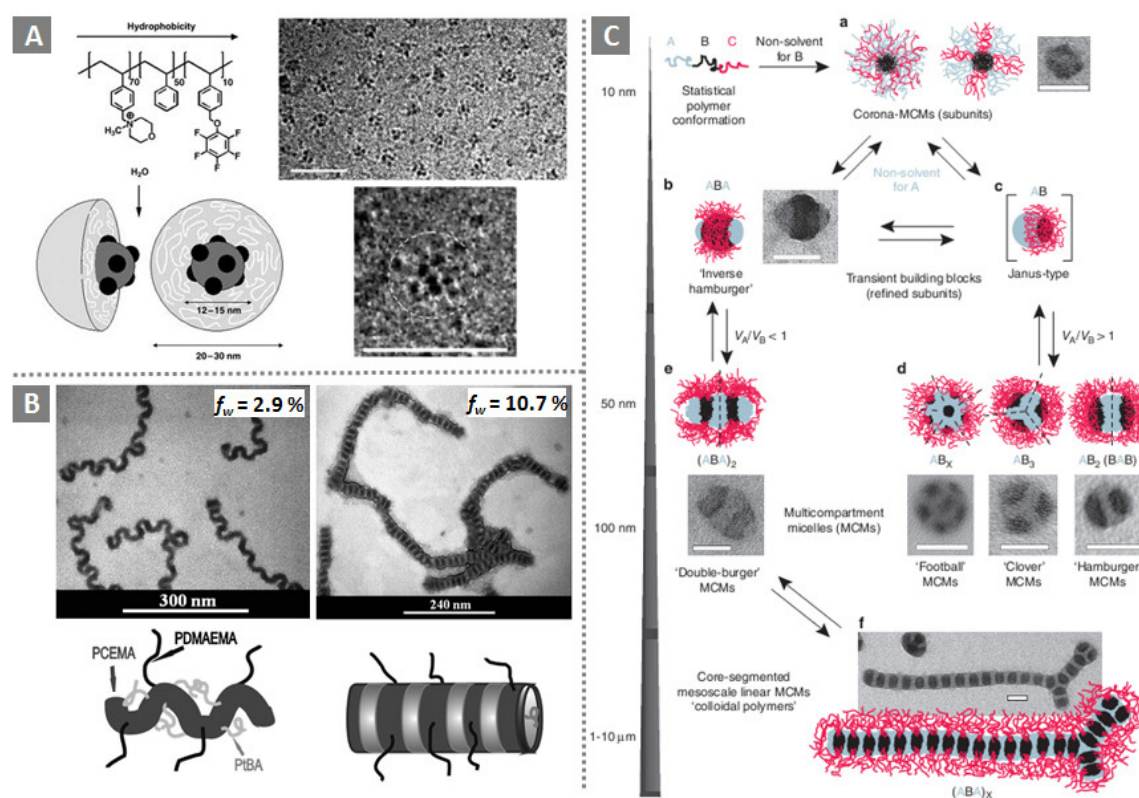


**Figure 1-3.** (A) Schematic representation and cryo-TEM of multicompartment micelles from poly(4-methyl-4-(4-vinylbenzyl)morpholin-4-ium chloride)-*block*-polystyrene-*block*-poly(pentafluorophenyl 4-vinylbenzyl ether) in water.<sup>38</sup> (B) Aggregation of wormlike micelles from poly(*tert*-butyl acrylate)-*block*-poly(2-cinnamoyloxyethyl methacrylate)-*block*-poly(*N,N*-dimethylaminoethyl methacrylate) into “wiggled” and segmented structures for two different volume fractions,  $f_w$ , of water in methanol.<sup>50</sup> (C) Conceptual mechanism for the directed self-assembly of linear ABC terpolymers into different multicompartment structures by sequential decrease of the degrees of freedom.<sup>59</sup>

Recently, Gröschel *et al.* reported a general concept for constructing multicompartment structures from linear triblock terpolymers by the directed self assembly of various ABC systems by step-wise adjusting the solvent quality, without the need of additives.<sup>59</sup> The therefore required sequential reduction of the degrees of freedom is accomplished by dissolution of the polymer in a solvent selective for the A and C block (step 1) and consecutive dialysis to a solvent selective for exclusively the C block (step 2). Similar to the approach reported by Fang,<sup>48</sup> the micellar building units formed upon step 1 further aggregate into compartmentalized structures. Depending on the volume ratio of the two insoluble blocks,  $V_A/V_B$ , a multitude of multicompartment micellar structures with distinct number of patches, including “hamburgers”, “clovers”, “Maltese crosses”, “footballs”, “double hamburgers” and linear one-dimensional segmented structures, are accessible (Figure 1-3C). Additionally, the pH or solvent-induced colloidal polymerization of the structural subunits and the solvent-induced structure switching of MCM’s was impressively demonstrated by controlling step 2.

### 1.1.2.2 Miktoarm Star Terpolymers

As already mentioned earlier, in contrast to linear terpolymers, ABC miktoarm star terpolymers are inherently forced to assemble into structures with a compartmentalized core in solvents selective for one block as all three constituting blocks evolve from a common junction point (Figure 1-2D). Hillmyer, Lodge and coworkers utilized the high incompatibility of hydrophilic poly(ethylene oxide) and hydrophobic poly(ethylene) and poly(perfluoropropylene oxide) segments ( $\mu$ -EOF) to conduct detailed structural and mechanistical investigations of the corresponding miktoarm star terpolymers with various compositions.<sup>36,60,61</sup> Attributed to the polymer architecture no special self-assembly protocols had to be applied and the polymers readily formed compartmentalized structures upon slow dissolution in water. It was shown that decreasing the length of the solubilizing block “hamburger” micelles, segmented worm-like micelles and nanostructured vesicles were accessible as compartmentalized equivalents to micellar morphologies from AB diblock copolymers (see Figure 1-1B). On the way from the worm-like micelles to the nanostructured vesicles segmented ribbon-like branched micelles, segmented bilayers with anisotropic orientation and faceted polygonal bilayer sheets were identi-

fied as intermediate structures. Furthermore, for polymers with the degree of polymerization of the perfluorinated block being bigger than the block length of the hydrophobic block, a situation of “double frustration” occurred. Besides the architectural restraints the fluorophilic segment aims for minimization of the unfavourable surface with the aqueous medium and the hydrophilic corona, despite resembling the majority core-forming block. This results in further diversification of the self-assembled structures into “raspberry”-like micelles and their aggregation into multicompartment worms. These findings enabled the construction of a phase diagram for multicompartment structures from  $\mu$ -EOF miktoarm star terpolymers as depicted in Figure 1-4.<sup>61</sup>

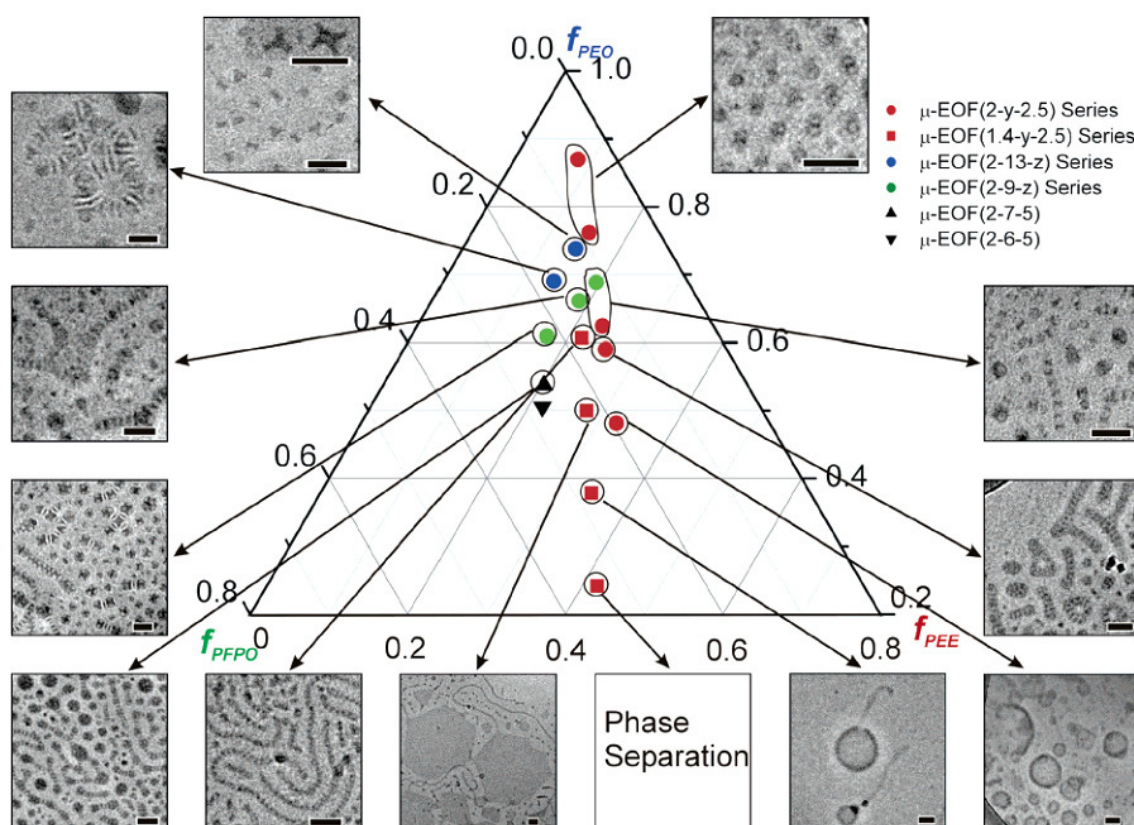


**Figure 1-4.** Phase diagram of multicompartment structures obtained from dilute aqueous solution of poly(ethylene)-arm-poly(ethylene oxide)-arm-poly(perfluoropropylene oxide) miktoarm star terpolymers ( $\mu$ -EOF) of various compositions.<sup>61</sup>

They also extended their studies to another system, where the perfluorinated block was exchanged with poly( $\gamma$ -methyl- $\epsilon$ -caprolactone) (PMCL), poly(ethylene)-arm-poly(ethylene oxide)-arm-poly( $\gamma$ -methyl- $\epsilon$ -caprolactone).<sup>62</sup> Due to the PMCL segment no “double frustration” was observed as in the case of  $\mu$ -EOF and therefore a transition of

“hamburger” micelles into segmented worm-like micelles and, finally, “raspberry”-like micelles occurred with increasing length of the polyester segment. Walther *et al.* demonstrated the formation of multicompartment micelles from another system (polystyrene-*arm*-polybutadiene-*arm*-poly(2-vinylpyridine)) with a segregated PS/PB core in aqueous solutions.<sup>63</sup> Interestingly, they observed the formation of hydrophobic bridges between individual MCMs by cryo-TEM. These evolve from the soft PB compartment and give rise to fusion processes.

Hillmyer, Lodge and co-workers reported the self-assembly of a double hydrophilic miktoarm star terpolymer system (polystyrene-*arm*-poly(ethylene oxide)-*arm*-poly(*N,N*-dimethylaminoethyl acrylate)) into spherical micelles with a mixed corona of PEO and PDMAEA at low pH (2.6).<sup>64</sup> Increasing the pH to 9.2 induced a transition to segmented worm-like micelles. Additionally, the groups of Jérôme<sup>65</sup> and Liu<sup>66-68</sup> reported the formation of micelles with a stimuli-responsive, mixed corona from bis-hydrophilic miktoarm star terpolymers in aqueous solution, however, without detailed discussion on the multicompartment character. On the contrary, a  $\mu$ -EOF miktoarm star terpolymer, forming compartmentalized disk-like micelles in water was shown to rearrange into micelles with a perfluorinated core and a mixed corona of PEO and polyethylene (PEE) upon addition of THF to the aqueous solution.<sup>69</sup> The sequential addition of THF gradually swells the PEE phase of the core and after passing nano-structured vesicles and segmented worm-like micelles completely dissolves the PEE compartment (Figure 1-5).

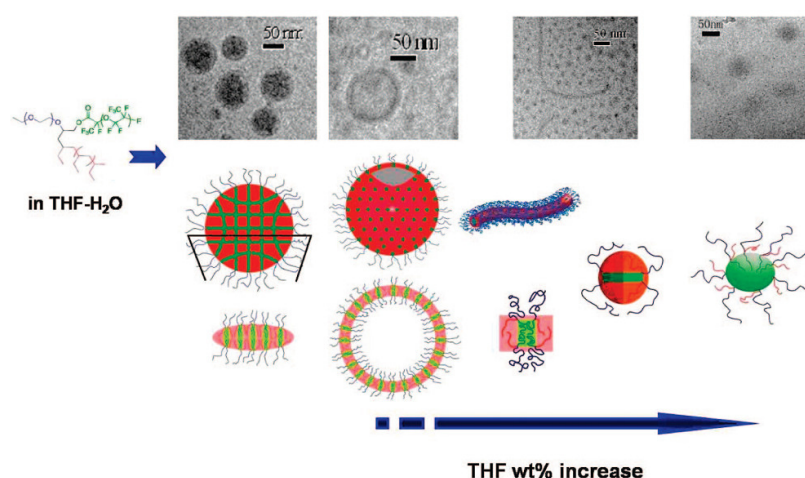
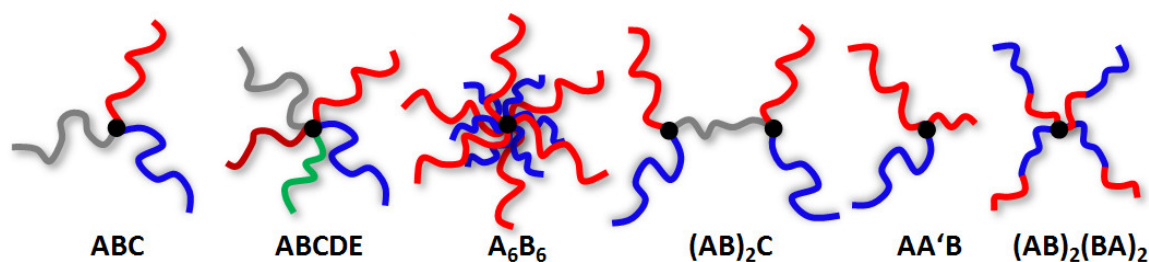


**Figure 1-5.** Transition of compartmentalized disk-like micelles from  $\mu$ -EOF into spherical micelles with a mixed corona, induced by changing the solvent composition.<sup>69</sup>

## 1.2 Miktoarm Star Polymers

In chapter 1.1.2 it was shown that due to their frustrated architecture ABC miktoarm star terpolymers inherently lead to compartmentalized structures upon dissolution in a selective solvent. This polymer architecture asks for special synthetic strategies. As compared to linear polymers, which are accessible by sequential controlled polymerization methods<sup>70-73</sup> there are less examples for the synthesis of miktoarm star polymers. Miktoarm star polymers in general are defined as star polymers with at least three arms of molecular weight, chemical or topological asymmetry (Scheme 1-1).<sup>28</sup> Various review articles dealing with the synthesis of miktoarm star polymer systems were published during the last two decades, highlighting the interest in such complex materials and their high potential.<sup>28,74-78</sup> However, in the following, the main focus will be set on ABC miktoarm star terpolymers, which display the corresponding branched analogues of the intensively studied linear ABC triblock terpolymers.<sup>79-84</sup>



**Scheme 1-1.** Examples of miktoarm star polymers with chemical (ABC, ABCDE,  $A_6B_6$ ,  $(AB)_2C$ ), molecular weight ( $AA'B$ ) or topological asymmetry ( $(AB)_2(BA)_2$ ).

### 1.2.1 Synthesis

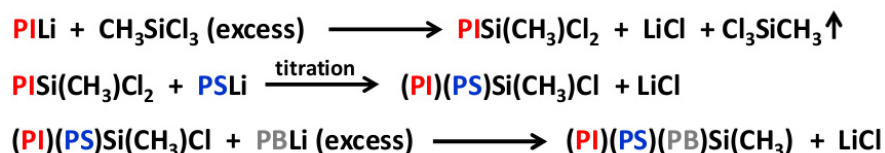
#### 1.2.1.1 ABC Miktoarm Star Terpolymers as Model System

ABC miktoarm star terpolymers resemble the basic system of miktoarm stars with chemical asymmetry. However, the synthetic requirements for the conjunction of the three polymer segments at a common junction point are the same as for the more complicated systems or also simplified  $A_2B$  systems or systems with asymmetry of molecular weight or topology. The different divergent and convergent synthetic strategies used therefore have to fulfill the criteria of exact mid-functionalization of diblock copolymers

or end-functionalization of homopolymers (1), with the stoichiometry of adequate linking reactions with pre-formed polymeric building blocks or initiator molecules (2). Even though in literature different classifications have been used, the synthesis of ABC miktoarm star terpolymers can be divided into four approaches of fundamentally differing chemistries. For the first three types anionic polymerization is utilized for the introduction of special functionalities in defined positions and/or selective reactivity of living anionic chain ends (A-C), whereas the fourth is based on multifunctional core molecules (D).

#### (A) Chlorosilane Method

Similar to the synthesis of regular stars by reaction of living anionic polymer chains with chlorosilanes,<sup>85,86</sup> these compounds can be used as linking agents for the construction of ABC miktoarm star terpolymers. Therefore, living anionic chain ends of different reactivity toward chlorine-silicon bonds have to be used to allow for step-wise substitution. Iatrou *et al.* synthesized a miktoarm star with polyisoprene, polystyrene and polybutadiene segments with trichloromethylsilane as trifunctional linking agent.<sup>87</sup> However, the synthesis can only be conducted in the specific sequence PS > PI > PB, due to the reactivity of the living anion toward the chlorosilane functionality. The less reactive and most sterically hindered polymer anion has to be added first, whereas the less sterically hindered and most reactive polymer anion has to be added at the end to guarantee full conversion. Even with this sequence (Scheme 1-2) the last step is time-consuming with reaction times of up to 4 weeks and for each step the stoichiometry is of outermost importance. Similarly, an ABCD miktoarm star quaterpolymer was synthesized by expanding the system with poly(4-methyl styrene) and using tetrachlorosilane.<sup>88</sup> The application of this approach to other less reactive polymer anions like poly(methyl methacrylate) or poly(2-vinylpyridine) requires a post- or pre-modification of the chlorosilane compound, respectively.<sup>89,90</sup>

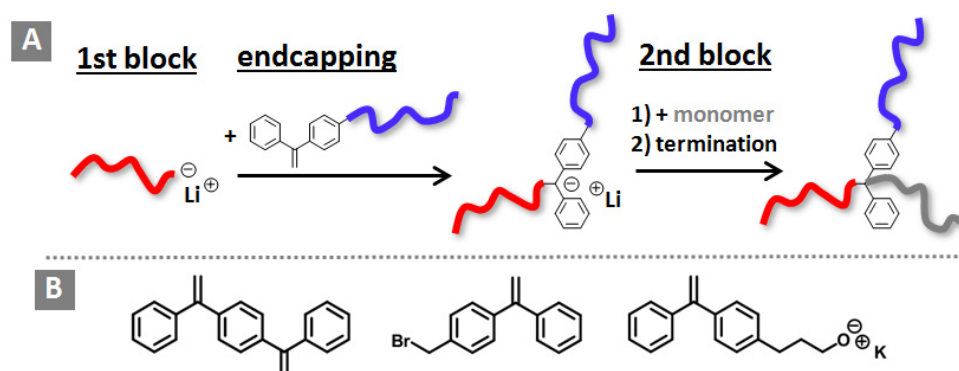


**Scheme 1-2.** Synthesis of an ABC miktoarm star terpolymer by the successive reaction of living polymer anions with trichlorosilane as linking agent.

### (B) Macromonomer Method

Apart from the special chemistry of chlorosilanes, diphenylethylene (DPE) and its double-diphenylethylene derivatives represent a powerful class of compounds, as their inability to homopolymerize permits selective functionalization of diblock copolymers.<sup>91</sup> Preformed macromonomers with a terminal DPE functionality can be applied for the sequential living anionic polymerization of diblock copolymers. By sequential addition of the macromonomer after polymerization of the first block, ABC miktoarm star terpolymers are accessible under control of the stoichiometry (Scheme 1-3A). For this purpose Quirk *et al.* used 1,4-bis(1-phenyl-ethenyl)benzene (Scheme 1-3B) to synthesize A<sub>2</sub>B and ABC miktoarm star polymers.<sup>92</sup> When the DPE derivative was used in two-fold excess for the linking reaction with polystyryl-lithium primarily monoaddition took place to generate the polystyrene macromonomer. Similarly, Hückstädt *et al.* demonstrated 1-(4-bromomethylphenyl)-1-phenylethylene (Scheme 1-3B) to be a suitable termination agent for living anions of polybutadiene<sup>93</sup> and polystyrene<sup>94</sup>. These served as macromonomers for the synthesis of a polybutadiene-*arm*-polystyrene-*arm*-poly(methyl methacrylate) miktoarm star terpolymer and series of polystyrene-*arm*-polybutadiene-*arm*-poly(2-vinylpyridine) miktoarm star terpolymers, respectively. However, also in the case of the bromo-functionalized DPE, formation of dimeric macromonomers can occur under inadequate reaction conditions as a result of Wurtz-analogous side reactions. Besides the use of DPE derivatives as termination agents for the macromonomer synthesis, Quirk and co-workers proved 1-(4-hydroxypropylphenyl)-1-phenylethylene to be a suitable initiator for the synthesis of poly(ethylene oxide) macromonomers after deprotonation with triphenylmethylpotassium (Scheme 1-3B).<sup>95</sup> In this way a polystyrene-*arm*-poly(ethylene oxide)-*arm*-poly(*tert*-butyl methacrylate) miktoarm star terpolymer was successfully synthesized. In a similar strategy a polystyrene-*arm*-poly(dimethylsiloxane)-*arm*-poly(*tert*-butyl methacrylate) miktoarm star terpolymer was

accessible by ring opening polymerization of hexamethylcyclotrisiloxane with lithiated *para*-(dimethylhydroxy)silyl- $\alpha$ -phenylstyrene as initiator.<sup>96</sup> For the synthesis involving macromonomers the stoichiometry of the endcapping reaction has to be considered to allow for simple purification of possible side products. Furthermore, the choice of monomer sequence is limited to the different reactivities of living anionic polymer chains.

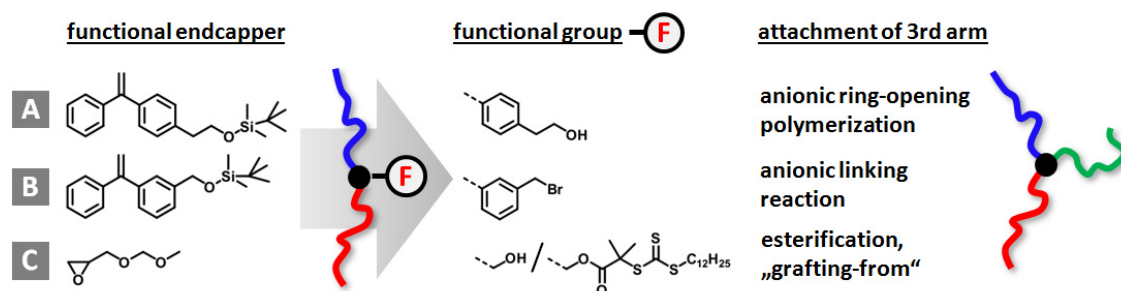


**Scheme 1-3.** (A) Schematic representation of the synthesis of ABC miktoarm star terpolymers *via* sequential anionic polymerization utilizing macromonomers. (B) DPE-derivatives used for the synthesis of macromonomers: 1,4-bis(1-phenyl-ethenyl)benzene,<sup>92</sup> 1-(4-bromomethylphenyl)-1-phenylethylene,<sup>93,94</sup> 1-(4-hydroxypropylphenyl)-1-phenylethylene deprotonated with trimethylphenylpotassium<sup>95</sup> (from left to right)

### (C) Mid-Functionalized Diblock Copolymers

Another possibility of constructing ABC miktoarm star terpolymers is the synthesis of mid-functional diblock copolymers. The third arm then is attached by adequate reactions with the functional group (Scheme 1-4). Again, DPE chemistry is advantageous within this context, as homopolymerization is excluded and therefore monofunctionalization is guaranteed under appropriate reaction conditions and polymerizations sequences. Exclusively hydroxyl-functionalized DPE's in their protected form have been used so far.<sup>97,98</sup> Lambert *et al.* synthesized mid-functional polystyrene-*block*-poly(ethylene oxide) and polystyrene-*block*-poly(methyl methacrylate) by sequential anionic polymerization with 1-[4-(2-*tert*-butyldimethylsiloxy)ethyl]phenyl-1-phenylethylene (Scheme 1-4A). After deprotection and deprotonation the hydroxyl-function served as initiator for the anionic ring opening polymerization of  $\epsilon$ -caprolactone<sup>97</sup> or L-lactide<sup>98</sup> in the case of polystyrene-*block*-poly(ethylene oxide) as diblock copolymer, or of ethylene oxide<sup>98</sup> in the case of polystyrene-*block*-poly(methyl

methacrylate). Using a similar DPE derivative, Hirao and co-workers synthesized hydroxy mid-functionalized polystyrene-*block*-poly(2-(perfluorooctyl)-ethyl methacrylate) diblock copolymers (Scheme 1-4B).<sup>99</sup> However, after transformation of the silyl-protected hydroxyl function into benzyl bromide, living anionic polymers of 2-vinylpyridine and methyl methacrylate were grafted to the diblock copolymers by anionic coupling reactions. Modification of the synthetic strategy and using a dual hydroxy-functionalized DPE further yielded A<sub>3</sub>B, ABC<sub>2</sub> and ABCD miktoarm star polymers. Another elegant way for introduction of a hydroxyl function at the border of two blocks is the use of 2-methoxymethoxymethylloxirane for the endcapping of living polymer anions (Scheme 1-4C).<sup>62,64,100</sup> The hydroxy function inherently generated during the coupling reaction with the endcapper is used for the ring opening polymerization of ethylene oxide as second block. After deprotection the second hydroxy function was used to attach a carboxyl-terminated poly(perfluoropropylene oxide) *via* esterification<sup>100</sup> or “grafting-from” of  $\gamma$ -methyl- $\epsilon$ -caprolactone<sup>62</sup> or *N,N*-dimethylaminoethyl acrylate<sup>64</sup> after post-modification of the alcohol to obtain amphiphilic ABC miktoarm star terpolymers. In a similar manner polystyrene-*block*-poly(ethylene oxide) diblock copolymers bearing an primary amino-<sup>101</sup> or allyl-function<sup>102</sup> at the block border were synthesized by Frey and co-workers from the corresponding functionalized glycidyl ethers. Due to their defined mid-functionality, these are of possible future interest for the construction of miktoarm star polymers. However, for such glycidyl compounds as endcapping agents, the polymerization method of the second block is restricted to anionic ring-opening polymerization. Also for the approaches utilizing DPE to generate the mid-functionality the choice of monomer sequence is dependent on the reactivity of the monomers.<sup>91</sup>

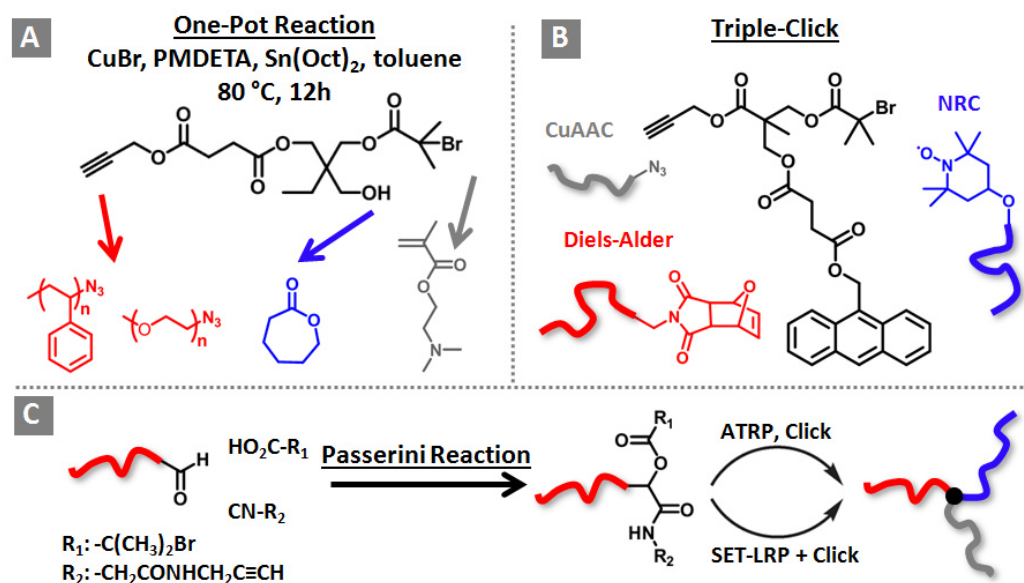


**Scheme 1-4.** Overview of mid-functional diblock copolymers for the construction of ABC miktoarm star terpolymers. Utilizing DPE chemistry (A,B)<sup>97-99</sup> or a glycidyl ether (C)<sup>62,64,100</sup> hydroxyl mid-functionalized diblock copolymers were synthesized which serve as precursor for the attachment of the third block *via* “grafting-from” or “grafting-to” approaches.

#### (D) Heterofunctional Core Molecules

All the examples discussed up to now take advantage of anionic polymerizations steps to generate well-defined and functionalized polymers as building blocks for the miktoarm star terpolymer synthesis. However, in the past decade, an increasing number of reactions fulfilling the criteria of click chemistry were utilized in polymer chemistry for the construction of various polymer architectures in combination with controlled radical polymerization methods.<sup>103</sup> Herein, heterofunctional core molecules can serve as common junction point for the “grafting-from” and “grafting-to” of different polymer segments by a combination of such click reactions with standard polymerization methods to construct miktoarm star terpolymers. For example Zhang *et al.* synthesized a trifunctional core molecule bearing an alkyne-, hydroxyl- and bromine-function.<sup>104</sup> Due to the compatibility and tolerance of the reaction conditions simultaneous azide-alkyne click chemistry, ring-opening polymerization and ATRP was possible to synthesize poly(styrene-*arm*-poly( $\epsilon$ -caprolactone)-*arm*-poly(*N,N*-dimethylaminoethyl methacrylate) or poly(ethylene oxide)-*arm*-poly( $\epsilon$ -caprolactone)-*arm*-poly(*N,N*-dimethylaminoethyl methacrylate) in a one-pot reaction (Scheme 1-5A). Based on the same principles, diverse other strategies are reported in literature where consecutive ATRP, ring-opening polymerization, click reactions like azide-alkyne or thiol-ene click chemistry, esterification and transformation reactions were combined to construct ABC miktoarm star terpolymers.<sup>66-68,77,105-110</sup> Furthermore, Tunca and co-workers presented an approach utilizing three orthogonal click reactions for the construction of a poly(ethylene oxide)-*arm*-poly( $\epsilon$ -caprolactone)-*arm*-poly(*N*-butyl oxanorboneneimide) miktoarm star

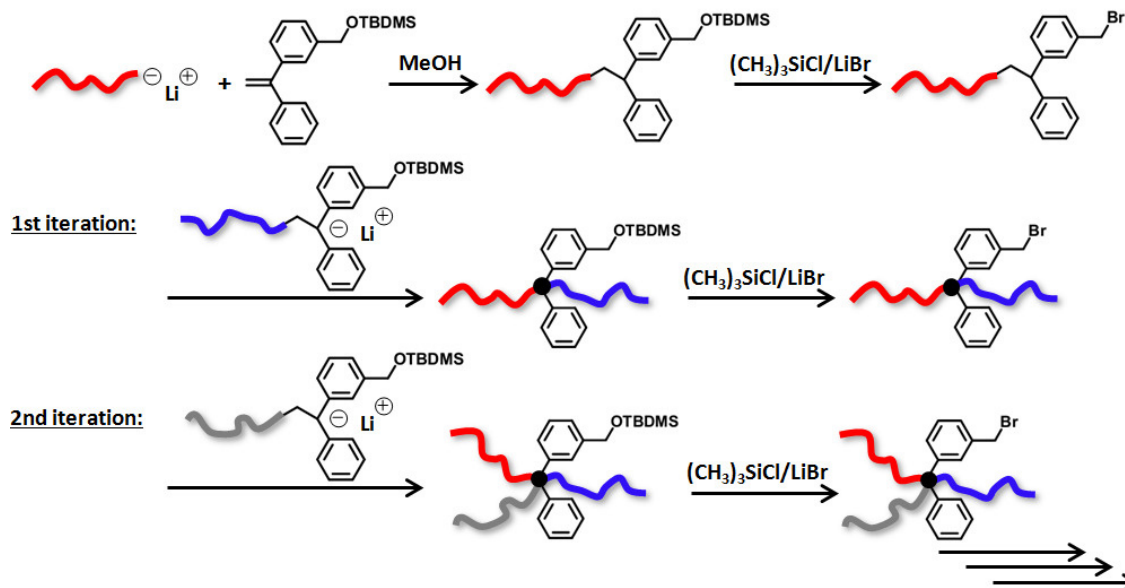
(Scheme 1-5B).<sup>111</sup> First the poly(ethylene oxide) segment was attached to the core molecule by a Diels-Alder click reaction, followed by the simultaneous ligation of the other two blocks by azide-alkyne cycloaddition and nitroxide radical coupling click reaction. Huan *et. al* reported a facile strategy for the construction of supramolecular ABC miktoarm star terpolymers using  $\beta$ -cyclodextrin as core molecule.<sup>112</sup> Recently, the group of Li demonstrated the Passerini three-component reaction to be a powerful method to simultaneously introduce an ATRP initiator and an alkyne-function to aldehyde end-functionalized poly(ethylene oxide).<sup>113</sup> Starting with this dual-functionalized PEO diverse ABC miktoarm star terpolymers were accessible either by consecutive ATRP and azide-alkyne cycloaddition or simultaneous SET-LRP and click reaction (Scheme 1-5C). Additionally, in literature different other miktoarm star architectures like ABCD,<sup>114</sup> star<sup>115</sup> and H-shaped ABCDE miktoarm stars<sup>116</sup> and the first ABC miktoarm star terpolymer with cyclic arms<sup>117</sup> are reported by modifications of these strategies with heterofunctional core molecules.



**Scheme 1-5.** Synthetic strategies for the construction of ABC miktoarm star terpolymers with heterofunctional core molecules *via* simultaneous ATRP, ROP and CuAAC (A),<sup>104</sup> consecutive triple click reactions (B)<sup>111</sup> or three-component Passerini reaction (C).<sup>113</sup>

### 1.2.1.2 Other Miktoarm Star Polymer Systems

Hirao and co-workers designed special reaction sequences which enable the iterative synthesis of asymmetric star branched polymers by repeating the sequence.<sup>76</sup> These individual steps involve the linking reaction of a living polymer anion with a polymer containing a suitable functional group (1), which is followed by the regeneration of the functional group at the reaction site (2). Based on the silyl-protected hydroxyl-functionalized DPE shown in Scheme 1-4B such an iterative methodology is possible, starting with a living polymer anion endcapped with this DPE derivative. After transformation of the protected hydroxy group into a benzyl bromide function a second living anion endcapped with this DPE is reacted with the bromide, which resembles step 1. Regeneration of the bromide function at the core from the newly introduced silyl-protected hydroxyl-function resembles step 2, which allows for repeating the cycle (Scheme 1-6). In this manner an ABCD miktoarm star polymer was synthesized.<sup>118</sup> However, as a prerequisite for the re-introduction of the functional group the living polymer anion used in the last step has to be nucleophilic enough to copolymerize with DPE. Therefore, for less nucleophilic living anions of polymers like poly(methyl methacrylate), a reintroduction of the functional group is not possible and they have to be attached in the last step. This methodology was also applied to bromide-functionalized DPE<sup>119</sup> or bromide-functionalized 1,3-butadiene,<sup>120</sup> which are used to re-introduce a non-homopolymerizable DPE or butadiene end-functionality. Repeating these steps, stars containing up to seven different arms could be achieved. Another functionality capable of such linking reactions without undergoing homopolymerization is the  $\alpha$ -phenyl acrylate, which can also copolymerize with less reactive monomers like *tert*-butyl methacrylate. Using a dual hydroxy-functionalized DPE derivative, which protecting groups can be selectively cleaved to esterify them with the  $\alpha$ -phenylacrylic acid in separate steps, ABCDE miktoarm stars were synthesized with an iterative methodology in the group of Hirao.<sup>121</sup> For all these strategies additional fractionation is necessary to obtain the pure miktoarm star polymers as the linking reactions are conducted with excess of the living anionic polymer chain to guarantee 100% conversion.



**Scheme 1-6.** Iterative methodology for the synthesis of star branched polymers *via* reaction of living polymer anions with a benzyl bromide function.<sup>118</sup>

Another widely used method is the divinylbenzene (DVB) method, based on the ability of preformed polystyrene arms to anionically copolymerize with divinylbenzene to form a core with active reaction sites.<sup>122</sup> Addition of a second monomer leads to polymer chains growing from this core. Therefore, with this “in-out” method, star systems of the type  $A_nB_n$  with symmetrical composition and different second blocks were easily accessible as shown by Tsitsilianis and co-workers.<sup>123-126</sup> By the addition of a third monomer furthermore  $A_n(\text{B-block-C})_n$  miktoarm star systems with a polystyrene and poly(2-vinylpyridine)-*block*-poly(*tert*-butyl acrylate) segments were synthesized.<sup>127</sup> However the number of arms represents an average value, which is only roughly adjustable by the amount of DVB and molecular weight of the starting polymer.

### 1.2.2 Self-Assembly in Bulk

In addition to the self-assembled structures of miktoarm star terpolymers in solution (see 1.1.2.2), their morphology in the bulk state represents an unique property. Already linear triblock terpolymers were shown to produce a wide variety of interesting morphologies due to the linear connection of three immiscible blocks with three different sets of interaction parameters.<sup>27,71,128-131</sup> However, for miktoarm star terpolymers of sufficient incompatibility the constitution of the three polymer segments at a common

point forces these to align in a one-dimensional fashion. In contrast to that the two different junction points in linear ABC triblock terpolymers are located at two-dimensional polymer interfaces. Consequently, completely segregating miktoarm star terpolymers are supposed to assemble into columnar bulk morphologies (Figure 1-6A).<sup>132</sup> The two-dimensional cross-sections of the spatial arrangement of these cylinders can be described by Archimedean tiling patterns.<sup>132-134</sup>

Due to the challenging synthesis of miktoarm star terpolymers systematic investigations of the compositional influence on the morphology are quite rare. Besides earlier morphological studies,<sup>135,136</sup> Thomas and co-workers proved the alignment of the junction points in a one-dimensional fashion for a system consisting of polystyrene, polyisoprene and poly(methyl methacrylate).<sup>137</sup> Hückstädt *et al.* gave the first detailed morphological study on a polystyrene-*arm*-polybutadiene-*arm*-poly(2-vinylpyridine) system of various compositions.<sup>94</sup> For another system containing polystyrene, polyisoprene and poly(2-vinylpyridine) arms the variation of the volume fractions yielded manifold structures of complex tiling patterns as exemplarily depicted in Figure 1-6B.<sup>138-141</sup> When miktoarm stars of more asymmetric compositions were investigated, transitions to highly periodic, substructured lamellar morphologies could be observed.<sup>142</sup> Similarly, Ikkala and co-workers reported the hierarchical smectic self-assembly for a miktoarm star terpolymer containing a  $\alpha$ -helical poly( $\epsilon$ -*tert*-butyloxycarbonyl-L-lysine) (PBLL) segment.<sup>143</sup> The morphology composed of an overall lamellar structure with one type of lamella of packed helices of PBLL and a second type formed from alternating rectangular cylinders of polystyrene and polyisoprene (Figure 1-6C). In addition Abetz *et al.* demonstrated that blending of polystyrene-*arm*-polybutadiene-*arm*-poly(2-vinylpyridine) miktoarm stars with diblock copolymers can be utilized to tune the obtained morphology within certain limits.<sup>144</sup>

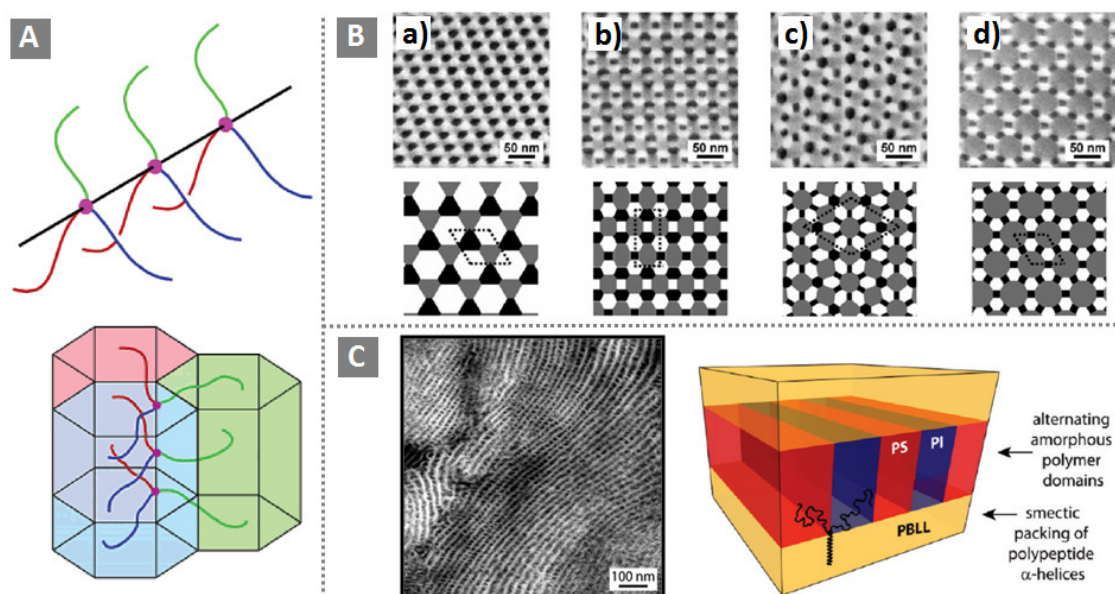


**Figure 1-6.** (A) Schematic illustration of the one-dimensional alignment of junction points and the resulting columnar arrangement of the individual blocks of ABC miktoarm star terpolymers.<sup>132</sup> (B) TEM micrographs of four polyisoprene-*arm*-polystyrene-*arm*-poly(2vinylpyridine) ( $\mu$ -ISV) miktoarm star terpolymers (top row) and the corresponding schematic tiling patterns (bottom row): (a)  $\mu$ -I<sub>1.0</sub>S<sub>1.8</sub>I<sub>1.0</sub>, (b)  $\mu$ -I<sub>1.0</sub>S<sub>1.8</sub>I<sub>1.6</sub>, (c)  $\mu$ -I<sub>1.0</sub>S<sub>1.8</sub>I<sub>2.0</sub>, (d)  $\mu$ -I<sub>1.0</sub>S<sub>1.8</sub>I<sub>2.9</sub> (the subscripts denote the corresponding volume ratios). The dark, light and gray domains correspond to PI, PS, and P2VP phases.<sup>141</sup> (C) TEM micrograph and schematic illustration of the bulk morphology of a  $\mu$ -(PS)(PI)(PBLL) miktoarm star. The sample is stained with OsO<sub>4</sub> (PI dark, PS and PBLL light).<sup>143</sup>

### 1.2.3 Application of ABC Miktoarm Star Terpolymers for Functional Materials

Due to the broad variety of hierarchies obtained both in solution and bulk (see 1.1.2.2 and 1.2.2), miktoarm star terpolymers are of special interest for the design of novel materials with compartmentalized structures. Up to now only a limited number of publications has been dealing with the application of miktoarm star terpolymers in materials research, most probably due to the complicated synthesis and accessibility of larger amounts of material. However, this situation will change with the advances obtained in miktoarm star synthesis during the last decade.

Already for linear diblock copolymers the infiltration in anodized aluminium oxide was demonstrated to be a powerful method for the fabrication of one-dimensional nanoscopic structures.<sup>145-148</sup> The phase behavior of symmetric ABC miktoarm star terpolymers in cylindrical nanopores was systematically investigated by Monte Carlo

simulations including different surface-polymer interactions and frustration parameters ( $D/L_0$ , resembling the ratio of pore diameter to long period of the bulk morphology).<sup>149</sup> As a consequence of the cylindrical confinement and the complex polymer architecture various new morphologies like *e.g.* A cylinder + BC single-strand helix or helical arranged ABC cylinders were predicted. In analogy, theoretical calculations for asymmetric miktoarm star terpolymers under cylindrical confinement were also conducted by another group.<sup>150</sup> Apart from theory, the unique hexagonal bulk morphology of a polystyrene-*arm*-polybutadiene-*arm*-poly(2-vinylpyridine) miktoarm star<sup>94</sup> was utilized to prepare one-dimensional nano-objects with perfectly parallel aligned compartments at the surface.<sup>151</sup> Similar to the synthesis of soft Janus particles from bulk,<sup>152,153</sup> the polybutadiene phase of the hexagonal morphology was crosslinked and the cylindrical structure subsequently transferred into solution. Selective decoration of the P2VP corona with metal nanoparticles yielded biaxial nanowires with the surface compartmentalization being adjustable by the solvent quality (Figure 1-7A).

Regarding self-assembled structures the core of multicompartement micelles is accessible for selective loading with small molecules. Hillmyer, Lodge and coworkers proved the basic concept of simultaneous loading of two chromophores (lipophilic and fluorophilic) as reference molecules into the respective compartments of a poly(ethylethylene)-*arm*-poly(ethylene oxide)-*arm*-poly(perfluoropropylene oxide) miktoarm star terpolymer in water.<sup>154</sup> On contrary, the miktoarm architecture can lead to micelles with a mixed corona if only one block is solvophobic. Sharma *et al.* took advantage of this fact by designing miktoarm star terpolymers with poly( $\epsilon$ -caprolactone) as storage block and a corona with poly(ethylene oxide) and triphenylphosphonium bromide (TPPBr) as biocompatible or mitochondriotropic moiety, respectively.<sup>155</sup> The obtained micelles displayed an extraordinarily high capability for loading with coenzyme Q10, which was successfully delivered to mitochondria as encoded by the targeting TPPBr block (Figure 1-7B). Hedrick and co-workers presented another promising example for miktoarm star terpolymers in biotechnology, namely as drug delivery vehicles for sustained release of the anticancer drug paclitaxel.<sup>156</sup> At the example of poly(ethylethylene)-*arm*-poly(ethylene oxide)-*arm*-poly( $\gamma$ -methyl- $\epsilon$ -caprolactone) miktoarm star systems it was shown that hydrolytic degradation of the caprolactone-

based segment can be used as trigger for morphological transitions in the multicompartiment micelle structure.<sup>157</sup> This pH-sensitive transition is regarded as a potential pathway for smart delivery systems.

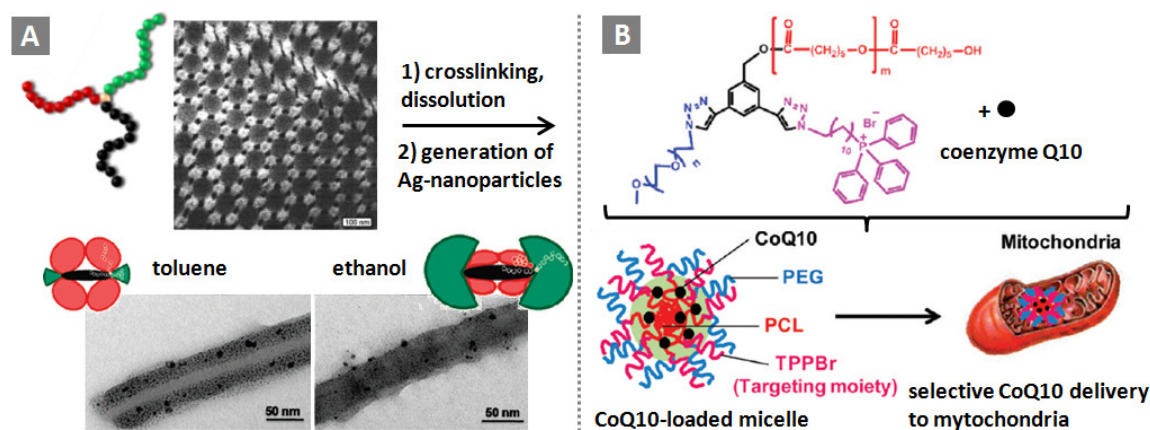


**Figure 1-7.** (A) Synthesis of bidirectional hybrid nanowires by crosslinking of the PB phase of the bulk morphology from a  $\mu$ -SBV miktoarm star terpolymer (PB = black, PS = red and P2VP = green), subsequent transfer into solution and generation of Ag-nanoparticles. By selective exposure to toluene the P2VP segment is collapsed, whereas in ethanol the PS compartment is collapsed.<sup>151</sup> (B) Schematic illustration for selective delivery of coenzyme Q10 (CoQ10) loaded micelles into mitochondria.<sup>155</sup>

## 1.3 Synthetic Strategies in Polymer Synthesis

### 1.3.1 DPE Chemistry in Anionic Polymerization

Living anionic polymerization is a versatile method for the synthesis of well-defined polymers as it combines perfect control over molecular weight, microstructure and tacticity with the possibility of sequential monomer addition to yield polymers with narrow molecular weight distribution in large quantity.<sup>158-160</sup> Within anionic polymerization, 1,1-diphenylethylene and its derivatives represent a beneficial class of compounds due to two fundamental properties: (i) The reaction of alkylolithium or polymeric organolithium compounds only results in monoaddition of the DPE as a consequence of steric hindrance and additionally stabilizes the anion.<sup>91</sup> (ii) Quantitative reaction of highly nucleophilic living anions, like polybutadienyl-lithium or polystyryl-lithium with DPE allows for attenuation of the nucleophilicity so that copolymerization with polar monomers of the methacrylate type is possible.<sup>161</sup> Without endcapping, termination occurs in polar solvents like THF by attack of the carbonyl function in the crossover step.

Therefore, block copolymers and homopolymers are accessible, carrying functional groups at defined positions ( $\alpha$ -,  $\omega$ -position, at the block junction or in an alternating manner) by simple sequential copolymerization with adequate DPE derivatives, which was termed as living functionalization.<sup>91</sup> In literature a variety of DPE compounds bearing functionalities including protected hydroxyl-groups<sup>97,99,118,162</sup> or primary amines,<sup>163</sup> tertiary amines,<sup>164</sup> protected carboxyl-functions,<sup>165,166</sup> fluorophores<sup>167-170</sup> or norbornene moieties<sup>171</sup> are reported. The reactive groups are afterwards accessible for polymer-analogous reactions. However, with regard to the reactivity of the used monomers the DPE derivatives can only be incorporated at distinct positions of homo- or block copolymers. Whereas styrene and butadiene as well as methacrylate-type monomers are amenable for initiation by organolithium adducts with DPE derivatives, endcapping of the living anions of methacrylates with DPE is not possible due to insufficient nucleophilicity.<sup>91</sup> Furthermore, it was shown that in the case of living anions of 2-vinylpyridine the addition of DPE is an equilibrium reaction lying on the educt side.<sup>172</sup> The plethora of synthetic approaches for the construction of miktoarm star polymers utilizing DPE chemistry discussed in 1.2.1 additionally demonstrates the versatility of DPE-chemistry for the generation of novel polymeric materials.

### 1.3.2 Click Chemistry

Since Sharpless' definition of the term "click chemistry" in 2001<sup>173</sup> reactions fulfilling the proposed criteria had a tremendous impact on the field of polymer-polymer conjugation, construction of polymer architectures and polymer functionalization.<sup>174-178</sup> The compressed definition claims for simple, highly efficient, easily applicable reactions without perceivable side-products, or byproducts which can be separated with little effort. Without aiming for new reactions, the purpose was rather to concentrate on adequate reactions fitting into this concept. Besides the initially considered reactions, like e.g. ring-opening of epoxides, hetero Diels-Alder reactions or 1,3-dipolar cycloaddition<sup>173</sup> an increasing number of strategies was applied in the last decade for the construction of polymeric materials. These include thiol-ene<sup>179,180</sup> and thiol-yne chemistry,<sup>181</sup> RAFT-hetero Diels-Alder,<sup>182,183</sup> tetrazene-norbornene chemistry<sup>184</sup> or thiol-*para* fluoro click reactions,<sup>185</sup> just to name a few. However, the copper-catalyzed alkyne-

azide cycloaddition (CuAAC) is the most frequently applied click reaction up to now.<sup>103,186-189</sup> This relies on several reasons. The educt functional groups are highly inert and stable under diverse conditions representing the orthogonality of the reaction. This was an initial disadvantage in the first reports on the uncatalyzed cycloaddition of azides and alkynes by Huisgen, which required high temperatures and long reaction times without the formation of stereospecific products. In contrast to that the Cu(I)-catalyzed modification yields exclusively 1,4-disubstituted 1,2,3-triazoles at ambient temperatures and time scales and with high efficiency (Scheme 1-7).<sup>190,191</sup> In addition diverse standardized methods have been developed within the last decade for the introduction of clickable functions into polymers *via* post-functionalization,<sup>192-195</sup> or functional initiators<sup>175,196-198</sup> and monomers,<sup>199-201</sup> making the building blocks for the construction of polymer architectures by combination of controlled/living polymerization methods and CuAAC easily accessible.



**Scheme 1-7.** Uncatalyzed (left side) and copper(I) catalyzed alkyne-azide cycloaddition (right side), leading to the formation of a mixture of 1,4- and 1,5-disubstituted triazoles or exclusively 1,4-adducts, respectively.

Due to the massive impact of click chemistry in polymer science, recently, a group of leading polymer chemists redefined the term click chemistry with regard to the demands in constructing polymeric materials.<sup>202</sup> In addition to the requirements of Sharpless' click concept<sup>173</sup> they emphasize that *equimolarity* is a key criterion for polymer-polymer ligation since polymer separation is challenging as compared to organic synthesis, especially on a large-scale. However, if such *large-scale purification* processes are operable in a simple manner they might be considered to conduct more simplified reaction pathways. On the other hand a *reasonable timescale* for completion of the reaction is more adequate than a *fast timescale* in polymer systems, even if the latter one is desirable. Additionally, the claim of *readily available starting materials* should be extended to materials that are *easily accessible by uncomplicated synthetic routes* as one of the great benefits of click chemistry in polymer science is modularity.

## 1.4 Aim of this thesis

The general objective of this thesis is the synthesis of novel amphiphilic miktoarm star terpolymer systems and the mechanistic and structural study of their self-assembly behavior in aqueous solutions.

Therefore, one key aspect is the development of a new strategy for the construction of polymers of this particular architecture with focus on the applicability to a broad range of monomers including functional groups and the modularity to obtain interesting materials. Anionic polymerization in combination with azide-alkyne cycloaddition are selected as suitable methods as they guarantee the synthesis of precisely functionalized diblock copolymers in high yields and combinatorial ligation with easily accessible azido-functional homopolymers.

Within the synthesized materials a star terpolymer bearing a quaternized poly(2-vinylpyridine) segment is shown to arrange into structures of outermost complexity in aqueous solution. At the example of this miktoarm star terpolymer the importance of the counterion nature on the mechanism of hierarchical self-assembly is to be studied. Based on the developed modular approach for the polymer synthesis this system is further expanded to other miktoarm star polymers for investigation of the influence of molecular composition and chemical nature of the constituting blocks. Therefore, this thesis is intended to cover the unique properties of miktoarm star polymers and the nature of the counterion as trigger for directing the self-assembly.

## 1.5 References

- (1) Whitesides, G. M.; Mathias, J. P.; Seto, C. T. *Science* **1991**, *254*, 1312-1319.
- (2) Whitesides, G. M.; Grzybowski, B. *Science* **2002**, *295*, 2418-2421.
- (3) Philp, D.; Stoddart, J. F. *Angew. Chem., Int. Ed.* **1996**, *35*, 1154-1196.
- (4) Mandelkern, M.; Elias, J. G.; Eden, D.; Crothers, D. M. *J. Mol. Biol.* **1981**, *152*, 153-161.
- (5) Zlotnick, A.; Stray, S. J. *Trends Biotechnol.* **2003**, *21*, 536-542.
- (6) Canetti, M.; Seves, A.; Secundo, F.; Vecchio, G. *Biopolymers* **1989**, *28*, 1613-1624.
- (7) Zhang, S. *Biotechnol. Adv.* **2002**, *20*, 321-339.
- (8) Rothmund, P. W. K. *Nature* **2006**, *440*, 297-302.
- (9) Andersen, E. S.; Dong, M.; Nielsen, M. M.; Jahn, K.; Subramani, R.; Mamdouh, W.; Golas, M. M.; Sander, B.; Stark, H.; Oliveira, C. L. P.; Pedersen, J. S.; Birkedal, V.; Besenbacher, F.; Gothelf, K. V.; Kjems, J. *Nature* **2009**, *459*, 73-76.
- (10) Pasparakis, G.; Krasnogor, N.; Cronin, L.; Davis, B. G.; Alexander, C. *Chem. Soc. Rev.* **2010**, *39*, 286-300.
- (11) Adams, D. J.; Topham, P. D., Assembly of Block Copolymers. In *Supramolecular Chemistry: From Molecules to Nanomaterials*, John Wiley & Sons, Ltd: Chichester, 2012.
- (12) Zhang, L.; Eisenberg, A. *Science* **1995**, *268*, 1728-1731.
- (13) Jain, S.; Bates, F. S. *Science* **2003**, *300*, 460-464.
- (14) Zehm, D.; Ratcliffe, L. P. D.; Armes, S. P. *Macromolecules* **2012**.
- (15) Shuai, X.; Ai, H.; Nasongkla, N.; Kim, S.; Gao, J. *J. Controlled Release* **2004**, *98*, 415-426.
- (16) Kataoka, K.; Harada, A.; Nagasaki, Y. *Adv. Drug Delivery Rev.* **2012**, *64*, Supplement, 37-48.
- (17) McHale, R.; Patterson, J. P.; Zetterlund, P. B.; O'Reilly, R. K. *Nat. Chem.* **2012**, *4*, 491-497.
- (18) Braun, C. H.; Richter, T. V.; Schacher, F.; Müller, A. H. E.; Crossland, E. J. W.; Ludwigs, S. *Macromol. Rapid Commun.* **2010**, *31*, 729-734.
- (19) Bouilhac, C.; Cloutet, E.; Taton, D.; Deffieux, A.; Borsali, R.; Cramail, H. *J. Poly. Sci., Part A: Polym. Chem.* **2009**, *47*, 197-209.
- (20) Wang, M.; Zhang, M.; Siegers, C.; Scholes, G. D.; Winnik, M. A. *Langmuir* **2009**, *25*, 13703-13711.
- (21) Bastakoti, B. P.; Guragain, S.; Yusa, S.-i.; Nakashima, K. *RSC Adv.* **2012**, *2*, 5938-5940.
- (22) Semsarilar, M.; Jones, E. R.; Blanz, A.; Armes, S. P. *Adv. Mater.* **2012**, *24*, 3378-3382.
- (23) Discher, B. M.; Won, Y.-Y.; Ege, D. S.; Lee, J. C. M.; Bates, F. S.; Discher, D. E.; Hammer, D. A. *Science* **1999**, *284*, 1143-1146.
- (24) Chécot, F.; Rodríguez-Hernández, J.; Gnanou, Y.; Lecommandoux, S. *Biomol. Engin.* **2007**, *24*, 81-85.
- (25) Du, J.; O'Reilly, R. K. *Soft Matter* **2009**, *5*, 3544-3561.
- (26) Leibler, L. *Macromolecules* **1980**, *13*, 1602-1617.
- (27) Bates, F. S.; Fredrickson, G. H. *Phys. Today* **1999**, *52*, 32-38.
- (28) Hadjichristidis, N. *J. Polym. Sci., Part A: Polym. Chem.* **1999**, *37*, 857-871.
- (29) Fustin, C. A.; Abetz, V.; Gohy, J. F. *Eur. Phys. J. E* **2005**, *16*, 291-302.
- (30) Walther, A.; Barner-Kowollik, C.; Müller, A. H. E. *Langmuir* **2010**, *26*, 12237-12246.
- (31) Du, J.; Armes, S. P. *Soft Matter* **2010**, *6*, 4851-4857.
- (32) Gohy, J.-F.; Willet, N.; Varshney, S.; Zhang, J.-X.; Jérôme, R. *Angew. Chem., Int. Ed.* **2001**, *40*, 3214-3216.
- (33) Ringsdorf, H.; Lehmann, P.; Weberskirch, R., Multicompartmentation - a Concept for the Molecular Architecture of Life. In *217th ACS National Meeting*, Anaheim, CA, 1999.
- (34) Yu, G.-e.; Eisenberg, A. *Macromolecules* **1998**, *31*, 5546-5549.
- (35) Moughton, A. O.; Hillmyer, M. A.; Lodge, T. P. *Macromolecules* **2012**, *45*, 2-19.
- (36) Li, Z.; Kesselman, E.; Talmon, Y.; Hillmyer, M. A.; Lodge, T. P. *Science* **2004**, *306*, 98-101.
- (37) Lodge, T. P.; Bang, J.; Li, Z.; Hillmyer, M. A.; Talmon, Y. *Faraday Discuss.* **2005**, *128*, 1-12.
- (38) Kubowicz, S.; Baussard, J.-F.; Lutz, J.-F.; Thünemann, A. F.; von Berlepsch, H.; Laschewsky, A. *Angew. Chem., Int. Ed.* **2005**, *44*, 5262-5265.
- (39) Skrabania, K.; Laschewsky, A.; Berlepsch, H. v.; Böttcher, C. *Langmuir* **2009**, *25*, 7594-7601.
- (40) Marsat, J.-N. I.; Heydenreich, M.; Kleinpeter, E.; Berlepsch, H. v.; Böttcher, C.; Laschewsky, A. *Macromolecules* **2011**, *44*, 2092-2105.
- (41) Skrabania, K.; Berlepsch, H. v.; Böttcher, C.; Laschewsky, A. *Macromolecules* **2009**, *43*, 271-281.
- (42) Berlepsch, H. v.; Böttcher, C.; Skrabania, K.; Laschewsky, A. *Chem. Commun.* **2009**, *0*, 2290-2292.

- (43) Wang, L.; Lin, J. *Soft Matter* **2011**, *7*, 3383-3391.
- (44) Babinot, J.; Renard, E.; Le Droumaguet, B.; Guigner, J.-M.; Mura, S.; Nicolas, J.; Couvreur, P.; Langlois, V. *Macromol. Rapid Commun.* **2012**, DOI: 10.1002/marc.201200692
- (45) Uchman, M.; Štěpánek, M.; Procházka, K.; Mountrichas, G.; Pispas, S.; Voets, I. K.; Walther, A. *Macromolecules* **2009**, *42*, 5605-5613.
- (46) Schacher, F.; Walther, A.; Müller, A. H. E. *Langmuir* **2009**, *25*, 10962-10969.
- (47) Schacher, F.; Walther, A.; Ruppel, M.; Drechsler, M.; Müller, A. H. E. *Macromolecules* **2009**, *42*, 3540-3548.
- (48) Fang, B.; Walther, A.; Wolf, A.; Xu, Y.; Yuan, J.; Müller, A. H. E. *Angew. Chem., Int. Ed.* **2009**, *48*, 2877-2880.
- (49) Dupont, J.; Liu, G.; Niihara, K.-i.; Kimoto, R.; Jinnai, H. *Angew. Chem., Int. Ed.* **2009**, *48*, 6144-6147.
- (50) Han, D.; Li, X.; Hong, S.; Jinnai, H.; Liu, G. *Soft Matter* **2012**, *8*, 2144-2151.
- (51) Pochan, D. J.; Chen, Z.; Cui, H.; Hales, K.; Qi, K.; Wooley, K. L. *Science* **2004**, *306*, 94-97.
- (52) Chen, Z.; Cui, H.; Hales, K.; Li, Z.; Qi, K.; Pochan, D. J.; Wooley, K. L. *J. Am. Chem. Soc.* **2005**, *127*, 8592-8593.
- (53) Li, Z.; Chen, Z.; Cui, H.; Hales, K.; Qi, K.; Wooley, K. L.; Pochan, D. J. *Langmuir* **2005**, *21*, 7533-7539.
- (54) Cui, H.; Chen, Z.; Wooley, K. L.; Pochan, D. J. *Macromolecules* **2006**, *39*, 6599-6607.
- (55) Li, Z.; Chen, Z.; Cui, H.; Hales, K.; Wooley, K. L.; Pochan, D. J. *Langmuir* **2007**, *23*, 4689-4694.
- (56) Cui, H.; Chen, Z.; Wooley, K. L.; Pochan, D. J. *Soft Matter* **2009**, *5*, 1269-1278.
- (57) Cui, H.; Chen, Z.; Zhong, S.; Wooley, K. L.; Pochan, D. J. *Science* **2007**, *317*, 647-650.
- (58) Dupont, J.; Liu, G. *Soft Matter* **2010**, *6*, 3654-3661.
- (59) Gröschel, A.; Schacher, F. H.; Schmalz, H.; Borisov, O. V.; Zhulina, E. B.; Walther, A.; Müller, A. H. E. *Nat. Commun.* **2012**, *3*, 710.
- (60) Li, Z.; Hillmyer, M. A.; Lodge, T. P. *Nano Lett.* **2006**, *6*, 1245-1249.
- (61) Li, Z.; Hillmyer, M. A.; Lodge, T. P. *Langmuir* **2006**, *22*, 9409-9417.
- (62) Saito, N.; Liu, C.; Lodge, T. P.; Hillmyer, M. A. *Macromolecules* **2008**, *41*, 8815-8822.
- (63) Walther, A.; Muller, A. H. E. *Chem. Commun.* **2009**, *0*, 1127-1129.
- (64) Liu, C.; Hillmyer, M. A.; Lodge, T. P. *Langmuir* **2009**, *25*, 13718-13725.
- (65) Butsele, K. V.; Fustin, C. A.; Gohy, J. F.; Jérôme, R.; Jérôme, C. *Langmuir* **2008**, *25*, 107-111.
- (66) Zhang, Y.; Liu, H.; Hu, J.; Li, C.; Liu, S. *Macromol. Rapid Commun.* **2009**, *30*, 941-947.
- (67) Liu, H.; Li, C.; Liu, H.; Liu, S. *Langmuir* **2009**, *25*, 4724-4734.
- (68) Li, C.; Ge, Z.; Liu, H.; Liu, S. *J. Polym. Sci., Part A: Polym. Chem.* **2009**, *47*, 4001-4013.
- (69) Liu, C.; Hillmyer, M. A.; Lodge, T. P. *Langmuir* **2008**, *24*, 12001-12009.
- (70) Giebeler, E.; Stadler, R. *Macromol. Chem. Phys.* **1997**, *198*, 3815-3825.
- (71) Schacher, F.; Yuan, J.; Schoberth, H. G.; Müller, A. H. E. *Polymer* **2010**, *51*, 2021-2032.
- (72) Germack, D. S.; Wooley, K. L. *Macromol. Chem. Phys.* **2007**, *208*, 2481-2491.
- (73) du Sart, G. G.; Rachmawati, R.; Voet, V.; van Ekenstein, G. A.; Polushkin, E.; ten Brinke, G.; Loos, K. *Macromolecules* **2008**, *41*, 6393-6399.
- (74) Hadjichristidis, N.; Iatrou, H.; Pitsikalis, M.; Mays, J. *Prog. Polym. Sci.* **2006**, *31*, 1068-1132.
- (75) Khanna, K.; Varshney, S.; Kakkar, A. *Polym. Chem.* **2010**, *1*, 1171-1185.
- (76) Higashihara, T.; Hayashi, M.; Hirao, A. *Prog. Polym. Sci.* **2011**, *36*, 323-375.
- (77) Altintas, O.; Vogt, A. P.; Barner-Kowollik, C.; Tunca, U. *Polymer Chemistry* **2011**, *3*, 34-45.
- (78) Iatridi, Z.; Tsitsilianis, C. *Polymers* **2011**, *3*, 1911-1933.
- (79) Breiner, U.; Krappe, U.; Stadler, R. *Macromol. Rapid Commun.* **1996**, *17*, 567-575.
- (80) Suzuki, J.; Furuya, M.; Iinuma, M.; Takano, A.; Matsushita, Y. *J. Polymer Sci., Part B: Polym. Phys.* **2002**, *40*, 1135-1141.
- (81) Erhardt, R.; Zhang, M.; Böker, A.; Zettl, H.; Abetz, C.; Frederik, P.; Krausch, G.; Abetz, V.; Müller, A. H. E. *J. Am. Chem. Soc.* **2003**, *125*, 3260-3267.
- (82) Fukushima, S.; Miyata, K.; Nishiyama, N.; Kanayama, N.; Yamasaki, Y.; Kataoka, K. *J. Am. Chem. Soc.* **2005**, *127*, 2810-2811.
- (83) Sperschneider, A.; Schacher, F.; Gawenda, M.; Tsarkova, L.; Müller, A. H. E.; Ulbricht, M.; Krausch, G.; Köhler, J. *Small* **2007**, *3*, 1056-1063.
- (84) Docampo, P.; Stefik, M.; Guldin, S.; Gunning, R.; Yufa, N. A.; Cai, N.; Wang, P.; Steiner, U.; Wiesner, U.; Snaith, H. J. *Adv. Energy Mater.* **2012**, *2*, 676-682.
- (85) Roovers, J. E. L.; Bywater, S. *Macromolecules* **1972**, *5*, 384-388.
- (86) Pennisi, R. W.; Fetters, L. J. *Macromolecules* **1988**, *21*, 1094-1099.
- (87) Iatrou, H.; Hadjichristidis, N. *Macromolecules* **1992**, *25*, 4649-4651.

- (88) Iatrou, H.; Hadjichristidis, N. *Macromolecules* **1993**, *26*, 2479-2484.
- (89) Sioula, S.; Tselikas, Y.; Hadjichristidis, N. *Macromolecules* **1997**, *30*, 1518-1520.
- (90) Mavroudis, A.; Hadjichristidis, N. *Macromolecules* **2005**, *39*, 535-540.
- (91) Quirk, R. P.; Yoo, T.; Lee, Y.; Kim, J.; Lee, B. *Adv. Polym. Sci.* **2000**, *153*, 67-162.
- (92) Quirk, R. P.; Yoo, T.; Lee, B. *J. Macromol. Sci. Pure Appl. Chem.* **1994**, *A31*, 911-926.
- (93) Hückstädt, H.; Abetz, V.; Stadler, R. *Macromol. Rapid Commun.* **1996**, *17*, 599-606.
- (94) Hückstädt, H.; Göpfert, A.; Abetz, V. *Macromol. Chem. Phys.* **2000**, *201*, 296-307.
- (95) Quirk, R. P.; Kim, Y. J. *Polym. Prepr. Am. Chem. Soc. Div. Polym. Chem.* **1996**, *37*, 643-644.
- (96) Fujimoto, T.; Zhang, H.; Kazama, T.; Isono, Y.; Hasegawa, H.; Hashimoto, T. *Polymer* **1992**, *33*, 2208-2213.
- (97) Lambert, O.; Dumas, P.; Hurtrez, G.; Riess, G. *Macromol. Rapid Commun.* **1997**, *18*, 343-351.
- (98) Lambert, O.; Reutenauer, S.; Hurtrez, G.; Riess, G. r.; Dumas, P. *Polym. Bull.* **1998**, *40*, 143-149.
- (99) Abouelmagd, A.; Sugiyama, K.; Hirao, A. *Macromolecules* **2011**, *44*, 826-834.
- (100) Li, Z.; Hillmyer, M. A.; Lodge, T. P. *Macromolecules* **2004**, *37*, 8933-8940.
- (101) Tonhauser, C.; Obermeier, B.; Mangold, C.; Lowe, H.; Frey, H. *Chem. Commun.* **2011**, *47*, 8964-8966.
- (102) Tonhauser, C.; Golriz, A. A.; Moers, C.; Klein, R.; Butt, H.-J.; Frey, H. *Adv. Mater.* **2012**, *24*, 5559-5563.
- (103) Binder, W. H.; Sachsenhofer, R. *Macromol. Rapid Commun.* **2007**, *28*, 15-54.
- (104) Zhang, Y.; Li, C.; Liu, S. *J. Polym. Sci., Part A: Polym. Chem.* **2009**, *47*, 3066-3077.
- (105) Altintas, O.; Hizal, G.; Tunca, U. *J. Polym. Sci., Part A: Polym. Chem.* **2006**, *44*, 5699-5707.
- (106) Yuan, Y.-Y.; Wang, Y.-C.; Du, J.-Z.; Wang, J. *Macromolecules* **2008**, *41*, 8620-8625.
- (107) Khanna, K.; Varshney, S.; Kakkar, A. *Macromolecules* **2010**, *43*, 5688-5698.
- (108) Gordin, C.; Delaite, C.; Medlej, H.; Josien-Lefebvre, D.; Hariri, K.; Rusu, M. *Polym. Bull.* **2009**, *63*, 789-801.
- (109) Iskin, B.; Yilmaz, G.; Yagci, Y. *J. Polym. Sci., Part A: Polym. Chem.* **2011**, *49*, 2417-2422.
- (110) Durmaz, H.; Dag, A.; Tunca, U.; Hizal, G. *J. Polym. Sci., Part A: Polym. Chem.* **2012**, *50*, 2406-2414.
- (111) Gunay, U. S.; Durmaz, H.; Gungor, E.; Dag, A.; Hizal, G.; Tunca, U. *J. Polym. Sci., Part A: Polym. Chem.* **2011**, *50*, 729-735.
- (112) Huan, X.; Wang, D.; Dong, R.; Tu, C.; Zhu, B.; Yan, D.; Zhu, X. *Macromolecules* **2012**, *45*, 5941-5947.
- (113) Li, L.; Kan, X.-W.; Deng, X.-X.; Song, C.-C.; Du, F.-S.; Li, Z.-C. *J. Polym. Sci., Part A: Polym. Chem.* **2012**, 865-873.
- (114) Yang, L.; Zhou, H.; Shi, G.; Wang, Y.; Pan, C.-Y. *J. Polym. Sci., Part A: Polym. Chem.* **2008**, *46*, 6641-6653.
- (115) Ye, C.; Zhao, G.; Zhang, M.; Du, J.; Zhao, Y. *Macromolecules* **2012**, *45*, 7429-7439.
- (116) Gungor, E.; Durmaz, H.; Hizal, G.; Tunca, U. *J. Polym. Sci., Part A: Polym. Chem.* **2008**, *46*, 4459-4468.
- (117) Jia, Z.; Lonsdale, D. E.; Kulis, J.; Monteiro, M. J. *ACS Macro Lett.* **2012**, *1*, 780-783.
- (118) Higashihara, T.; Nagura, M.; Inoue, K.; Haraguchi, N.; Hirao, A. *Macromolecules* **2005**, *38*, 4577-4587.
- (119) Zhao, Y.; Higashihara, T.; Sugiyama, K.; Hirao, A. *J. Am. Chem. Soc.* **2005**, *127*, 14158-14159.
- (120) Hirao, A.; Higashihara, T.; Inoue, K. *Macromolecules* **2008**, *41*, 3579-3587.
- (121) Ito, S.; Goseki, R.; Senda, S.; Hirao, A. *Macromolecules* **2012**, *45*, 4997-5011.
- (122) Eschwey, H.; Burchard, W. *Polymer* **1975**, *16*, 180-184.
- (123) Tsitsilianis, C.; Chaumont, P.; Rempp, P. *Makromol. Chem.* **1990**, *191*, 2319-2328.
- (124) Tsitsilianis, C.; Lutz, P.; Graff, S.; Lamps, J. P.; Rempp, P. *Macromolecules* **1991**, *24*, 5897-5902.
- (125) Tsitsilianis, C.; Papanagopoulos, D.; Lutz, P. *Polymer* **1995**, *36*, 3745-3752.
- (126) Tsitsilianis, C.; Voulgaris, D. *Macromol. Chem. Phys.* **1997**, *198*, 997-1007.
- (127) Stavrouli, N.; Kyriazis, A.; Tsitsilianis, C. *Macromolecular Chemistry and Physics* **2008**, *209*, 2241-2247.
- (128) Krappe, U.; Stadler, R.; Voigt-Martin, I. *Macromolecules* **1995**, *28*, 4558-4561.
- (129) Breiner, U.; Krappe, U.; Thomas, E. L.; Stadler, R. *Macromolecules* **1998**, *31*, 135-141.
- (130) Brinkmann, S.; Stadler, R.; Thomas, E. L. *Macromolecules* **1998**, *31*, 6566-6572.
- (131) Ludwigs, S.; Böker, A.; Abetz, V.; Müller, A. H. E.; Krausch, G. *Polymer* **2003**, *44*, 6815-6823.
- (132) Matsushita, Y. *Macromolecules* **2007**, *40*, 771-776.
- (133) Matsushita, Y.; Hayashida, K.; Takano, A. *Macromol. Rapid Commun.* **2010**, *31*, 1579-1587.

- (134) Zhang, G.; Qiu, F.; Zhang, H.; Yang, Y.; Shi, A.-C. *Macromolecules* **2010**, *43*, 2981-2989.
- (135) Okamoto, S.; Hasegawa, H.; Hashimoto, T.; Fujimoto, T.; Zhang, H.; Kazama, T.; Takano, A.; Isono, Y. *Polymer* **1997**, *38*, 5275-5281.
- (136) Sioula, S.; Hadjichristidis, N.; Thomas, E. L. *Macromolecules* **1998**, *31*, 5272-5277.
- (137) Sioula, S.; Hadjichristidis, N.; Thomas, E. L. *Macromolecules* **1998**, *31*, 8429-8432.
- (138) Takano, A.; Wada, S.; Sato, S.; Araki, T.; Hirahara, K.; Kazama, T.; Kawahara, S.; Isono, Y.; Ohno, A.; Tanaka, N.; Matsushita, Y. *Macromolecules* **2004**, *37*, 9941-9946.
- (139) Takano, A.; Kawashima, W.; Noro, A.; Isono, Y.; Tanaka, N.; Dotera, T.; Matsushita, Y. *J. Polym. Sci., Part B: Polym. Phys.* **2005**, *43*, 2427-2432.
- (140) Hayashida, K.; Kawashima, W.; Takano, A.; Shinohara, Y.; Amemiya, Y.; Nozue, Y.; Matsushita, Y. *Macromolecules* **2006**, *39*, 4869-4872.
- (141) Hayashida, K.; Takano, A.; Arai, S.; Shinohara, Y.; Amemiya, Y.; Matsushita, Y. *Macromolecules* **2006**, *39*, 9402-9408.
- (142) Takano, A.; Kawashima, W.; Wada, S.; Hayashida, K.; Sato, S.; Kawahara, S.; Isono, Y.; Makihara, M.; Tanaka, N.; Kawaguchi, D.; Matsushita, Y. *J. Polym. Sci., Part B: Polym. Phys.* **2007**, *45*, 2277-2283.
- (143) Junnila, S.; Houbenov, N.; Hanski, S.; Iatrou, H.; Hirao, A.; Hadjichristidis, N.; Ikkala, O. *Macromolecules* **2010**, *43*, 9071-9076.
- (144) Abetz, V.; Jiang, S. *e-Polymers* **2004**, no. 054.
- (145) Shin, K.; Xiang, H.; Moon, S. I.; Kim, T.; McCarthy, T. J.; Russell, T. P. *Science* **2004**, *306*, 76.
- (146) Dobriyal, P.; Xiang, H.; Kazuyuki, M.; Chen, J.-T.; Jinnai, H.; Russell, T. P. *Macromolecules* **2009**, *42*, 9082-9088.
- (147) Wang, Y.; Qin, Y.; Berger, A.; Yau, E.; He, C.; Zhang, L.; Gösele, U.; Knez, M.; Steinhart, M. *Adv. Mater.* **2009**, *21*, 2763-2766.
- (148) Wang, Y.; Tong, L.; Steinhart, M. *ACS Nano* **2011**, *5*, 1928-1938.
- (149) Song, J.; Shi, T.; Chen, J.; An, L. *J. Phys. Chem. B* **2010**, *114*, 16318-16328.
- (150) Xu, Y.; Li, W.; Qiu, F.; Yang, Y.; Shi, A.-C. *J. Phys. Chem. B* **2009**, *113*, 11153-11159.
- (151) Walther, A.; Yuan, J.; Abetz, V.; Müller, A. H. E. *Nano Lett.* **2009**, *9*, 2026-2030.
- (152) Erhardt, R.; Böker, A.; Zettl, H.; Kaya, H.; Pyckhout-Hintzen, W.; Krausch, G.; Abetz, V.; Müller, A. H. E. *Macromolecules* **2001**, *34*, 1069-1075.
- (153) Wolf, A.; Walther, A.; Müller, A. H. E. *Macromolecules* **2011**, *44*, 9221-9229.
- (154) Lodge, T. P.; Rasdal, A.; Li, Z.; Hillmyer, M. A. *J. Am. Chem. Soc.* **2005**, *127*, 17608-17609.
- (155) Sharma, A.; Soliman, G. M.; Al-Hajaj, N.; Sharma, R.; Maysinger, D.; Kakkar, A. *Biomacromolecules* **2012**, *13*, 239-252.
- (156) Nederberg, F.; Appel, E.; Tan, J. P. K.; Kim, S. H.; Fukushima, K.; Sly, J.; Miller, R. D.; Waymouth, R. M.; Yang, Y. Y.; Hedrick, J. L. *Biomacromolecules* **2009**, *10*, 1460-1468.
- (157) Saito, N.; Liu, C.; Lodge, T. P.; Hillmyer, M. A. *ACS Nano* **2010**, *4*, 1907-1912.
- (158) Szwarc, M. *Nature* **1956**, *178*, 1168-1169.
- (159) Hadjichristidis, N.; Pitsikalis, M.; Pispas, S.; Iatrou, H. *Chem. Rev.* **2001**, *101*, 3747-3792.
- (160) Baskaran, D.; Müller, A. H. E., Anionic Vinyl Polymerization. In *Controlled and Living Polymerizations*, Müller, A. H. E.; Matyjaszewski, K., Eds. Wiley-VCH: Weinheim, 2009; pp 1-56.
- (161) Auschra, C.; Stadler, R. *Polym. Bull.* **1993**, *30*, 257-264.
- (162) Heitz, T.; Höcker, H. *Makromol. Chem.* **1988**, *189*, 777-789.
- (163) Quirk, R. P.; Lynch, T. *Macromolecules* **1993**, *26*, 1206-1212.
- (164) Quirk, R. P.; Zhu, L.-F. *Brit. Polym. J.* **1990**, *23*, 47-54.
- (165) Summers, G. J.; Quirk, R. P. *Polym. Int.* **1996**, *40*, 79-86.
- (166) Summers, G. J.; Quirk, R. P. *J. Polym. Sci., Part A: Polym. Chem.* **1998**, *36*, 1233-1241.
- (167) Quirk, R. P.; Perry, S.; Mendicuti, F.; Mattice, W. L. *Macromolecules* **1988**, *21*, 2294-2295.
- (168) Quirk, R. P.; Schock, L. E. *Macromolecules* **1991**, *24*, 1237-1241.
- (169) Hruska, Z.; Vuillemin, B.; Riess, G.; Katz, A.; Winnik, M. A. *Makromol. Chem.* **1992**, *193*, 1987-1994.
- (170) Hruska, Z.; Vuillemin, B.; Riess, G. *Polym. Bull.* **1994**, *32*, 163-167.
- (171) Cheng, C.; Yang, N.-L. *Macromolecules* **2010**, *43*, 3153-3155.
- (172) Helary, G.; Fontanille, M.; Khan, I. M.; Hogen-Esch, T. E. *Makromol. Chem.* **1989**, *190*, 341-348.
- (173) Kolb, H. C.; Finn, M. G.; Sharpless, K. B. *Angew. Chem., Int. Ed.* **2001**, *40*, 2004-2021.
- (174) Mansfeld, U.; Pietsch, C.; Hoogenboom, R.; Becer, C. R.; Schubert, U. S. *Polym. Chem.* **2010**, *1*, 1560-1598.

- (175) Goldmann, A. S.; Quémener, D.; Millard, P.-E.; Davis, T. P.; Stenzel, M. H.; Barner-Kowollik, C.; Müller, A. H. E. *Polymer* **2008**, *49*, 2274-2281.
- (176) Iha, R. K.; Wooley, K. L.; Nyström, A. M.; Burke, D. J.; Kade, M. J.; Hawker, C. J. *Chem. Rev.* **2009**, *109*, 5620-5686.
- (177) Altintas, O.; Vogt, A. P.; Barner-Kowollik, C.; Tunca, U. *Polym. Chem.* **2012**, *3*, 34-45.
- (178) Sumerlin, B. S.; Vogt, A. P. *Macromolecules* **2009**, *43*, 1-13.
- (179) Justynska, J.; Hordyjewicz, Z.; Schlaad, H. *Polymer* **2005**, *46*, 12057-12064.
- (180) Goldmann, A. S.; Walther, A.; Nebhani, L.; Joso, R.; Ernst, D.; Loos, K.; Barner-Kowollik, C.; Barner, L.; Müller, A. H. E. *Macromolecules* **2009**, *42*, 3707-3714.
- (181) Lowe, A. B.; Hoyle, C. E.; Bowman, C. N. *J. Mater. Chem.* **2010**, *20*, 4745-4750.
- (182) Inglis, A. J.; Stenzel, M. H.; Barner-Kowollik, C. *Macromol. Rapid Commun.* **2009**, *30*, 1792-1798.
- (183) Glassner, M.; Delaittre, G.; Kaupp, M.; Blinco, J. P.; Barner-Kowollik, C. *J. Am. Chem. Soc.* **2012**, *134*, 7274-7277.
- (184) Hansell, C. F.; O'Reilly, R. K. *ACS Macro Lett.* **2012**, *1*, 896-901.
- (185) Becer, C. R.; Babiuch, K.; Pilz, D.; Hornig, S.; Heinze, T.; Gottschaldt, M.; Schubert, U. S. *Macromolecules* **2009**, *42*, 2387-2394.
- (186) Fournier, D.; Hoogenboom, R.; Schubert, U. S. *Chem. Soc. Rev.* **2007**, *36*, 1369-1380.
- (187) Binder, W. H.; Sachsenhofer, R. *Macromol. Rapid Commun.* **2008**, *29*, 952-981.
- (188) Qin, A.; Lam, J. W. Y.; Tang, B. Z. *Macromolecules* **2010**, *43*, 8693-8702.
- (189) Robb, M. J.; Hawker, C. J., 'Click' Chemistry in Polymer Science: CuAAC and Thiol-Ene Coupling for the Synthesis and Functionalization of Macromolecules. In *Synthesis of Polymers: New Structures and Methods*, Schlüter, A. D.; Hawker, C. J.; Sakamoto, J., Eds. Wiley-VCH: Weinheim, 2012; Vol. 2, pp 923-971.
- (190) Rostovtsev, V. V.; Green, L. G.; Fokin, V. V.; Sharpless, K. B. *Angew. Chem., Int. Ed.* **2002**, *41*, 2596-2599.
- (191) Tornøe, C. W.; Christensen, C.; Meldal, M. *J. Org. Chem.* **2002**, *67*, 3057-3064.
- (192) Gao, H.; Matyjaszewski, K. *J. Am. Chem. Soc.* **2007**, *129*, 6633-6639.
- (193) Lian, X.; Wu, D.; Song, X.; Zhao, H. *Macromolecules* **2010**, *43*, 7434-7445.
- (194) Nasrullah, M. J.; Vora, A.; Webster, D. C. *Macromol. Chem. Phys.* **2011**, *212*, 539-549.
- (195) Reinicke, S.; Schmalz, H. *Colloid Polym. Sci.* **2011**, *289*, 497-512.
- (196) Mantovani, G.; Admiral, V.; Tao, L.; Haddleton, D. M. *Chem. Commun.* **2005**, *0*, 2089-2091.
- (197) Touris, A.; Mays, J. W.; Hadjichristidis, N. *Macromolecules* **2011**, *44*, 1886-1893.
- (198) Fleischmann, S.; Komber, H.; Appelhans, D.; Voit, B. I. *Macromol. Chem. Phys.* **2007**, *208*, 1050-1060.
- (199) Sumerlin, B. S.; Tsarevsky, N. V.; Louche, G.; Lee, R. Y.; Matyjaszewski, K. *Macromolecules* **2005**, *38*, 7540-7545.
- (200) Lang, A. S.; Neubig, A.; Sommer, M.; Thelakkat, M. *Macromolecules* **2010**, *43*, 7001-7010.
- (201) Pfeifer, S.; Lutz, J.-F. *Chemistry – Eur. J.* **2008**, *14*, 10949-10957.
- (202) Barner-Kowollik, C.; Du Prez, F. E.; Espeel, P.; Hawker, C. J.; Junkers, T.; Schlaad, H.; Van Camp, W. *Angew. Chem., Int. Ed.* **2011**, *50*, 60-62.



## 2 – Overview of the Thesis

This dissertation contains three publications, presented from chapter 3 to 5.

Novel miktoarm star terpolymers are the common issue connecting the three publications within this thesis. The main focus of the investigations is based on the synthesis of such materials on the one side and on the characterization of the micellar structures obtained by self-assembly of the polymers in solution on the other side. Therefore, a new approach for the synthesis of various ABC miktoarm star terpolymers was developed. Mid-alkyne functionalized diblock copolymers, which were synthesized by anionic polymerization utilizing 1,1-diphenylethylene (DPE) chemistry, form the key building blocks. These allowed modular ligation with azido-functionalized homopolymers *via* azide-alkyne Huisgen cycloaddition, which is presented in **Chapter 3**.

For a miktoarm star terpolymer containing a poly(2-vinylpyridine block) (P2VP) the mechanism of hierarchical superstructure formation was investigated. The polymer architecture, quaternization of P2VP and triiodide as counterion were found to be prerequisites for the directed self-assembly into complex “woodlouse”-shaped aggregates. The formation of cylindrical structures from spherical micelles, the meander-like arrangement of these cylinders and, finally, the fusion into lamellar aggregates of barrel-like shape was shown to be the underlying mechanism. **Chapter 4** includes the results of this counterion-mediated hierarchical superstructure formation.

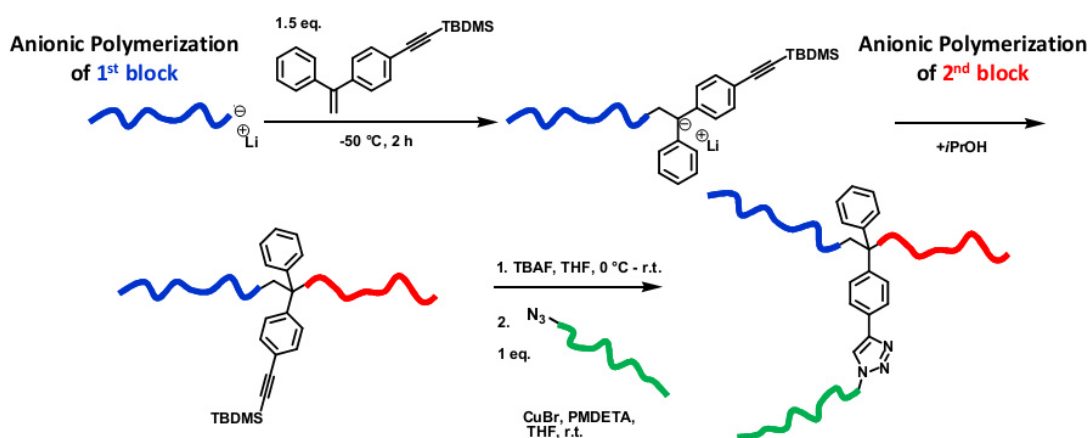
With the knowledge of the necessary parameters for such a directed self-assembly, this study was further expanded to other ABC miktoarm star terpolymers and an ABA' miktoarm star copolymer. Enabled by our modular approach the influence of molecular and chemical composition on the obtained superstructure was evaluated (**Chapter 5**). Herein, structures similar to the “woodlouse” aggregates were observed, however from a different mechanism starting with vesicles as primary building units instead of micelles.

Below, an overview over the most important results of each of the three following chapters is given. The reader is referred to the corresponding chapter for an extensive

discussion on the particular topic of synthesis and self-assembly of the miktoarm star terpolymers.

## 2.1 Modular Synthesis of Miktoarm Star Terpolymers

Besides routes relying exclusively on anionic polymerization, the synthesis of miktoarm star terpolymers is typically accomplished by a combination of different polymerization methods. Therefore, specially designed linking reactions in combination with precisely functionalized diblock copolymers and postfunctionalization/transformation reactions have to be conducted. In this chapter we present a more generalized method, which can be applied to a broad variety of (functional) monomers. The synthetic steps involve sequential anionic polymerization of alkyne mid-functionalized diblock copolymers and subsequent ligation with azido-functionalized diblock copolymers (Scheme 2-1).



**Scheme 2-1.** Synthetic route for ABC miktoarm star terpolymers by the combination of anionic polymerization in THF with DPE chemistry and click chemistry.

For the preparation of the alkyne mid-functionalized diblock copolymer we utilized DPE chemistry, as it allows exact incorporation of exactly one DPE unit at the block border under appropriate choice of monomer sequence. For this purpose, we synthesized a novel DPE derivative carrying a protected alkyne-function (click-DPE, 1-[(4-(*tert*-butyldimethylsilyl)-ethynyl)phenyl]-1-phenylethylene). Due to the conjugation of the  $\pi$ -system with the alkyne-function in *para*-position the corresponding living anion exhibits a bathochromic shift in the UV-spectrum as compared to unsubstituted DPE (Figure 2-1A).

As a consequence of this altered electronic configuration click-DPE was shown to copolymerize with living anions of poly(2-vinylpyridine) (P2VP) by MALDI-ToF MS investigation of an appropriate test reaction (Figure 2-1B), in contrast to other DPE derivatives reported in literature. Hence, the living anion of click-DPE can principally both be used to start the anionic polymerization 2-vinylpyridine (2VP) and for endfunctionalization of living anions of P2VP.

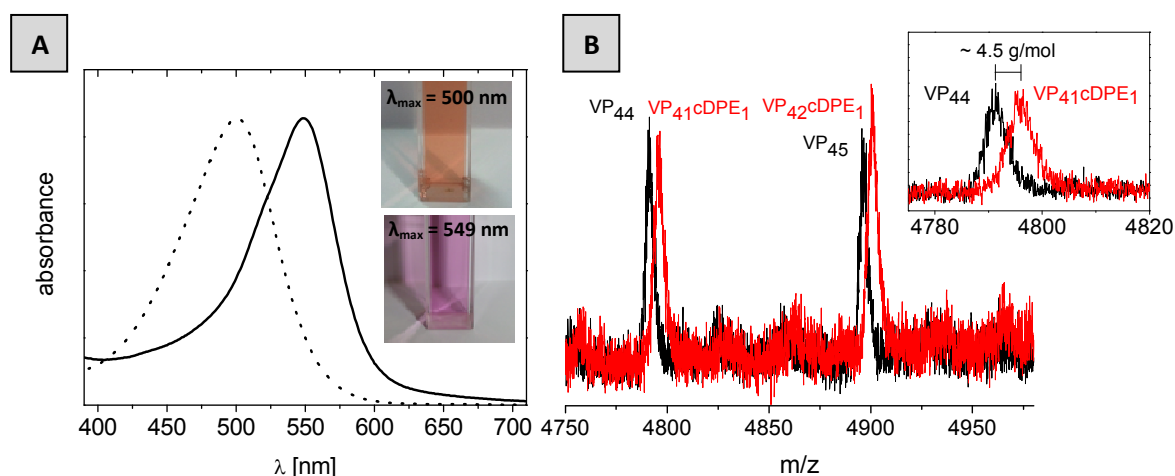


**Figure 2-1.** (A) UV-vis absorption spectrum of the adduct of 1,1-diphenylethylene (dotted line) and 1-[(4-(*tert*-butyldimethylsilyl)ethynyl)phenyl]-1-phenylethylene (solid line) with *sec*-BuLi in THF. The inset shows the picture of the cuvette containing the living anion of the unsubstituted DPE (top) and the click-DPE (bottom). (B) MALDI-ToF MS spectra of poly(2-vinylpyridine) before (black line) and after addition of click-DPE (cDPE, red line), recorded in reflectron mode (B) with AgTFA as ionization agent.

Here, we prepared different alkyne mid-functionalized diblock copolymers with polybutadiene as first block and poly(2-vinylpyridine), poly(*tert*-butyl methacrylate) (PtBMA), or poly(*N,N*-dimethylaminoethyl methacrylate) (PDMAEMA) as second block. Except hydrolysis no further transformation reactions are necessary to generate the alkyne-function. We determined the degree of alkyne-functionalization by a test click reaction with an azido-functional perylene bisimide as chromophore in combination with UV measurements. For the diblock copolymers with P2VP as second block only a slight over-incorporation of the click-DPE could be achieved under appropriate reaction conditions (~120% alkyne-functionalization). This is due to the addition of a second DPE unit for some chains. In contrast, for PtBMA as second block near-quantitative functionalization was proven (~93% alkyne functionalization).

By a modular combination of these mid-functional diblock copolymers with azido-functionalized homopolymers we synthesized different novel ABC miktoarm star terpolymers *via* copper-catalyzed azide-alkyne Huisgen cycloaddition. For the example of a PB-*b*-PtBMA diblock copolymer (cBT2) the miktoarm star terpolymers obtained after click reaction with azido-functional polystyrene (PS), poly(ethylene oxide) (PEO) and PDMAEMA homopolymers are listed in Table 2-1. The corresponding SEC eluograms are depicted in Figure 2-2. In all cases narrowly distributed miktoarm star terpolymers were obtained. We further showed for click-reactions with PEO and PDMAEMA homopolymers that a reaction pathway with an excess of the homopolymer was possible and monomodal miktoarm star terpolymers were achieved after appropriate purification procedures, like *e.g.* dialysis (Figure 2-2B).

**Table 2-1. Molecular Characterization of ABC Miktoarm Star Terpolymers Obtained from Click Reactions with Alkyne Mid-Functionalized PB<sub>111</sub>-*b*-PtBMA<sub>42</sub> Diblock Copolymer cBT2 (Subscripts Denote the Corresponding Degrees of Polymerization)**

sample ID <sup>a</sup>	DP(3 <sup>rd</sup> block) <sup>b</sup>	$M_{n,th.}$ <sup>c</sup> [kg/mol]	$M_{n,app}$ <sup>d</sup> [kg/mol]	$\bar{D}$ <sup>d</sup>
$\mu$ -BT2S1, ( $\mu$ -B <sub>38</sub> T <sub>38</sub> S <sub>23</sub> <sup>15.9</sup> )	36	15.9	20.5	1.03
$\mu$ -BT2S2, ( $\mu$ -B <sub>33</sub> T <sub>33</sub> S <sub>33</sub> <sup>18.1</sup> )	57	18.1	22.4	1.03
$\mu$ -BT2E, ( $\mu$ -B <sub>32</sub> T <sub>32</sub> E <sub>35</sub> <sup>18.8</sup> )	150	18.8	25.4	1.03
$\mu$ -BT2D, ( $\mu$ -B <sub>34</sub> T <sub>34</sub> D <sub>31</sub> <sup>17.6</sup> )	34	17.6	20.8	1.11

<sup>a</sup>The superscript denotes the theoretical number average molecular weight of the ABC miktoarm star terpolymer, as calculated from the respective values of the diblock copolymer and homopolymer and the indices the theoretical weight fraction of the respective blocks. <sup>b</sup>Calculated from the molecular weight of the 3<sup>rd</sup> block. <sup>c</sup>Theoretical molecular weight. <sup>d</sup>Apparent molecular weight and dispersity determined by SEC with polystyrene calibration. For the miktoarm star terpolymers containing PDMAEMA THF-SEC with additional 0.25 wt% tetrabutylammonium bromide (TBAB) was used.

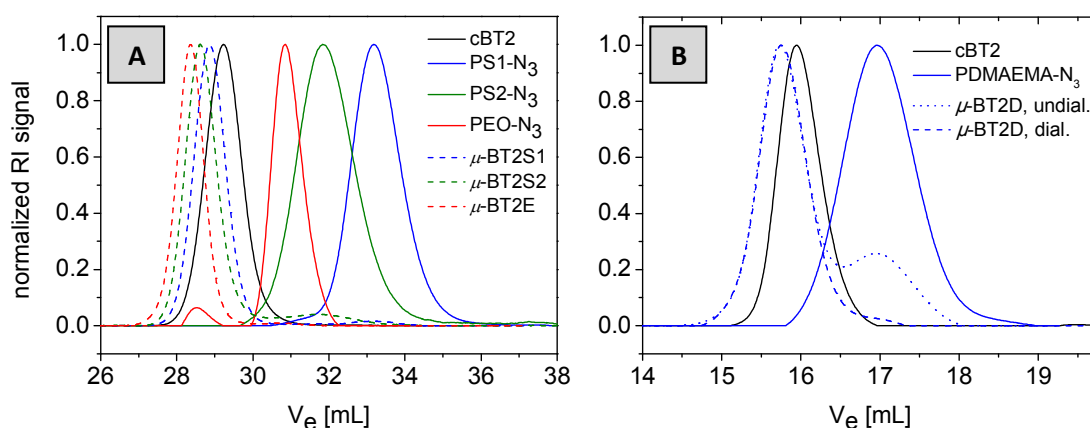


**Figure 2-2.** SEC traces of miktoarm star terpolymers from click reactions of a polybutadiene-*block*-poly(*tert*-butyl methacrylate) diblock copolymer (cBT2) with (A) two polystyrene homopolymers (PS1-N<sub>3</sub>, PS2-N<sub>3</sub>) and a poly(ethylene oxide) homopolymer (PEO-N<sub>3</sub>) and (B) a poly(*N,N*-dimethylaminoethyl methacrylate) homopolymer (PDMAEMA-N<sub>3</sub>). For (B) THF-SEC with additional salt was used and as the click reaction was conducted with 2 equiv of the PDMAEMA-N<sub>3</sub>, excess homopolymer was removed *via* dialysis.

With this modular approach a variety of functional miktoarm star terpolymers are accessible. Furthermore, click-DPE offers novel synthetic advantages in the construction of polymeric architectures *via* a combination of anionic polymerization and click-chemistry. The miktoarm star terpolymers synthesized herein all carry a polybutadiene block, which can be used for further modification and functionalization *via* thiol-ene chemistry. Moreover new amphiphilic miktoarm star terpolymers were synthesized, which carry hydrophilic (PEO, PDMAEMA) and stimuli-responsive arms (PDMAEMA, PtBMA after hydrolysis).

## 2.2 Counterion-Mediated Hierarchical Self-Assembly of an ABC Miktoarm Star Terpolymer Containing a Poly(*N*-methyl-2-vinylpyridinium iodide) Segment

For a miktoarm star terpolymer containing a polybutadiene, poly(*tert*-butyl methacrylate) and poly(2-vinylpyridine) segment ( $\mu$ -BVT), quaternization with methyl iodide and transfer into aqueous solution was observed to yield two structurally completely differing limiting cases of aggregation forms: spherical micelles ( $d_{\text{micelle}} = 24.5 \pm 2.0$  nm) and particles with a complex lamellar interior (200-500 nm in longitudinal axis). The concentration of triiodide as polarizable counterion for the quaternized P2VP

phase (P2VPq) was identified to be responsible for the formation of superstructures with lamellar compartmentalization, termed “woodlouse” aggregates. The triiodide ions are generated by the reaction of iodide as initial counterion from the quaternization with methyl iodide, together with elemental iodine as photodecomposition product of the quaternization agent. Increasing triiodide concentration leads to decreasing hydrophilicity of the P2VPq phase and induces aggregation thereof. Furthermore, subsequent addition of iodine is capable of triggering the superstructure formation into the next level of hierarchy. In this manner, by variation of the amount of triiodide a step-wise increase in hierarchy is the underlying mechanism for the formation of supramolecular self-assemblies, starting with spherical micelles (level 1, Figure 2-3A) as initial building blocks into cylindrical micelles (level 2) and their aggregates (Figure 2-3B), highly intertwined superstructures thereof (Figure 2-3C) and, finally, into up to 1  $\mu\text{m}$  long particles with a highly periodic lamellar fine-structure (“woodlouse” aggregates, Figure 2-3D).

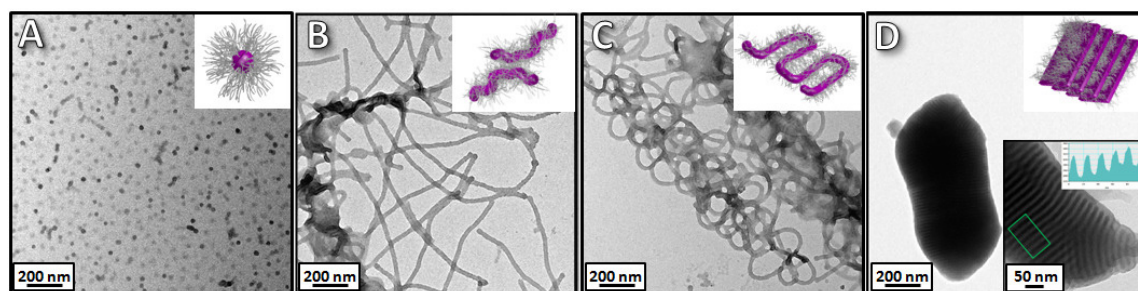


**Figure 2-3.** TEM micrographs from 0.2 g/L aqueous micellar solution of  $\mu$ -BVqT after dialysis in the presence of different amounts of iodine. The solutions were prepared without (A), and with 0.08 (B), 0.25 (C) or 0.42 (D) equiv of supplementary iodine with respect to P2VPq monomer units. The schematic illustrations represent the dominant aggregate morphology.

All different structures and intermediate stages were thoroughly investigated by a combination of scanning and (cryogenic) transmission electron microscopy (SEM, TEM) and further supported by small-angle X-ray scattering (SAXS) measurement. Apart from this mechanistic study the bulk morphology of the perfect “woodlouse” structure was systematically analyzed *via* electron microscopy, including cryo-TEM tilt angle-series and TEM tomography of thin-film cuts of resin-embedded samples. Figure 2-4 gives an overview of some of the results. The “woodlouse” aggregates clearly consist of a lamellar structure throughout the whole particle. The one type of lamella is composed of

a partially mixed PB/PtBMA phase whereas the other lamella is formed by a swollen P2VPq phase, which keeps the aggregate together due to its decreased hydrophilicity, as mediated by the counterion. The undulated shape of the PB/PtBMA lamellae is hereby attributed to preferential formation of a PtBMA/P2VPq interface, which induces partial demixing. All these results give a detailed, even though basic, understanding on the directed self-assembly of the  $\mu$ -BVqT miktoarm star terpolymer and the obtained complex “woodlouse” structures.

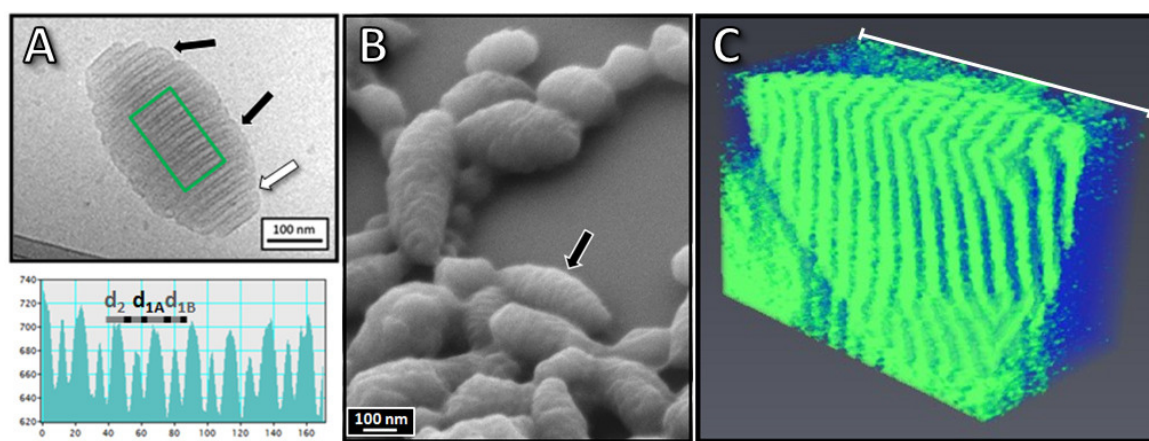


**Figure 2-4.** Cryo-TEM (A) and REM images (B) of “woodlouse” aggregates. For cryo-TEM the concentration was 0.6 g/L and the regular pattern originates from the P2VPq phase ( $d_{1A} + d_{1B}$ ) PB/PtBMA phase ( $d_2$ ). The black arrows in (A) highlight an area where the lamellae are bent, whereas the white arrow shows stacked lamellae. The concentration for REM was 0.02g/L and a regular corrugated surface of the compact particles is visible (black arrow in (B)). In (C) the TEM tomography 3D reconstruction of a slice of the “woodlouse” structure with view into the lamellar morphology is depicted. The tomography image was obtained from a 150 nm thick cut of the freeze-dried and resin-embedded particles. OsO<sub>4</sub> staining (PB phase) was performed and the approximate length of the white marked edge is 290 nm.

### 2.3 Application of the Triiodide-Directed Self-Assembly to other ABC and ABA’ Miktoarm Star Polymers with a Poly(*N*-methyl-2-vinylpyridinium iodide) Segment

Based on the results summarized in chapter 2.2 two other miktoarm star terpolymer systems consisting of different monomer units were subjected to the same triiodide directed self-assembly process. For the first system, composed of arms of polybutadiene, poly(2-vinylpyridine) and polystyrene, different molecular compositions and therefore different amphiphilicities were used to investigate their influence on the

obtained structures. For the structures obtained by dialysis of the quaternized polymers from dioxane to water without added iodide spherical micelles, oligomeric structures of spherical micelles and vesicles were obtained with decreasing length of the P2VPq block. These results are consistent with the theory for diblock copolymers where decreasing the length of the solvophilic block leads to a transition of the micellar morphology from spherical micelles to cylindrical micelles and, finally, vesicles. However, the addition of iodine before dialysis to water decreased the solubility of the corona and induced superstructure formation. Whereas for the two samples with the longest hydrophilic block ( $w_{\text{hydrophilic}} = 0.60$  and  $0.46$ ) similar to  $\mu$ -BqVT an aggregation of micelles into lamellar superstructures occurred, the sample with the shortest hydrophilic block  $\mu$ -BV3qS ( $w_{\text{hydrophilic}} = 0.23$ ) yielded multilamellar vesicles (Figure 2-5). In the latter case the fusion of the vesicles was visualized by cryo-TEM (inset in Figure 2-5AC) and the vesicular primary structure was retained during hierarchical superstructure formation.

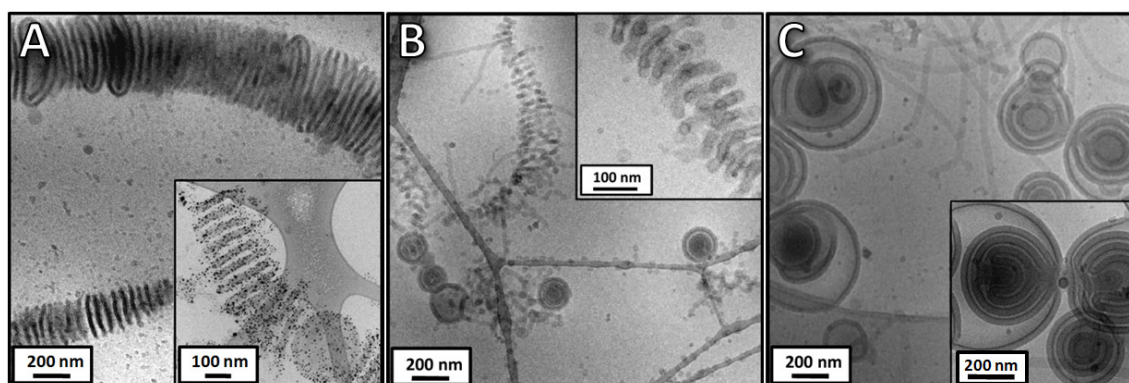


**Figure 2-5.** Cryo-TEM micrographs of micellar aggregates obtained from  $\mu$ -BVq1S,  $\mu$ -BVq2S and  $\mu$ -BVq3S miktoarm star terpolymers with 0.25 equiv  $I_2$  (with respect to P2VPq units) to water. The inset in (A) shows a sample, where Au nanoparticles were generated within the P2VPq corona. The concentration was approximately 0.35 g/L.

Despite the high values for the incompatibility parameter,  $\chi_{SB}N$ , and the presence of the glass transition of the PB phase in DSC measurements, no phase segregation between the PS and PB blocks could be visualized in TEM images of  $\mu$ -BVq3S with selective staining of the PB phase. This is most probably attributed to the differences in the interfacial energy of PS/P2VP and PB/P2VP. Despite the miktoarm architecture a lamellar structure of the vesicle walls with the PB phase in the centre and a thin PS phase close to the surface, surrounded by a P2VPq corona. Additionally, nanohybrids

were formed by the generation of gold nanoparticles within the P2VPq corona (inset in Figure 2-5A).

For the second system the low- $T_g$  PB block was substituted with a glassy PS block with different length than the first PS arm, yielding  $\mu$ -SVS'. After quaternization and dialysis to water again mainly vesicles were observed as primary building units (Figure 2-6A). Upon drying, it was demonstrated that these vesicles with a robust wall completely collapse into “kippah”-like structures, due to minute amounts of triiodide, which induce coronal attraction to a distinct degree (inset in Figure 2-6A). However, if the polymer was dialyzed with medium amounts of iodine (0.08 equiv regarding P2VPq units) – in contrast to  $\mu$ -BV3qS with an elastic PB segment – aggregation of vesicles instead of fusion into multilamellar vesicles was observed. Additionally, nascent bilayer sheets as pre-stages of vesicles were visualized (Figure 2-6B). In case of dialysis with higher amounts of iodine ( $\geq 0.15$  equiv) anisotropic aggregation of deformed vesicles with partial rearrangement was observed, which yielded “woodlouse” structures similar to  $\mu$ -BVqT (Figure 2-6C). However, these evolved *via* a complete different mechanism from vesicular building units. SAXS of the freeze-dried samples supported the presence of an internal lamellar structure with a periodicity of  $d_{\text{lam}} = 16.5 \pm 1.0$  nm (Figure 2-6D). The whole process was monitored by dynamic light scattering (DLS) as depicted in Figure 2-6E.

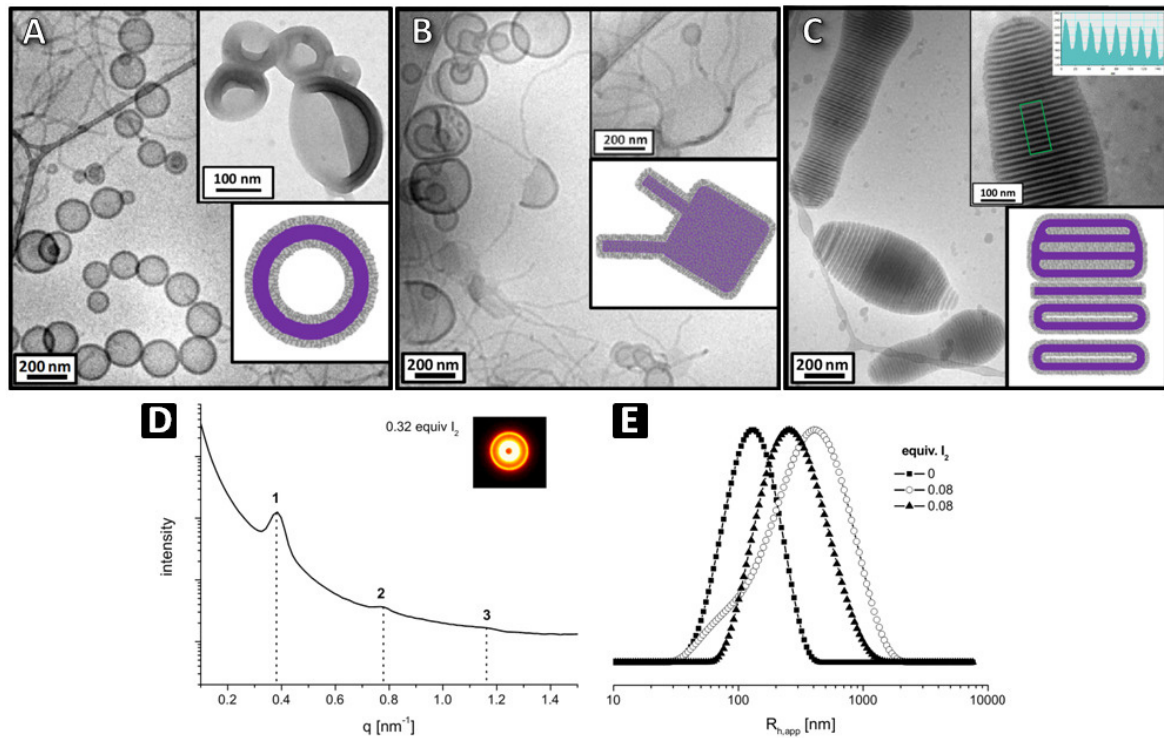


**Figure 2-6.** Cryo-TEM micrographs of micellar aggregates obtained from  $\mu$ -SVq1S' miktoarm star copolymer with 0 (A), 0.08 (B) and 0.25 equiv  $I_2$  (C) with respect to P2VPq units to water. The upper inset in (A) shows a TEM image of the dried sample, where the vesicles collapse into the "kippah" structure. The lower insets represent schematic illustrations of the main aggregation forms. The concentrations were  $\sim 0.4$  g/L. In (D) the SAXS pattern of the freeze-dried sample from (C) is shown and in (E) the DLS Contin plots of the respective solutions.

## 2.4 Individual Contributions to Joint Publications

The results presented in this dissertation were obtained in collaboration with others, and have been published or submitted to publication as indicated below. The contributions of all these co-authors to the different publications are stated below. The asterisk denotes the corresponding author.

### Chapter 3

This work is published in *Macromolecules* **2012**, *45*, 8300-8309 under the title:

**“A Modular Route for the Synthesis of ABC Miktoarm Star Terpolymers via a New Alkyne-Substituted Diphenylethylene Derivative”**

*by Andreas Hanisch, Holger Schmalz, and Axel H. E. Müller\**

I wrote the publication and conducted the experiments.

Holger Schmalz and Axel H. E. Müller were involved in scientific discussions and correction of the manuscript.

### Chapter 4

This work is published in *ACS Nano* **2013**, *7*, 4030-4041 under the title:

**“Counterion-Mediated Hierarchical Self-Assembly of an ABC Miktoarm Star Terpolymer”**

*by Andreas Hanisch, André H. Gröschel, Melanie Förtsch, Markus Drechsler, Hiroshi Jinnai, Thomas M. Ruhland, Felix H. Schacher,\* and Axel H. E. Müller\**

I wrote the publication and conducted most of the experiments.

Exceptions are stated below:

- Andre H. Gröschel recorded some of the TEM micrographs and was involved in discussions and in correction of the manuscript.
- Melanie Förtsch performed the majority of the TEM and cryo-TEM measurements.
- Markus Drechsler helped with the cryo-TEM tilt image series.
- Thomas M. Ruhland recorded the SEM images.
- Felix H. Schacher performed the TEM tomography measurements at the chair of Prof. Hiroshi Jinnai.

- Felix H. Schacher, Hiroshi Jinnai and Axel H. E. Müller were involved in scientific discussions and correction of the manuscript.

## Chapter 5

This work is published in *Polymer* **2013**, *54*, 4528-4537 under the title:

### **“Hierarchical Self-Assembly of Miktoarm Star Polymers Containing a Polycationic Segment: A General Concept”**

*by Andreas Hanisch, André H. Gröschel, Melanie Förtsch, Tina I. Löbling, Felix H. Schacher,\* and Axel H. E. Müller\**

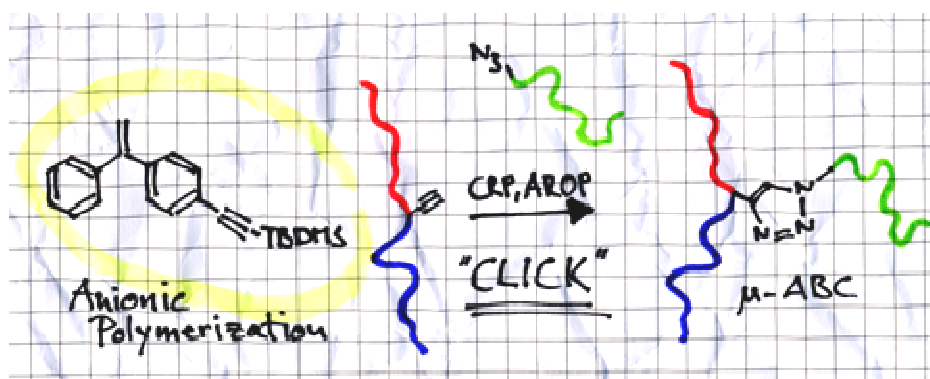
I wrote the publication and conducted most of the experiments.

Exceptions are stated below:

- André H. Gröschel was involved in scientific discussions.
- Melanie Förtsch performed almost all TEM and cryo-TEM measurements.
- Tina I. Löbling recorded some of the TEM micrographs.
- Felix H. Schacher and Axel H. E. Müller were involved in scientific discussions and correction of the manuscript.

### 3 – A Modular Route for the Synthesis of ABC Miktoarm Star Terpolymers via a New Alkyne-Substituted Diphenylethylene Derivative

Andreas Hanisch, Holger Schmalz, and Axel H. E. Müller



**ABSTRACT:** We introduce a modular route for the synthesis of well-defined ABC miktoarm star terpolymers. To this aim, the synthesis of a 1,1-diphenylethylene derivative bearing a protected alkyne function (1-[(4-(*tert*-butyldimethylsilyl)ethynyl)phenyl]-1-phenylethylene) was developed. This compound was for the first time employed in sequential anionic polymerization to readily prepare alkyne mid-functionalized diblock copolymers with polybutadiene as first and a poly(alkyl methacrylate) (poly(*tert*-butyl methacrylate), poly(*N,N*-dimethylaminoethyl methacrylate)) as second block. For the third arm controlled radical polymerization methods (polystyrene, poly(*tert*-butyl methacrylate), poly(*N,N*-dimethylaminoethyl methacrylate)) and anionic ring-opening polymerization (poly(ethylene oxide)) were used to separately prepare homopolymers with an azido function. Afterward, azide-alkyne Huisgen cycloaddition was successfully employed to synthesize a library of ABC miktoarm star terpolymers with different molecular weights and chemical compositions *via* modular combination of the functionalized diblock copolymers and homopolymers. The resulting new ABC miktoarm star terpolymers showed narrow, monomodal molecular weight distributions with dispersities typically below 1.10, as determined by size exclusion chromatography.

### 3.1 Introduction

Polymer architecture and composition is a decisive factor for controlling structure formation both in bulk and in solution. Besides the choice of monomer and the number and sequence of polymeric building blocks the way of molecular conjunction of these blocks is of outermost importance. Compared to their linear analogues, miktoarm star terpolymers, where the polymer chains are connected at one common junction point,<sup>1</sup> present a much more complex system. A variety of unique bulk morphologies were found,<sup>2-4</sup> which are inaccessible by linear triblock terpolymers. This is a direct consequence of the confined geometry of the polymer chains, which forces the common junction points of the three different blocks to be aligned in a 1-dimensional fashion. These miktoarm star terpolymer morphologies were also utilized for generating cylindrical, compartmentalized particles by selective crosslinking of one block.<sup>5</sup> In addition, theoretical studies suggest that even more complex morphologies are expected under cylindrical confinement of ABC miktoarm star terpolymers.<sup>6</sup> Depending on the length ratio of the respective arms, Hillmyer, Lodge and co-workers<sup>7,8</sup> obtained different multicompartiment structures in aqueous solution from ABC miktoarm star terpolymers with a fluorinated segment. These ranged from hamburger micelles to segmented wormlike micelles and nanostructured vesicles.

The conjunction of three chains at one common linking point leads to special requirements concerning the synthetic strategy. The main difficulties are (1) the exact functionalization of a diblock copolymer with a functional group or polymer block at the junction of the two blocks and (2) the stoichiometry of the linking reaction. Four different synthetic strategies have been reported so far for miktoarm star terpolymers.

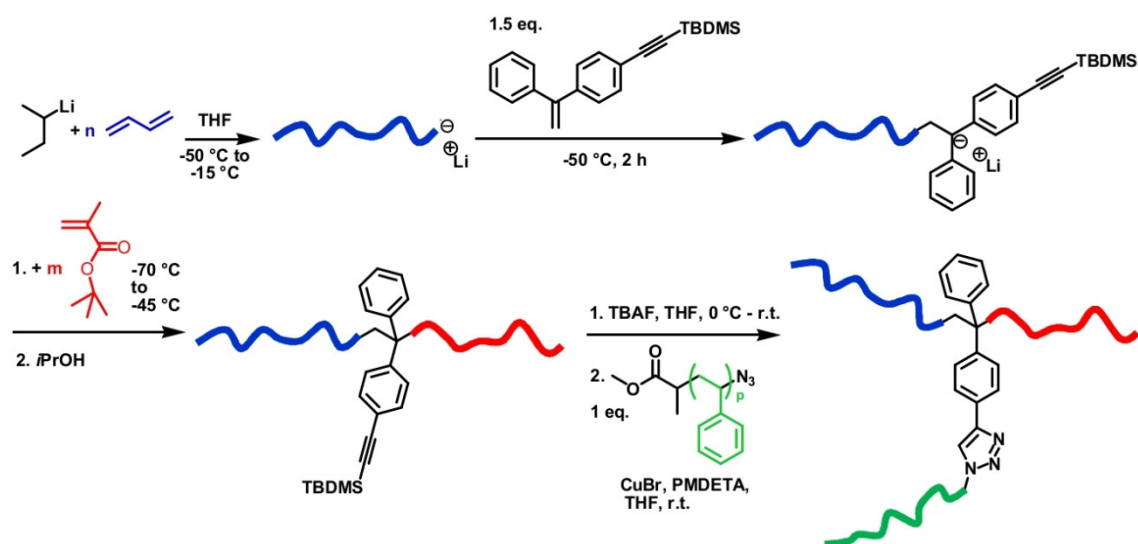
One approach uses the different reactivity of living anionic polymer chains toward the chlorine-silicon groups of trichlorosilanes. Using methyltrichlorosilane as linking agent, Hadjichristidis and coworkers synthesized a miktoarm star terpolymer consisting of polyisoprene, polystyrene, and polybutadiene.<sup>9</sup> However, the sequence of introduction of arms is strongly limited to the reactivity and steric demand of the polymeric anions, and adaption to other monomers requires a modification of the method.<sup>10,11</sup> The second anionic approach utilizes macromonomers with nonhomopolymerizable endgroups

which were directly sequentially copolymerized with two sorts of monomers.<sup>2,12-14</sup> In another approach, first diblock copolymers were synthesized carrying functional groups at the junction point of the two blocks. Again, nonhomopolymerizable compounds or special polymerization strategies have to be employed to assure that only one functional group is located exactly in between the two polymeric building blocks. Up to now, mainly hydroxyl-functions were used to conjugate the third block, which were introduced *via* a 1,1-diphenylethylene (DPE) derivative<sup>15,16</sup> or 2-methoxymethyloxymethyloxirane<sup>17-19</sup> as end-capping molecule. This hydroxyl function serves as anchoring point for the third block, which can be “grafted from” by anionic ring opening polymerization (AROP)<sup>15-17</sup> or controlled radical polymerization (CRP) after appropriate modification<sup>19</sup> or “grafted to” *via* direct esterification.<sup>18</sup> Hirao and co-workers recently used in-chain-benzyl bromide-functionalized diblock copolymers for the miktoarm star terpolymer synthesis involving specially designed anionic linking reactions.<sup>20</sup>

The possibility of constructing complex polymeric architectures with controlled radical polymerization methods increased within the last decade.<sup>21,22</sup> This supported the development of new strategies for the synthesis of ABC miktoarm star terpolymers where anionic polymerization is not involved. In addition, click reactions in general, or copper(I)-catalyzed azide-alkyne cycloaddition (CuAAC) in particular have become powerful tools for highly efficient linking of polymeric building blocks.<sup>23-25</sup> These novel synthetic routes take advantage of the orthogonality of the different polymerization/ligation methods, which is a prerequisite for the synthesis of well-defined ABC miktoarm star terpolymers. By designing special core molecules with three different functionalities, the arms can be “grafted onto” or “grafted from” in different steps.<sup>26-31</sup>

Herein, we present a more general method by combining anionic polymerization, employed for the synthesis of readily alkyne mid-functionalized diblock copolymers, with other polymerization techniques *via* azide-alkyne Huisgen cycloaddition (Scheme 3-1). Barner-Kowollik and co-workers already reported the ligation of alkyne mid-functionalized homopolymers with azide-bearing homopolymers.<sup>32</sup> However, only A<sub>2</sub>B miktoarm star terpolymers were accessible. The synthesis of an alkyne mid-functionalized diblock copolymer consisting of polystyrene and poly(*tert*-butyl acrylate) was also reported.<sup>33,34</sup> Nevertheless, multiple polymer analogous reactions had to be

conducted and/or switching the polymerization system was necessary. Thus, we synthesized 1-[(4-(*tert*-butyldimethylsilyl)ethynyl)phenyl]-1-phenylethylene to directly prepare mid-chain alkyne-substituted diblock copolymers *via* sequential anionic polymerization. Because of the direct introduction of the alkyne-group into the diblock copolymer by the use of DPE chemistry, a wide variety of functional diblock copolymers are accessible, and except hydrolysis no tedious transformation reactions have to be conducted. The obtained diblock copolymers were afterward ligated with different azide-bearing homopolymers prepared by atom transfer radical polymerization (ATRP), reversible addition-fragmentation chain transfer (RAFT) polymerization, and anionic ring opening polymerization *via* azide-alkyne click chemistry. Different novel ABC miktoarm star terpolymers were synthesized utilizing this modular combination.



**Scheme 3-1.** Synthetic route for the synthesis of ABC miktoarm star terpolymers for the example of a star consisting of arms of polybutadiene, poly(*tert*-butyl methacrylate), and polystyrene

### 3.2 Experimental Section

**Materials.** For the purification of monomers, reagents and solvent and the synthesis of used compounds see the Supporting Information.

**Synthesis of 1-[(4-(*tert*-Butyldimethylsilyl)ethynyl)phenyl]-1-phenylethylene (Click-DPE).** The starting molecule 1-(4-bromophenyl)-1-phenylethylene was synthesized as described elsewhere.<sup>35</sup> The synthetic protocol for the coupling reaction with the protected alkyne derivative was adopted from the literature.<sup>36</sup> First, 1-(4-bromophenyl)-1-phenylethylene was dissolved in piperidine (~50 mg/mL) and bis(triphenylphosphine)palladium(II) dichloride (0.03 equiv) and CuI (0.004 equiv) were added under a nitrogen atmosphere. After degassing with nitrogen for 30 minutes, *tert*-butyldimethylsilylacetylene (1.2 equiv) was added dropwise at 50 °C, and the solution was stirred overnight. The reaction mixture was filtered, the solvent evaporated, and the crude product was dissolved in THF. After addition of water, the product was extracted with hexane for three times. The organic fractions were dried over sodium sulfate, and the solvent was evaporated to obtain a brown oil. This was further purified by column chromatography with hexane as solvent to obtain a clear oil. Distillation of the product was not possible even under high vacuum conditions. Before the use in anionic polymerization, the compound was freeze-dried from benzene solution on a high vacuum line and subsequently dissolved in dry THF to obtain a stock solution of low viscosity. *sec*-BuLi was added dropwise (typically 1-2 drops) under nitrogen flow until a deeply violet color was obtained. Besides proving the absence of impurities, the persistent color also served as indication for the purity of the stock solution. <sup>1</sup>H NMR (300 MHz, CDCl<sub>3</sub>):  $\delta$  = 7.50-7.27 (m, 9H, Ar), 5.50 (s, 2H, -C=CH<sub>2</sub>), 1.03 (s, 9H, SiC(CH<sub>3</sub>)<sub>3</sub>), 0.22 (s, 6H, SiCH<sub>3</sub>)

**Polymerizations.** *Sequential Living Anionic Polymerization in THF.* All polymerizations were carried out at low temperatures in a thermostated laboratory autoclave (Büchi) under dry nitrogen atmosphere using THF as solvent. The day before polymerization, freshly distilled THF (~250 mL for 15 g of polymer) was treated with 1 mL of *sec*-BuLi per 100 mL of solvent at -20 °C, followed by stirring overnight to form lithium alkoxides. These exhibit stabilizing effects on the living chain end of polybutadiene and furthermore in the case of methacrylate-type monomers no addition of LiCl is necessary to ob-

tain well-defined polymers.<sup>37</sup> For the diblock copolymers, first butadiene was initiated with *sec*-BuLi at -70 °C and then polymerized at -50 to -15 °C depending on the block length of the different polymerizations. To ensure complete consumption of the butadiene the polymerization was followed by in-line NIR fiber-optic spectroscopy. The living polybutadienyl anion was end-capped with 1-[(4-(*tert*-butyldimethylsilyl)ethynyl)phenyl]-1-phenylethylene (1.1-1.5 equiv) at -50 °C for 2 h. Before and after the addition of the click-DPE samples for SEC and MALDI-ToF MS were withdrawn. In the case of poly(2-vinylpyridine) (P2VP) as second block the monomer was added at -70 °C and polymerized for 5 minutes. After termination with degassed methanol the polymer (cBV) was isolated by precipitation in water. For the diblock copolymers with *tert*-butyl methacrylate (*t*BMA) the monomer addition was conducted at -70 °C and the polymerization took place at -45 °C for 1 h before it was terminated with degassed methanol. After the addition of the *t*BMA the violet color of the DPE end-capped living anion slowly faded away. The final polymer (cBT) was precipitated in a mixture of isopropanol/water 3/1 (v/v). For the third type of diblock the *N,N*-dimethylaminoethyl methacrylate (DMAEMA) was injected into the reactor at -70 °C and polymerized for 1 h. Immediately after addition of the monomer the color of the DPE end-capped polybutadienyl anion vanished completely. After termination with degassed methanol, the resulting polymer (cBD) was dialyzed against THF and finally freeze-dried from dioxane. The molecular weights of the diblock copolymers with P2VP or PDMAEMA as second block were calculated by a combination of MALD-ToF MS and <sup>1</sup>H NMR. Therefore, the  $M_n$  of the polybutadiene (PB) precursor polymer was determined by mass spectrometry. By the relative molar ratios of the characteristic signals of PB (5.10-5.60 ppm, 2H 1,2-PB; 5.70-5.15 ppm, 1H 1,2-PB and 2H 1,4-PB) and P2VP (8.50-8.00 ppm, 1H) or PDMAEMA (4.30-3.90 ppm, 2H) the overall molecular weight was calculated using the PB precursor molecular weight as reference. The  $M_n$  of the PB-*b*-*Pt*BMA diblock copolymers was directly measured by MALDI-ToF MS. All the data for the diblock characterization are summarized in Table 3-1.

**Alkyne Deprotection.** For the deprotection procedure, the respective polymer was dissolved in THF (~0.1 g/mL) and degassed for 30 min. Then, 10 equiv of tetrabutylammonium fluoride (1 M solution in THF) relative to alkyne functions were

added at 0 °C and stirred at this temperature for 2 h. After warming up to room temperature the solution was stirred overnight. The polymer was precipitated in pure water or isopropanol/water 3/1 (v/v) for PB-*b*-P2VP and PB-*b*-PtBMA, respectively. Afterward, the polymer was dissolved in THF and dialyzed against THF (MWCO 1 000 g/mol) to remove impurities. Finally, the polymers were freeze-dried from dioxane. In the case of the diblock copolymer with DMAEMA the reaction mixture was directly dialyzed against THF prior to freeze-drying.

**Click Reactions.** For the determination of the degree of functionalization with alkyne-substituted DPE, test click reactions with *N*-(1-heptyloctyl)-*N'*-(hexyl-6'-azido)-perylene-3,4,9,10-tetracarboxylic acid bisimide were conducted. In a typical run, 100 mg of the deprotected diblock copolymer were dissolved in 5 mL THF in a screw-cap glass. Then, 2 equiv of the azido-functionalized perylene bisimide relative to the alkyne function was added. After purging with nitrogen for 10 min, 1 equiv of CuBr was added, followed by further degassing for 10 min. By addition of 1 equiv of *N,N,N',N',N''*-pentamethyldiethylenetriamine (PMDETA) as ligand, the click reaction was started and stirred at room temperature for 3 days. After termination by exposure to air, the remaining copper was removed by filtration over a short silica gel column. Preparative SEC with THF as eluent was employed to remove excess perylene. An intense red-colored polymer was obtained after freeze-drying from dioxane.

The click reactions for the construction of the miktoarm star terpolymers were conducted in a similar manner. Typically, the molar ratios of alkyne function:azido function:CuBr:PMDETA was set to 1:1:1:1 (if not stated elsewhere), and the polymer concentration was ~20 mg/mL in THF. The reactions were conducted at room temperature and followed by withdrawing samples for SEC measurements. Finally, when no further changes in the SEC eluograms were observed, the resulting miktoarm star terpolymer was purified by passing through a small silica gel column to remove copper. The polymers were obtained as white powders after freeze-drying from dioxane.

### 3.3 Results and Discussion

#### 3.3.1 Synthesis of 1-[(4-(*tert*-Butyldimethylsilyl)ethynyl)phenyl]-1-phenylethylene (Click-DPE)

The key compound of this modular route toward ABC miktoarm star terpolymers (Scheme 3-1) was directly synthesized by the palladium-catalyzed Sonogashira coupling reaction between 1-(4-bromophenyl)-1-phenylethylene and *tert*-butyldimethylsilyl protected acetylene. Similar compounds, like 4-(trimethylsilyl)ethynylstyrene<sup>36</sup> and methacrylate derivatives as 3-trimethylsilyl-2-propynyl methacrylate,<sup>38</sup> have already been synthesized and used in anionic polymerization to obtain polymers with predictable molecular weights and narrow distributions. As known for DPE and its derivatives homopolymerization of such compounds is not possible due to steric hindrance.<sup>39</sup> In contrast to methods reported in literature,<sup>33,34</sup> this synthetic advantage enables us to use one sequential polymerization process to selectively incorporate exactly one alkyne function between the two polymeric blocks under adequate choice of monomers. The click-DPE was purified *via* column chromatography to give a clear viscous oil. The chemical structure and the purity were confirmed by <sup>1</sup>H NMR spectroscopy (Figure 3-1a).

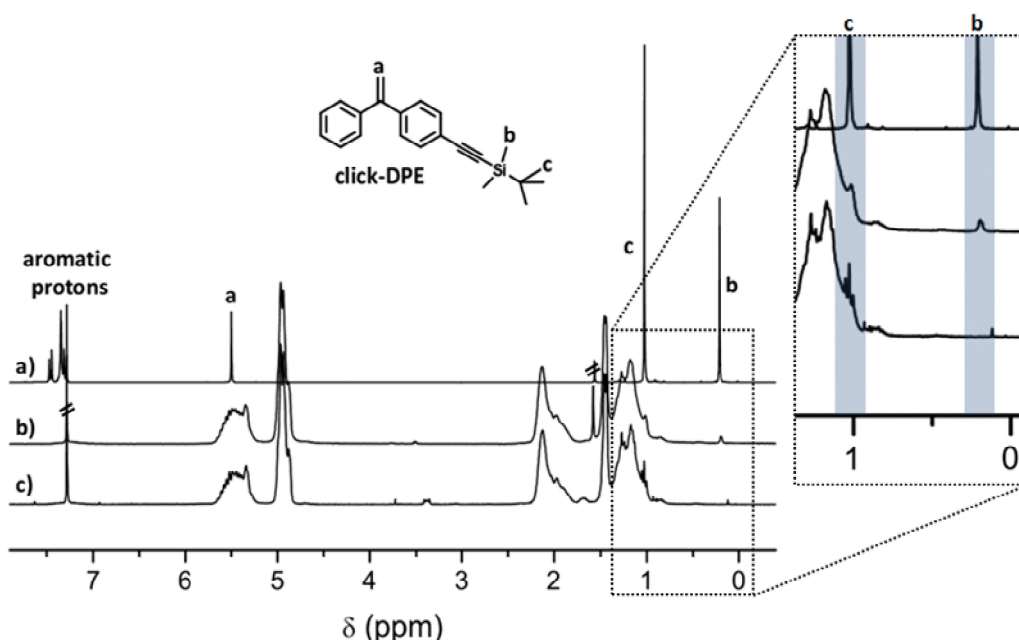


**Figure 3-1.** <sup>1</sup>H NMR spectra of (a) 1-[(4-(*tert*-butyldimethylsilyl)ethynyl)phenyl]-1-phenylethylene (click-DPE), (b) the protected alkyne-functionalized diblock cBT2, and (c) the corresponding diblock after hydrolysis of the silyl-protecting group (solvent signals are striked out).

The UV-vis spectrum of the deeply violet solution of the living anion (Figure 3-2) generated by reaction of 1-[(4-(*tert*-butyldimethylsilyl)ethynyl)phenyl]-1-phenylethylene with *sec*-BuLi shows a maximum at 549 nm. In contrast, the living anion of unsubstituted 1,1-diphenylethylene has a deep red color, and we determined the absorption maximum at around 500 nm under the same conditions.<sup>40</sup> This clear bathochromic shift originates from the conjugation of the  $\pi$ -system with the protected alkyne group. Similarly, Tsuda *et al.* reported a brownish-red color in the anionic polymerization of 4-(trimethylsilyl)ethylenestyrene,<sup>36</sup> in contrast to the orange color of polystyryl anions.<sup>41</sup>

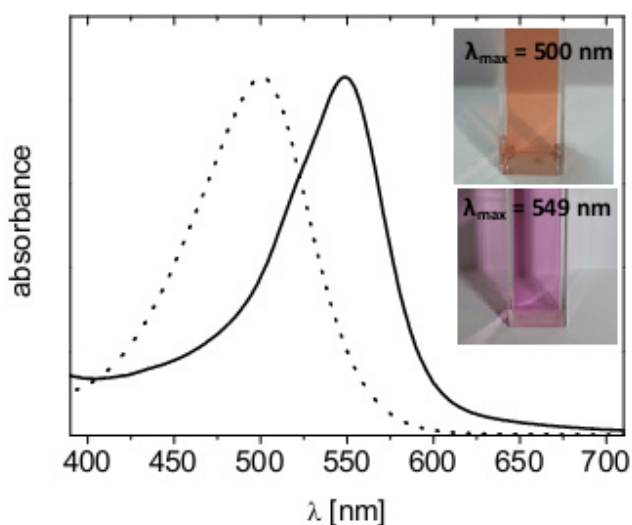


**Figure 3-2.** UV-vis absorption spectrum of the adduct of 1,1-diphenylethylene (dotted line) and 1-[(4-(*tert*-butyldimethylsilyl)ethynyl)phenyl]-1-phenylethylene (solid line) with *sec*-BuLi in THF. The inset shows the picture of the cuvette containing the living anion of the unsubstituted DPE (top) and the click-DPE (bottom).

### 3.3.2 Synthesis of Alkyne Mid-Functionalized Diblock Copolymers

Butadiene was chosen for the first block and for the second block 2-vinylpyridine (2VP) or methacrylate type monomers as *tert*-butyl methacrylate (tBMA) and *N,N*-dimethylaminoethyl methacrylate (DMAEMA). The anionic polymerization of butadiene was conducted in THF at -50 to -15 °C (depending on the respective block length) using *sec*-BuLi as initiator. After complete conversion – as followed *in situ* with fiber-optics NIR spectroscopy – 1.1 to 1.5 equiv of the click-DPE stock solution was added *via* syringe at -50 °C. The addition of the diphenylethylene derivative was clearly visible by the imme-

diate change in color from a slight yellow to intensive dark violet. To ensure complete end-capping of the polybutadienyl anions, the solution was stirred at -50 °C for another 2 h. During this period, no fading or change in color was detected. Samples of the polybutadiene (PB) precursors for SEC analysis were withdrawn before and after addition of the click-DPE, respectively. As the pristine polybutadiene carries no chromophore, no UV signal was detected at 260 nm. After reaction with the click-DPE, a significant UV signal was detected, coinciding with the RI trace. No change in the shape of the peak was detectable, indicating the absence of unwanted side reactions. Furthermore, a small shift of the whole peak toward lower elution volumes took place (Figure 3-S1). The molecular weight of the polybutadiene precursor was 5 910 g/mol before and 6 270 g/mol after the addition of the click-DPE, as determined by MALDI-ToF MS (Figure 3-S2). This is in good accordance with the expected increase of 320 g/mol for a click-DPE monoaddition.

With this new alkyne substituted DPE derivative we prepared three different types of midchain alkyne-functionalized diblock copolymers with narrow molecular weight distributions. In the case of 2-vinylpyridine as second block, the monomer was added at -70 °C and the polymerization was quenched after 5 min by the addition of degassed methanol. The overall composition and number-average molecular weight of the three different diblock copolymers (cBV1, cBV2, and cBV3) was determined by a combination of MALDI-ToF MS and <sup>1</sup>H NMR. The characterization of the synthesized diblock copolymers is given in detail in Table 3-1.

**Table 3-1. Molecular Characterization of Alkyne Mid-Functionalized PB-*b*-P2VP, PB-*b*-PtBMA, and PB-*b*-PDMAEMA Diblock Copolymers**

sample ID <sup>a</sup>	$M_n$ PB-precursor <sup>b</sup> [kg/mol]	$N(\text{PB})^b$	$N(\text{2nd block})^c$	$M_n$ diblock <sup>d</sup> [kg/mol]	$\bar{D}$ diblock <sup>e</sup>	$f_{\text{alkyne}}^f$
cBV1 (cB <sub>40</sub> V <sub>58</sub> <sup>14.7</sup> )	5.9	109	81	14.7	1.02	1.16
cBV2 (cB <sub>22</sub> V <sub>76</sub> <sup>14.0</sup> )	3.1	58	101	14.0	1.03	1.20
cBV3 (cB <sub>70</sub> V <sub>28</sub> <sup>17.2</sup> )	12.0	223	46	17.2	1.02	n.d.
cBT1 (cB <sub>76</sub> T <sub>22</sub> <sup>17.1</sup> )	13.0	242	27	17.1	1.03	0.93
cBT2 (cB <sub>49</sub> T <sub>49</sub> <sup>12.3</sup> )	6.0	111	42	12.3	1.03	n.d.
cBD (cB <sub>58</sub> D <sub>40</sub> <sup>17.0</sup> )	9.8	181	44	17.0	1.06	n.d.

<sup>a</sup>The subscripts denote the molecular weight fraction and the superscript the overall molecular weight including the click-DPE unit. <sup>b</sup>Determined by MALDI-ToF MS. <sup>c</sup>Calculated by <sup>1</sup>H NMR or in the case of PtBMA as second block by the difference in the MALDI-ToF MS spectra of diblock and precursor. <sup>d</sup>The overall molecular weight was determined by a combination of MALDI-ToF MS and <sup>1</sup>H NMR in the case of cBV's and cBD and by MALDI-ToF MS in the case of cBT's. The molecular weight of the diblock includes the DPE unit. <sup>e</sup>Measured from THF-SEC calibrated with polystyrene standards; in the case of cBD salt-THF-SEC was used. <sup>f</sup>The degree of alkyne functionalization  $f_{\text{alkyne}}$  was determined by UV-vis measurements of the perylene modified diblock copolymers.

In addition, we also prepared different diblock copolymers with PtBMA (cBT1 and cBT2) or PDMAEMA (cBD) as the second block. The polymerization conditions for polybutadiene and the end-capping reaction were similar to the diblock copolymers consisting of butadiene and 2-vinylpyridine (cBV's). The *t*BMA polymerization was started at -70 °C. As the violet color of the anionic click-DPE chain end did not disappear the temperature was stepwise raised to -45 °C where the color slowly faded away. This indicated the start of the polymerization. In the case of cBD the monomer was also added at -70 °C; however, the color of the end-capped polybutadienyl anion disappeared immediately after the addition of the monomer. DMAEMA polymerized faster and already at -70 °C, as it shows a higher reactivity than *t*BMA. Similar to *t*BMA no change from colorless to violet was observed after complete consumption of the monomer. This substantiates the hypothesis that the click-DPE is only inserted after the polybutadiene block and not within or at the end of the methacrylate block. All data for the polybutadiene precursors and the final diblock copolymers are listed in Table 3-1.

Theoretically, in combination with *sec*-BuLi, our click-DPE can be used to initiate methacrylates for the generation of  $\alpha$ -alkyne-functionalized homopolymers or block copolymers. In addition  $\omega$ -alkyne terminated homo- or block copolymers of nucleophilic monomers like styrene, butadiene and their derivatives can be prepared by end-capping with this alkyne-substituted DPE. The alkyne function is directly introduced into the polymers *via* DPE-chemistry. Except hydrolysis, no further polymer-analogous reaction steps are therefore necessary.

### 3.3.3 Hydrolysis of the Alkyne Mid-Functionalized Diblock Copolymers

The tetra-*n*-butylammonium fluoride-mediated hydrolysis of the protecting group was monitored *via*  $^1\text{H}$  NMR by the disappearance of the characteristic methyl signals of the silyl group at 1.03 and 0.22 ppm. The signal at 1.03 is overlapping with the backbone signals of polybutadiene, whereas the signal at 0.22 is well separated from other signals. Therefore, for the latter signal the complete disappearance indicates the quantitative deprotection (Figure 3-1b,c).

As the molecular weights of the diblock copolymers exceeded 10 000 g/mol, the direct determination of the degree of alkyne substitution from the characteristic signals of the protecting group was too imprecise. Thus, to determine the degree of alkyne functionalization, a modification of the diblock copolymers with an azido-functionalized perylene bisimide<sup>42</sup> was conducted *via* click chemistry at the example of cBV1, cBV2, and cBT1. After deprotection of the alkyne function and subsequent click reaction with 2 equiv of *N*-(1-heptyloctyl)-*N'*-(hexyl-6'-azido)-perylene-3,4,9,10-tetracarboxylic acid bisimide ( $\text{N}_3$ -PBI), functionalization of the diblock copolymer was proven qualitatively by SEC measurements at a wavelength of 458 nm. The nonlabeled diblock copolymers did not show any significant UV activity at this wavelength, whereas perylene is UV-active. After complete removal of excess perylene by preparative SEC (as confirmed by SEC measurements at 458 nm), UV spectra were recorded in dichloromethane at a polymer concentration of  $10^{-5}$  mol/L. Thus, by measuring the optical density and comparing the value of UV absorption at the maximum of the spectra ( $\lambda = 525$  nm) with a pure  $\text{N}_3$ -PBI solution with  $c = 10^{-5}$  mol/L, the degree of alkyne-functionalization was determined to be  $\sim 116\%$  for cBV1 (see Figure 3-S3A and Table 3-1). There might be some minor sources

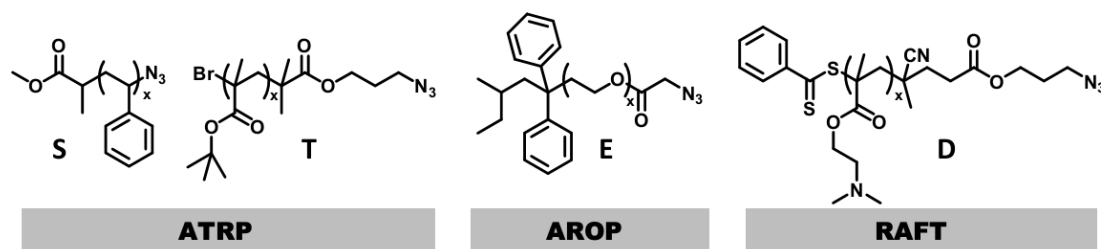
of error by weighing and by determination of the number-average molecular weight of the polymer by a combination of MALDI-ToF MS and  $^1\text{H}$  NMR. Nevertheless, this value gives rise to the assumption that there might be incorporation of more than one click-DPE in the block copolymer even under the applied conditions. Multiple incorporation of the DPE derivative in the polybutadiene block can be excluded, as complete consumption of the monomer was guaranteed by *in situ* NIR-spectroscopy. Similar results were obtained for the  $\text{N}_3$ -PBI-labeled cBV2, where also functionalization with more than one click-DPE took place (concluded from the determined degree of functionalization of 120%). Test reactions showed that living 2VP anions can attack click-DPE after extended reaction times (a more detailed description and the corresponding MALDI-ToF MS spectra can be found in the Supporting Information). Here, one has to note that for the test reaction the conditions were dissimilar to the diblock synthesis as a 2-fold excess of click-DPE was used, and the reaction mixture was stirred for an additional hour after addition of the click-DPE. In contrast to this, for the synthesis of the diblock copolymers the excess of click-DPE was already present during the course of polymerization. Nevertheless, we suppose that the click-DPE is incorporated after complete consumption of the 2VP monomer. As can be seen from the determined degree of alkyne-functionalization for the cBV's the values of 116 - 120% were lower than the maximal value of 150% deduced from the use of 1.5 equiv of click-DPE regarding initiator. Consequently, even though the P2VP polymerization was terminated immediately after consumption of all monomer, to a small extent diblock copolymers were obtained, which partially might bear an additional click-DPE unit in, or more probably, at the end of the P2VP block.

Since methacrylates are generally not capable of adding diphenylethylene, incorporation of only one click-DPE unit at the block junction is expected for the diblock copolymers with butadiene as first and a methacrylate as second block.<sup>39,43</sup> This is supported by the determined degree of alkyne-functionalization of 93% for the perylene modified cBT1 (Figure 3-S3B). Taking into account the errors of weighing and determination of the number-average molecular weight, this can be assumed to be quantitative. Therefore, well-defined diblock copolymers bearing exactly one alkyne function in between the two blocks can be synthesized with our approach, if the second block is a

methacrylate. Generally, also well-defined alkyne mid-functionalized diblock copolymers consisting of poly(2-vinylpyridine) as first block and a methacrylate type monomer as second block are accessible utilizing click-DPE.

### 3.3.4 Synthesis of $\omega$ -Azido Homopolymers

In principle, every homopolymer bearing an azido function can be clicked to the synthesized alkyne mid-functionalized diblock copolymers. Different polymerization methods are capable of generating azido-functionalized polymers *in situ*<sup>44,45</sup> or by appropriate termination reactions<sup>46</sup> or postfunctionalization methods.<sup>47</sup> To demonstrate the broad applicability and modular strategy of our approach, we synthesized azido-functionalized homopolymers utilizing three different polymerizations methods (Chart 3-1, for details of the corresponding synthetic procedure see the Experimental Section in the Supporting Information). Azido-functionalized polystyrene (PS-N<sub>3</sub>) as model compound was synthesized *via* ATRP and subsequent transformation of the bromine end group with sodium azide.<sup>47</sup> By using an azido-functionalized initiator, poly(*tert*-butyl methacrylate) was directly synthesized *via* ATRP.<sup>45</sup> This can be hydrolyzed to yield poly(acrylic acid). Similarly poly(*N,N*-dimethylaminoethyl methacrylate) as functional stimuli-responsive polymer was polymerized *via* RAFT employing an azido-functionalized chain transfer agent (CTA).<sup>44</sup> Poly(ethylene oxide) was achieved *via* anionic ring-opening polymerization (AROP) and can serve as water-soluble block. Therefore, we utilized the possibility of quenching living polymer anions with azido acid chlorides<sup>46</sup> to obtain azido-terminated PEO. In all cases the presence of an azido function was proven by IR measurements and additionally with MALDI-ToF MS or <sup>1</sup>H NMR except for PtBMA-N<sub>3</sub> (see characterization of  $\omega$ -azido homopolymers in the Supporting Information). The advantage of the applied “grafting-onto” method is that the third arm is polymerized and characterized separately. The molecular characterizations of the different polymers are summarized in Table 3-2.

**Chart 3-1. Azido-Functionalized Homopolymers Synthesized *via* Different Polymerization Methods****Table 3-2. Molecular Characterization of Azido-Functional Homopolymers**

sample ID	$M_n$ [kg/mol]	$\bar{D}$
PS1-N3 <sup>a</sup>	3.7	1.07
PS2-N3 <sup>a</sup>	5.9	1.10
PS3-N3 <sup>a</sup>	8.3	1.06
PEO-N3 <sup>b</sup>	6.6	1.02
PtBMA-N3 <sup>c</sup>	7.6	1.17
PDMAEMA-N3 <sup>d</sup>	5.4	1.20

<sup>a</sup>Molecular weights and dispersities were determined by THF SEC using polystyrene standards. <sup>b</sup>Molecular weights and dispersities were determined by THF SEC using poly(ethylene oxide) standards. <sup>c</sup>Molecular weights and dispersities were determined by THF SEC using poly(*tert*-butyl methacrylate) standards. <sup>d</sup>MALDI-ToF MS was employed for determination of molecular weight and dispersity.

### 3.3.5 Synthesis of Miktoarm Star Terpolymers *via* Click Chemistry

Copper-catalyzed alkyne-azide cycloaddition (CuAAC) was utilized for the modular synthesis of ABC miktoarm star terpolymers *via* combination of alkyne mid-functionalized diblock copolymers with  $\omega$ -azido-functionalized homopolymers of different length and monomer structure (Chart 3-1). Here, only the alkyne mid-functionalized diblock copolymers with a methacrylate as second block (cBT's and cBD) were used, as for 2-vinylpyridine partial incorporation of the click-DPE in or most probably at the end of the P2VP block could not be excluded completely.

*Click Reactions with  $\omega$ -Azido-Functionalized Polystyrene.* To demonstrate the feasibility of this approach, we first conducted click reactions of the alkyne-functionalized diblock copolymers with different azido-functionalized PS homopolymers. One prerequisite of our approach is the 100% efficiency of the click reaction step, so that no laborious purification steps are needed when the educts are added in equimolar amounts.<sup>48</sup> Even though in literature linear and well-defined star shaped polymers with molecular

weights close to 100 000 g/mol were produced *via* CuAAC,<sup>49,50</sup> we suppose that in our case the alkyne function at the block junction is sterically less amenable than an alkyne function in  $\alpha$ - or  $\omega$ -position. Our first trials with higher molecular weight polymers (exceeding 40 000-50 000 g/mol for the individual compounds) were not successful. Therefore, we chose moderate molecular weights of the individual compounds, so that the overall molecular weight did not exceed 25 000 g/mol and the functional groups were not too diluted. The course of the click reactions with cBT diblock copolymers was followed by SEC. The reactions were conducted under equimolar conditions. After 24 h the molecular weight distribution of the diblock copolymers cBT1 and cBT2 shifted completely (see Figure 3-3 and Figure 3-S4), resembling the successful generation of the desired miktoarm star terpolymer. However, despite equimolar reaction conditions in both cases there was still a minor amount of unreacted homopolymer left. Further SEC measurements showed that the peak of the PS1-N<sub>3</sub> already disappeared nearly completely after 11.5 h (Figure 3-S5) for the click reaction with cBT2. Increasing the reaction time did not lead to any change in the eluogramm. Therefore, we additionally carried out a reaction between cBT1 and only 0.8 equiv of PS1-N<sub>3</sub>. Under the same reaction conditions, again, a comparable amount of homopolymer was left (results not shown). We assume that during polymerization and work-up of the homopolymer, a minor part of the bromine group is eliminated, as already reported in literature.<sup>51</sup> This leads to a small amount of non-azido-functionalized homopolymer which cannot take part in the click reaction (see discussion of MALDI-TOF spectrum in the Supporting Information). This was also confirmed by the click reaction of cBT2 with PS3-N<sub>3</sub> (Figure 3-S6). Under equimolar reaction conditions no further ligation took place after 15 h, leading to a non-negligible amount of unreacted diblock and homopolymer. In contrast to the click reactions with lower molecular weight polystyrenes the conversion of the click reaction with PS3-N<sub>3</sub> was much lower after 3.25 h (where the reaction was more or less finished in the other cases). Further addition of 0.5 equiv of homopolymer resulted in a complete shift of the diblock due to complete click efficiency as depicted in Figure 3-S6. Thus, the degree of unfunctionalized polystyrene increased with increasing molecular weight.

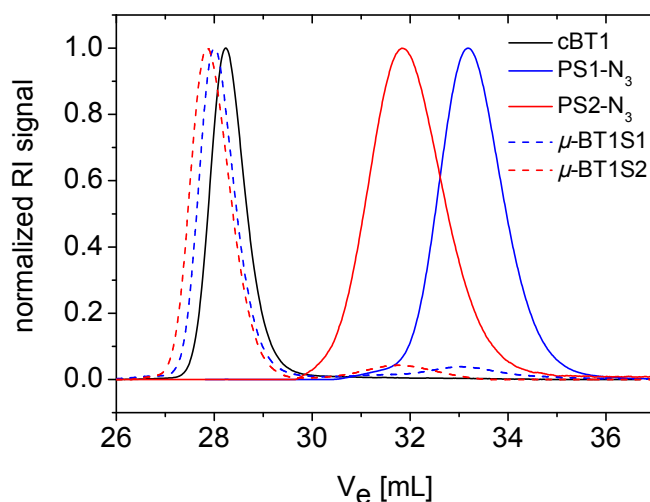


**Figure 3-3.** THF-SEC (RI signal) of alkyne-functionalized diblock cBT1, azido-functionalized PS (PS1-N<sub>3</sub>, PS2-N<sub>3</sub>) and the corresponding ABC miktoarm star terpolymers ( $\mu$ -BT1S1 and  $\mu$ -BT1S2) obtained after equimolar click reaction for 24 h.

Nevertheless, complete shifts of the molecular weight distributions of the miktoarm star terpolymers toward lower elution volumes compared to the pristine diblock copolymers were detected in all cases. This demonstrates the successful formation of ABC miktoarm star terpolymers. Additionally, the overall shifts of the resulting ABC miktoarm star terpolymers were not too distinct. This is in accordance with theory, where the hydrodynamic radius of star polymers is expected to be smaller than the hydrodynamic radius of a linear polymer with the same composition and molecular weight due to the higher segmental density of star polymers.<sup>52</sup> All synthesized  $\mu$ -BTS star terpolymers exhibited symmetrical peaks with a narrow molecular weight distribution. The theoretical molecular weights were calculated from the known molecular weights of the ligated diblock copolymers. These are shown together with the apparent molecular weights and the respective dispersities in Table 3-3. Furthermore an exemplarily <sup>1</sup>H NMR of  $\mu$ -BT1S1 is shown in Figure 3-S7. All characteristic signals of the polymeric building blocks are present in the obtained miktoarm star terpolymer.

**Table 3-3. Molecular Characterization of ABC Miktoarm Star Terpolymers Obtained from Click Reactions with Alkyne Mid-Functionalized Diblock Copolymers**

sample ID <sup>a</sup>	DP(PB) <sup>b</sup>	DP(2nd block) <sup>c</sup>	DP(3rd block) <sup>d</sup>	$M_{n,th.}$ <sup>e</sup> [kg/mol]	$M_{n,app}$ <sup>f</sup> [kg/mol]	$\mathcal{D}$ <sup>f</sup>
$\mu$ -BT1S1 ( $\mu$ -B <sub>63</sub> T <sub>18</sub> S <sub>18</sub> <sup>20.7</sup> )	242	27	36	20.7	28.0	1.03
$\mu$ -BT1S2 ( $\mu$ -B <sub>57</sub> T <sub>17</sub> S <sub>26</sub> <sup>22.9</sup> )	242	27	57	22.9	30.0	1.03
$\mu$ -BT1E ( $\mu$ -B <sub>55</sub> T <sub>16</sub> E <sub>28</sub> <sup>23.6</sup> )	242	27	150	23.6	32.7	1.04
$\mu$ -BT1D ( $\mu$ -B <sub>58</sub> T <sub>17</sub> D <sub>24</sub> <sup>22.4</sup> )	242	27	34	22.4	31.5	1.10
$\mu$ -BT2S1 ( $\mu$ -B <sub>38</sub> T <sub>38</sub> S <sub>23</sub> <sup>15.9</sup> )	111	42	36	15.9	20.5	1.03
$\mu$ -BT2S2 ( $\mu$ -B <sub>33</sub> T <sub>33</sub> S <sub>33</sub> <sup>18.1</sup> )	111	42	57	18.1	22.4	1.03
$\mu$ -BT2S3 <sup>g</sup> ( $\mu$ -B <sub>29</sub> T <sub>29</sub> S <sub>40</sub> <sup>20.5</sup> )	111	42	80	20.5	25.0	1.03
$\mu$ -BT2E ( $\mu$ -B <sub>32</sub> T <sub>32</sub> E <sub>35</sub> <sup>18.8</sup> )	111	42	150	18.8	25.4	1.03
$\mu$ -BT2D ( $\mu$ -B <sub>34</sub> T <sub>34</sub> D <sub>31</sub> <sup>17.6</sup> )	111	42	34	17.6	20.8	1.11
$\mu$ -BDT <sup>g</sup> ( $\mu$ -B <sub>40</sub> D <sub>28</sub> T <sub>31</sub> <sup>24.5</sup> )	181	44	53	24.5	26.3	1.08
$\mu$ -BDE <sup>g</sup> ( $\mu$ -B <sub>42</sub> D <sub>29</sub> E <sub>28</sub> <sup>23.5</sup> )	181	44	150	23.5	32.5	1.06

<sup>a</sup>The number-average molecular weight of the ABC miktoarm star terpolymer was calculated from the respective values of diblock copolymers and the homopolymers. Therefore, the superscript denotes the theoretical number-average molecular weight of the ABC miktoarm star terpolymer and the indices the theoretical weight fraction of the respective blocks. <sup>b</sup>Degree of polymerization (DP) determined from MALDI-ToF MS of the PB-precursor. <sup>c</sup>Calculated by the difference in  $M_n$  determined by the MALDI-ToF MS spectra of diblock and precursor. <sup>d</sup>Calculated from the molecular weight of the 3<sup>rd</sup> block. <sup>e</sup>Theoretical molecular weight. <sup>f</sup>Apparent molecular weight and dispersity determined by SEC with polystyrene calibration. For the miktoarm star terpolymers containing PDMAEMA THF-SEC with additional 0.25 wt% tetrabutylammonium bromide (TBAB) was used. <sup>g</sup>In these cases the apparent molecular weight and dispersity were determined excluding the separated homopolymer peak.

*Click Reactions with  $\omega$ -Azido-Functionalized Poly(ethylene oxide).* These first successful test reactions with azido-functionalized polystyrene prove the feasibility of our approach. To prepare amphiphilic miktoarm star terpolymers we conducted click reactions with PEO-N<sub>3</sub>. First attempts under equimolar reaction conditions led to a non-negligible amount of unreacted diblock copolymer. Therefore, the click reactions were carried out with an excess of the functionalized PEO-N<sub>3</sub>. By stepwise addition of PEO-N<sub>3</sub> to the reaction mixture, the equivalents necessary for a complete click reaction were determined

(Figure 3-S8). Therefore, in a first step, the reaction with 1 equiv of PEO-N<sub>3</sub> was followed by SEC. As after 24 h no further change in the eluogram was detected, and still a significant amount of unreacted diblock copolymer was left over, 0.5 equiv of PEO-N<sub>3</sub> was added subsequently. Finally, after 3.5 h reaction time, further 0.2 equiv of PEO-N<sub>3</sub> was added to the click reaction containing already 1.5 equiv. As this did not result in a change compared to the eluogram after reaction with 1.5 equiv of PEO-N<sub>3</sub>, the equivalents necessary for complete ligation were determined to be 1.5 equiv.

The reason for the use of such a huge excess of PEO-N<sub>3</sub> still remains unclear. From the amount of coupled product (~6 wt% from SEC) only a slight excess of the azido-functionalized compound would be reasonable. However, maybe partial elimination of the azido group of PEO or uncomplete functionalization due to side reaction during the end-capping reaction could be a feasible explanation (see discussion of MALDI-ToF spectrum in the Supporting Information). The respective SEC traces for the click reactions with cBT1, cBT2, and CBD (where the ratio of cBX:PEO-N<sub>3</sub> was minimum 1:1.5) are shown in Figure 3-4. In case of the diblock copolymers with PtBMA as second block the excess PEO-N<sub>3</sub> was easily removed during purification from copper with a short column of silica due to interactions with the column. Using PEO-N<sub>3</sub> in excess and subsequent removal of unreacted homopolymer guaranteed the complete conversion of the alkyne function.

However, in the case of the diblock CBD containing DMAEMA a higher amount of PEO homopolymer was left over after work-up. Further purification with a column, crystallization from cold THF, or dialysis in aqueous media did not reduce the amount of the undesired PEO homopolymer. A possible explanation could be that PEO forms hydrogen bonds with PDMAEMA, which therefore prevent the complete removal of excess PEO homopolymer. Here, one has to notice that for further applications, where the PEO serves as corona in aqueous solutions, this minor amount of PEO homopolymer is not problematic.

In contrast to the previous click reactions, distinct shifts of the molecular weight distributions of the ABC miktoarm star terpolymers compared to the corresponding diblock precursors were detected. The absence of a peak from residual diblock also gives evidence that all diblock copolymer chains carry an alkyne function. Like for the click reac-

tions with PS-N<sub>3</sub> low dispersities of the resulting ABC miktoarm star terpolymers were detected (Table 3-3).

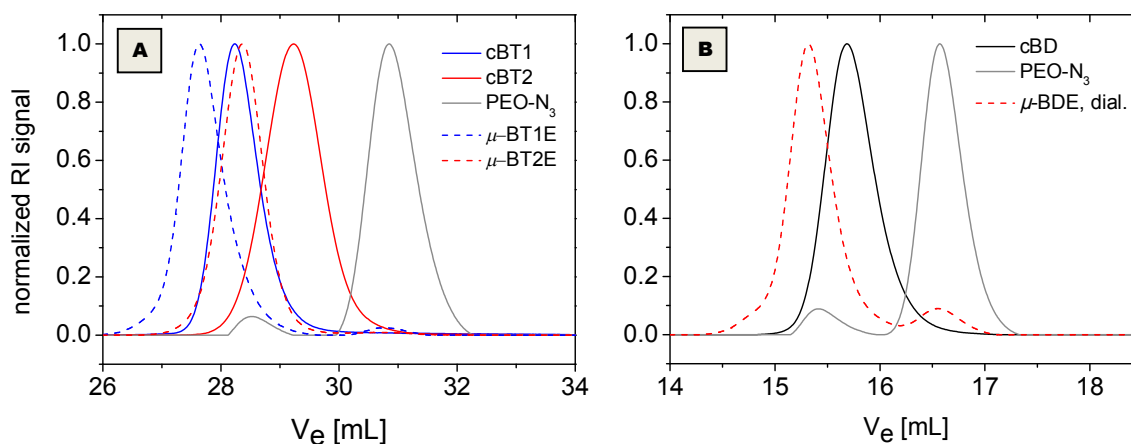


**Figure 3-4.** THF-SEC (A) of alkyne-functionalized diblock copolymers cBT1, cBT2, the azido-functionalized PEO-N<sub>3</sub>, and the corresponding ABC miktoarm star terpolymers ( $\mu$ -BT1E and  $\mu$ -BT2E) obtained after azide-alkyne click coupling and salt-THF-SEC traces (B) of cBD, PEO-N<sub>3</sub>, and the resulting ABC miktoarm star terpolymer ( $\mu$ -BDE) after dialysis. In all cases the RI-signals are shown.

#### Click Reactions with $\omega$ -Azido-Functionalized Poly(*N,N*-dimethylaminoethyl methacrylate).

To obtain PDMAEMA as a water-soluble polymer, which responds both to pH and temperature,<sup>53</sup> we used an azido-substituted CTA.<sup>44</sup> As the general applicability of our approach under equimolar conditions was proven we conducted the click reactions with a 2-fold excess of PDMAEMA-N<sub>3</sub> for 5 days, without optimizing the reaction time. With this reaction pathway we were also able to guarantee 100% conversion of the alkyne-compound. The SEC traces of the raw product of the click reactions of the azido-functionalized PDMAEMA-N<sub>3</sub> with the two cBT diblock copolymers are shown in Figure 3-5A and 3-5B, respectively. In both cases the molecular weight distributions of the miktoarm star terpolymers shifted completely in the corresponding SEC-traces compared to their diblock copolymer precursors. The excess PDMAEMA-N<sub>3</sub> was removed by dialysis in a mixture of methanol/isopropanol (2/1 v/v), where the miktoarm star terpolymer forms micelles with a polybutadiene core. Therefore, a dialysis membrane with a cut-off (50 000 g/mol) much higher than the molecular weight of the homopolymer was used. The SEC traces of the obtained miktoarm star terpolymers are plotted in Figure 3-5A and B. In the case of  $\mu$ -BT1D the tiny coupling shoulder at lower elution volume became more pronounced after dialysis. Therefore, we assume that this

shoulder might be the result of some aggregation effects, which occurred for this reaction. Another explanation could be the oxidation of the amine, which leads to the formation of amine oxide. For the dialysis of  $\mu$ -BT2D even under extensive exchange of the solvent, the small residual peak from unreacted PDMAEMA- $N_3$  could not be removed completely. However, compared to the product peak this peak is negligible. The molecular characterization of the  $\mu$ -BTD miktoarm star terpolymers is listed in Table 3-3. In a similar way a  $\mu$ -BDT miktoarm star terpolymer consisting of the same monomer units was synthesized by ligation of cBD with PtBMA- $N_3$  (see Supporting Information and Table 3-3).

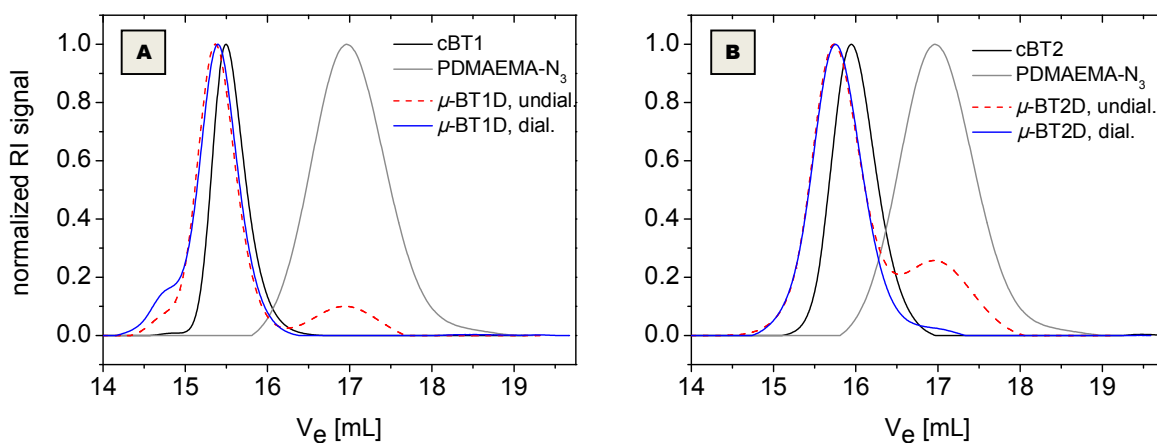


**Figure 3-5.** Salt-THF-SEC (RI signal) of  $\mu$ -BTD miktoarm star terpolymers obtained by click coupling of the alkyne-functionalized diblock copolymers (A) cBT1 and (B) cBT2 with the azido-functionalized PDMAEMA- $N_3$ . As in both cases 2 equiv of PDMAEMA were used within the click reaction, SEC traces of the raw product and the miktoarm star terpolymer after dialysis are shown.

### 3.4 Conclusions

This general modular route for the synthesis of ABC miktoarm star terpolymers combines anionic polymerization techniques with CRP methods and anionic ring opening polymerization using azide-alkyne Huisgen cycloaddition as ligation method. For this purpose, we successfully employed our alkyne-modified DPE derivative in sequential anionic polymerization. In the case of methacrylate-type monomers well-defined alkyne midfunctional diblock copolymers consisting of a first block of PB and a second block of either PtBMA or PDMAEMA were synthesized. Click reactions with azido-functionalized perylene bisimide verified the successful incorporation of only one DPE unit at the block junction. In contrast to other DPE derivatives, we observed that click-DPE can copolymerize with 2VP, which offers the advantage of producing alkyne mid-functionalized diblock copolymers with P2VP as first block and a methacrylate as second block. Therefore, 2VP and butadiene and styrene and their derivatives can be used as first blocks and methacrylate type monomers as second block to obtain well defined-diblock copolymers bearing an alkyne function at the block junction. By using a toolbox of different azido-functionalized homopolymers, we demonstrate that a variety of well-defined ABC miktoarm star terpolymers is accessible *via* this modular approach. These exhibited monomodal molecular weight distributions with small dispersities close to 1.10 or even lower.

The obtained miktoarm star terpolymers are interesting new polymers regarding their bulk morphologies and solution-based self-assembly. Results from the self-assembly of these ABC miktoarm star terpolymers will be reported in subsequent publications. A further advantage is that due to the use of anionic polymerization miktoarm star terpolymers with a polybutadiene block are accessible, which can afterward be functionalized through thiol-ene click chemistry<sup>54</sup> or used for selective crosslinking.<sup>5,55</sup> Furthermore, the ABC miktoarm star terpolymer containing arms of polybutadiene, poly(*N,N*-dimethylaminoethyl methacrylate) and poly(ethylene oxide) is a promising candidate in the field of biotechnological applications like gene delivery.<sup>56-58</sup> Our approach enables the upscaling of the synthesis of ABC miktoarm star terpolymers to more than one gram. Both synthetic steps for diblock and homopolymer synthesis are well-established polymerization methods, and no further complex synthetic procedures are

necessary, as compared to other methods. Because of the strong versatility of click chemistry and the increasing amount of publications dealing with it, we expect our click-DPE to offer a variety of new possibilities in the design of novel custom polymer architectures and materials.

**Supporting Information.** Materials section, polymerization procedures, characterization section, characterization of  $\omega$ -azido homopolymers, click reaction with poly(*tert*-butyl methacrylate) and discussion of the reactivity of click-DPE toward living P2VP-Li; UV-vis spectra of perylene-labeled diblock copolymers, SEC traces of polybutadiene precursors, poly(ethylene oxide) and click reactions, MALDI-ToF mass spectra of polybutadiene precursors and an exemplarily  $^1\text{H}$  NMR spectrum of  $\mu$ -BT1S1. This Information is available free of charge *via* the Internet at <http://pubs.acs.org/>.

**Acknowledgments.** This work was supported by the Deutsche Forschungsgemeinschaft within SPP 1165 (Mu896/22). We thank Christo B. Tsvetanov and Markus Müllner for fruitful discussion. Melanie Förtsch, Annika Pfaffenberger, and Christopher V. Synatschke are acknowledged for performing MALDI-ToF MS measurements and Marietta Böhm, Katharina Neumann, and Robin Pettau for conducting SEC measurements. We further thank André H. Gröschel for providing one of the polystyrene homopolymers, Stefan Reinicke for the synthesis of the azidoacetyl chloride, and Julia Ewert for RAFT polymerization of the PDMAEMA homopolymer. Andreas S. Lang is acknowledged for providing the azido-functionalized perylene bisimide.

### 3.5 References

- (1) Hadjichristidis, N. *J. Polym. Sci., Part A: Polym. Chem.* **1999**, *37*, 857-871.
- (2) Hückstädt, H.; Göpfert, A.; Abetz, V. *Macromol. Chem. Phys.* **2000**, *201*, 296-307.
- (3) Junnila, S.; Houbenov, N.; Hanski, S.; Iatrou, H.; Hirao, A.; Hadjichristidis, N.; Ikkala, O. *Macromolecules* **2010**, *43*, 9071-9076.
- (4) Matsushita, Y.; Hayashida, K.; Takano, A. *Macromol. Rapid Commun.* **2010**, *31*, 1579-1587.
- (5) Walther, A.; Yuan, J.; Abetz, V.; Müller, A. H. E. *Nano Lett.* **2009**, *9*, 2026-2030.
- (6) Song, J.; Shi, T.; Chen, J.; An, L. *J. Phys. Chem. B* **2010**, *114*, 16318-16328.
- (7) Li, Z.; Hillmyer, M. A.; Lodge, T. P. *Langmuir* **2006**, *22*, 9409-9417.
- (8) Li, Z.; Hillmyer, M. A.; Lodge, T. P. *Nano Lett.* **2006**, *6*, 1245-1249.
- (9) Iatrou, H.; Hadjichristidis, N. *Macromolecules* **1992**, *25*, 4649-4651.
- (10) Sioula, S.; Tselikas, Y.; Hadjichristidis, N. *Macromolecules* **1997**, *30*, 1518-1520.
- (11) Mavroudis, A.; Hadjichristidis, N. *Macromolecules* **2005**, *39*, 535-540.
- (12) Fujimoto, T.; Zhang, H.; Kazama, T.; Isono, Y.; Hasegawa, H.; Hashimoto, T. *Polymer* **1992**, *33*, 2208-2213.
- (13) Hückstädt, H.; Abetz, V.; Stadler, R. *Macromol. Rapid Commun.* **1996**, *17*, 599-606.
- (14) Quirk, R. P.; Yoo, T.; Lee, B. *J. Macromol. Sci.* **1994**, *31*, 911-926.
- (15) Lambert, O.; Dumas, P.; Hurtrez, G.; Riess, G. *Macromol. Rapid Commun.* **1997**, *18*, 343-351.
- (16) Lambert, O.; Reutenauer, S.; Hurtrez, G.; Riess, G.; Dumas, P. *Polym. Bull.* **1998**, *40*, 143-149.
- (17) Saito, N.; Liu, C.; Lodge, T. P.; Hillmyer, M. A. *Macromolecules* **2008**, *41*, 8815-8822.
- (18) Li, Z.; Hillmyer, M. A.; Lodge, T. P. *Macromolecules* **2004**, *37*, 8933-8940.
- (19) Liu, C.; Hillmyer, M. A.; Lodge, T. P. *Langmuir* **2009**, *25*, 13718-13725.
- (20) Abouelmagd, A.; Sugiyama, K.; Hirao, A. *Macromolecules* **2011**, *44*, 826-834.
- (21) Matyjaszewski, K.; Tsarevsky, N. V. *Nat. Chem.* **2009**, *1*, 276-288.
- (22) Gregory, A.; Stenzel, M. H. *Prog. Polym. Sci.* **2012**, *37*, 38-105.
- (23) Huisgen, R. *Angew. Chem., Int. Ed.* **1963**, *2*, 633-645.
- (24) Binder, W. H.; Sachsenhofer, R. *Macromol. Rapid Commun.* **2008**, *29*, 952-981.
- (25) Huisgen, R. *Angew. Chem., Int. Ed.* **1963**, *2*, 565-598.
- (26) Liu, H.; Li, C.; Liu, H.; Liu, S. *Langmuir* **2009**, *25*, 4724-4734.
- (27) Zhang, Y.; Liu, H.; Dong, H.; Li, C.; Liu, S. *J. Polym. Sci., Part A: Polym. Chem.* **2009**, *47*, 1636-1650.
- (28) Khanna, K.; Varshney, S.; Kakkar, A. *Macromolecules* **2010**, *43*, 5688-5698.
- (29) Iskin, B.; Yilmaz, G.; Yagci, Y. *J. Polym. Sci., Part A: Polym. Chem.* **2011**, *49*, 2417-2422.
- (30) Zhang, Y.; Li, C.; Liu, S. *J. Polym. Sci., Part A: Polym. Chem.* **2009**, *47*, 3066-3077.
- (31) Gunay, U. S.; Durmaz, H.; Gungor, E.; Dag, A.; Hizal, G.; Tunca, U. *J. Polym. Sci., Part A: Polym. Chem.* **2011**, 729-735.
- (32) Wong, E. H. H.; Stenzel, M. H.; Junkers, T.; Barner-Kowollik, C. *Macromolecules* **2010**, *43*, 3785-3793.
- (33) Wang, G.; Luo, X.; Liu, C.; Huang, J. *J. Polym. Sci., Part A: Polym. Chem.* **2008**, *46*, 2154-2166.
- (34) Ye, C.; Zhao, G.; Zhang, M.; Du, J.; Zhao, Y. *Macromolecules* **2012**, DOI: 10.1021/ma3015118.
- (35) Schlosser, M.; Schaub, B. *Chimia* **1982**, *36*, 396-397.
- (36) Tsuda, K.; Ishizone, T.; Hirao, A.; Nakahama, S.; Kakuchi, T.; Yokota, K. *Macromolecules* **1993**, *26*, 6985-6991.
- (37) Auschra, C.; Stadler, R. *Polym. Bull.* **1993**, *30*, 257-264.
- (38) Ishizone, T.; Uehara, G.; Hirao, A.; Nakahama, S.; Tsuda, K. *Macromol. Chem. Phys.* **1998**, *199*, 1827-1834.
- (39) Quirk, R.; Yoo, T.; Lee, Y.; Kim, J.; Lee, B. *Adv. Polym. Sci.* **2000**, *153*, 67-162.
- (40) Waack, R.; Doran, M. A. *J. Am. Chem. Soc.* **1969**, *91*, 2456-2461.
- (41) Giebeler, E.; Stadler, R. *Macromol. Chem. Phys.* **1997**, *198*, 3815-3825.
- (42) Lang, A. S.; Neubig, A.; Sommer, M.; Thelakkat, M. *Macromolecules* **2010**, *43*, 7001-7010.
- (43) Hsieh, H. L.; Quirk, R. P. In *Anionic Polymerization: Principles and Practical Applications*; Marcel Dekker: New York, 1996.
- (44) Gondi, S. R.; Vogt, A. P.; Sumerlin, B. S. *Macromolecules* **2007**, *40*, 474-481.
- (45) Mantovani, G.; Ladmiral, V.; Tao, L.; Haddleton, D. M. *Chem. Commun.* **2005**, 2089-2091.
- (46) Reinicke, S.; Schmalz, H. *Colloid Polym. Sci.* **2011**, *289*, 497-512.
- (47) Coessens, V.; Matyjaszewski, K. *J. Macromol. Sci.* **1999**, *36*, 667-679.

- (48) Barner-Kowollik, C.; Du Prez, F. E.; Espeel, P.; Hawker, C. J.; Junkers, T.; Schlaad, H.; Van Camp, W. *Angew. Chem., Int. Ed.* **2011**, *50*, 60-62.
- (49) Durr, C. J.; Emmerling, S. G. J.; Lederhose, P.; Kaiser, A.; Brandau, S.; Klimpel, M.; Barner-Kowollik, C. *Polym. Chem.* **2012**, *3*, 1048-1060.
- (50) Inglis, A. J.; Pierrat, P.; Muller, T.; Brase, S.; Barner-Kowollik, C. *Soft Matter* **2010**, *6*, 82-84.
- (51) Zhong, M.; Matyjaszewski, K. *Macromolecules* **2011**, *44*, 2668-2677.
- (52) Roovers, J.; Hadjichristidis, N.; Fetters, L. J. *Macromolecules* **1983**, *16*, 214-220.
- (53) Plamper, F. A.; Schmalz, A.; Penott-Chang, E.; Drechsler, M.; Jusufi, A.; Ballauff, M.; Müller, A. H. E. *Macromolecules* **2007**, *40*, 5689-5697.
- (54) Justynska, J.; Hordyjewicz, Z.; Schlaad, H. *Polymer* **2005**, *46*, 12057-12064.
- (55) Walther, A.; Goldmann, A. S.; Yelamanchili, R. S.; Drechsler, M.; Schmalz, H.; Eisenberg, A.; Müller, A. H. E. *Macromolecules* **2008**, *41*, 3254-3260.
- (56) van de Wetering, P.; Cherng, J.-Y.; Talsma, H.; Hennink, W. E. *J. Controlled Release* **1997**, *49*, 59-69.
- (57) Schallon, A.; Jérôme, V.; Walther, A.; Synatschke, C. V.; Müller, A. H. E.; Freitag, R. *React. Funct. Polym.* **2010**, *70*, 1-10.
- (58) Majewski, A. P.; Schallon, A.; Jérôme, V.; Freitag, R.; Müller, A. H. E.; Schmalz, H. *Biomacromolecules* **2012**, *13*, 857-866.

## 3.6 Supporting Information

### 3.6.1 Additional Experimental Section

**Materials.** *sec*-Butyllithium (*sec*-BuLi, Acros, 1.3 M in cyclohexane/hexane: 92/8) and the phosphazene base *t*-BuP<sub>4</sub> (Fluka, 1 M in hexane) were used without further purification. Butadiene (Rießner-Gase, 2.5) was passed through columns filled with molecular sieves (4 Å) and basic aluminum oxide and stored over dibutylmagnesium (1 M solution in heptane, Aldrich). 2-Vinylpyridine (2VP, Aldrich) was degassed, stirred with triethylaluminium (1 M solution in hexanes, Aldrich) for 2 h and condensed on a high vacuum line into storage ampoules. *tert*-Butyl methacrylate (*t*BMA, BASF) and *N,N*-dimethylaminoethyl methacrylate (DMAEMA, Aldrich) were purified in a similar manner, except that DMAEMA was stirred with tri-*n*-octylaluminium (25 wt.% solution in hexanes, Aldrich) instead of triethylaluminium. Ethylene oxide (Linde, 3.0) was condensed onto CaH<sub>2</sub> and stirred at 0 °C for 3 h before being transferred into a glass ampoule for storage. Prior to use the ethylene oxide was additionally purified over *n*-BuLi and condensed into a sampling ampoule. THF (Sigma-Aldrich) was distilled from CaH<sub>2</sub> and K metal under dry nitrogen. 1,1-Diphenylethylene (Aldrich, 97%) was purified by stirring with *sec*-BuLi under N<sub>2</sub> followed by distillation. *N,N,N',N',N''*-Pentamethyldiethylenetriamine (PMDETA) was purchased from Aldrich and distilled and degassed. CuBr (Aldrich) was treated with pure acetic acid and filtered. The monomers for ATRP and RAFT, which were *tert*-butyl methacrylate, styrene and *N,N*-dimethylaminoethyl methacrylate were destabilized by passing through a column filled with basic alumina. Azidoacetyl chloride was synthesized according to literature<sup>1</sup> and cryodistilled on a high vacuum line before use. The synthesis of 4-cyano-4-methyl-4-thiobenzoylsulfanyl-butyric acid 3-azidopropyl ester<sup>2</sup> and *N*-(1-heptyloctyl)-*N'*-(hexyl-6'-azido)-perylene-3,4,9,10-tetracarboxylic acid bisimide<sup>3</sup> is described in literature. If not stated elsewhere, all other chemicals were purchased in analytical grade and used as received. The dialysis membranes used for purification were purchased from Roth (SpectraPor) with molecular weight cut-offs (MWCO) of 1 000 g/mol and 50 000 g/mol.

**Polymerization.** *Model-Reaction of click-DPE toward P2VP-Homopolymer.* To investigate the endcapping efficiency of click-DPE toward living poly(2-vinylpyridine) anions, a test

polymerization was performed, similar to the previous reported procedures with the same setup. The monomer was directly initiated with *sec*-BuLi in THF at -70 °C and polymerized for 45 minutes. After withdrawing a precursor, the click-DPE was added in a two-fold excess regarding the living chain ends. Finally the polymerization was terminated with 1 mL of degassed methanol after 1 h. The polymer was isolated by precipitation in water.

*Azido-functionalized Poly(ethylene oxide) (PEO-N<sub>3</sub>) using Anionic Ring Opening Polymerization.* The azido-functionalized poly(ethylene oxide) was synthesized *via* anionic ring opening polymerization in THF using the phosphazene base *t*-BuP<sub>4</sub> as additive and azidoacetyl chloride as functional termination agent.<sup>1</sup> First, the initiator diphenylhexyllithium was directly generated by reaction of *sec*-BuLi with 1.1 equiv of 1,1-diphenylethylene at -70 °C. Afterward, the purified ethylene oxide was added *via* ampoule and allowed to stir for 30 min. As ethylene oxide is not able to polymerize with lithium as counterion and only monoaddition takes place, the reaction mixture was warmed up to 10 °C and then the phosphazene base (2 equiv relative to the initiator) was added to the reaction mixture.<sup>4,5</sup> After polymerization at 50 °C for 15 h the temperature was lowered to 20 °C again and the freshly cryo-distilled azidoacetyl chloride (2 equiv with regard to the living anionic chain ends) was added. The reaction mixture was stirred for two additional hours. Finally, the product was isolated by precipitation in cold diethyl ether and subsequent drying in a vacuum oven.

*Azido-end-functionalized Polymers via Atom Transfer Radical Polymerization (ATRP).* All polymerizations were conducted according to standard polymerization procedures.<sup>6</sup> To obtain azido-functionalized poly(*tert*-butyl methacrylate) (PtBMA-N<sub>3</sub>) homopolymer, 2-bromo-isobutyric acid 3-azidopropylester was chosen as initiator. This was synthesized according to literature.<sup>7</sup> The azido-functionalized initiator (205 mg, 0.82 mmol) and *t*BMA (5.95 g, 41.8 mmol) were mixed with 11 mL anisole in a screw cap glass, sealed with a rubber septum and purged with nitrogen for 10 minutes. Then, CuBr (118 mg, 0.82 mmol) was added and the solution was de-oxygenated with nitrogen for further 15 min. Degassed ligand PMDETA (42 mg, 0.82 mmol) was injected and the polymerization was conducted at 40 °C. Samples were withdrawn with time to follow the conversion *via* <sup>1</sup>H NMR. The reaction solution was concentrated on a rotary evaporator and redissolved

in cyclohexane. The cyclohexane solution was filtrated over a column filled with silica gel to remove copper. After precipitation in a mixture of water/methanol (40/60, v/v) it was filtrated and dried in a vacuum oven.

As the ATRP of styrene with the already mentioned azido-functionalized ATRP initiator was not successful, the polymers were synthesized in a two step reaction. First, styrene was polymerized in anisole with CuBr as catalyst, PMDETA as ligand and methyl-2-bromopropionate as initiator at 100 °C. After purification and precipitation in methanol the bromine endgroup was transformed into an azide function by treatment with 10 equivalents of sodium azide (relative to the bromine endgroups) in a 1/1 mixture of DMF/THF (v/v). The polymer was isolated by precipitation in methanol and extensively washed with water to remove residual  $\text{NaN}_3$ .<sup>8</sup>

*Azido-end-functionalized Poly(N,N-dimethylaminoethyl methacrylate) (PDMAEMA- $\text{N}_3$ ) via RAFT.* A mixture of 4-cyano-4-methyl-4-thiobenzoylsulfanyl-butyric acid 3-azidopropyl ester (67 mg, 0.186 mmol), DMAEMA (1.5 g, 9.54 mmol), AIBN (6 mg, 0.038 mmol) and 8.6 mL of anisole in a screw cap glass, sealed with a rubber septum, were purged with nitrogen for 30 minutes. Afterward, the polymerization flask was put in an oil bath at 65 °C. Samples were withdrawn to follow the conversion *via*  $^1\text{H}$  NMR. For termination, the reaction mixture was cooled down and exposed to air. The polymer was purified by precipitation in cold *n*-hexane, dried in a vacuum oven and subsequently freeze-dried from dioxane solution.

**Characterization.** *Size Exclusion Chromatography (SEC).* SEC measurements were performed on a set of 30 cm SDV-gel columns of 5  $\mu\text{m}$  particle size having a pore size of  $10^5$ ,  $10^4$ ,  $10^3$ , and  $10^2$  Å with refractive index and UV ( $\lambda = 260$  nm) detection. THF was used as eluent at a flow rate of 1 mL/min using toluene as internal standard. The system was calibrated with PS, PtBMA, 1,4-PB and PEO standards. The characterization of the PDMAEMA homopolymer was conducted with a set of a PSS GRAM columns (7  $\mu\text{m}$  particle size with pore sizes of  $10^2$  and  $10^3$  Å) with DMAc containing 0.5 M LiBr as mobile phase. The flow rate was 0.7 mL/min and the columns were thermostatted at 60 °C. The Agilent 1200 system was equipped with RI and UV ( $\lambda = 260$  nm) detection. The diblock copolymers and miktoarm star terpolymers containing PDMAEMA were characterized with another system using THF with additional 0.25 wt% tetrabutylammonium bromide

(TBAB) as eluent. This was necessary as the polybutadiene block of the miktoarm star terpolymers is insoluble in DMAc. The Waters instrument was equipped with PSS SDV gel columns (30 x 8 mm, 5  $\mu\text{m}$  particle size) with  $10^5$ ,  $10^4$ ,  $10^3$ ,  $10^2$  Å pore sizes, using RI and UV detection ( $\lambda = 254$  nm). The flow rate was 0.5 mL/min and the obtained data were evaluated applying a PS calibration.

*<sup>1</sup>H NMR Spectroscopy.* <sup>1</sup>H NMR spectra were recorded on a Bruker Ultrashield 300 spectrometer at an operating frequency of 300 MHz. CDCl<sub>3</sub> was used as solvent and tetramethylsilane as internal standard.

*Matrix-Assisted Laser Desorption Ionization Time-of-Flight Mass Spectrometry (MALDI-ToF MS).* MALDI-ToF MS analysis was performed on a Bruker Reflex III apparatus equipped with a N<sub>2</sub> laser ( $\lambda = 337$  nm) at an acceleration voltage of 20 kV. *trans*-2-[3-(4-*tert*-Butylphenyl)-2-methyl-2-propenylidene]malononitrile (DCTB, Fluka, 99.0%) was used as a matrix material and silver trifluoroacetate (AgTFA, Sigma-Aldrich, 99.99%) as ionization agent. Samples were prepared from THF solution by mixing matrix, polymer, and salt in a ratio of 20/5/1 (v/v).

*Fourier Transform Infrared (FTIR) Spectroscopy.* FTIR spectra were recorded using a Perkin Elmer Spectrum 100 FTIR spectrometer.

*UV-Vis spectroscopy.* UV-vis spectra were recorded on a Hitachi 3000 spectrophotometer. For the measurement of the living anions of 1-[(4-(*tert*-butyldimethylsilyl)ethynyl)phenyl]-1-phenylethylene a  $5 \times 10^{-4}$  M solution of the DPE compound in distilled THF was prepared under inert gas and 2 equiv of *sec*-BuLi were added. The solution was directly transferred into a specially designed cuvette, which can be evacuated and closed under nitrogen atmosphere. Upon injection into the cuvette the intensity of the color decreased, so that the actual concentration for the measurements is lower than  $5 \times 10^{-4}$  M. Nevertheless, the concentration was high enough to obtain the desired UV-vis spectra of the living anions.

## 3.6.2 Additional Figures

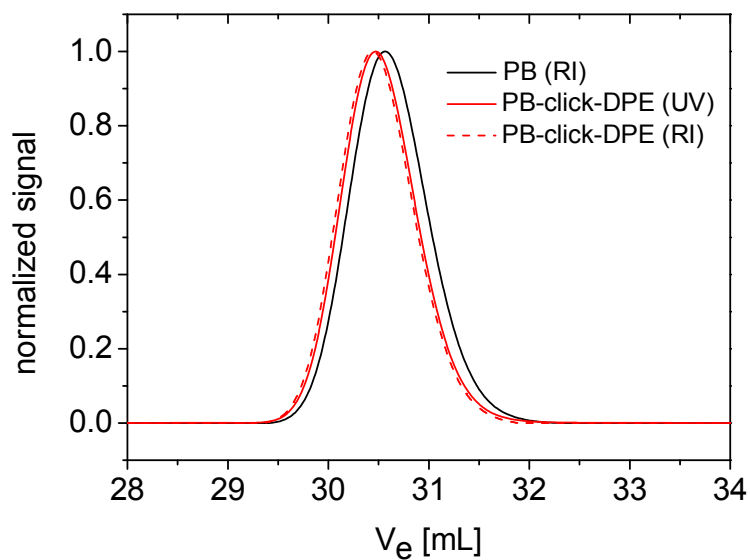


**Figure 3-S1.** SEC traces of precursor samples from polybutadiene before (black) and after reaction with 1-[(4-(*tert*-butyldimethylsilyl)ethynyl)phenyl]-1-phenylethylene (red).

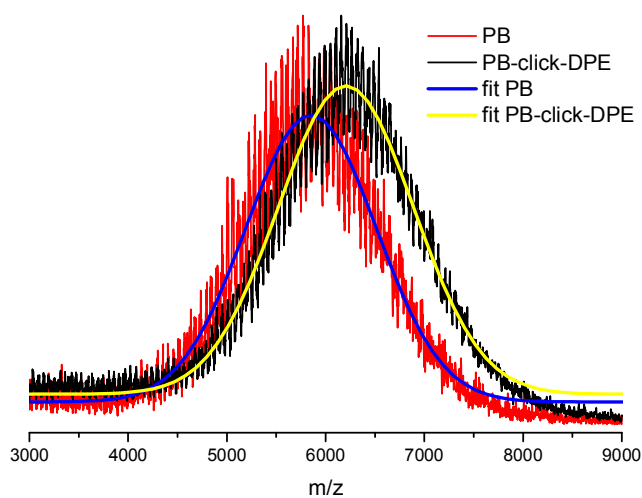


**Figure 3-S2.** MALDI-ToF MS spectra of polybutadiene before (red) and after reaction with 1-[(4-(*tert*-butyldimethylsilyl)ethynyl)phenyl]-1-phenylethylene (black) and their corresponding fits.

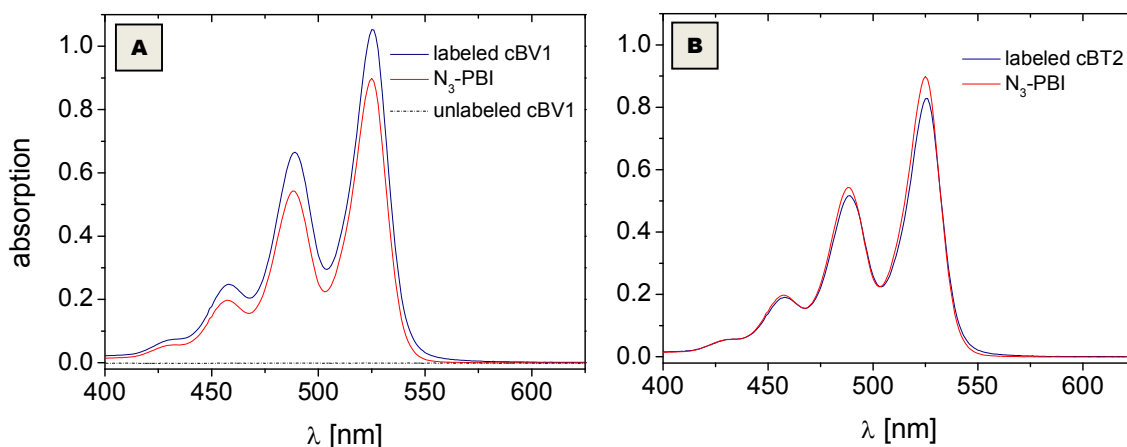


**Figure 3-S3.** UV-vis spectra of  $10^{-5}$  M  $\text{CH}_2\text{Cl}_2$  solutions of *N*-(1-heptyloctyl)-*N'*-(hexyl-6'-azido)-perylene-3,4,9,10-tetracarboxylic acid bisimide ( $\text{N}_3$ -PBI) and the respective perylene-labeled diblock copolymers (A) cBV1 and (B) cBT1.

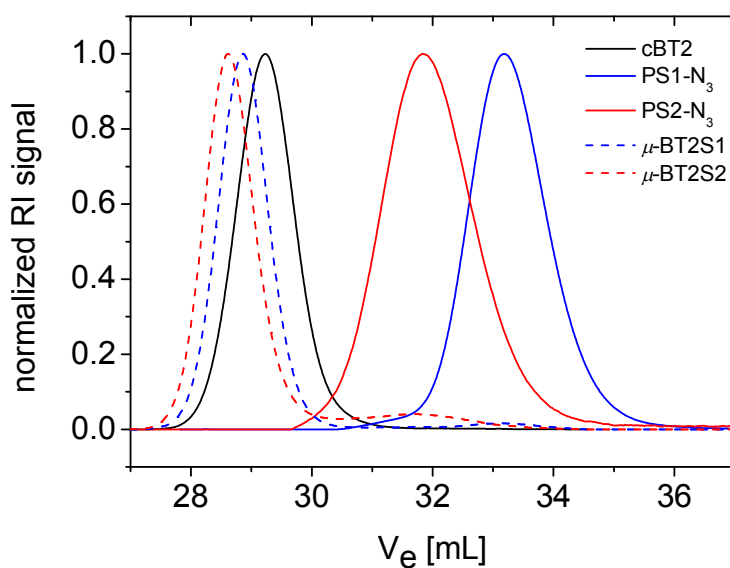


**Figure 3-S4.** THF-SEC (RI signal) of alkyne-functionalized diblock cBT2, azido functionalized polystyrenes (PS1-N<sub>3</sub>, PS2-N<sub>3</sub>) and the corresponding ABC miktoarm star terpolymers ( $\mu$ -BT2S1 and  $\mu$ -BT2S2) obtained after equimolar click reaction for 24 h.

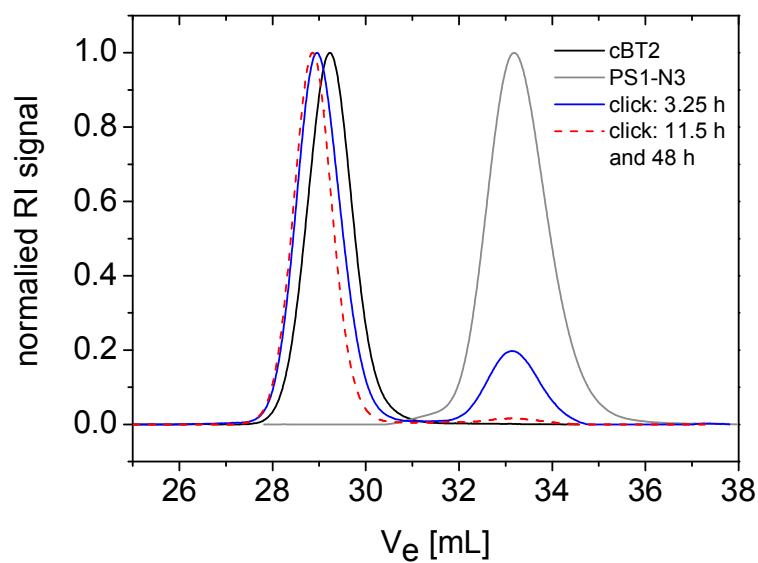


**Figure 3-S5.** THF-SEC (RI-signal) of samples withdrawn during equimolar click reaction between cBT2 and PS1-N<sub>3</sub> after 3.25 h (-), 11.5 h and 48 h (---).

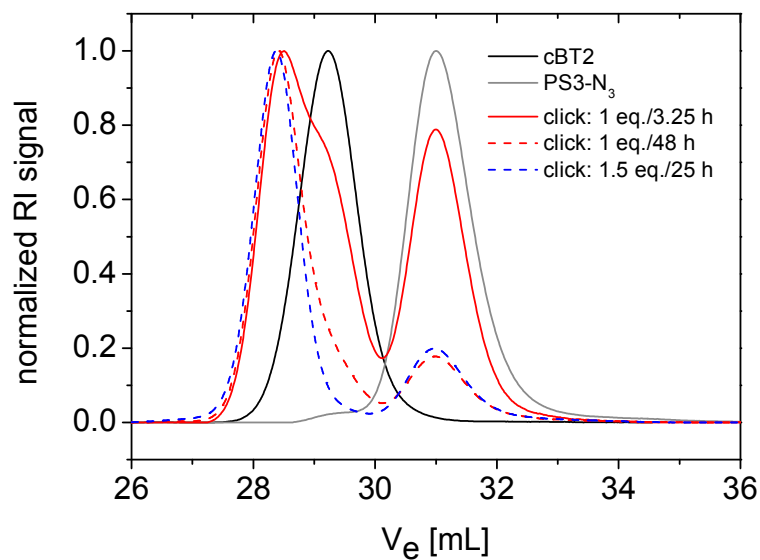


**Figure 3-S6.** THF-SEC (RI signal) of click reaction between cBT2 and PS3-N<sub>3</sub> with further addition of 0.5 equiv PS3-N<sub>3</sub> 48 h after start of the click reaction. 25 h after addition of the second portion of PS3-N<sub>3</sub> a final sample was taken for SEC.

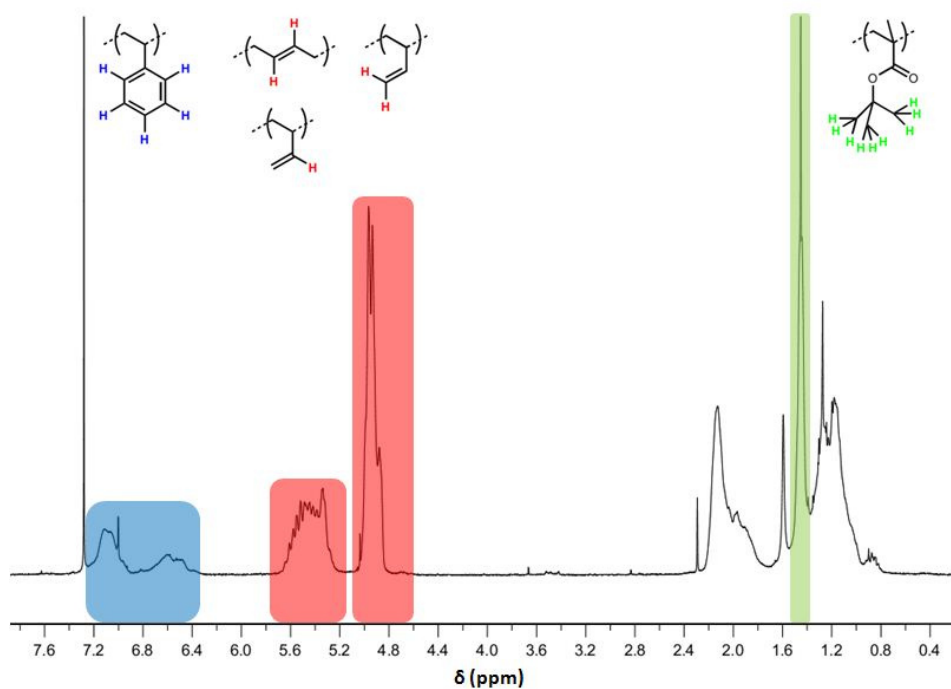


**Figure 3-S7.**  $^1\text{H}$  NMR spectrum of  $\mu\text{-BT1S1}$  in  $\text{CDCl}_3$ . The characteristic signals of the respective polymer blocks are highlighted.

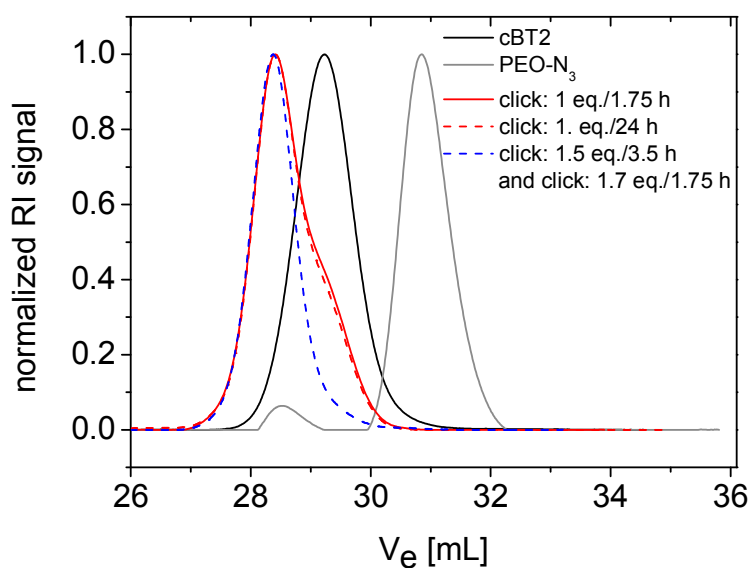


**Figure 3-S8.** THF-SEC (RI signal) of click reaction between cBT2 and  $\text{PEO-N}_3$  with stepwise addition of  $\text{PEO-N}_3$ . Further 0.5 equiv  $\text{PEO-N}_3$  were added 24 h after start of the click reaction and 3.5 h later further 0.2 equiv  $\text{PEO-N}_3$  were added. The corresponding reaction times are relative to the point of addition of a further  $\text{PEO-N}_3$  portion. The excess of  $\text{PEO-N}_3$  is not visible as the PEO is adsorbed at the silica column used for removing copper catalyst.

### 3.6.3 Test Polymerization with P2VP and Click-DPE

In contrast to polybutadienyl and polystyryl lithium, the living anion of poly(2-vinylpyridine) is less nucleophilic and hence, the initial assumption was that it is not able to attack excess click-DPE. This would lead to the desired diblock copolymers with only one click-DPE at the block junction. If the 2VP would incorporate more units of click-DPE the diblock would carry more than one alkyne function, which would result in star terpolymers with more than three arms. Hogen-Esch *et al.* reported that the endcapping of P2VPLi with unsubstituted DPE is an equilibrium reaction<sup>9</sup> and that even the addition of a large excess of 1,1-diphenylethylene to living poly(2-vinylpyridine) does not lead to a significant endcapping of the anion.<sup>10</sup> Hirao *et al.* showed that silyl-protected hydroxyl-functionalized DPE, 1-(3-*tert*-butyldimethylsilyloxymethylphenyl)-1-phenylethylene did not undergo copolymerization with living poly(2-vinylpyridine) anions.<sup>11</sup> Also, in previous tests on the endcapping of poly(2-vinylpyridine) with DPE functionalized polybutadiene macromonomers, we found no significant coupling between the two polymeric chains. Therefore, a test reaction was conducted to verify whether the alkyne-substituted click-DPE can be attacked by a living P2VPLi as a result of the altered electronic configuration of the DPE derivative. For this purpose, 2-vinylpyridine was polymerized in THF at -70 °C with *sec*-BuLi as initiator, yielding a molecular weight of 5 000 g/mol. Then, a 2-fold excess of the alkyne-functionalized click-DPE was added at the same temperature. Directly after injection, the color of the P2VPLi anion changed from red to violet giving a first qualitative indication for the addition of the click-DPE. <sup>1</sup>H NMR determined the degree of alkyne functionalization as around 98%.

MALDI-ToF MS supported a quantitative end-functionalization (Figure 3-S9A). Before addition the  $M_n$  of the P2VP was 4 750 g/mol. After 1 h reaction with click-DPE the  $M_n$  increased to 5 230 g/mol. These values indicate that click-DPE addition took place quantitatively, considering the accuracy of the determination method. Moreover, the molecular weight distribution shifted completely and in the case of the reflectron mode a distinct shift of the individual peaks was noticeable (Figure 3-S9B). This proved the presence of only one species after addition of click-DPE. The shift of the peaks with a difference of around 4.5 g/mol is in good agreement with the expected 3 g/mol difference ( $M(2VP) = 105.14$  g/mol,  $M(\text{click-DPE}) = 318.53$  g/mol;  $\Delta = 318.53$  g/mol - 3 x 105.14

g/mol = 3.11 g/mol). For example, the peak at  $m/z = 4791.6$  in the P2VP precursor, *i.e.* before addition of click-DPE, corresponds to 44 repeating units of 2VP with a *sec*-butyl residue and  $\text{Ag}^+$  as counter-ion. This is in accordance with the theoretical  $m/z$  value of 4792.0. In the spectrum after click-DPE addition, the modified P2VP with the same number of repeating units and an additional click-DPE was detected at  $m/z = 5111.1$ . Also here, this value is consistent with the expected 5110.5 (= 4792.0 + 318.5). Hence, click-DPE adds to living poly(2-vinylpyridine) anions quantitatively, in contrast to other DPE derivatives reported in literature.

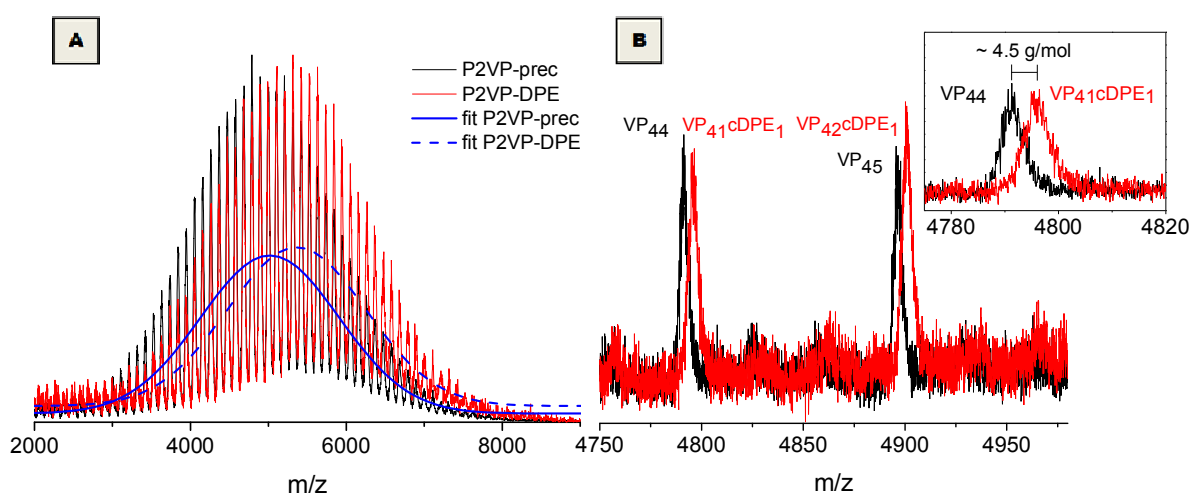


**Figure 3-S9.** MALDI-ToF MS spectra of poly(2-vinylpyridine) before (black line) and after addition of click-DPE (cDPE, red line), recorded in linear (A) and reflectron mode (B) with  $\text{AgTFA}$  as ionization agent.

In summary, the anion of the alkyne-functionalized DPE has a nucleophilicity comparable to P2VPLi, whereas the anion of unsubstituted DPE is more nucleophilic than P2VPLi. One reason for this might be the electron withdrawing effect of the *tert*-butyldimethylsilyl group which leads to a reduction of the electron density in the double bond and thus decreases the nucleophilicity of the click-DPE as compared to the unsubstituted DPE.<sup>12</sup> As the living anion of the click-DPE is able to start the polymerization of P2VP and click-DPE also adds to P2VPLi, it is possible to copolymerize P2VP and click-DPE. Therefore, if the click-DPE is used in a slight excess and not under equimolar conditions, the DPE derivative might also be incorporated in or most probably after consumption of all 2VP monomer at the end of the P2VP block for the aimed PB-*b*-P2VP diblock copolymers. In contrast to butadiene and styrene, methacrylates are known to be not nucleophilic enough to attack diphenylethylene and its derivatives.<sup>13,14</sup> Conse-

quently, monomers like *t*BMA and DMAEMA can be polymerized as second block to obtain well-defined diblock copolymers with exactly one alkyne function at the block junction.

Due to the altered reactivity of the click-DPE toward living P2VP-Li compared to other DPE derivatives both  $\alpha$ - and  $\omega$ -alkyne modified P2VP homopolymers are accessible. In addition, alkyne mid-functionalized diblock copolymers with poly(2-vinylpyridine) as first and a methacrylate-type monomer as second block can be synthesized.

### 3.6.4 Characterization of $\omega$ -Azido Homopolymers

Besides the qualitative proof of the presence of an azido function *via* IR (Figure 3-S10) the degree of azide-functionalization was additionally tried to be quantified by MALDI-ToF MS or  $^1\text{H}$  NMR.

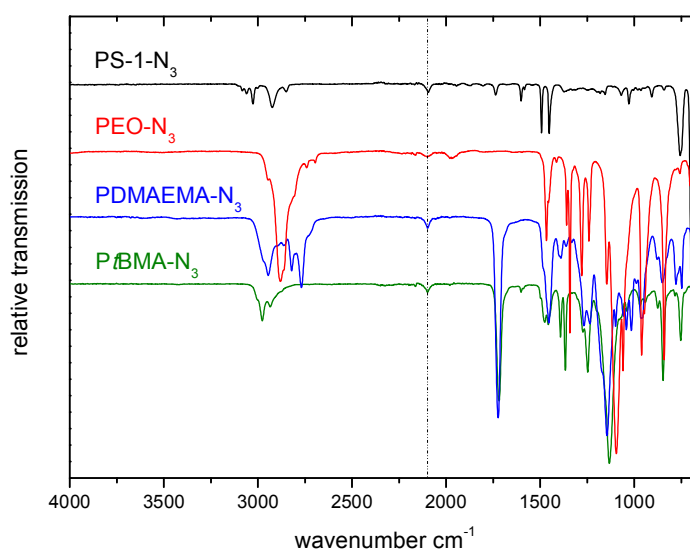


**Figure 3-S10.** IR spectra of the corresponding homopolymers show the characteristic stretching vibration of the azido group at  $\sim 2098\text{ cm}^{-1}$ .

In case of PS1-N<sub>3</sub> and PEO-N<sub>3</sub> mass spectrometry in reflectron mode was possible. The respective spectra are shown in Figure 3-S11 and 3-S12. In the case of the azido-terminated PS1-N<sub>3</sub> only a small peak resembling the desired functional species is present. As already reported in literature formation of postsource metastable ions from azido-functionalized polymers is possible under high laser powers in reflectron mode.<sup>15</sup>

Therefore, by comparing the relative intensities of the azido-functionalized species and the corresponding metastable ion with the intensity of the unfunctionalized species, as main population the azido-terminated polystyrene is clearly concluded. We have to mention here that the peak at the left side of the proton-terminated polystyrene could not be assigned clearly.

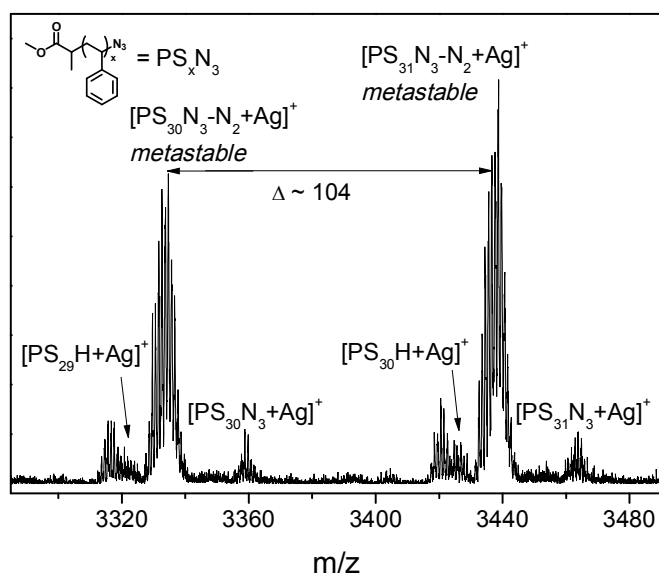


**Figure 3-S11.** MALDI-ToF MS spectrum of PS1-N<sub>3</sub> recorded in reflectron mode with AgTFA as ionization agent.

In the MALDI spectrum of PEO-N<sub>3</sub> (Figure 3-S12) two series of peaks were present. Here, the main population resembles the azido-terminated PEO. The second population could be attributed to azido-terminated PEO with a proton as counter ion. Another possible explanation could be deduced from SEC measurements, where a small second peak at lower elution volume was detected (around 6 wt.%, see Figure 3-S13). This originates from minimal residual amounts of thionyl chloride which was used for the synthesis of the azidoacetyl chloride and is hard to remove completely despite thorough purification.<sup>1</sup> This population cannot take part in the click reaction. For the molecular characterization, only the major peak was taken into consideration. The molecular weight determined by MALDI-ToF MS was consistent with the values from SEC. Therefore, the second population in MALDI can be interpreted as the lower molecular weight side of the coupling product with thionyl chloride. Even though the main peak corresponds to the de-

sired functionalized PEO, one has to notice that chains where  $\text{HN}_3$  was eliminated ( $\Delta \sim 43$  g/mol) and chains which were terminated with a proton instead of the acid chloride ( $\Delta \sim 5$  g/mol) would not be distinguishable and could possibly be present.

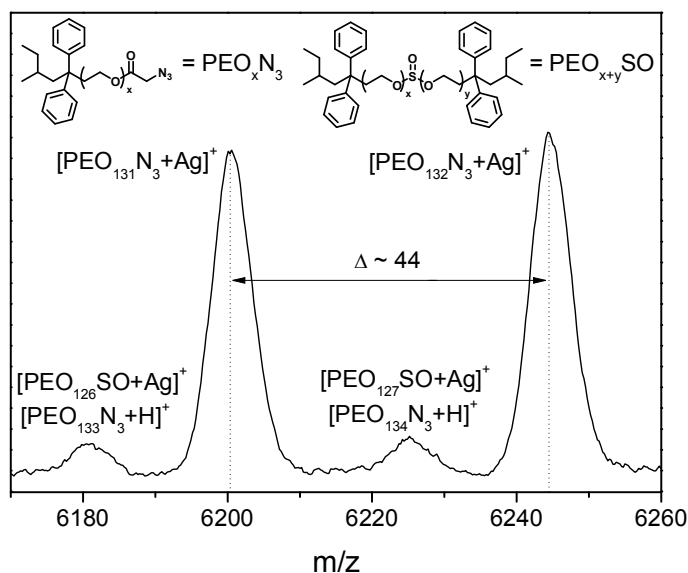


**Figure 3-S12.** MALDI-ToF MS spectrum of PEO- $\text{N}_3$  recorded in reflectron mode with AgTFA as ionization agent.

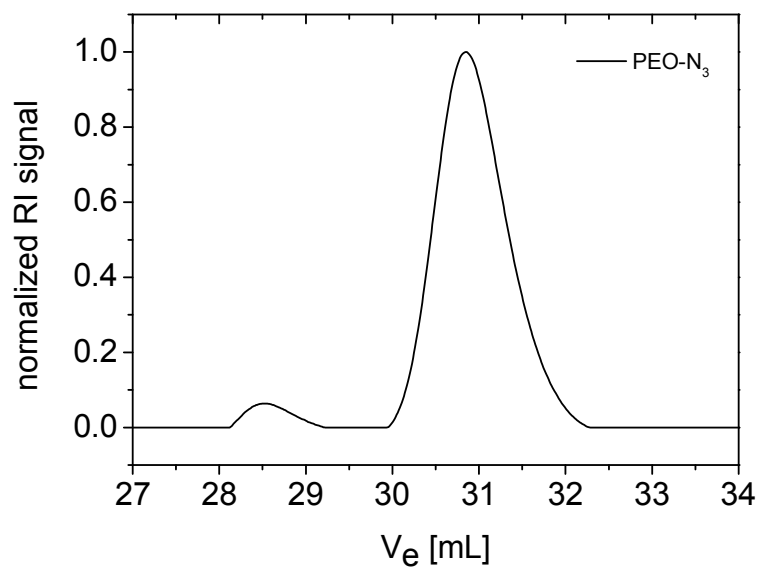


**Figure 3-S13.** THF-SEC (RI signal) of azido-functionalized poly(ethylene oxide).

Both in case of PtBMA- $\text{N}_3$  and PDMAEMA- $\text{N}_3$  endgroup determination was not possible *via* MALDI-ToF MS. In contrast to PtBMA- $\text{N}_3$  for the DMAEMA homopolymer calculation

of the degree of azido-functionalization was possible from the characteristic signals in the  $^1\text{H}$  NMR spectrum (Figure 3-S14). According to the calculated value of approximately 96 %, quantitative azido-functionalization of the polymer was assumed.

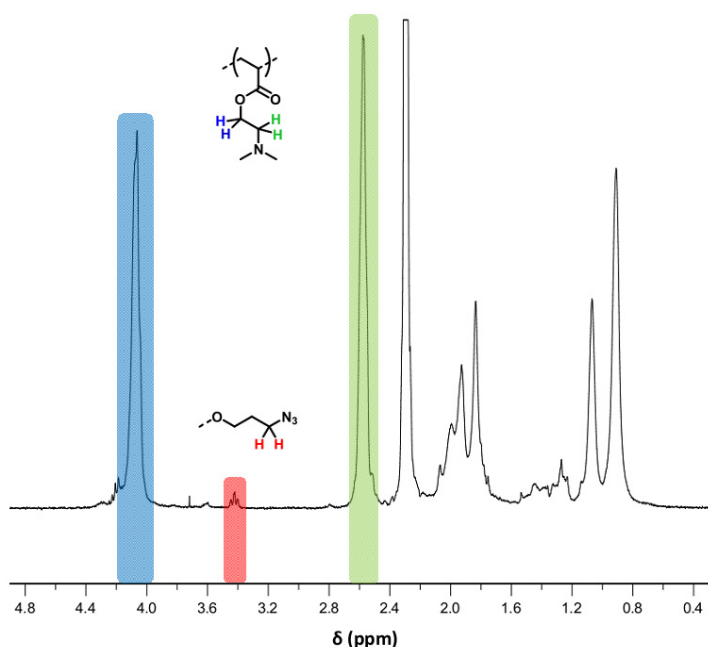


**Figure 3-S14.**  $^1\text{H}$  NMR spectrum of PDMAEMA- $\text{N}_3$  in  $\text{CDCl}_3$ . The characteristic signals of the monomer unit and chain transfer agent are highlighted.

### 3.6.5 Click Reaction with $\omega$ -Azido-Functionalized Poly(*tert*-butyl methacrylate)

Since we also synthesized an alkyne-functionalized diblock with DMAEMA as second block (cBD), a  $\mu$ -BDT miktoarm star terpolymer was achievable by click reaction with the azido-terminated PtBMA. Similar to the click reactions with PDMAEMA- $\text{N}_3$ , the reaction conditions were not optimized. The ligation was conducted for 3 days with 1.3 equiv of azido-functionalized homopolymer to guarantee 100 % conjugation of the diblock. The SEC of the click-product after dialysis in methanol/isopropanol (2/1 v/v) is shown in Figure 3-S15 and a complete shift of the molecular weight distribution of the miktoarm star terpolymer compared to the diblock terpolymer was detected. This demonstrates the efficiency of our approach. Even though we were not able to remove all excess homopolymer, we showed that formation of a  $\mu$ -BDT miktoarm star terpolymer is possi-

ble starting from two different diblock copolymers. The molecular parameters of the obtained ABC miktoarm star terpolymer are summarized in Table 3-3.

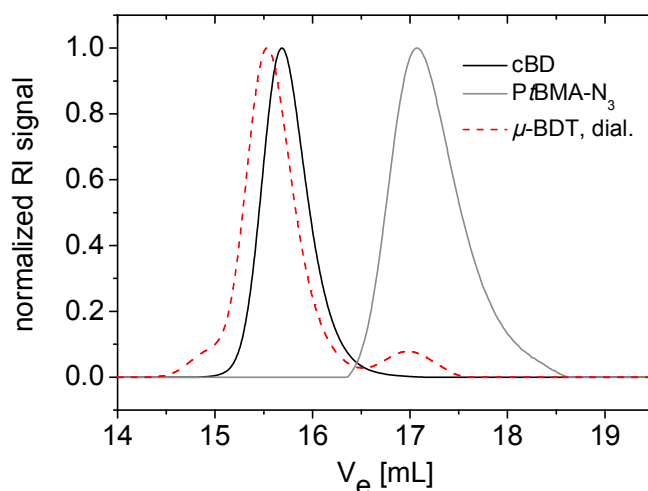


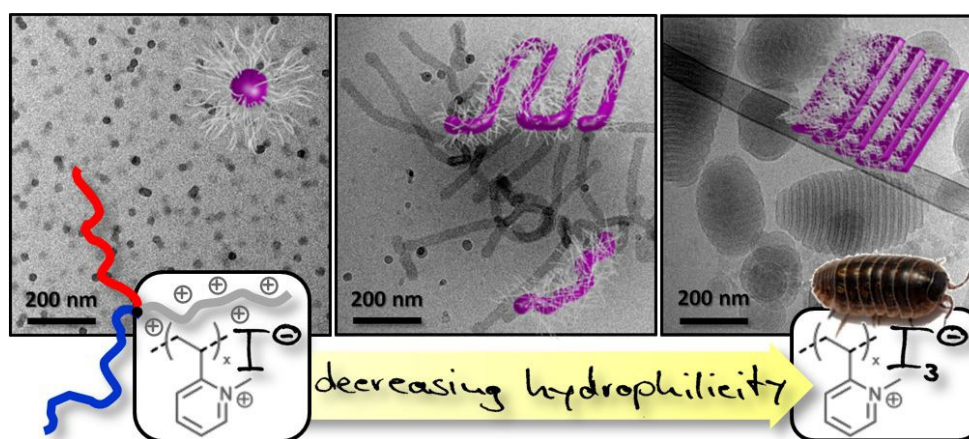
**Figure 3-S15.** Salt-THF-SEC (RI-signal) of the  $\mu$ -BDT miktoarm star terpolymers obtained after click reaction of alkyne-functionalized diblock cBD with the azido functionalized PtBMA-N<sub>3</sub>.

### 3.6.6 References

- (1) Reinicke, S.; Schmalz, H. *Colloid Polym. Sci.* **2011**, *289*, 497-512.
- (2) Gondi, S. R.; Vogt, A. P.; Sumerlin, B. S. *Macromolecules* **2007**, *40*, 474-481.
- (3) Lang, A. S.; Neubig, A.; Sommer, M.; Thelakkat, M. *Macromolecules* **2010**, *43*, 7001-7010.
- (4) Eßwein, B.; Möller, M. *Angew. Chem.* **1996**, *108*, 703-705.
- (5) Schmalz, H.; Lanzendörfer, M. G.; Abetz, V.; Müller, A. H. E. *Macromol. Chem. Phys.* **2003**, *204*, 1056-1071.
- (6) Schmalz, A.; Hanisch, M.; Schmalz, H.; Müller, A. H. E. *Polymer* **2010**, *51*, 1213-1217.
- (7) Mantovani, G.; Ladmiral, V.; Tao, L.; Haddleton, D. M. *Chem. Commun.* **2005**, 2089-2091.
- (8) Coessens, V.; Matyjaszewski, K. *J. Macromol. Sci.* **1999**, *36*, 667-679.
- (9) Helary, G.; Fontanille, M.; Khan, I. M.; Hogen-Esch, T. E. *Makromol. Chem.* **1989**, *190*, 341-348.
- (10) Yin, R.; Hogen-Esch, T. E. *J. Polym. Sci., Part A: Polym. Chem.* **1994**, *32*, 363-368.
- (11) Hirao, A.; Murao, K.; Abouelmagd, A.; Uematsu, M.; Ito, S.; Goseki, R.; Ishizone, T. *Macromolecules* **2011**, *44*, 3302-3311.
- (12) Tsuda, K.; Ishizone, T.; Hirao, A.; Nakahama, S.; Kakuchi, T.; Yokota, K. *Macromolecules* **1993**, *26*, 6985-6991.
- (13) Hsieh, H. L.; Quirk, R. P. In *Anionic Polymerization: Principles and Practical Applications*; Marcel Dekker: New York, 1996.
- (14) Quirk, R.; Yoo, T.; Lee, Y.; Kim, J.; Lee, B. *Adv. Polym. Sci.* **2000**, *153*, 67-162.
- (15) Li, Y.; Hoskins, J. N.; Sreerama, S. G.; Grayson, S. M. *Macromolecules* **2010**, *43*, 6225-6228.

## 4 – Counterion-Mediated Hierarchical Self-Assembly of an ABC Miktoarm Star Terpolymer

Andreas Hanisch, André H. Gröschel, Melanie Förtsch, Markus Drechsler, Hiroshi Jinnai,  
Thomas M. Ruhland, Felix H. Schacher, and Axel H. E. Müller



**ABSTRACT:** Directed self-assembly processes of polymeric systems represent a powerful approach for the generation of structural hierarchy in analogy to biological systems. Herein, we utilize triiodide as a strongly polarizable counterion to induce hierarchical self-assembly of an ABC miktoarm star terpolymer comprising a polybutadiene (PB), a poly(*tert*-butyl methacrylate) (PtBMA), and a poly(*N*-methyl-2-vinylpyridinium) (P2VPq) segment. Hereby, the miktoarm architecture in conjunction with an increasing ratio of triiodide *versus* iodide counterions allows for a stepwise assembly of spherical micelles as initial building blocks into cylindrical structures and superstructures thereof. Finally, micrometer-sized multicompartments with a periodic lamellar fine structure are observed, for which we introduce the term “woodlouse”. The counterion-mediated decrease in hydrophilicity of the corona-forming P2VPq block is the underlying trigger to induce this hierarchical structure formation. All individual steps and the corresponding intermediates toward these well-defined superstructures were intensively studied by scattering and electron microscopic techniques, including transmission electron microtomography.

**Keywords:** ABC Miktoarm Star Terpolymer, Hierarchical Self-Assembly, Polyelectrolytes, Multicompartments Micelles, Poly(2-vinylpyridine)

## 4.1 Introduction

Self-assembly processes<sup>1</sup> are of particular importance in biological systems for the formation of defined, monodisperse structures on multiple length scales.<sup>2</sup> Inspired by nature, low molecular weight amphiphiles (*e.g.*, surfactants and lipids) represent a class of well-studied compounds.<sup>3,4</sup> However, amphiphilic AB diblock copolymers are superior to their low molecular weight analogues as they combine high functionality and compositional diversity as well as different assembly pathways to obtain a multitude of thermodynamically or kinetically controlled morphologies in solution.<sup>5,6</sup> Such structures are of high potential use for a variety of applications in the field of nano- and biotechnology.<sup>7-11</sup>

During the last decade, advances in polymer synthesis and macromolecular conjugation reactions led to progressively complex polymer architectures and compositions being accessible. The introduction of an additional block to obtain ABC triblock terpolymers results in the formation of nanostructures of increased complexity.<sup>12,13</sup> Three individual building blocks give rise to core-shell-corona structures as well as core- or corona-compartmentalized aggregates *via* adequate choice of a selective solvent. For example, different multicompartiment micelles could be fabricated by direct dispersion of ABC miktoarm star terpolymers in a selective solvent for one of the blocks. Depending on the relative block ratios, “hamburger” micelles, segmented worm-like micelles, nanostructured vesicles, and raspberry-like micelles were observed for different systems.<sup>14-17</sup>

Examples of compartmentalized structures from linear triblock terpolymers involve, for example, materials containing fluorocarbon segments<sup>18,19</sup> or interpolyelectrolyte complexes.<sup>20,21</sup> Interestingly, also the formation of double and triple helices from achiral (meth)acrylate-type triblock terpolymers was reported.<sup>22</sup> In this case, Liu and co-workers showed that for distinct solvent mixtures a time-dependent hierarchical transition from spherical to cylindrical micelles and finally helices took place. Jiang *et al.* obtained giant segmented worm-like micelles from linear ABC triblock terpolymers with a poly(2-vinylpyridine) block by decreasing the solubility of the latter.<sup>23</sup> Recently, we presented a general concept for the generation of multicompartiment micelles from linear ABC triblock terpolymers by a step-by-step reduction of the conformational degrees of freedom.<sup>24</sup> Using different ternary systems and compositions, reversible step-growth

polymerization of multicompartment micelles as well as the solution-based preparation of Janus structures could be demonstrated.<sup>25</sup> Another strategy for creating hierarchical and compartmentalized structures is crystallization-driven self-assembly.<sup>26-28</sup> This facile process enables the construction of A-B, A-B-A, and, very recently, even A-B-C block co-micelles *via* the stepwise addition of crystalline-coil polyferrocenylsilane block copolymers. Furthermore, cylindrical A-B-C block co-micelles were shown to act as giant amphiphiles and assembled into micrometer-sized supermicelles, similar to micelle formation from linear ABC triblock terpolymers.<sup>28</sup> In all these systems, the formation of hierarchical superstructures is directed by the terpolymer architecture,<sup>14-17</sup> the self-assembly pathway,<sup>24,25</sup> electrostatic interactions,<sup>20,21</sup> the solvent composition,<sup>22,23,28</sup> or certain characteristics of one of the segments, like perfluorinated<sup>18,19</sup> or crystallizable blocks.<sup>26-29</sup>

Apart from that, the use of additives represents an interesting alternative trigger. Wooley, Pochan, and co-workers exploited the interaction of triblock terpolymers consisting of polystyrene, poly(methyl acrylate) and poly(acrylic acid) (PAA) segments with divalent organic counterions. By adjusting the electrostatic complexation of the PAA block with diamines in mixtures of THF and water, spherical, cylindrical, and disk-like micelles as well as the corresponding superstructures or toroidal aggregates were generated.<sup>30-34</sup> The nature and the overall amount of the added diamine in combination with solvent quality or the block sequence were identified as main set screws.<sup>35</sup>

In this contribution, we present the hierarchical self-assembly of a polybutadiene-*arm*-poly(*N*-methyl-2-vinylpyridinium iodide)-*arm*-poly(*tert*-butyl methacrylate) miktoarm star terpolymer ( $\mu$ -BVqT) in aqueous solution. We show that the hydrophilicity of the corona-forming poly(*N*-methyl-2-vinylpyridinium iodide) block (P2VPq) is controlled by the nature of the counterion, which is crucial in directing the self-assembly process. The addition of iodine results in the formation of triiodide counterions from iodide. By increasing the amount of triiodide in the system, the assembly of spherical micelles into cylindrical micelles, followed by intertwining of these cylinders into compact particles, resembles a step-by-step increase in hierarchy. All intermediate steps are visualized using (cryogenic) transmission electron microscopy (cryo-TEM and TEM). In this context, we found a unique micellar morphology, which we call “woodlouse” struc-

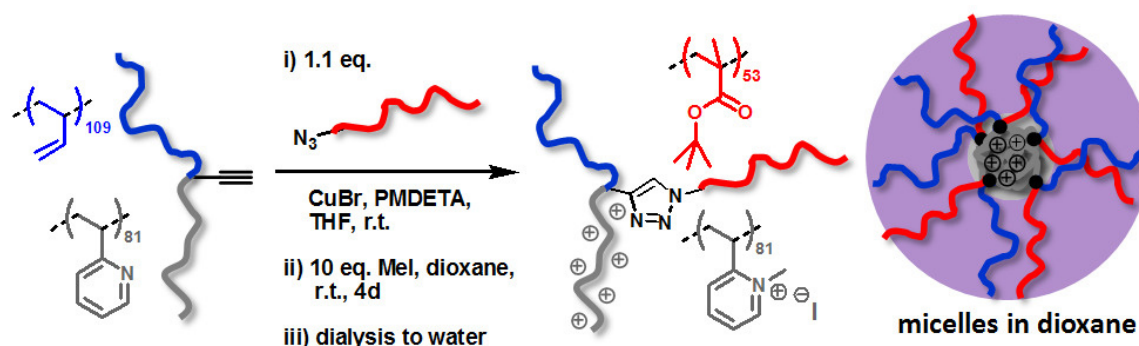
ture. This example of a compartmentalized block copolymer particle was comprehensively studied by (cryo-)TEM and TEM tomography (TEMT), enabling a detailed illustration of the underlying mechanism and the final superstructure morphology.

## 4.2 Results and Discussion

### 4.2.1 Synthesis and Characterization of the PB-P2VP-PtBMA Miktoarm Star Terpolymer

The precursor polybutadiene-*arm*-poly(2-vinylpyridine)-*arm*-poly(*tert*-butyl methacrylate) miktoarm star terpolymer ( $\mu$ -BVT) was synthesized *via* a combination of anionic polymerization, atom transfer radical polymerization (ATRP), and azide-alkyne Huisgen cycloaddition in a similar way as has been reported recently by our group (Scheme 4-1).<sup>36</sup> Details on the synthetic procedure and material characterization are given in the Supporting Information. The polymer  $\mu$ -B<sub>109</sub>V<sub>81</sub>T<sub>53</sub> has a number-average molecular weight,  $M_n = 22.2$  kg/mol and a polydispersity index of 1.07. The subscripts denote the degrees of polymerization of the corresponding blocks.

Besides optional post-polymerization functionalization of the polybutadiene block (PB), for example, *via* thiol-ene chemistry<sup>37</sup> or crosslinking,<sup>38</sup>  $\mu$ -BVT features a pH-responsive poly(2-vinylpyridine) block (P2VP)<sup>39</sup> and a poly(*tert*-butyl methacrylate) segment (PtBMA) that can be hydrolyzed to poly(methacrylic acid), a weak polyelectrolyte.<sup>40</sup> For the research reported here, we transformed P2VP into the strong polyelectrolyte poly(*N*-methyl-2-vinylpyridinium iodide) (P2VPq) by quaternization with methyl iodide.<sup>21</sup>



**Scheme 4-1.** Route for the synthesis of  $\mu$ -BVqT and color code of the arms.

### 4.2.2 Self-Assembly Behavior of $\mu$ -BVqT

Inspired by the diversity of structures formed by ABC miktoarm star terpolymers in solution,<sup>14,15,17,41</sup> we were interested in the self-assembly of  $\mu$ -BVT in aqueous media. First, the P2VP block was quaternized in dioxane using methyl iodide to yield  $\mu$ -BVqT.<sup>21</sup> Owing to the low solubility of P2VPq in dioxane, micelles with an ionic P2VPq core and a corona consisting of PB and PtBMA are formed as shown by TEM (Figure 4-1A) and DLS (Supporting Information Figure 4-S2). In TEM only the micellar core ( $d_{\text{core}} \sim 7.5$  nm, compared to  $R_{\text{n,app}} = 12.5$  nm from DLS) is visible due to the high electron density of the iodide counterions in P2VPq. We assume a mixed corona of PB and PtBMA as a consequence of the miktoarm star architecture (Scheme 4-1).

The as-prepared  $\mu$ -BVqT micelles were subsequently transferred into water, leading to an inversion of the solubility of the constituting segments. P2VPq now forms the corona, whereas both PB and PtBMA are hydrophobic and build up the core. From simple solubility tests of the respective homopolymers, we know that during dialysis the PB block collapses first, followed by PtBMA. At the same time, P2VPq swells and stabilizes the whole aggregate. At about 20 vol% water in dioxane, P2VPq is fully solubilized while PtBMA and PB are insoluble. This is supported by the respective solubility parameters,  $\delta$ , in (MPa)<sup>1/2</sup>: PB<sub>90%1,2</sub>: 17.4;<sup>42</sup> PtBMA: 18.0;<sup>43</sup> 1,4-dioxane: 20.5;<sup>44</sup> water: 47.9.<sup>44</sup> Consequently, during the dialysis to water, an intermediate stage will be reached where the solubility of the constituting blocks is inverted and micelles with a P2VPq corona are formed.

In terms of micellar morphology, two limiting cases were observed after dialysis to water under comparable preparation conditions: in one case, spherical micelles were found in TEM (Figure 4-1B,  $d_{\text{micelle}} = 24.5 \pm 2.0$  nm). We propose that these consist of a mixed PB/PtBMA core and a P2VPq corona. In another batch, a completely different morphology was observed. TEM and cryo-TEM images revealed rather complex aggregates with an internal lamellar fine structure (Figure 4-1C,D and Figure 4-S3). The particles feature an elongated barrel-like shape and were mostly in a size range of 200-500 nm. Due to their shape, we named those substructured particles “woodlouse” aggregates. In some cases, also spherical, multilamellar aggregates were observed (see inset

in Figure 4-1C). We were initially puzzled by the fact that two entirely different morphologies evolved from the same  $\mu$ -BVqT system. Partial crosslinking of the PB block was excluded by repeated SEC measurements of  $\mu$ -BVT after some months of storage.

Two questions arise from these observations: (A) Which parameter is responsible for these different levels of structure formation, and (B) how are the individual  $\mu$ -BVqT star terpolymer molecules arranged within such a highly periodic structure? We first dissect the underlying mechanism of superstructure formation and later present a more detailed structural investigation of the “woodlouse” aggregates.

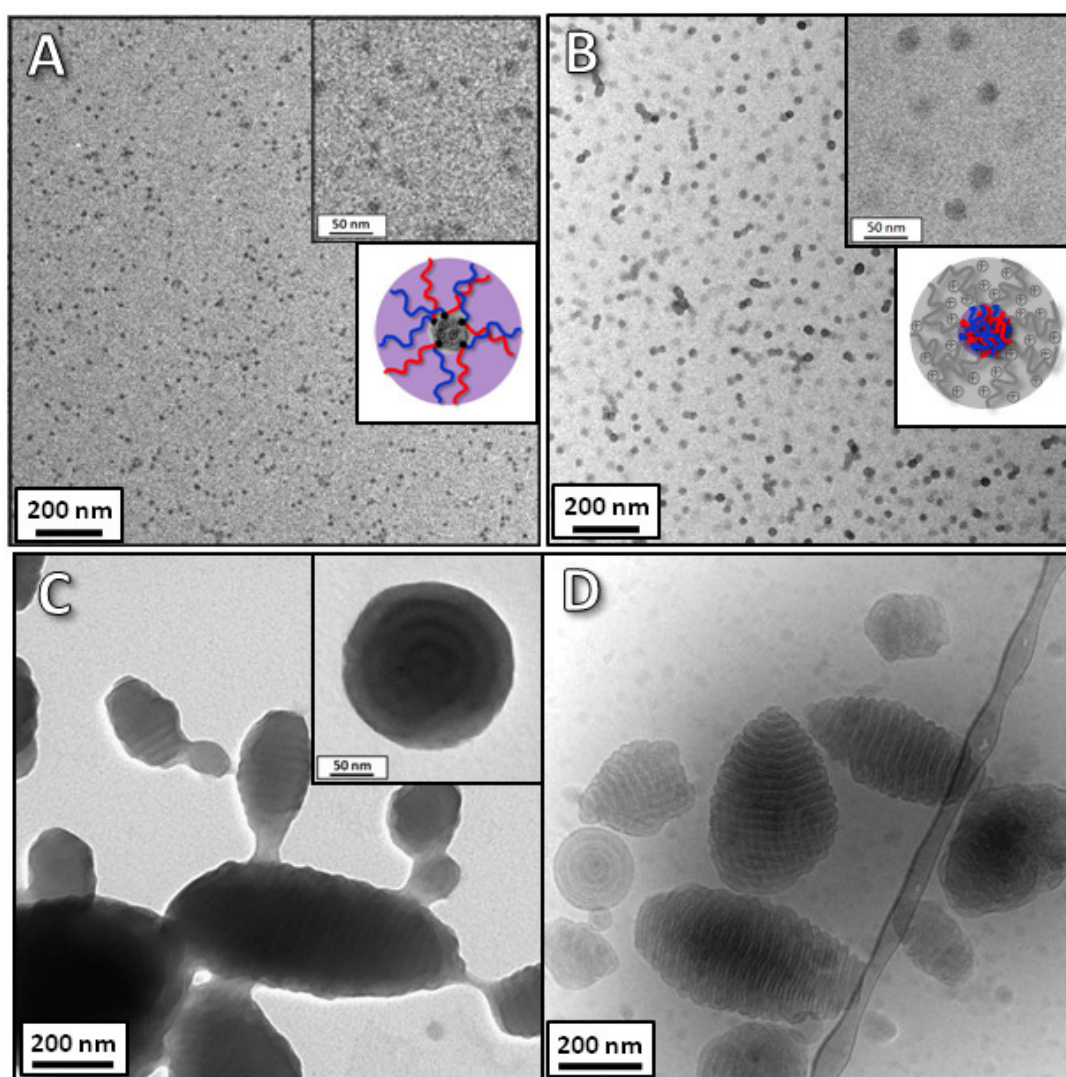


**Figure 4-1.** TEM micrographs of spherical micelles of  $\mu$ -BVqT in dioxane (A) and the aggregates obtained thereof by dialysis to water: inverted spherical micelles (B) and “woodlouse” aggregates (C) with a corresponding cryo-TEM image (D). Concentrations: 0.2 g/L (B), 0.1 g/L (C) and  $\sim$ 0.6 g/L (D). As no additional staining was performed, the contrast emerges solely from the iodide counterion of the P2VPq phase.

Before studying the self-assembly mechanism in detail, we were interested in the influence of the polymer structure itself on the obtained aggregates. Therefore, materials of similar chemical composition but different architecture were used, more precisely a diblock copolymer ( $B_{109}V_{81}$ ) and a linear triblock terpolymer ( $B_{1108}V_{142}T_{93}$ ). However, only ill-defined aggregates were obtained from these linear polymers after quaternization and comparable preparation conditions (see representative micrographs of the triblock terpolymer in Figure 4-S4). These findings demonstrate that the miktoarm architecture itself is an important criterion for the hierarchical self-assembly into substructured particles. Hadjichristidis and co-workers already showed both experimentally and by theoretical investigations that the micellization behaviour of  $A_2B$  miktoarm systems is different compared to linear  $AB$  diblock copolymers due to topological differences at the core-corona interface.<sup>45</sup>

#### 4.2.2.1 Hierarchical Superstructure Formation

According to cryo-TEM (Figure 4-1D), the “woodlouse” aggregates can be preliminarily described as either superstructures from cylindrical micelles or lamellae. However, as the periodicity of these particles is in the size range of the diameter observed for the spherical micelles in Figure 4-1B, we assume these to act as primary building blocks. The different structures observed would then simply correspond to different levels of superstructure formation. Regarding the overall morphology, similar structures, such as laterally structured vesicles or layered structures, were already predicted by simulations of  $ABC$  miktoarm star terpolymers with two solvophobic blocks.<sup>46,47</sup> More detailed information about the superstructure formation was gained from investigations of the intermediate structures obtained under comparable preparation conditions (Figure 4-2A). Here, the aggregates clearly consist of several intertwined and partially wrapped-up cylindrical micelles. Again, the dimensions of the cylinders are in good agreement with the diameter of the spherical micelles ( $d_{\text{cylinder}} = 27.5 \pm 2.5$  nm, as compared to  $d_{\text{micelle}} = 24.5 \pm 2.0$  nm), which corroborates the assumption that spherical micelles are indeed the underlying building blocks. Staining with  $OsO_4$  reveals a PB (or mixed PB/PtBMA) core of the cylinders (Figure 4-2B). Subsequently, these cylinders align in a parallel, ribbon-like fashion, which we regard as another intermediate level on the way toward highly periodic

lamellar “woodlice”. Our assumption of a mixed PB/PtBMA core is further supported by the calculated phase segregation parameter, for PB/PtBMA,  $\chi N \sim 1.1$ .<sup>48</sup> According to the theory of phase separation for diblock copolymers, this is in the disordered regime due to the small degrees of polymerization for our system.<sup>49,50</sup> Furthermore, cast films of PB-*b*-PtBMA diblock copolymers with comparable molecular weights did not show any phase separation in the bulk (results not shown).

Cryo-TEM shows highly intertwined and entangled cylindrical micelles (Figure 4-2C). A surprisingly highly regular packing of individual cylinders can be observed in some cases, highlighted in the insets and gray scale analysis of Figure 4-2C. Remarkably, some of the structures show long-range order and dimensions of up to 1  $\mu\text{m}$  in length.

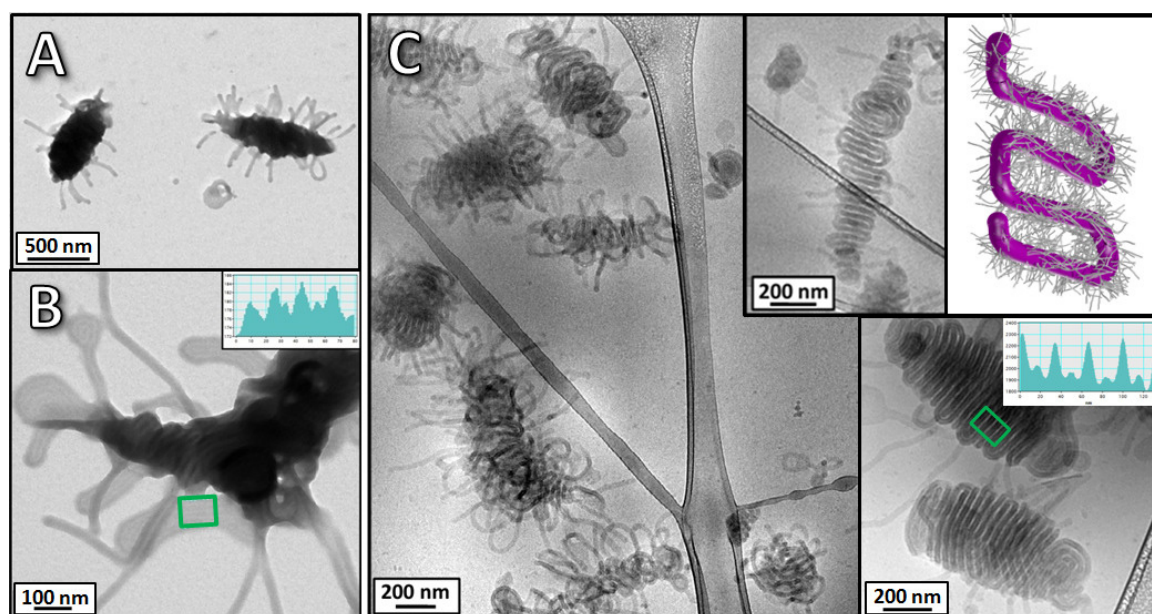


**Figure 4-2.** TEM (A,B) and cryo-TEM micrographs (C) of intermediate micellar structures from  $\mu$ -BVqT in aqueous solution. The final polymer concentration was 0.2 g/L for TEM and 0.4 g/L for cryo-TEM. Whereas for (A) no staining was performed, the sample in (B) was stained with  $\text{OsO}_4$ . Here, the gray scale analysis of the highlighted area reveals a ribbon-like arrangement of cylinders.

With the example of these intermediate structures, we further investigated the influence of two other parameters during the process of structure formation (for details see Supporting Information): (i) the solutions were thermally annealed, and (ii) the time in between quaternization in dioxane and dialysis to water was increased to up to 1 month. Whereas thermal annealing did not result in higher structural perfection at all, the structures were slightly more developed after 1 month in dioxane prior to dialysis (Figure 4-S5). Nonetheless, from all the TEM investigations discussed so far, different

levels of hierarchy from approximately 20 nm to 1  $\mu$ m were detected for  $\mu$ -BVqT, starting from spherical micelles (level 1), which aggregate into cylinders (level 2), and finally into multilamellar superstructures (level 3).

#### 4.2.2.2 Importance of the Nature of the Counterion

It is known that methyl iodide can undergo photodecomposition to form free iodine.<sup>51</sup> Based on this fact, one hypothesis for the observed structural differences was the presence of varying amounts of elementary iodine in the respective dioxane solutions. In combination with the iodide counterion, this then forms triiodide,  $I_3^-$ , which is a strongly polarizable counterion,<sup>52,53</sup> already described for quaternized poly(4-vinylpyridine) (P4VPq).<sup>54</sup> The increased hydrophobicity of P2VPq with triiodide as counterion is clearly demonstrated by DLS measurements of a P2VPq homopolymer in water (Figure 4-S8). Higher amounts of added iodine led to an increase of the hydrodynamic radii, which we assign to hydrophobic interactions. In contrast, chloride or methyl sulfate counterions did not lead to the formation of any hierarchically structured aggregates for the  $\mu$ -BVqT system (see Supporting Information).

However, addition of supplementary iodine to an aqueous micellar solution of  $\mu$ -BVqT (Figure 4-1B) did not induce significant structural changes. We attribute this to two different reasons: first, owing to the reduced core dynamics, rearrangement processes are suppressed. Second and most important, iodine itself is not soluble in water but is solubilized by the formation of triiodide. However, the iodide counterions are mainly located within the micellar corona – approximately 90% according to investigations of quaternized poly(*N,N*-dimethylaminoethyl methacrylate) stars<sup>55</sup> – leading to very slow exchange processes. Consequently, we added different amounts of iodine to the  $\mu$ -BVqT solution in dioxane prior to dialysis. The samples were allowed to equilibrate for 2 h to guarantee the conversion to triiodide and then dialyzed to water. Already the addition of 0.08 equiv of  $I_2$  induced drastic structural changes (Figure 4-3A), as worm-like micelles and elongated superstructures were observed in contrast to spherical micelles in the absence of iodine (Figure 4-1B). Again, the diameter of these cylindrical aggregates refers to the initially observed spherical micelles ( $d_{\text{micelle}} = 24.5 \pm 2.0$  nm and  $d_{\text{cylinder}} = 25.0 \pm 2.0$  nm). The corona-forming P2VPq block can be clearly distinguished in cryo-TEM

(inset in Figure 4-3A and Figure 4-S9A). For 0.25 equiv, almost exclusively superstructures from aggregated and intertwined cylindrical micelles are found. In addition, fewer protrusions and an increased tendency of the cylinders to form meander-like structures were observed. The inset in Figure 4-3B depicts an area where the cylinders form pre-stages of ribbons. When 0.42 equiv of  $I_2$  was added, “woodlouse” aggregates with a periodic, multilayered structure were found ( $d_{\text{lam}} = 19.5 \pm 1.0$  nm, Figure 4-3C). This pattern is also clearly visible in cryo-TEM, accompanied by areas where the lamellae are less densely packed (highlighted area in Figure 4-S9B) or particles which seem to be trapped as cylindrical superstructures (inset in Figure 4-S9B). A minor fraction of micelles and cylinders was found, as well.

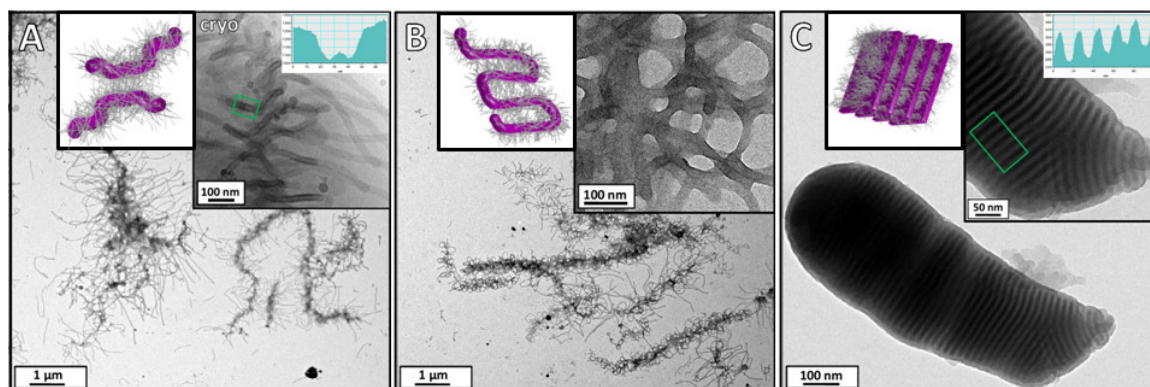


**Figure 4-3.** TEM micrographs from 0.2 g/L aqueous micellar solutions of  $\mu$ -BVqT after dialysis in the presence of different amounts of iodine. The solutions were prepared with 0.08 (A), 0.25 (B) and 0.42 (C) equiv of iodine with respect to P2VPq monomer units. The inset in (A) shows the corresponding cryo-TEM micrograph. The schematic illustrations represent the dominant aggregate morphology. For the respective sample without additional iodine, see Figure 4-1B.

To evaluate this lamellar packing within the particles in more detail, additional SAXS measurements were conducted from freeze-dried powders of the sample depicted in Figure 4-3C. The SAXS pattern (Figure 4-4A) shows peaks with a  $q$  ratio of 1:2:3, representing the [100], [200], and [300] reflections, thus confirming the lamellar structure. The long period was calculated to  $d_{\text{lam}} = 20.0 \pm 1.5$  nm and is in perfect agreement with the values observed in TEM ( $d_{\text{lam}} = 19.5 \pm 1.0$  nm). In the SAXS pattern for the intermediate structure (as shown in Figure 4-S5), the reflections were less pronounced (Figure 4-4B). This was already expected from the TEM images (Figure 4-S5), which reveal a less regular arrangement. However, the assumption of an overall lamellar morphology and the presence of the [100] and [200] reflections allow the calculation of  $d_{\text{lam}} = 22.5 \pm 2.0$

nm. Comparable long periods from “woodlice” and aggregated cylinders further support our proposed mechanism of superstructure formation.

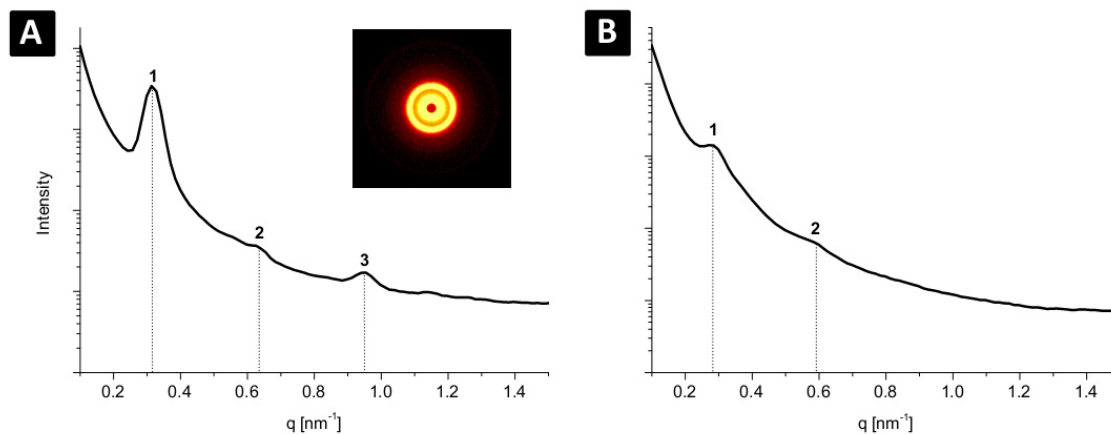


**Figure 4-4.** SAXS pattern of a freeze-dried powder from (A) the “woodlouse” structure (Figure 4-3C) and (B) the intermediate structure (Figure 4-S5). The integer numbers indicate the relative reflex positions, and the inset in A depicts the scattering pattern observed at the 2D detector.

These different levels of hierarchical self-assembly of  $\mu$ -BVqT into spherical micelles (level 1), followed by cylinders (level 2), superstructures thereof and, finally, the stacking and back-folding of lamellae into compartmentalized micrometer-sized polymer particles (level 3) can be attributed to surface minimization due to decreasing hydrophilicity of the P2VPq corona triggered by the presence of triiodide counterions. Hereby, the superstructure formation of lamellae *via* folding (or stacking) is supported by simulations on the sphere-cylinder-lamellae transition in diblock copolymer systems.<sup>56</sup> As we are most probably dealing with non-equilibrium structures formed during dialysis, the folded cylinders are supposed to be transient intermediate structures on the way toward lamellae. Similar structures were already reported for linear ABC triblock terpolymers, where either the addition of a diamine in the case of poly(acrylic acid) as solubilizing block<sup>31-33</sup> or changes in solvent quality for the P2VP corona<sup>23</sup> triggered the formation of superstructures. However, in our case, this is clearly caused by changes in the polarizability of the counterion, triggered by the addition of iodine. The amount of triiodide represents the essential trigger here. Both the assembly pathway and a delicate balance of iodide/triiodide regulate structural precision and the overall colloidal stability of the substructured particles. Furthermore, here, the well-defined compact structures

clearly evolve through a complex aggregation and fusion *via* cylindrical building units in contrast to the stacking of disk-like structures as reported in literature.<sup>23,31-33</sup> The system presented here is relative simple as no sophisticated preparation pathways utilizing bifunctional additives have to be applied, and the structures are obtained in aqueous solution rather than in solvent mixtures. Also, the directed self-assembly is induced by the monovalent counterion, and the structural integrity is rather unaffected by the pH of the solution (see aggregates within acidic media of pH 3 as depicted in Figure 4-S10)

### 4.2.3 Structural Characterization of “Woodlouse” Aggregates

So far, we have described the triiodide-mediated hierarchical self-assembly of  $\mu$ -BVqT into compartmentalized particles. The highly periodic internal fine structure is confirmed by gray-scale analysis of the TEM micrographs of individual particles (Figure 4-5A). Here, the darker domains correspond to the P2VPq phase containing iodide/triiodide counterions ( $d_1 = 8$  nm), whereas the contrast is inverted when staining with OsO<sub>4</sub> was performed (selective for the PB phase,  $d_2 = 11$  nm Figure 4-5B). The wider lamellae presumably consist of a mixed PtBMA/PB phase as already discussed above.

In cryo-TEM, even three different repeating distances are visible (Figure 4-5C). Here, the observed periodicities can be explained in a similar way. The 8 nm of  $d_2$  represent a mixed phase of PB and PtBMA, which is slightly broadened in TEM ( $d_2$  in Figure 4-5B), as the lamella is flattened and collapsed onto the carbon film in the dried state. On the other hand, both  $d_{1A}$  and  $d_{1B}$  represent P2VPq, serving as the corona for the mixed PB/PtBMA domains. At the interface ( $d_{1A}$ ), the density of P2VPq chains is higher as compared to the periphery ( $d_{1B}$ ), leading to an increased electron density. The proposed chain packing and the corresponding dimensions are illustrated in Figure 4-5D. Hereby, the individual lamellar sheets of the superstructures can either stack (white arrow in Figure 4-5C) or back-fold (black arrows in Figure 4-5C), leading to “open” or “closed” structures at the edge of the particles.

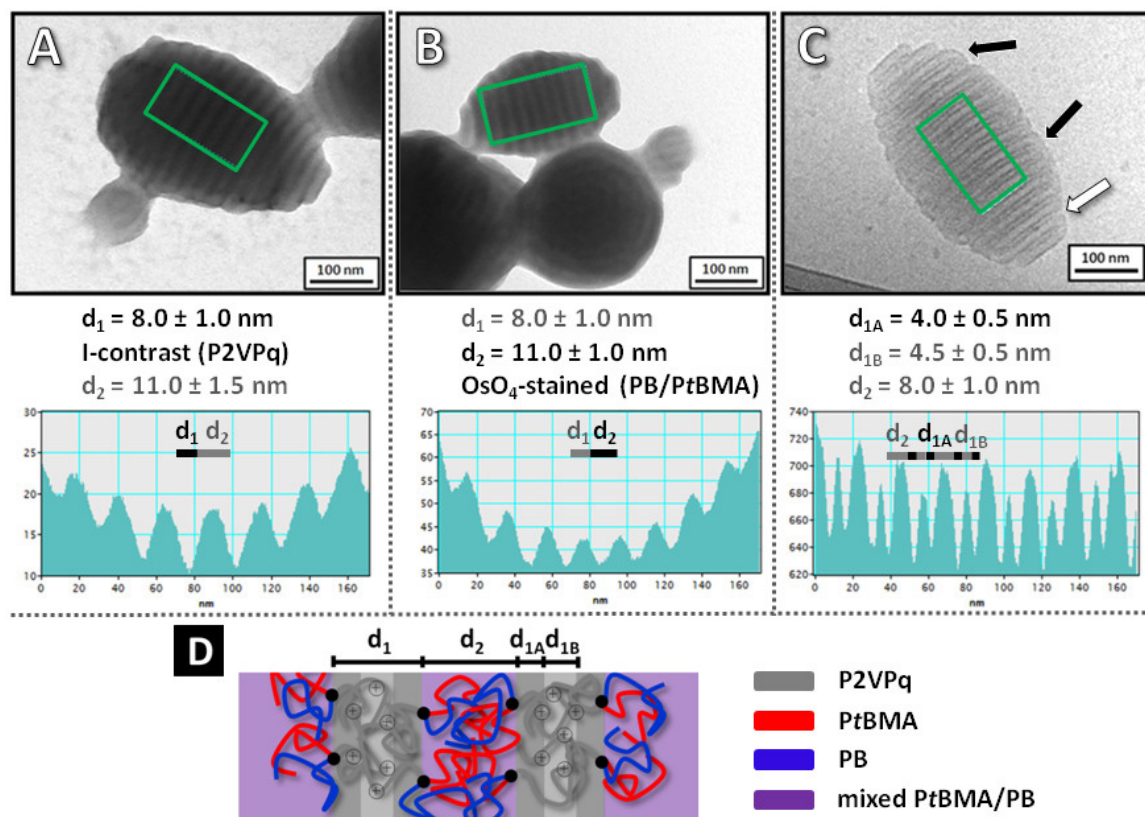


**Figure 4-5.** TEM micrographs of “woodlouse” aggregates of  $\mu$ -BVqT obtained *via* dialysis from dioxane into water (A,B). The concentration was 0.1 g/L. In (A), the contrast emerges solely from the iodide counterion of the P2VPq phase, whereas (B) was stained with OsO<sub>4</sub>. In cryo-TEM (C), a regular pattern of three distances is visible. The concentration was 0.6 g/L. The corresponding gray scale analyses are shown below the micrographs. The proposed arrangement of the miktoarm star terpolymers is illustrated in (D).

We additionally performed cryo-TEM at different tilt angles (Figure 4-S11 and video 4-S3). Thereby, the influence of the woodlouse orientation within the vitrified film was examined, and from the projections at different tilt angles, a circular cross section of the aggregates can be clearly deduced. Again, the presence of flat two-dimensional assemblies can be excluded, which is additionally supported by SEM of the dried particles (Figure 4-S12). In the cryo-TEM tilt images, the internal fine structure is only visible if the particles are oriented perpendicular to the beam direction. If the stage is tilted further, the structural features blur and, finally, disappear completely. The fact that such structural features are only visible under specific viewing angles has already been observed.<sup>57</sup>

Cross-sectional analysis of the “woodlice” within thin film cuts of epoxy resin embedded particles (Figure 4-6A and 4-S13) clearly showed a periodic fine structure, further confirming our assumption that the particles are not hollow. When the sample was treated with OsO<sub>4</sub> (staining of PB, Figure 4-6A), undulated lamellae are visualized as al-

ready discussed for the intermediate structures. The rather undulated shape of the PB/PtBMA lamella might be related to partial demixing of PB and PtBMA, despite the rather low  $\chi N$ . This could be a consequence of the longer DP of the PB block (109) as compared to PtBMA (DP = 53), as well as different  $\chi$  for the PB/P2VP and the PtBMA/P2VP interactions, leading to minimization of the PB/P2VP interface.<sup>48,58</sup> Additionally, from DSC measurements of the miktoarm star terpolymer, the presence of a  $T_g$  at -2 °C also hints toward the presence of a separated PB phase in the bulk state (Figure 4-S14). This leads to a direct PtBMA/P2VPq interface, accompanied by an interface of P2VPq with the adjacent mixed PB/PtBMA phase and, finally, a pure PB domain without a PB/P2VPq interface. The proposed arrangement of the constituting segments is illustrated in Figure 4-6B. Staining with OsO<sub>4</sub> enhances contrast mainly in the PB phase, but also the mixed phase appears darker (Figure 4-6A), whereas the pure PtBMA domains appear brighter. Similarly, the TEM micrographs of the cylindrical intermediate aggregates under the same sample preparation method also hint toward an undulated phase boundary (Figure 4-S6B).

Finally, the volume morphology of the “woodlice” was investigated using TEM tomography (TEMT). We therefore prepared thicker slices (~150 nm) of the resin-embedded sample and performed staining with OsO<sub>4</sub> to provide maximum contrast. In Figure 4-6C, a three-dimensional reconstruction of a slice of a woodlouse particle with view into the lamellar bulk morphology is shown. Additionally, Figure 4-6D shows three different slices of the same reconstruction for a single particle. Both three-dimensional reconstructions clearly confirm the presence of lamellae with an undulated surface throughout the entire sample (also see video 4-S4). Hereby, the formation of well-defined lamellar structures as compared to micellar clusters (observed for linear polymers; see Figure 4-S4) is probably a direct consequence of the miktoarm architecture. In accordance with both theory and experimental work,<sup>59</sup> the increased segmental density has a distinctive effect on the surface curvature and, in the case of our system, facilitates the formation of lamellae with low surface curvature.

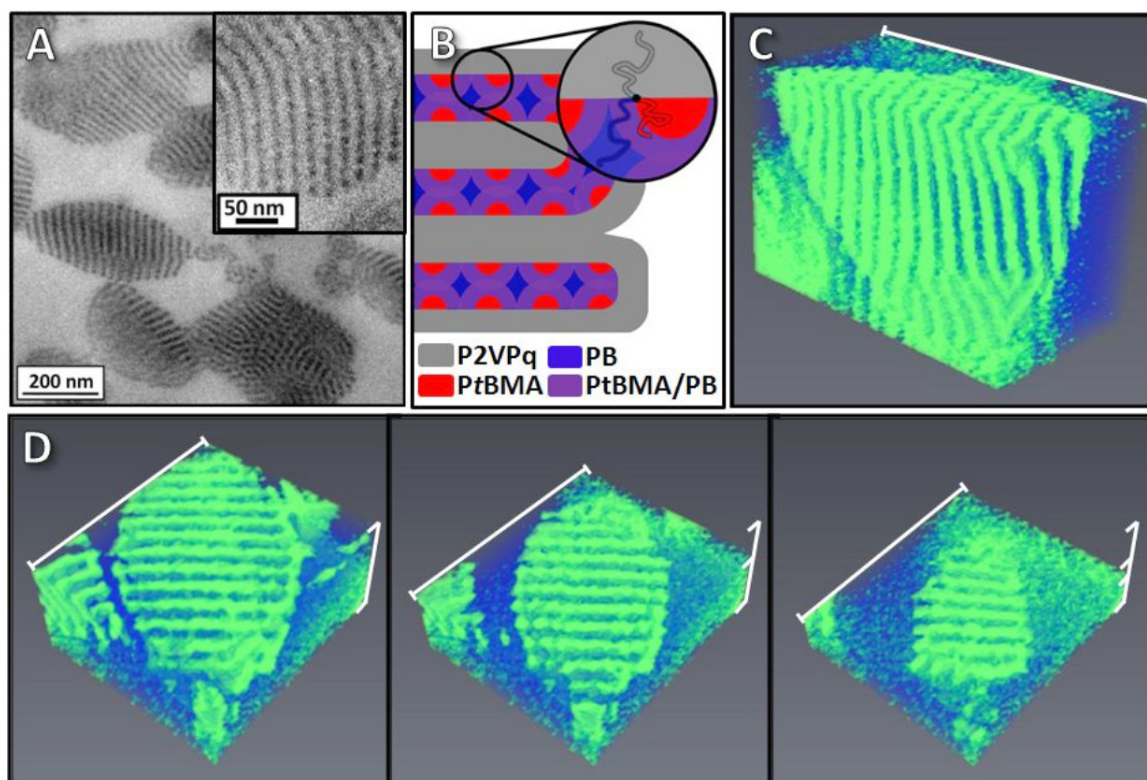


**Figure 4-6.** (A) TEM micrograph of 50 nm thick cuts from freeze-dried and embedded samples of  $\mu$ -BVqT aggregates, stained with  $\text{OsO}_4$ . (B) Schematic illustration of the block arrangement within the “woodlouse” structure is depicted, with the two possibilities of bent (upper part) and stacked lamellae (lower part). The gray areas resemble the P2VPq phase; PtBMA is red, and PB is blue. The violet domains represent a mixed PB/PtBMA phase. TEM tomography 3D reconstructions of a slice of the “woodlouse” structure (C) and cross-sectional analysis of a single particle (D). The tomography images were obtained from a 150 nm thick cut, which was additionally treated with  $\text{OsO}_4$  to selectively stain the mixed PB/PtBMA phase (plotted in green). The approximate length of the long marked edge of the reconstructions is 280 nm in (C) and 220 nm in (D).

### 4.3 Conclusions

We have demonstrated the hierarchical self-assembly of an ABC miktoarm star terpolymer into substructured particles of up to  $1\mu\text{m}$  in size, which we term “woodlouse” particles. Spherical micelles with a mixed PB/PtBMA core and a P2VPq corona act as the basic building blocks (level 1). Stepwise aggregation of these results in cylindrical micelles (level 2), followed by superstructures thereof, and finally compartmentalized particles of up to  $1\mu\text{m}$  in size. These particles feature a highly periodic, lamellar fine structure (level 3). The presence and amount of triiodide as a highly polarizable counterion for the P2VPq corona is an essential trigger to induce this superstructure formation into different levels of hierarchy (Figure 4-7). All intermediates of increasing hierarchy involved on the way to the final “woodlice” are visualized by TEM and cryo-TEM. The iodide/triiodide system is an elegant approach for directing the hierarchical self-assembly of such materials. The nature of the counterion, the miktoarm star architecture, and the assembly pathway are essential parameters and influence structural perfection and the final morphology. To recapitulate, a detailed understanding of the self-assembly mechanism into complex superstructures was obtained, which bear structural similarities to biological systems such as mitochondria. Applying these results to other miktoarm star terpolymer systems with higher segmental incompatibility might lead to completely phase-separated cores and represents an interesting approach to core-compartmentalized structures of complex shape. Further functionalization and modification of these structures will enable the preparation of a variety of stimuli-responsive highly structured materials with defined internal periodicity.

The question arises whether this approach is applicable to other miktoarm star systems containing polycationic segments in general or whether the combination of P2VPq and a “dynamic”, low  $T_g$  segment like PB is a prerequisite. This will be the subject of future work. The use of iodide/triiodide as a setscrew to direct the self-assembly of different materials into well-defined hierarchical superstructures would be advantageous and desirable.

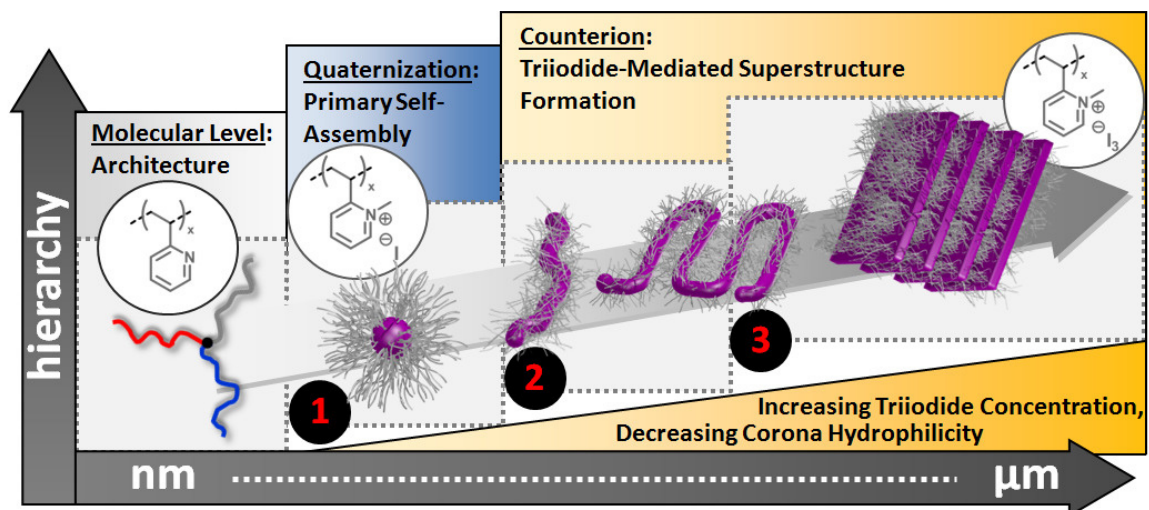


**Figure 4-7.** Proposed mechanism for the triiodide-triggered superstructure formation of the  $\mu$ -BVqT miktoarm star terpolymer *via* different hierarchy levels from the nanometer to the micrometer scale: spherical micelles (level 1), cylindrical micelles (level 2), and lamellar superstructures (level 3).

## 4.4 Experimental Section

### Materials

Butadiene (Rießner-Gase) was passed through columns filled with molecular sieves (4 Å) and basic aluminium oxide and stored over dibutylmagnesium (1 M solution in heptane, Aldrich). 2-Vinylpyridine (Aldrich) was degassed, stirred with triethylaluminium (1 M solution in hexanes, Aldrich), and condensed on a high vacuum line. THF (Sigma-Aldrich) was distilled from CaH<sub>2</sub> and Na/K alloy. *sec*-Butyllithium (Acros, 1.3 M in cyclohexane/hexane: 92/8) was used without further purification. *tert*-Butyl methacrylate (*t*BMA, Sigma-Aldrich) for ATRP was filtered over basic aluminium oxide. *N,N,N',N',N''*-Pentamethyldiethylenetriamine (PMDETA) and CuBr were purchased from Aldrich and distilled and degassed or treated with pure acetic acid and filtered, respectively. 1-[(4-(*tert*-Butyldimethylsilyl)ethynyl)phenyl]-1-phenylethylene was synthesized from 1-(4-bromophenyl)-1-phenylethylene as already reported.<sup>36</sup> The aqueous solutions were prepared with distilled desalinated water. All other chemicals were of analytical grade and used as received. The dialysis membrane used for all steps was purchased from Roth (Spectra Por), with a molecular weight cut-off (MWCO) of 1 000 g/mol.

### Synthesis of Polybutadiene-*arm*-Poly(2-vinylpyridine)-*arm*-Poly(*tert*-butyl methacrylate) ( $\mu$ -BVT) Miktoarm Star Terpolymer

The detailed procedures for the synthesis of the individual polymeric building blocks and the ligation by azide-alkyne Huisgen cycloaddition have already been reported elsewhere.<sup>36</sup> The alkyne mid-functionalized diblock copolymer polybutadiene-*b*-poly(2-vinylpyridine) (PB-*b*-P2VP) was synthesized *via* anionic polymerization using an alkyne-substituted DPE. The poly(*tert*-butyl methacrylate) (PtBMA) arm was synthesized in a separate polymerization procedure *via* ATRP using an azido-functionalized initiator.<sup>60</sup>

Finally, the ligation of the alkyne-functionalized diblock copolymer with the azido-functionalized homopolymer was conducted by azide-alkyne Huisgen cycloaddition.<sup>61</sup> Therefore, a mixture of the diblock copolymer and 1.1 equiv of the homopolymer were dissolved in THF at a concentration of ~20 g/L and degassed for 10 minutes. After addition of 1 equiv of CuBr the solution was degassed for further 15 minutes. PMDETA (1 equiv) was added to complex the copper and start the reaction, which was followed by

SEC. After 2 days, the resulting miktoarm star terpolymer was purified by passing the solution through a small column with basic alumina to remove copper and finally freeze-dried from dioxane.

### **Quaternization of $\mu$ -BVT and Preparation of Aqueous Micellar Solutions**

The transformation of the P2VP compartment into a strong cationic polyelectrolyte (P2VPq) was conducted using methyl iodide as quaternization agent. The miktoarm star terpolymer was dissolved in dioxane at a concentration of 2 g/L. After the addition of a 10-fold excess of methyl iodide compared to 2VP units, the solution was allowed to stir at room temperature for 3 days. To remove excess quaternization agent, the solution was dialyzed against dioxane. During this step, the solution typically turned yellow. Finally, the solution was diluted with dioxane to obtain a concentration of 1 g/L, and then the solvent was subsequently exchanged against water. The dialysis water was changed three times. The concentrations of the obtained aqueous solutions ranged from 0.3 to 0.7 g/L. It was observed that some samples precipitated after a few days or weeks, whereas others were still colloidally stable after 2 years (even though prepared under comparable conditions). As the amount of triiodide was proven to be responsible for the different aggregation structure, we attribute subtle differences in the ratio of iodide/triiodide to have an impact on the long-term stability of the “woodlouse” aggregates.

To simplify matters, in case of all quaternized solutions, the given concentrations resemble the concentration of the pristine miktoarm star terpolymer before quaternization, thus neglecting the increase of mass due to quaternization.

For the preparation of the triiodide complexes, an iodine stock solution was prepared with dioxane as solvent at 15 g/L. Then, this iodine solution was added to the agitated dioxane solution of the quaternized star terpolymer until the desired ratio of iodine to 2VP was achieved. Afterward, the solutions were stirred for 2 h and then treated with ultrasound for 15 min. Subsequently, the solutions were dialyzed against water, as described above. The solutions were obtained with concentrations ranging from 0.3 to 0.7 g/L. Whereas the solutions with low iodine contents were long-term stable, the solutions with high amounts of iodine slowly precipitated with time. However, these solu-

tions were easily redispersible by shaking without leaving macroscopic precipitate.

### **Transmission Electron Microscopy (cryo-TEM and TEM)**

TEM micrographs were taken with a Zeiss CEM 902 or 922 OMEGA electron microscope operated at 80 kV or 200 kV, respectively. Both machines were equipped with an in-column energy filter. For sample preparation, 2  $\mu$ L of the solution (typically 0.1-0.2 g/L) were deposited on a TEM grid (copper, 200 mesh). Afterward, the remaining solvent was removed with a blotting paper. For investigation of the particle films, the freeze-dried polymer was embedded into a resin (EpoTek 301). Then, 50 nm thin cuts were prepared with a Leica EM UC7 microtome equipped with a diamond knife and deposited onto TEM grids (copper, 200 mesh). Selective staining of the B phase was achieved by treating the samples with OsO<sub>4</sub> vapour for 30 s.

For cryo-TEM studies, a drop (~2 mL) of the aqueous micellar solution ( $c \approx 0.4$ -0.7 g/L) was placed on a lacey carbon-coated copper TEM grid (200 mesh, Science Services), where most of the liquid was removed with blotting paper, leaving a thin film stretched over the grid holes. The specimens were shock vitrified by rapid immersion into liquid ethane in a temperature-controlled freezing unit (Zeiss Cryobox, Zeiss NTS GmbH) and cooled to approximately 90 K. The temperature was monitored and kept constant in the chamber during all of the preparation steps. After freezing the specimens, they were inserted into a cryo-transfer holder (CT3500, Gatan) and transferred to a Zeiss EM922 OMEGA EFTEM instrument. Examinations were carried out at temperatures around 90 K. The microscope was operated at an acceleration voltage of 200 kV. Zero-loss filtered images ( $\Delta E = 0$  eV) were taken under reduced dose conditions. All images were registered digitally by a bottom-mounted CCD camera system (Ultrascan 1000, Gatan), combined, and processed with a digital imaging processing system (Gatan Digital Micrograph 3.9 for GMS 1.4).

Evaluation of the respective length scales of the structures was achieved by measuring 50-100 different spots within the sample with the UTHSCSA ImageTool V. 3.00.

### TEM-Tomography (TEMT)

For TEMT measurements, samples (~200 nm thickness) were microtome cut onto Cu mesh grids with a carbon film and an additional underlying polyvinyl formal coating. Prior to TEMT, samples were stained using OsO<sub>4</sub> vapour and Au nanoparticles with a diameter of approximately 5 nm (BB International Ltd, UK) were deposited onto the microtome star terpolymer films. TEMT measurements were performed on a JEM-2200FS (JEOL Co., Ltd., Japan) at an accelerating voltage of 200 kV and equipped with a slow-scan CCD camera (GATAN USC4000, Gatan Inc., USA). The TEM micrographs were obtained at 1° increment between -65° and 65° tilt angle. The image set was processed according to the same protocol described elsewhere.<sup>62</sup> Subsequently, the tilt series of the TEM images were aligned by using the previously deposited Au nanoparticles as fiducial markers and then reconstructed on the basis of the filtered-back-projection (FBP) method.<sup>63</sup> The reconstructed images were further visualized using the software platform Avizo® (Visualization Sciences Group, <http://www.vsg3d.com>).

### Small-Angle X-Ray Scattering (SAXS)

SAXS measurements of the freeze-dried powders were performed on a Bruker AXS Nanostar (Bruker, Karlsruhe, Germany), equipped with a microfocus X-ray source (Incoatec  $I\mu S_{Cu}$  E025, Incoatec Geesthacht, Germany), operating at  $\lambda = 1.54 \text{ \AA}$ . A pinhole setup with 750, 400, and 1000  $\mu\text{m}$  (in the order from source to sample) was used and the sample-to-detector distance was 107 cm. Samples were mounted on a metal rack and fixed using tape. The scattering patterns were corrected for the beam stop and the background (Scotch tape) prior to evaluations. The measurement time for the samples was 4h in all cases.

**Conflict of Interest:** The authors declare no competing financial interest.

**Acknowledgements.** This work was supported by the *Deutsche Forschungsgesellschaft* within SPP 1165 (Mu896/22). We thank Prof. M. Ballauff, D.V. Pergushov and H. Schmalz for fruitful discussions. F. Wieberger is acknowledged for performing some of the SEM

measurements, and Annika Pfaffenberger for recording some of the TEM micrographs. H.J. gratefully acknowledges the financial support received through Grants-in-Aid No. 24310092 from the Ministry of Education, Culture, Sports, Science, and Technology. F.H.S. acknowledges a fellowship from the Verband der Chemischen Industrie (VCI) and funding from the Thuringian Ministry for Education, Science and Culture (TMBWK, Grant No. B514-09051, NanoConSens, and Grant No. B515-11028, SWAXS-JCSM).

**Supporting Information Available.** Additional experimental section. Molecular characterization and SEC eluograms of  $\mu$ -BVT and its precursor polymers. DLS of micellar  $\mu$ -BVqT solution and P2VPq homopolymer. DSC of  $\mu$ -BVT. Additional SEM, TEM and cryo-TEM of micellar aggregates. Videos of cryo-TEM tilt-series and a TEM-tomography 3D reconstruction. This material is available free of charge *via* the Internet at <http://pubs.acs.org>.

## 4.5 References

- (1) Whitesides, G. M.; Grzybowski, B. Self-Assembly at All Scales. *Science* **2002**, *295*, 2418-2421.
- (2) Zhang, S. Emerging Biological Materials Through Molecular Self-Assembly. *Biotechnol. Adv.* **2002**, *20*, 321-339.
- (3) Nagarajan, R.; Ruckenstein, E. Theory of Surfactant Self-Assembly: a Predictive Molecular Thermodynamic Approach. *Langmuir* **1991**, *7*, 2934-2969.
- (4) Svenson, S. Controlling Surfactant Self-Assembly. *Curr. Opin. Colloid Interface Sci.* **2004**, *9*, 201-212.
- (5) Zhang, L.; Eisenberg, A. Multiple Morphologies of "Crew-Cut" Aggregates of Polystyrene-*b*-poly(acrylic acid) Block Copolymers. *Science* **1995**, *268*, 1728-1731.
- (6) Mai, Y.; Eisenberg, A. Self-Assembly of Block Copolymers. *Chem. Soc. Rev.* **2012**, *41*, 5969-5985.
- (7) Antonietti, M.; Förster, S. Vesicles and Liposomes: A Self-Assembly Principle Beyond Lipids. *Adv. Mater.* **2003**, *15*, 1323-1333.
- (8) Hamley, I. W. Nanotechnology with Soft Materials. *Angew. Chem., Int. Ed.* **2003**, *42*, 1692-1712.
- (9) Schacher, F. H.; Rupa, P. A.; Manners, I. Functional Block Copolymers: Nanostructured Materials with Emerging Applications. *Angew. Chem., Int. Ed.* **2012**, *51*, 7898-7921.
- (10) Savić, R.; Luo, L.; Eisenberg, A.; Maysinger, D. Micellar Nanocontainers Distribute to Defined Cytoplasmic Organelles. *Science* **2003**, *300*, 615-618.
- (11) H. Cabral; Y. Matsumoto; K. Mizuno; Q. Chen; M. Murakami; M. Kimura; Y. Terada; M. R. Kano; K. Miyazono; M. Uesaka; N. Nishiyama; K. Kataoka. Accumulation of Sub-100 nm Polymeric Micelles in Poorly Permeable Tumours Depends on Size. *Nat. Nanotechnol.* **2011**, *6*, 815-823.
- (12) Holder, S. J.; Sommerdijk, N. A. J. M. New Micellar Morphologies from Amphiphilic Block Copolymers: Disks, Toroids and Bicontinuous Micelles. *Polym. Chem.* **2011**, *2*, 1018-1028.
- (13) Bates, F. S.; Hillmyer, M. A.; Lodge, T. P.; Bates, C. M.; Delaney, K. T.; Fredrickson, G. H. Multiblock Polymers: Panacea or Pandora's Box? *Science* **2012**, *336*, 434-440.
- (14) Li, Z.; Kesselman, E.; Talmon, Y.; Hillmyer, M. A.; Lodge, T. P. Multicompartment Micelles from ABC Miktoarm Stars in Water. *Science* **2004**, *306*, 98-101.
- (15) Li, Z.; Hillmyer, M. A.; Lodge, T. P. Morphologies of Multicompartment Micelles Formed by ABC Miktoarm Star Terpolymers. *Langmuir* **2006**, *22*, 9409-9417.
- (16) Saito, N.; Liu, C.; Lodge, T. P.; Hillmyer, M. A. Multicompartment Micelles from Polyester-Containing ABC Miktoarm Star Terpolymers. *Macromolecules* **2008**, *41*, 8815-8822.
- (17) Liu, C.; Hillmyer, M. A.; Lodge, T. P. Multicompartment Micelles from pH-Responsive Miktoarm Star Block Terpolymers *Langmuir* **2009**, *25*, 13718-13725.
- (18) Kubowicz, S.; Baussard, J.-F.; Lutz, J.-F.; Thünemann, A. F.; von Berlepsch, H.; Laschewsky, A. Multicompartment Micelles Formed by Self-Assembly of Linear ABC Triblock Copolymers in Aqueous Medium. *Angew. Chem., Int. Ed.* **2005**, *44*, 5262-5265.
- (19) Fang, B.; Walther, A.; Wolf, A.; Xu, Y.; Yuan, J.; Müller, A. H. E. Undulated Multicompartment Cylinders by the Controlled and Directed Stacking of Polymer Micelles with a Compartmentalized Corona. *Angew. Chem., Int. Ed.* **2009**, *48*, 2877-2880.
- (20) Schacher, F.; Betthausen, E.; Walther, A.; Schmalz, H.; Pergushov, D. V.; Müller, A. H. E. Interpolyelectrolyte Complexes of Dynamic Multicompartment Micelles. *ACS Nano* **2009**, *3*, 2095-2102.
- (21) Schacher, F.; Walther, A.; Müller, A. H. E. Dynamic Multicompartment-Core Micelles in Aqueous Media. *Langmuir* **2009**, *25*, 10962-10969.
- (22) Dupont, J.; Liu, G.; Niihara, K.-i.; Kimoto, R.; Jinnai, H. Self-Assembled ABC Triblock Copolymer Double and Triple Helices. *Angew. Chem., Int. Ed.* **2009**, *48*, 6144-6147.
- (23) Zhu, J.; Jiang, W. Self-Assembly of ABC Triblock Copolymer into Giant Segmented Wormlike Micelles in Dilute Solution. *Macromolecules* **2005**, *38*, 9315-9323.
- (24) Gröschel, A. H.; Schacher, F. H.; Schmalz, H.; Borisov, O. V.; Zhulina, E. B.; Walther, A.; Müller, A. H. E. Precise Hierarchical Self-Assembly of Multicompartment Micelles. *Nat. Commun.* **2012**, *3*, 710.
- (25) Gröschel, A. H.; Walther, A.; Löblich, T. I.; Schmelz, J.; Hanisch, A.; Schmalz, H.; Müller, A. H. E. Facile, Solution-Based Synthesis of Soft, Nanoscale Janus Particles with Tunable Janus Balance. *J. Am. Chem. Soc.* **2012**, *134*, 13850-13860.

- (26) Wang, H.; Lin, W.; Fritz, K. P.; Scholes, G. D.; Winnik, M. A.; Manners, I. Cylindrical Block Co-Micelles with Spatially Selective Functionalization by Nanoparticles. *J. Am. Chem. Soc.* **2007**, *129*, 12924-12925.
- (27) Wang, X.; Guerin, G.; Wang, H.; Wang, Y.; Manners, I.; Winnik, M. A. Cylindrical Block Copolymer Micelles and Co-Micelles of Controlled Length and Architecture. *Science* **2007**, *317*, 644-647.
- (28) Rupar, P. A.; Chabanne, L.; Winnik, M. A.; Manners, I. Non-Centrosymmetric Cylindrical Micelles by Unidirectional Growth. *Science* **2012**, *337*, 559-562.
- (29) Schmelz, J.; Karg, M.; Hellweg, T.; Schmalz, H. General Pathway toward Crystalline-Core Micelles with Tunable Morphology and Corona Segregation. *ACS Nano* **2011**, *5*, 9523-9534.
- (30) Cui, H.; Chen, Z.; Zhong, S.; Wooley, K. L.; Pochan, D. J. Block Copolymer Assembly via Kinetic Control. *Science* **2007**, *317*, 647-650.
- (31) Cui, H.; Chen, Z.; Wooley, K. L.; Pochan, D. J. Controlling Micellar Structure of Amphiphilic Charged Triblock Copolymers in Dilute Solution via Coassembly with Organic Counterions of Different Spacer Lengths. *Macromolecules* **2006**, *39*, 6599-6607.
- (32) Li, Z.; Chen, Z.; Cui, H.; Hales, K.; Wooley, K. L.; Pochan, D. J. Controlled Stacking of Charged Block Copolymer Micelles. *Langmuir* **2007**, *23*, 4689-4694.
- (33) Pochan, D. J.; Chen, Z.; Cui, H.; Hales, K.; Qi, K.; Wooley, K. L. Toroidal Triblock Copolymer Assemblies. *Science* **2004**, *306*, 94-97.
- (34) Cui, H.; Chen, Z.; Wooley, K. L.; Pochan, D. J. Origins of Toroidal Micelle Formation Through Charged Triblock Copolymer Self-Assembly. *Soft Matter* **2009**, *5*, 1269-1278.
- (35) Chen, Z.; Cui, H.; Hales, K.; Li, Z.; Qi, K.; Pochan, D. J.; Wooley, K. L. Unique Toroidal Morphology from Composition and Sequence Control of Triblock Copolymers. *J. Am. Chem. Soc.* **2005**, *127*, 8592-8593.
- (36) Hanisch, A.; Schmalz, H.; Müller, A. H. E. A Modular Route for the Synthesis of ABC Miktoarm Star Terpolymers via a New Alkyne-Substituted Diphenylethylene Derivative. *Macromolecules* **2012**, *45*, 8300-8309.
- (37) Justynska, J.; Hordyjewicz, Z.; Schlaad, H. Toward a Toolbox of Functional Block Copolymers via Free-Radical Addition of Mercaptans. *Polymer* **2005**, *46*, 12057-12064.
- (38) Walther, A.; Gödel, A.; Müller, A. H. E. Controlled Crosslinking of Polybutadiene Containing Block Terpolymer Bulk Structures: A Facile Way Towards Complex and Functional Nanostructures. *Polymer* **2008**, *49*, 3217-3227.
- (39) Martin, T. J.; Procházka, K.; Munk, P.; Webber, S. E. pH-Dependent Micellization of Poly(2-vinylpyridine)-block-poly(ethylene oxide). *Macromolecules* **1996**, *29*, 6071-6073.
- (40) Burkhardt, M.; Martinez-Castro, N.; Tea, S.; Drechsler, M.; Babin, I.; Grishagin, I.; Schweins, R.; Pergushov, D. V.; Gradzielski, M.; Zezin, A. B.; Müller, A. H. E. Polyisobutylene-block-poly(methacrylic acid) Diblock Copolymers: Self-Assembly in Aqueous Media. *Langmuir* **2007**, *23*, 12864-12874.
- (41) Saito, N.; Liu, C.; Lodge, T. P.; Hillmyer, M. A. Multicompartment Micelle Morphology Evolution in Degradable Miktoarm Star Terpolymers. *ACS Nano* **2011**, *4*, 1907-1912.
- (42) He, T.; Li, B.; Ren, S. Glass Transition Temperature and Chain Flexibility of 1,2-Polybutadiene. *J. Appl. Polym. Sci.* **1986**, *31*, 873-884.
- (43) Barton, A. F. M. In *CRC Handbook of Polymer-Liquid Interaction Parameters and Solubility Parameters*; Boston, 1990.
- (44) Brandrup, J.; Immergut, E. H.; Grulke, E. A. In *Polymer Handbook*; Fourth Edition ed.; Wiley: New York, 1999.
- (45) Pispas, S.; Hadjichristidis, N.; Potemkin, I.; Khokhlov, A. Effect of Architecture on the Micellization Properties of Block Copolymers: A<sub>2</sub>B Miktoarm Stars vs AB Diblocks. *Macromolecules* **2000**, *33*, 1741-1746.
- (46) Kong, W.; Li, B.; Jin, Q.; Ding, D.; Shi, A.-C. Helical Vesicles, Segmented Semivesicles, and Noncircular Bilayer Sheets from Solution-State Self-Assembly of ABC Miktoarm Star Terpolymers. *J. Am. Chem. Soc.* **2009**, *131*, 8503-8512.
- (47) Wang, L.; Xu, R.; Wang, Z.; He, X. Kinetics of Multicompartment Micelle Formation by Self-Assembly of ABC Miktoarm Star Terpolymer in Dilute Solution. *Soft Matter* **2012**.
- (48) Schacher, F.; Yuan, J.; Schoberth, H. G.; Müller, A. H. E. Synthesis, Characterization, and Bulk Crosslinking of Polybutadiene-block-poly(2-vinyl pyridine)-block-poly(*tert*-butyl methacrylate) Block Terpolymers. *Polymer* **2010**, *51*, 2021-2032.

- (49) Leibler, L. Theory of Microphase Separation in Block Copolymers. *Macromolecules* **1980**, *13*, 1602-1617.
- (50) Bates, F. S.; Fredrickson, G. H. Block Copolymer Thermodynamics: Theory and Experiment. *Annu. Rev. Phys. Chem.* **1990**, *41*, 525-557.
- (51) West, W.; Schlessinger, L. The Mechanism of the Photodecomposition of Methyl and Ethyl Iodides. *J. Am. Chem. Soc.* **1938**, *60*, 961-966.
- (52) Palmer, D. A.; Ramette, R. W.; Mesmer, R. E. Triiodide Ion Formation Equilibrium and Activity Coefficients in Aqueous Solution. *J. Solution Chem.* **1984**, *13*, 673-683.
- (53) Zhang, F. S.; Lynden-Bell, R. M. Interactions of Triiodide Cluster Ion with Solvents. *Eur. Phys. J. D* **2005**, *34*, 129-132.
- (54) Chernov'yants, M.; Burykin, I.; Pisanov, R.; Shalu, O. Synthesis and Antimicrobial Activity of Poly(*N*-methyl-4-vinylpyridinium triiodide). *Pharm. Chem. J.* **2010**, *44*, 61-63.
- (55) Plamper, F. A.; Schmalz, A.; Penott-Chang, E.; Drechsler, M.; Jusufi, A.; Ballauff, M.; Müller, A. H. E. Synthesis and Characterization of Star-Shaped Poly(*N,N*-dimethylaminoethyl methacrylate) and Its Quaternized Ammonium Salts. *Macromolecules* **2007**, *40*, 5689-5697.
- (56) Zhulina, E. B.; Adam, M.; LaRue, I.; Sheiko, S. S.; Rubinstein, M. Diblock Copolymer Micelles in a Dilute Solution. *Macromolecules* **2005**, *38*, 5330-5351.
- (57) McKenzie, B. E.; Nudelman, F.; Bomans, P. H. H.; Holder, S. J.; Sommerdijk, N. A. J. M. Temperature-Responsive Nanospheres with Bicontinuous Internal Structures from a Semicrystalline Amphiphilic Block Copolymer. *J. Am. Chem. Soc.* **2010**, *132*, 10256-10259.
- (58) Schacher, F. H.; Sugimori, H.; Hong, S.; Jinnai, H.; Müller, A. H. E. Tetragonally Perforated Lamellae of Polybutadiene-*block*-poly(2-vinylpyridine)-*block*-poly(*tert*-butyl methacrylate) (BVT) Triblock Terpolymers in the Bulk: Preparation, Cross-Linking, and Dissolution. *Macromolecules* **2012**, *45*, 7956-7963.
- (59) Dyer, C.; Driva, P.; Sides, S. W.; Sumpter, B. G.; Mays, J. W.; Chen, J.; Kumar, R.; Goswami, M.; Dadmun, M. D. Effect of Macromolecular Architecture on the Morphology of Polystyrene-Polyisoprene Block Copolymers. *Macromolecules* **2013**, *46*, 2023-2031.
- (60) Mantovani, G.; Ladmiral, V.; Tao, L.; Haddleton, D. M. One-Pot Tandem Living Radical Polymerisation-Huisgens Cycloaddition Process ("click") Catalysed by *N*-alkyl-2-pyridylmethanimine/Cu(i)Br Complexes. *Chem. Commun.* **2005**, 2089-2091.
- (61) Binder, W. H.; Sachsenhofer, R. 'Click' Chemistry in Polymer and Materials Science. *Macromol. Rapid Commun.* **2007**, *28*, 15-54.
- (62) Jinnai, H.; Spontak, R. J.; Nishi, T. Transmission Electron Microtomography and Polymer Nanostructures. *Macromolecules* **2010**, *43*, 1675-1688.
- (63) Crowther, R. A.; DeRosier, D. J.; Klug, A. The Reconstruction of a Three-Dimensional Structure from Projections and its Application to Electron Microscopy. *Proc. R. Soc. London A* **1970**, *317*, 319-340.

## 4.6 Supporting Information

### 4.6.1 Additional Experimental Section

#### Synthesis

##### Quaternization of 2-Vinylpyridine Homopolymers (P2VP) and Preparation of Aqueous Solutions

The quaternization procedure was similar to the method described for the miktoarm star terpolymer with slight modifications. After three days of reaction with methyl iodide 10 vol% of water were added to the partially precipitated reaction mixture in dioxane and it was allowed to stir for an additional day. Afterward, it was first dialyzed to a mixture of dioxane:water (90:10) and then the solvent composition was gradually increased to (80:20). The obtained stock solution in the dioxane:water mixture was afterward dialyzed to water. The triiodide complexes were prepared in the same manner as described in the manuscript.

##### Preparation of $\mu$ -BVqT with Different Counterions

The exchange of the iodide counter ion with chloride was achieved by dialysis of the dioxane stock solution to 50 mM solution of LiCl in THF. Afterward the solution was dialyzed against pure THF to remove excess salt. Before dialysis to water, the solvent was again changed to dioxane through dialysis.

The quaternizations with dimethyl sulfate were conducted either in THF or dioxane. A polymer solution was prepared with a concentration of 2 g/L and then degassed for 15 minutes. Afterward, 10 equiv of dimethyl sulfate regarding 2VP units were added and the reaction mixture was allowed to stir at 40 °C for 3 days. Finally the solution was purified from the excess quaternization agent by dialysis with the respective reaction medium. After dilution to a concentration of 1 g/L the solutions were dialyzed to water.

#### Characterization

##### Size Exclusion Chromatography (SEC)

SEC measurements were performed on a set of 30 cm SDV-gel columns (5  $\mu$ m bead size, with pore sizes of  $10^5$ ,  $10^4$ ,  $10^3$  and  $10^2$  Å) using refractive index and UV ( $\lambda = 254$  nm)

detection. THF was used as eluent at a flow rate of 1 mL/min. Toluene was used as internal standard and the system was calibrated with PS and 1,4-PB standards.

### **$^1\text{H}$ NMR Spectroscopy**

$^1\text{H}$  NMR spectra were recorded on a Bruker Ultrashield 300 spectrometer at an operating frequency of 300 MHz.  $\text{CDCl}_3$  was used as solvent and tetramethylsilane as internal standard.

### **Matrix-Assisted Laser Desorption Ionization Time-of-Flight Mass Spectrometry (MALDI-ToF MS)**

MALDI-ToF MS analysis was performed on a Bruker-Reflex III apparatus equipped with a  $\text{N}_2$  laser ( $\lambda = 337$  nm) at an acceleration voltage of 20 kV. *trans*-2-[3-(4-*tert*-Butylphenyl)-2-methyl-2-propenylidene]malonitrile (DCTB, Fluka, 99,0 %) was used as matrix and silver trifluoroacetate (AgTFA, Sigma-Aldrich, 99.99%) as ionization agent. Samples were prepared from THF solution by mixing matrix, polymer and salt in a ratio of 20/5/1 (v/v).

### **Scanning Electron Microscopy (SEM)**

The particles were analyzed by field emission scanning electron microscopy on a Zeiss LEO 1530 Gemini microscope equipped with a field emission cathode operating at 0.5-5 kV. Specimen preparation was accomplished as follows: silicon wafers were cleaned using isopropanol and acetone in a standard procedure. To obtain areas of different concentration of particles, the wafer was first dip-coated from 0.02 g/L solution and then a further drop of the solution was deposited and allowed to dry. The specimens were coated with a thin platinum layer using a sputter coater (Cressington 208HR) to render the specimen conductive.

### **Dynamic Light Scattering (DLS)**

DLS measurements were performed on an ALV DLS/SLS-SP 5022F compact goniometer system with an ALV 5000/E cross correlator and a He-Ne laser ( $\lambda = 632.8$  nm). The measurements were carried out in cylindrical scattering cells ( $d = 10$  mm) at an angle of  $90^\circ$  and a temperature of  $20^\circ\text{C}$ . Prior to the light scattering measurements, the sample solutions were filtered using nylon filters (Magna, Roth) with a pore size of  $5\ \mu\text{m}$ . The CON-

TIN algorithm was applied to analyze the obtained correlation functions. Apparent hydrodynamic radii were calculated according to the Stokes-Einstein equation.

## DSC

Thermal analysis and determination of the glass transition temperatures was performed on a Perkin–Elmer Diamond DSC at a heating rate of 20 K/min.

### 4.6.2 Synthesis and Characterization of PB-*arm*-P2VP-*arm*-PtBMA Miktoarm Star Terpolymer

The synthesis of the PB-*arm*-P2VP-*arm*-PtBMA miktoarm star terpolymer was accomplished by combining sequential anionic polymerization with azide-alkyne Huisgen cycloaddition. Therefore, an alkyne-functionalized polybutadiene-*b*-poly(2-vinylpyridine) (PB-*b*-P2VP) diblock copolymer was directly prepared by anionic polymerization using an alkyne-functionalized DPE derivative (click-DPE). The molecular characterization of the diblock copolymer is listed in Table 4-S1. As already reported, in the case of the click-DPE, incorporation in, or most probably at the end of the poly(2-vinylpyridine) (P2VP) block takes place. This leads to diblock copolymers which bear additional alkyne-functions in or at the end of the P2VP block, as the DPE derivative is used in excess. Nevertheless, under appropriate reaction conditions, *i.e.* using only a slight excess of click-DPE, low temperatures and short reaction times an overall degree of alkyne-functionalization of 116 % was achieved.<sup>1</sup> Taking into account the errors of the determination method this resembles only a slight over-incorporation of click-DPE into the material.

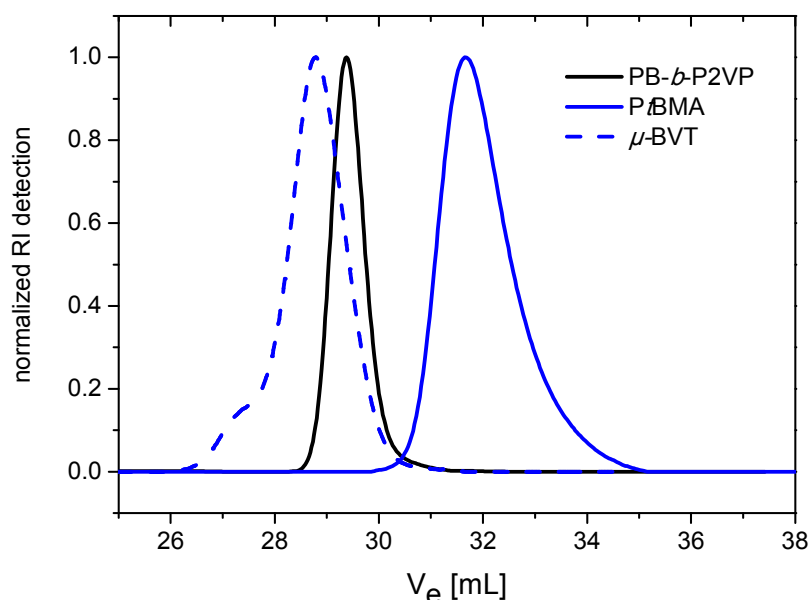
The alkyne group is then used to attach the third block, poly(*tert*-butyl methacrylate) (PtBMA), *via* azide-alkyne Huisgen cycloaddition. Thus, in the following click reaction an excess of 10% of azido-functionalized homopolymer chains relative to the diblock chains was used to ensure that all diblock chains undergo conjugation. As a direct consequence the obtained miktoarm star terpolymer contains a minor fraction with more than one chain of PtBMA. Figure 4-S1 displays the SEC traces of the precursor homopolymer and diblock copolymer, and the obtained miktoarm star terpolymer. Table 4-S1 lists the corresponding characterization data. Due to the use of an azido-functionalized ATRP initia-

tor for the PtBMA polymerization in case of recombination polymers bearing two azido end-groups are formed. Therefore, a small percentage of  $\alpha,\omega$ -azido-bifunctionalized homopolymer could lead to H-shaped miktoarm star terpolymers and explain the observed higher molecular weight shoulder. From test click reactions with PS homopolymers, where the bromo-function was transformed into an azide after polymerization, no such coupling shoulder was detected, supporting our assumption.

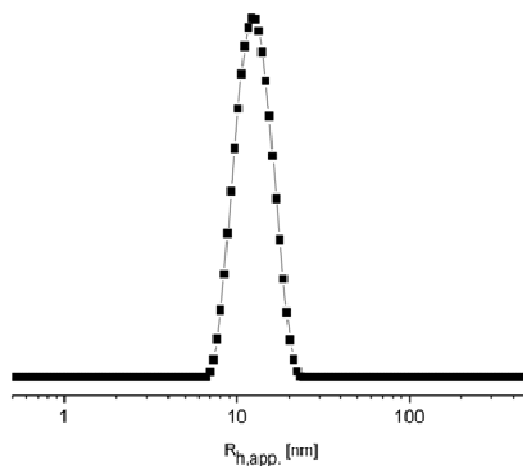
**Table 4-S1. Molecular Characteristics of Poly(*tert*-butyl methacrylate) (T), Polybutadiene-*block*-poly(2-vinylpyridine) (BV), and  $\mu$ -BVT**

Polymer <sup>a</sup>	$M_n^b$ / kg/mol	PDI <sup>c</sup>
T <sub>53</sub>	7.6	1.17
B <sub>109</sub> V <sub>81</sub>	14.7	1.02
$\mu$ -B <sub>109</sub> V <sub>81</sub> T <sub>53</sub>	22.2	1.07

<sup>a</sup>The subscripts denote the degrees of polymerization of the corresponding blocks as calculated from the respective number average molecular weights. <sup>b</sup>For the PtBMA homopolymer the number average molecular weight was determined by SEC using a PtBMA calibration. For the diblock copolymer the molecular weight was calculated from <sup>1</sup>H NMR using the molecular weight of the PB as reference. This was measured directly *via* MALDI-ToF MS. For the ABC miktoarm star terpolymer the overall molecular weight was calculated from the corresponding precursor polymers. <sup>c</sup>Determined by SEC in THF calibrated with PS standards or in the case of PtBMA homopolymer with PtBMA standards.



**Figure 4-S1.** SEC eluograms of the PB-*arm*-P2VP-*arm*-PtBMA miktoarm star terpolymer ( $\mu$ -BVT), the precursor diblock copolymer (PB-*b*-P2VP), and the homopolymer (PtBMA). In all cases the RI signal is shown.

4.6.3 Self-Assembly of  $\mu$ -BVqT

**Figure 4-S2.** Intensity-weighted DLS CONTIN plot (A) of quaternized  $\mu$ -BVT ( $\mu$ -BVqT) in 1 g/L dioxane solution,  $R_{h,app} = 12.5$  nm.

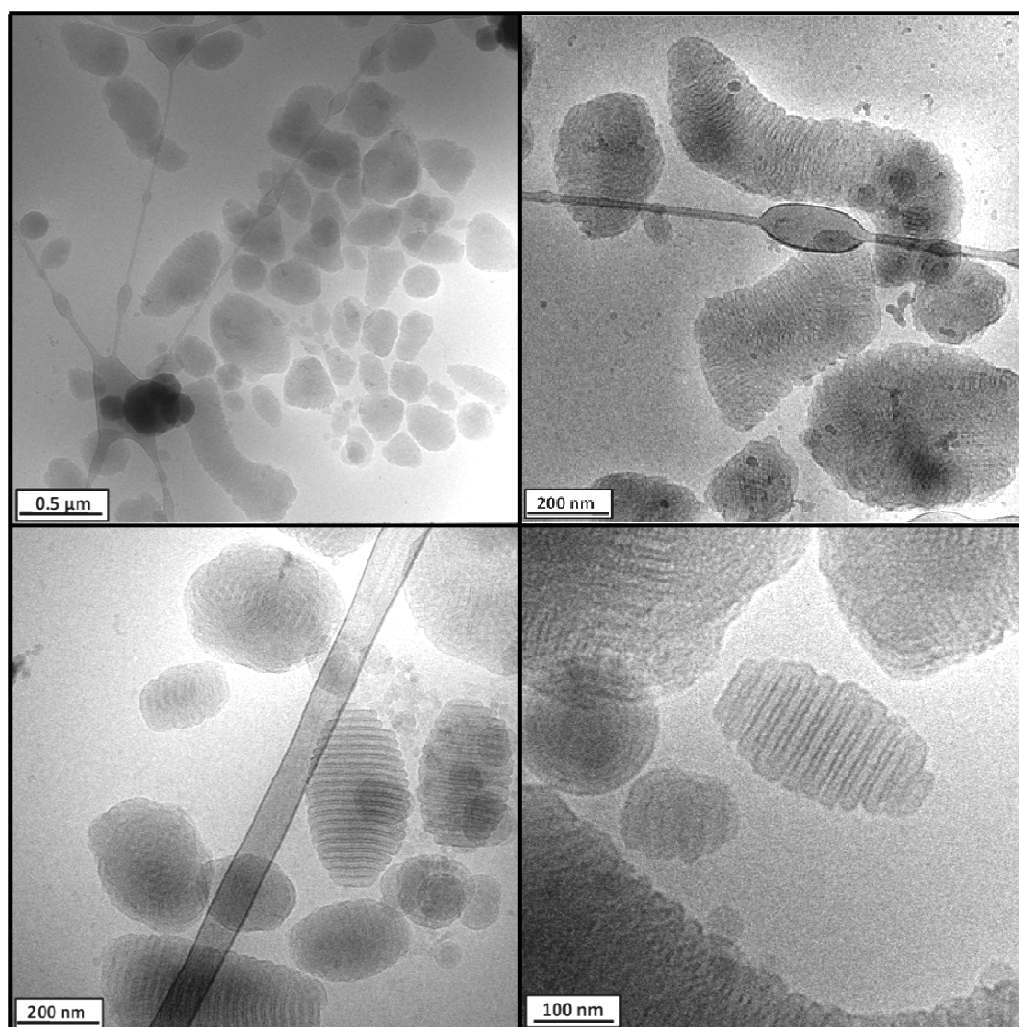


**Figure 4-S3.** Overview of various cryo-TEM images of different “woodlouse” aggregation forms observed in  $\sim 0.6$  g/L aqueous solutions of  $\mu$ -BVqT.

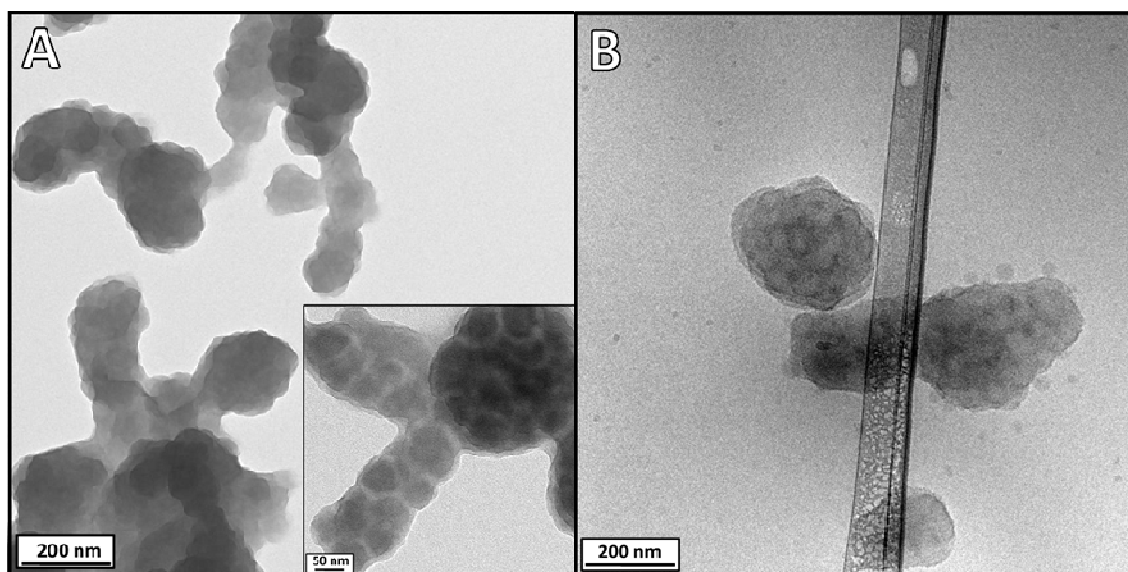


**Figure 4-S4.** (A) TEM and (B) cryo-TEM micrographs from aqueous solutions of linear  $B_{1108}Vq_{142}T_{93}$  at 0.2 and 0.65 g/L, respectively. After dialysis to water precipitation occurred gradually. Whereas the image in (A) is unstained, the inset in (A) shows an enlarged area after staining with  $OsO_4$ . In both cases micellar clusters can be seen, without any internal fine structure (see staining in the inset in (A) or the brighter areas in the cryo-TEM in (B)). Please note that the molecular weight of the triblock terpolymer was much higher and also the molar fractions were different to the studied miktoarm star terpolymer  $\mu$ - $B_{101}V_{81}T_{53}$ . Additionally, the sequence was PB-*b*-P2VP-*b*-PtBMA due to the restrictions of anionic polymerization and therefore the middle block forms the corona. This leads to a folding of the polymer chain to shield the hydrophobic end blocks.

#### 4.6.3.1 Intermediate Structures of “Woodlouse” Aggregates

The dioxane solution of  $\mu$ -BVqT, which yielded the intermediate structures (Figure 4-2), was allowed to age for an additional month before dialysis to water. TEM analysis showed that the obtained aggregates were of slightly higher structural order and the internal fine structure of the “woodlouse” was already visible for some objects (Figure 4-S5A). Nevertheless, the structures seem to be kinetically trapped during the process, as further ageing of aqueous solutions did not lead to any increase in order. As observed by cryo-TEM the superstructures were more densely packed (Figure 4-S5B). Less cylindrical protrusions emanate from the center of the aggregates, and the gray-scale analysis confirms three periodic distances ( $d_1 = 4.5 \pm 1.0$  nm,  $d_2 = 4.5 \pm 1.0$  nm,  $d_3 = 9.0 \pm 1.0$  nm). The structure was further visualized using different tilt angles in cryo-TEM (Supporting videos 4-S1 and 4-S2), confirming a 3-dimensional array of the cylinders.

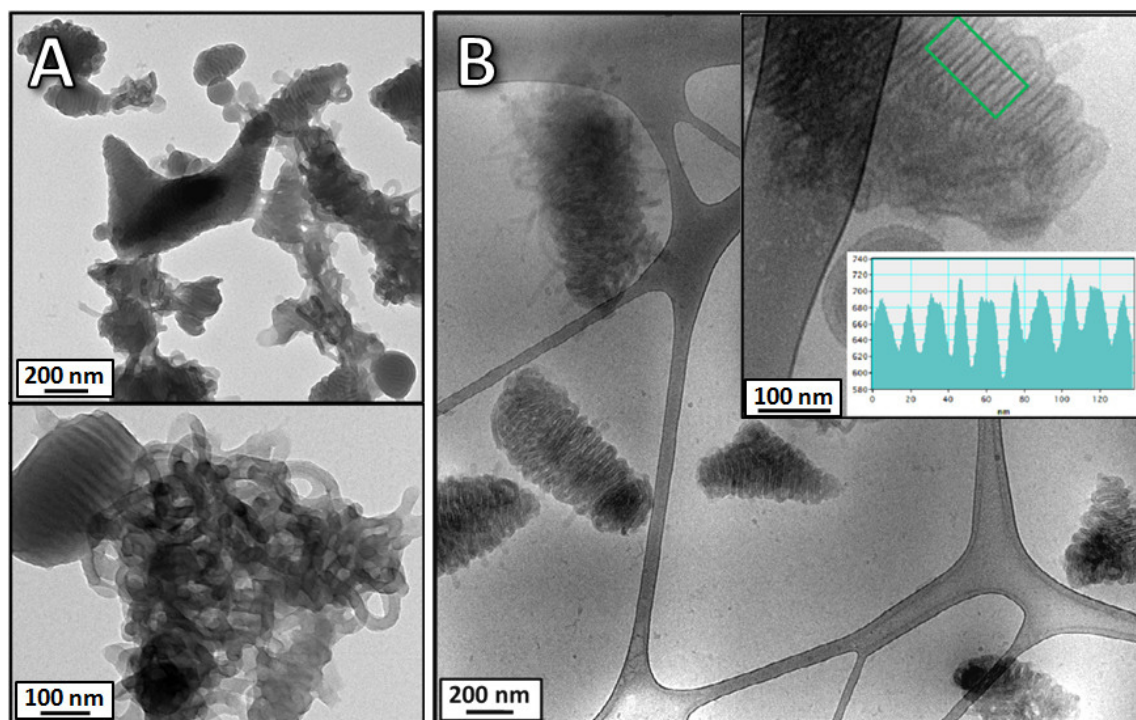


**Figure 4-S5.** TEM (A) and cryo-TEM micrographs (B) of intermediate micellar structures of  $\mu$ -BVqT obtained by dialysis to water after ageing of the dioxane solution for one month. The final polymer concentration was 0.2 g/L for TEM and 0.4 g/L in case of cryo-TEM. The upper inset in (B) displays a gray-scale analysis of the highlighted area.

We further prepared thin film cuts of this structural intermediate by freeze-drying of the solution and embedding the particles into an epoxy resin. The corresponding TEM micrographs from thin slices (with and without additional  $\text{OsO}_4$  staining) are shown in Figure 4-S6 and an internal lamellar structure can be observed (black arrows in Figure 4-S6). Additionally,  $\text{OsO}_4$  staining revealed an undulated shape of the lamellae, which can also be interpreted as a dense packing of spheres (Figure 4-S6B). The same observation was made for some of the cylindrical structures (white arrows in Figure 4-S6B). As indicated by the white arrows for the non-stained micrographs in Figure 4-S6A (only P2VPq is visible), cylindrical protrusions with a tubular nature were also identified. These findings confirm our initial assumption of cylindrical micelles as intermediates. Furthermore, the absence of structures with a diffuse core region supports the assumption of compact particles. The presence of both cylindrical protrusions and elongated particles of rather compact shape with a spherical cross section were further confirmed *via* SEM measurements (Figure 4-S7).

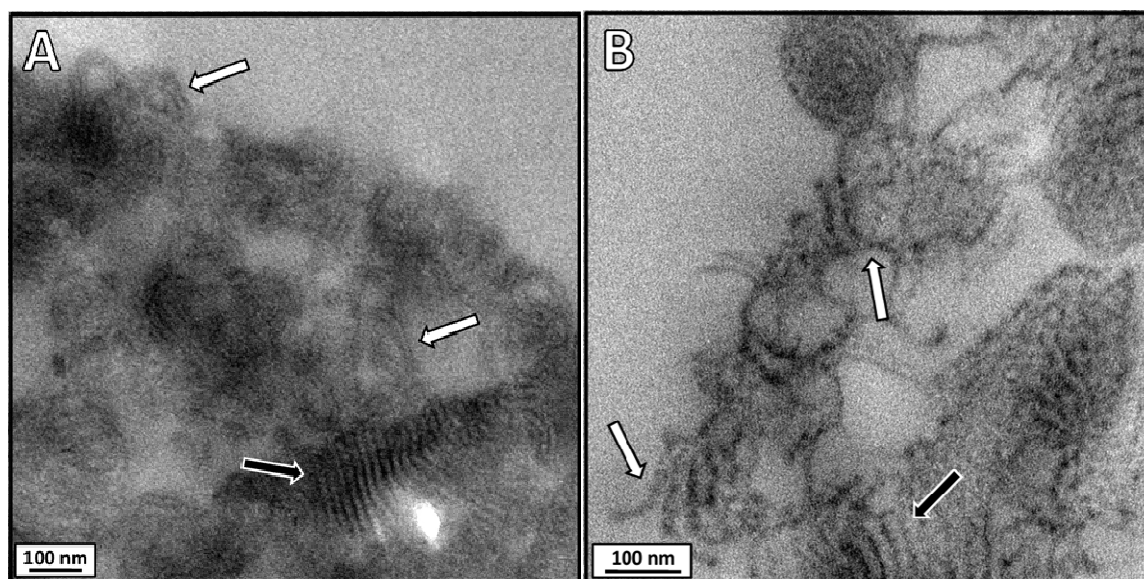


**Figure 4-S6.** TEM micrographs of 50 nm thick cuts from freeze-dried and resin embedded samples of the intermediate structures. This was obtained from the sample depicted in Figure 4-S5. The micrograph (A) is unstained, whereas for (B) staining with  $\text{OsO}_4$  was performed. The black arrows indicate areas where the lamellar structure of the more densely packed particles could be observed, whereas the white arrows highlight spots, where the cylindrical building units are clearly evident.

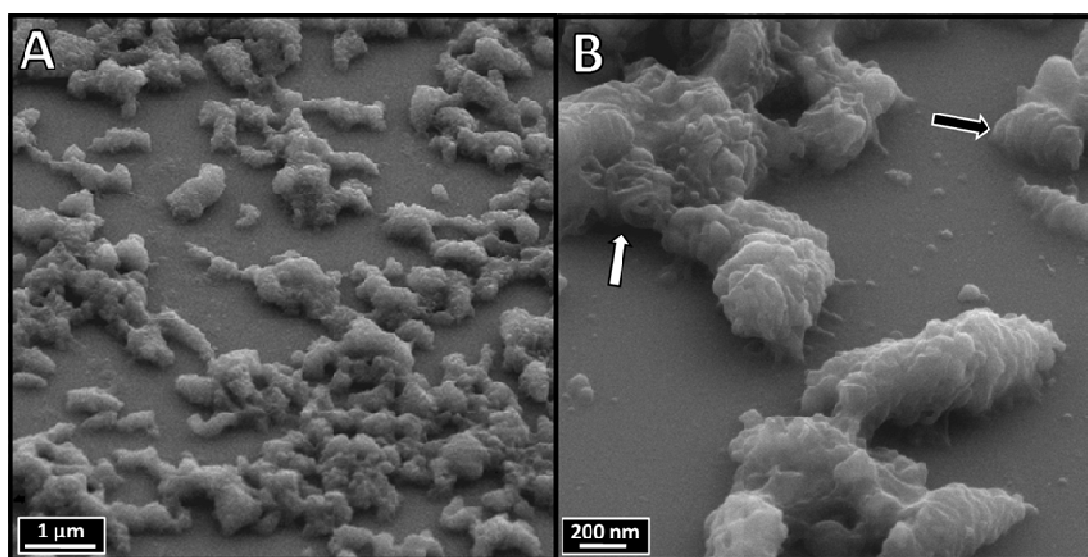


**Figure 4-S7.** SEM images of intermediate structures obtained from aqueous solutions of  $\mu$ -BVqT ( $c = 0.02$  g/L). The samples were measured on a tilted stage. An irregular array of cylinders is present within the sample. The sample was prepared by dialysis of a quaternized dioxane solution, which was allowed to age for 1 month. Besides ill-shaped aggregates (white arrow in B) also some more defined structures are present in the sample (black arrow in B).

#### 4.6.3.2 Importance of the Counterion Nature

To screen the influence of iodine on Poly(*N*-metlyl-2-vinylpyridinium iodide), different amounts were added to a homopolymer solution in dioxane/water mixtures as reference system. Subsequent dialysis to water, followed by DLS measurements (Figure 4-S8) revealed the formation of aggregates already for the sample without additional iodine. We attribute this to incomplete quaternization due to the decreasing solubility of P2VPq during the reaction.<sup>2</sup> However, with additional iodine an increase of the hydrodynamic radii can be clearly observed. Therefore, we assume that the so-formed triiodide counterion leads to a decreased hydrophilicity of the P2VPq segment, inducing further aggregation. Hereby, the addition of iodine prior to dialysis to water is important due to its low solubility in water. In test reactions where an ethanol solution of iodine was added to the aqueous solution of  $\mu$ -BVqT, a brown rim was formed in the vial during slow evaporation of the organic co-solvent. This hints towards its low solubility in water and slow reaction with the iodide counterions mainly located within the corona.

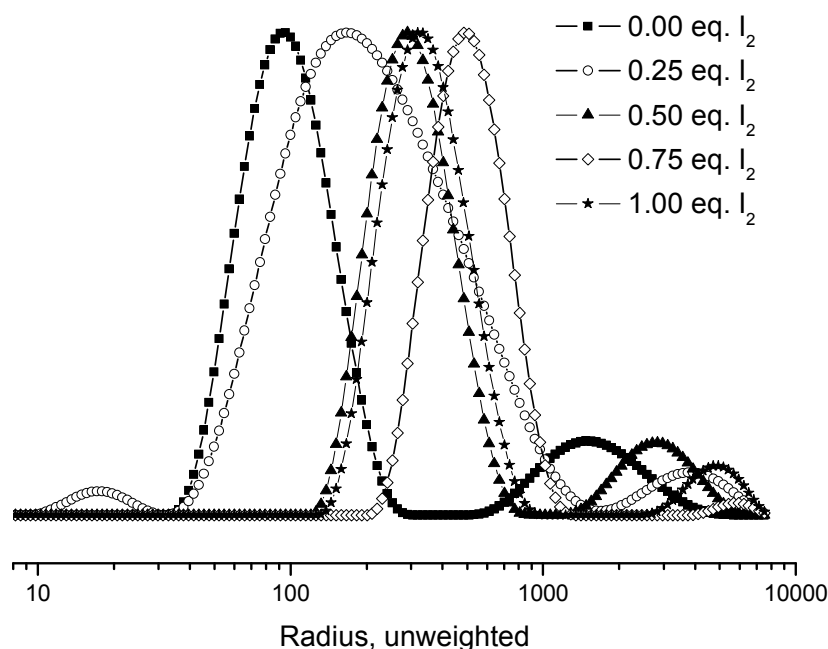


**Figure 4-S8.** DLS CONTIN plots of solutions of linear P2VPq dialyzed from dioxane:water (80:20) mixtures with different amounts of additional iodine with respect to 2VP monomer units to water. The polymer concentration was  $\sim 0.4$  g/L.

To further substantiate the necessity of iodide as counterion for our system to form triiodide, reference solutions of quaternized  $\mu$ -BVT with chloride or methyl sulfate as counterions were prepared. In the first case, the dioxane solution of  $\mu$ -BVqT was dialyzed against a 50 mM solution of LiCl in THF. Subsequent dialysis to water only yielded ill-defined micellar clusters. When the miktoarm star terpolymer was directly quaternized with dimethyl sulfate, the solution precipitated during the dialysis step to water, both from dioxane and THF solution.

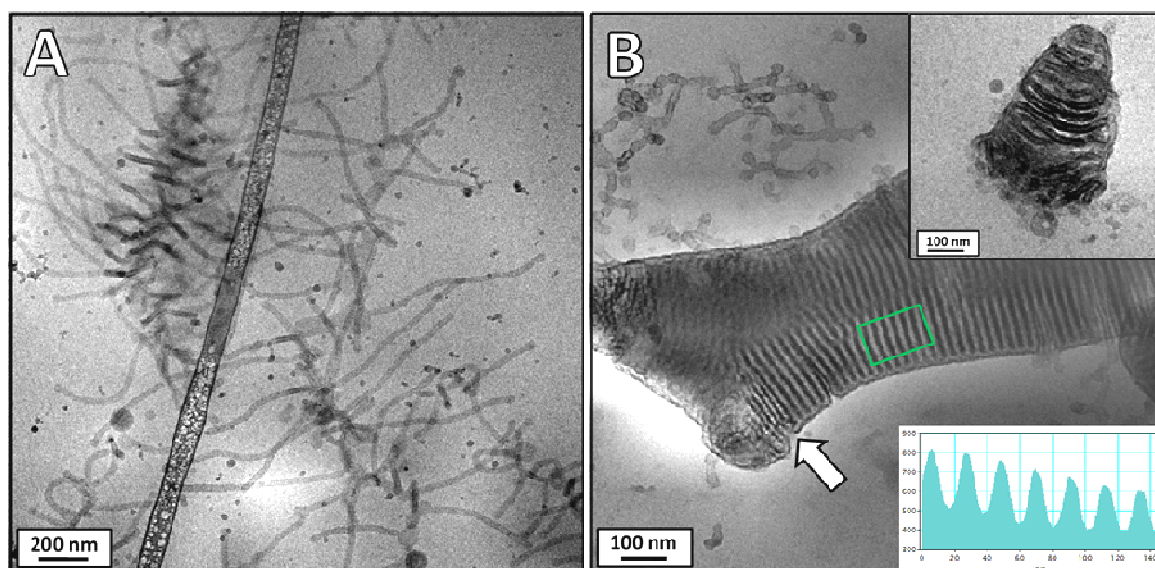


**Figure 4-S9.** cryo-TEM micrograph of cylindrical aggregates obtained from a micellar solution of  $\mu$ -BVqT to which 0.08 (A) and 0.42 (B) equiv of iodine were added before dialysis to water. The polymer concentration was  $\sim 0.4$  g/L. The white arrow in B indicates an area, where the lamellae are less densely packed.

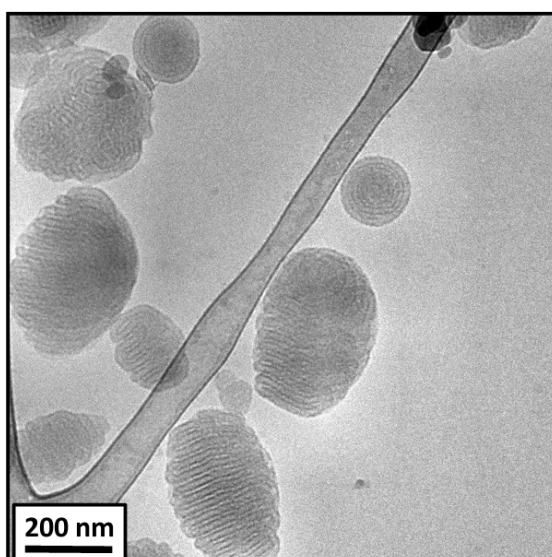


**Figure 4-S10.** cryo-TEM micrograph of a solution of the “woodlouse” aggregates as depicted in Figure 4-S3 which was subsequently dialyzed to a pH3 solution. The polymer concentration was  $\sim 0.6$  g/L.

## 4.6.3.3 Structural Characterization of “Woodlouse” Aggregates

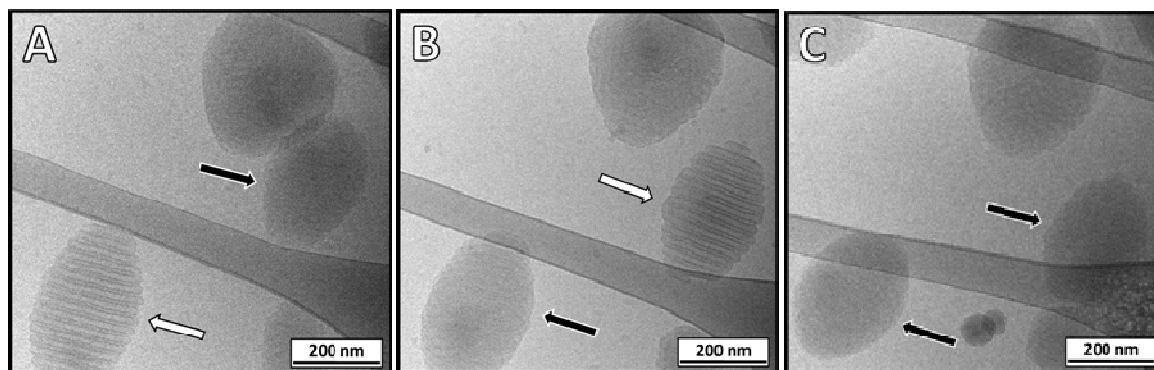


**Figure 4-S11.** cryo-TEM micrograph tilt series of an aqueous solution of the “woodlouse” structure (0.6 g/L,  $\mu$ -BVqT) at 30° (A), 0° (B) and -30° (C) angle. The internal fine structure of the aggregate is only visible, when the longitudinal axis of the object is exactly perpendicular to the direction of the electron beam, as indicated by the white arrows. During tilting the sample the objects leave this optimum position and the fine structure is not visible any more (black arrows).

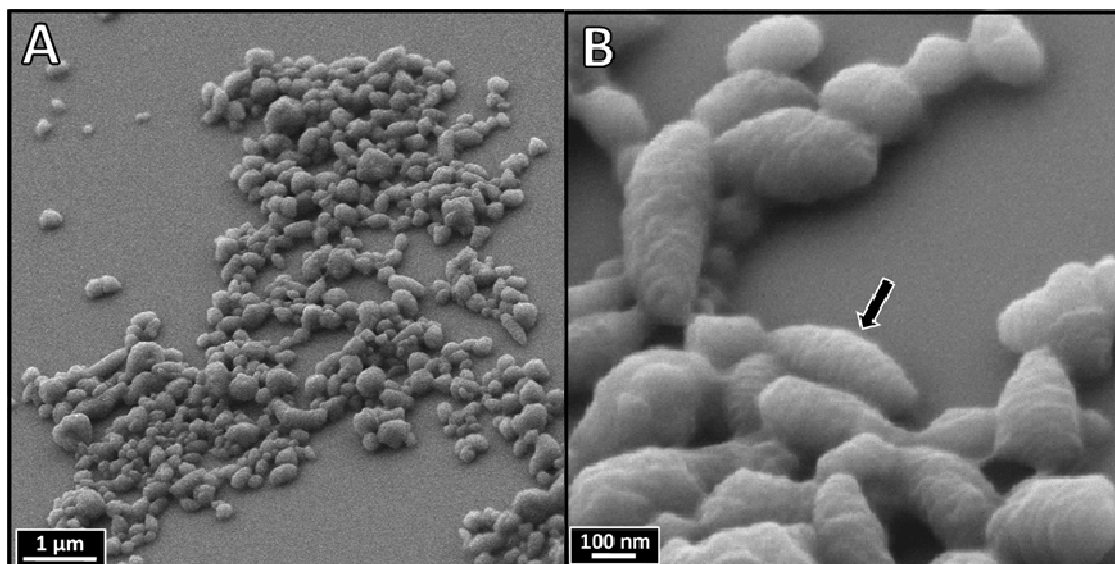


**Figure 4-S12.** SEM images of “woodlouse”-structured aggregates of  $\mu$ -BVqT at  $c = 0.02$  g/L measured on a tilted sample stage. This allows gaining more information about the depth profile of the structure. The aggregates are not flattened on the surface and retain their circular cross section and 3-dimensional shape as assumed from TEM-tomography. This also supports the assumption of compact non hollow particles. Second, at appropriate angles for some particles a regularly corrugated surface profile was observed (see black arrow in B). This is a direct consequence of the regularly belted structure as detected with TEM/cryo-TEM.

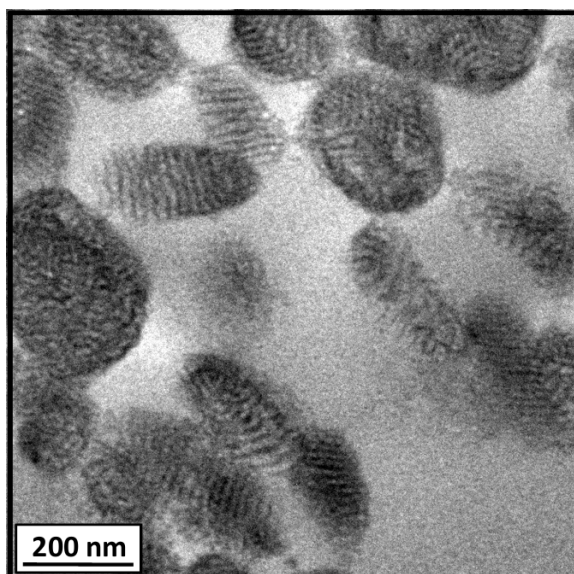


**Figure 4-S13.** Unstained TEM micrograph of a 50 nm thick cut from a freeze-dried and embedded sample of  $\mu$ -BVqT aggregates.

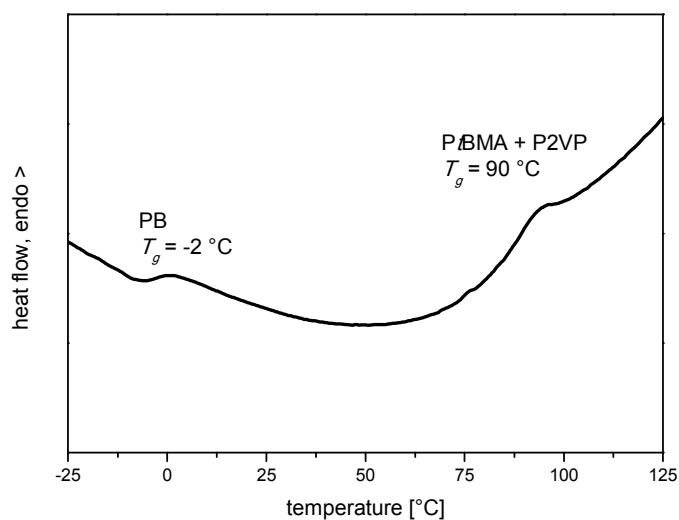


**Figure 4-S14.** DSC plot for the second heating scan of  $\mu$ -BVT. The  $T_g$  of the polybutadiene precursor homopolymer was determined to be  $-8.5$  °C (not shown). For the miktoarm star terpolymers the transition at  $-2$  °C corresponds to the  $T_g$  of the polybutadiene phase, therefore indicating that ligation leads to an increase in  $T_g$ . The transition at  $90$  °C resembles the  $T_g$  of PtBMA and P2VP. Similar to literature we attribute this to consist of two nonresolved peaks.<sup>3</sup>

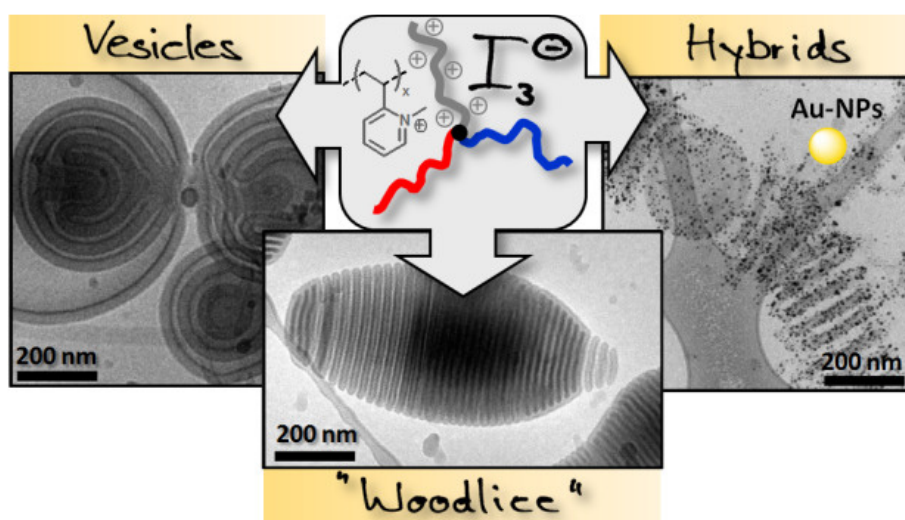
#### 4.6.4 References

- (1) Hanisch, A.; Schmalz, H.; Müller, A. H. E. A Modular Route for the Synthesis of ABC Miktoarm Star Terpolymers *via* a New Alkyne-Substituted Diphenylethylene Derivative. *Macromolecules* **2012**, *45*, 8300-8309.
- (2) Schacher, F.; Walther, A.; Müller, A. H. E. Dynamic Multicompartment-Core Micelles in Aqueous Media. *Langmuir* **2009**, *25*, 10962-10969.
- (3) du Sart, G. G.; Rachmawati, R.; Voet, V.; van Ekenstein, G. A.; Polushkin, E.; ten Brinke, G.; Loos, K. Poly(*tert*-butyl methacrylate-*b*-styrene-*b*-4-vinylpyridine) Triblock Copolymers: Synthesis, Interactions, and Self-Assembly. *Macromolecules* **2008**, *41*, 6393-6399.



## 5 – Hierarchical Self-Assembly of Miktoarm Star Polymer Systems Containing a Polycationic Segment: A General Concept

Andreas Hanisch, André H. Gröschel, Melanie Förtsch, Tina I. Löbling, Felix H. Schacher, and Axel H. E. Müller



**ABSTRACT:** We recently introduced a concept for the counterion-mediated hierarchical self-assembly of amphiphilic miktoarm star terpolymers in aqueous media into micrometer-sized compartmentalized particles with a highly periodic lamellar fine structure (“woodlice”). Herein, we extend this concept to different miktoarm star polymer systems containing a polycationic segment. The presence of a poly(*N*-methyl-2-vinylpyridinium) (P2VPq) block and its interaction with iodide/triiodide counterions is crucial. In analogy to linear diblock copolymer systems the hydrophilic/hydrophobic balance of polybutadiene-*arm*-poly(*N*-methyl-2-vinylpyridinium iodide)-*arm*-polystyrene miktoarm star terpolymers determines the morphology of the primary building blocks (spherical micelles and cylindrical micelles/vesicles) and the obtained superstructures (stacked lamellar structures and multilamellar vesicles) during this hierarchical process. When an ABA’ miktoarm star copolymer (polystyrene-*arm*-poly(*N*-methyl-2-vinylpyridinium iodide)-*arm*-polystyrene) without a dynamic core-forming block was investigated, a different mechanism into “woodlouse”-structured aggregates *via* aggregation and deformation of intermediate vesicles was found. The individual steps of the

different self-assembly processes were investigated by transmission electron microscopy and additionally supported by dynamic light scattering, differential scanning calorimetry, and small-angle X-ray scattering.

**Keywords:** Miktoarm Star Polymer, Polyelectrolyte, Hierarchical Self-Assembly

## 5.1 Introduction

One straightforward method to control the morphology of self-assembled structures from block copolymers is changing the volume fraction of the constituting segments. This led to a diversity of morphologies in the bulk<sup>1-4</sup> and in solution.<sup>5-10</sup> In the latter case, predominantly spherical micelles are formed, but also cylindrical or vesicular structures, as well as the corresponding intermediates have been reported.<sup>11</sup>

Despite the plethora of nanostructures being accessible today, the structural diversity and complexity reached in biological systems still represents the ultimate benchmark. Here, self-organization of diverse biomacromolecules induces hierarchy over several length scales through intra- and intermolecular interactions by encoding utmost functionality *via* the individual building blocks. Such processes can be considered as convergent since the cooperativity of a multitude of (different) weak interactions leads to the formation of primary building blocks, which further assemble into structures of increased complexity at a thermodynamic minimum. The accumulation of weak interactions within and between the building blocks compensates for the loss in entropy.<sup>12,13</sup> For example, proteins fold into complex three-dimensional structures guided by the information encoded within the primary structure of the amino acid sequence.<sup>14</sup> Commonly, these structures are monodisperse, as shown for the tobacco mosaic virus (TMV), where 2130 identical protein subunits arrange around a single strand of RNA in a helical fashion to produce a rigid rod of 18 x 300 nm.<sup>15</sup>

Even though the dimensions obtained in natural systems are difficult to reach by directed self-assembly of synthetic macromolecules in general, this still provides a straightforward approach for the design of well-defined functional materials. Increasing the transcribed chemical information of the system by an additional block (AB to ABC) already leads to a drastic increase of the mere number of morphologies being accessible.<sup>16</sup> This is a consequence of three unlike polymer-polymer interaction parameters and the possibility of solvents being selective for one or two segments. Depending on the individual solubility, this enables the preparation of corona- or core-compartmentalized structures.<sup>17-19</sup> In this context Hillmyer, Lodge and co-workers gave a detailed investigation of the compartmentalization in micellar systems by using miktoarm star

terpolymers. Through this unique macromolecular architecture “hamburger” micelles, segmented worm-like micelles, and substructured vesicles could be obtained as core-compartmentalized analogs to spherical, worm-like and vesicular structures.<sup>20-22</sup> Moreover, in the field of triblock terpolymers it is well demonstrated that the complexation with single stranded DNA<sup>23</sup> or the use of diamines as additives<sup>24,25</sup> display additional triggers for hierarchical structure formation. Especially “kinetic control” allowed for the stepwise self-assembly of poly(acrylic acid)-*block*-poly(methyl acrylate)-*block*-polystyrene triblock terpolymers into toroids, stacks of disk-like micelles, and lamellar phase separated droplets. Hereby, the structures were influenced by the polymer sequence, composition, the nature of the divalent counterion, the solvent mixture, and the preparation pathway and the control of these parameters allowed for manipulation of the obtained aggregation forms.<sup>25-30</sup>

Recently, we reported the counterion-directed self-assembly of a polybutadiene-*arm*-poly(*N*-methyl-2-vinylpyridinium iodide)-*arm*-poly(*tert*-butyl methacrylate) ( $\mu$ -BVqT) miktoarm star terpolymer into multilayered “woodlouse” aggregates, taking advantage of both the polymer architecture and the tunability of the counterion.<sup>31</sup> The presence of iodide as counterion for the quaternized poly(2-vinylpyridine) segment was crucial to achieve superstructure formation. Iodine as additive led to the formation of triiodide, a highly polarizable counterion, which induced hierarchical self-organization from spherical micelles into cylindrical structures and well-defined superstructures thereof. Besides the nature of the counterion and the miktoarm star architecture also the preparation pathway was essential to obtain well-defined aggregates. Here, we try to obtain a more detailed insight into the underlying mechanism of this process by expanding it to other miktoarm star polymer systems. We take advantage of our newly developed modular approach for the straightforward synthesis of such materials.<sup>32</sup> First, the influence of the molecular composition on the obtained building units from three different polybutadiene-*arm*-poly(*N*-methyl-2-vinylpyridinium iodide)-*arm*-polystyrene miktoarm star terpolymers ( $\mu$ -BVqS) and the resulting counterion-directed superstructures will be elaborated. In this context, the P2VPq corona was additionally utilized for the generation and hosting of Au nanoparticles. Second, the triiodide-directed self-assembly of a

polystyrene-*arm*-poly(*N*-methyl-2-vinylpyridinium iodide)-*arm*-polystyrene mikroarm star copolymer ( $\mu$ -SVqS') as a model system without a low  $T_g$  segment is investigated.

## 5.2 Experimental Part

### Synthesis

#### Materials

Butadiene (Rießner-Gase) was passed through columns filled with molecular sieves (4 Å) and basic aluminium oxide and stored over dibutylmagnesium (1 M solution in heptane, Aldrich). 2-Vinylpyridine (2-VP, Aldrich) was degassed, stirred with triethylaluminium (1 M solution in hexanes, Aldrich) and condensed on a high vacuum line. Styrene (BASF) was purified in a similar manner, except that it was stirred with dibutylmagnesium (1 M solution in heptane, Aldrich) instead of triethylaluminium. THF (Sigma-Aldrich) was distilled from CaH<sub>2</sub> and Na/K alloy. *sec*-Butyllithium (Acros, 1.3 M in cyclohexane/hexane: 92/8) was used without further purification. *tert*-Butyl methacrylate (*t*BMA, Sigma-Aldrich) and styrene (Sigma-Aldrich) for ATRP were filtered over basic aluminium oxide before use. *N,N,N',N',N''*-Pentamethyldiethylenetriamine (PMDETA) and CuBr were purchased from Aldrich and distilled and degassed or treated with pure acetic acid and filtered, respectively. 1-(4-*tert*-butyldimethylsilyl)ethynylphenyl)-1-phenylethylene (click-DPE) was synthesized from 1-(4-bromophenyl)-1-phenylethylene as already reported<sup>32</sup>. The aqueous solutions were prepared with distilled desalinated water. All other chemicals were of analytical grade and used as received. The dialysis membrane used for all steps was purchased from Roth (Spectra Por), with a molecular weight cut-off (MWCO) of 1 000 g/mol.

#### Synthesis and Quaternization of Miktoarm Star Ter- and Copolymers

The detailed procedures for the synthesis of the alkyne mid-functional diblock copolymers (polybutadiene-*block*-poly(2-vinylpyridine)) and azido-functionalized homopolymers (polystyrene and poly(*tert*-butyl methacrylate)) have already been reported elsewhere.<sup>32</sup> Similarly, another alkyne mid-functionalized diblock copolymer, polystyrene-*block*-poly(2-vinylpyridine) (PS-*b*-P2VP), was also synthesized *via* anionic polymerization in THF utilizing the alkyne-substituted diphenylethylene (click-DPE) derivative. Therefore, styrene was initiated with *sec*-BuLi at -70 °C and allowed to polymerize at this temperature for 25 minutes before the click-DPE was added (1.1 equiv relative to living chains). After stirring at -50 °C for 2 h the temperature was set to -70 °C and 2VP was added and allowed to polymerize for 5

minutes before termination with degassed isopropanol. The polymer was purified by precipitation in water.

Finally, the ligations of the alkyne-functionalized diblock copolymers with the azido-functionalized homopolymers were conducted by azide-alkyne Huisgen cycloaddition.<sup>33</sup> Therefore, a mixture of the diblock copolymer and 1.1 equiv of the respective homopolymer were dissolved in THF at a concentration of ~20 g/L and degassed for 10 min. After addition of 1 equiv CuBr, the solution was degassed for further 15 min. PMDETA (1 equiv) was added to complex the copper and start the reaction, which was followed by SEC. After 2 days, the resulting miktoarm star terpolymers were purified by passing the solution through a small column with basic alumina to remove copper and finally freeze-dried from dioxane.

### **Preparation of Aqueous Micellar Solutions**

The transformation of the P2VP compartment into a strong cationic polyelectrolyte (P2VPq) was conducted using methyl iodide as quaternization agent. The detailed procedure is given in the literature.<sup>31</sup> To simplify matters, in case of all quaternized solutions the given concentrations resemble the concentration of the pristine miktoarm star terpolymer before the modification, thus neglecting the increase of mass due to quaternization.

For the preparation of the triiodide complexes an iodine stock solution was prepared with dioxane as solvent at 15 g/L. This iodine solution was then added to the dioxane solution of the quaternized star terpolymers until the desired ratio of iodine to amino-function was achieved. Afterwards, the solutions were stirred for 2 h and then treated with ultrasound for 15 min. Subsequently, the solutions were dialyzed against water, as described above and obtained with concentrations ranging from 0.3 to 0.7 g/L. Some of the solutions were colloidally stable over months, whereas others sedimented with time.

### **Generation of Au Nanoparticles**

To 1.5 mL of an aqueous solution of  $\mu$ -BVq1S, which was obtained from dialysis of the corresponding dioxane solution with additional 0.25 equiv I<sub>2</sub> (regarding P2VPq units), was added a highly concentrated aqueous solution of HAuCl<sub>4</sub> until an Au:N ratio of 0.6 was reached. Directly after addition, precipitation occurred, and therefore the sample was treated with ultrasound for 30 minutes. After stirring for 90 minutes the solution was subjected to centrifugation. The supernatant liquid was decanted and the solid content was redispersed in 1.5 mL

of water. A freshly prepared solution of  $\text{NaBH}_4$  was added (5 M equiv with respect to Au) and then the solution was stirred over night. After centrifugation to remove excess reagents, the solid content was again redispersed in 1.5 mL of water to obtain a solution of characteristic red-violet color.

## Characterization

### Transmission Electron Microscopy (cryo-TEM and TEM)

TEM micrographs were taken with a Zeiss CEM 902 or 922 OMEGA electron microscope operated at 80 kV or 200 kV, respectively. Both machines were equipped with an in column energy filter. For sample preparation 2  $\mu\text{L}$  of the solution (typically 0.1-0.2 g/L) were deposited on a hydrophilized TEM grid (copper, 200 mesh). Afterwards, the remaining solvent was removed with a blotting paper. In another preparation pathway a drop of the solution was deposited on a TEM grid on a piece of parafilm, immediately frozen with liquid nitrogen and afterwards freeze-dried. For investigation of the particle film the freeze-dried polymer was embedded into a resin (EpoTek 301). 50 nm thin cuts were prepared with a Leica EM UC7 microtome equipped with a diamond knife and deposited onto TEM grids (copper, 200 mesh). For cryo-TEM studies, a drop ( $\sim 2$  mL) of the aqueous micellar solution ( $c \sim 0.4$ - $0.7$  g/L) was placed on a lacey carbon-coated copper TEM grid (200 mesh, Science Services), where most of the liquid was removed with blotting paper, leaving a thin film stretched over the grid holes. The specimens were shock vitrified by rapid immersion into liquid ethane in a temperature-controlled freezing unit (Zeiss Cryobox, Zeiss NTS GmbH) and cooled to approximately 90 K. The temperature was monitored and kept constant in the chamber during all of the preparation steps. After freezing the specimens, they were inserted into a cryo-transfer holder (CT3500, Gatan) and transferred to a Zeiss EM922 OMEGA EFTEM instrument. Examinations were carried out at temperatures around 90 K. The microscope was operated at an acceleration voltage of 200 kV. Zero-loss filtered images ( $\Delta E = 0$  eV) were taken under reduced dose conditions. All images were registered digitally by a bottom-mounted CCD camera system (Ultrascan 1000, Gatan), combined, and processed with a digital imaging processing system (Gatan Digital Micrograph 3.9 for GMS 1.4). Evaluation of the respective length scales of the structures was achieved by measuring 50-100 different spots within the sample with the UTHSCSA ImageTool V. 3.00.

### **UV-Vis Spectroscopy**

UV-vis spectra were recorded on a Hitachi 3000 spectrophotometer.

### **Dynamic Light Scattering (DLS)**

DLS measurements were performed on an ALV DLS/SLS-SP5022F compact goniometer system equipped with an ALV 5000/E cross correlator and a He-Ne laser ( $\lambda = 632.8$  nm). The measurements were carried out in cylindrical scattering cells ( $d = 10$  mm) at an angle of  $90^\circ$  and a temperature of  $20^\circ\text{C}$ . The solutions were measured without filtration. The CONTIN algorithm was applied to analyze the obtained correlation functions. Apparent hydrodynamic radii were calculated according to the Stokes-Einstein equation.

### **Small-Angle X-Ray Scattering (SAXS)**

SAXS measurements of the freeze-dried powders were performed on a Bruker AXS Nanostar (Bruker, Karlsruhe, Germany), equipped with a microfocus X-ray source (Incoatec  $I\mu\text{S}_{\text{Cu}}$  E025, Incoatec Geesthacht, Germany), operating at  $\lambda = 1.54$  Å. A pinhole setup with 750, 400, and 1000  $\mu\text{m}$  (in the order from source to sample) was used and the sample-to-detector distance was 107 cm. Samples were mounted on a metal rack and fixed using tape. The scattering patterns were corrected for the beam stop and the background (Scotch tape) prior to evaluations. The measurement time was 12 h.

### **Differential Scanning Calorimetry (DSC)**

Thermal analyses and determination of the glass transition temperatures were performed on a Perkin-Elmer Diamond DSC at a heating rate of 20 K/min.

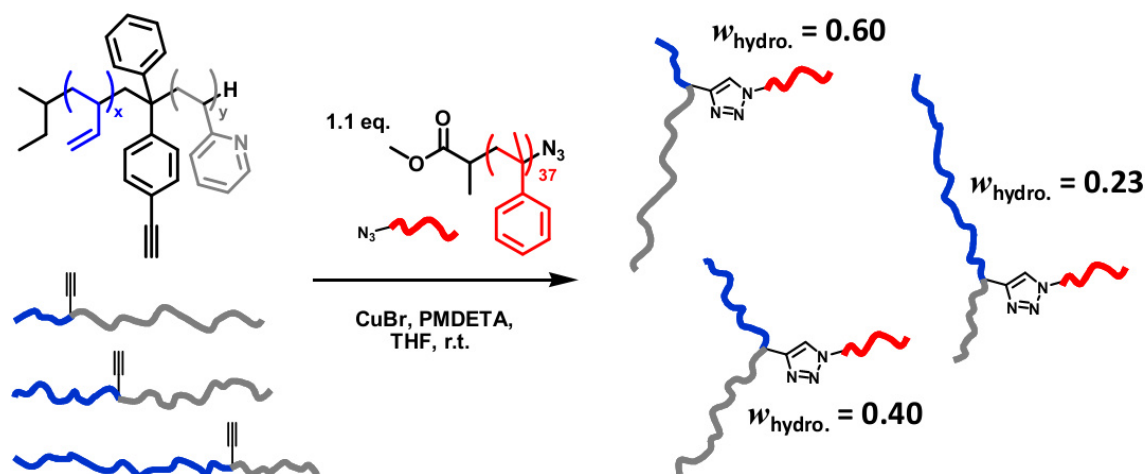
The description of the SEC, NMR and MALDI-ToF experiments is given in the Supporting Information

## 5.3 Results and Discussion

### 5.3.1 Miktoarm Star Ter- and Copolymer Synthesis

We recently demonstrated that triiodide as counterion is capable of guiding the self-assembly of a polybutadiene-*arm*-poly(*N*-methyl-2-vinylpyridinium iodide)-*arm*-poly(*tert*-butyl methacrylate) miktoarm star terpolymer ( $\mu$ -BVqT) into barrel-shaped aggregates with a highly periodic lamellar fine structure (“woodlice”).<sup>31</sup> The miktoarm architecture facilitates the formation of well-defined lamellar aggregates instead of irregular clusters. To extend this concept to other miktoarm star polymers, we synthesized two different systems of miktoarm stars using our previously reported modular approach.<sup>32</sup>

As first system polybutadiene-*arm*-poly(2-vinylpyridine)-*arm*-polystyrene ( $\mu$ -BVS) was selected since PB/PS exhibits a higher incompatibility ( $\chi_{SB} = 0.061$ )<sup>34</sup> as compared to PB/PtBMA ( $\chi_{BT} = 0.007$ )<sup>35</sup> in our previous studies. Starting with polybutadiene-*block*-poly(2-vinylpyridine) (PB-*b*-P2VP) diblock copolymers of different composition (BV1 = B<sub>58</sub>V<sub>101</sub>, BV2 = B<sub>109</sub>V<sub>81</sub> and BV3 = B<sub>223</sub>V<sub>46</sub>, with the subscripts denoting the degree of polymerization of the corresponding blocks), the ligation with azide-terminated polystyrene (PS-N<sub>3</sub>) yielded three  $\mu$ -BVS miktoarm star terpolymers with varying weight fractions of the pH-sensitive P2VP block,  $w_{\text{hydrophilic}}$  (Scheme 5-1). This allows assessing the influence of differences in the hydrophilic/hydrophobic balance during counterion-mediated hierarchical structure formation. The advantage of this strategy compared to ligation of the same diblock copolymer with polystyrene homopolymers of different molecular weight is achieving a broad range of values for  $w_{\text{hydrophilic}}$  without drastic changes in the overall molecular weight. For the second system, we exchanged the dynamic (low  $T_g$ ) polybutadiene block with a glassy polystyrene segment to obtain a  $\mu$ -SVS' (polystyrene-*arm*-poly(2-vinylpyridine)-*arm*-polystyrene) miktoarm star copolymer. This should drastically affect the mobility of the core-forming segments and, thus, have an impact on the obtained structures. The molecular characterization of the miktoarm star polymers and all materials involved is summarized in Table 5-1. The corresponding SEC traces are shown in the Supporting Information (Figure 5-S1 to 5-S4).



Scheme 5-1. Modular synthesis of  $\mu$ -BVS miktoarm star terpolymers of different composition.

Table 5-1. Molecular Characteristics of Homopolymers, Diblock Copolymers, the Obtained  $\mu$ -BVT and  $\mu$ -BVS Miktoarm Star Terpolymers, and the  $\mu$ -SVS' Miktoarm Star Copolymer

sample	polymer composition <sup>a</sup>	$M_n^b$ / kg/mol	PDI <sup>c</sup>	$w_{\text{hydrophilic}}$
S-N <sub>3</sub>	S <sub>36</sub>	3.7	1.07	
T-N <sub>3</sub>	T <sub>53</sub>	7.6	1.17	
BV1	B <sub>58</sub> V <sub>101</sub>	14.0	1.03	
$\mu$ -BV1S	$\mu$ -B <sub>58</sub> V <sub>101</sub> S <sub>36</sub>	17.6	1.04	0.60
BV2	B <sub>109</sub> V <sub>81</sub>	14.7	1.02	
$\mu$ -BV2T <sup>d</sup>	$\mu$ -B <sub>109</sub> V <sub>81</sub> T <sub>53</sub>	22.2	1.07	0.38
$\mu$ -BV2S	$\mu$ -B <sub>109</sub> V <sub>81</sub> S <sub>36</sub>	18.3	1.04	0.46
BV3	B <sub>223</sub> V <sub>46</sub>	17.2	1.02	
$\mu$ -BV3S	$\mu$ -B <sub>223</sub> V <sub>46</sub> S <sub>36</sub>	20.8	1.02	0.23
SV	S <sub>52</sub> V <sub>65</sub>	12.6	1.04	
$\mu$ -SVS'	$\mu$ -S <sub>52</sub> V <sub>65</sub> S <sub>36</sub>	16.2	1.05	0.42

<sup>a</sup>The subscripts denote the degrees of polymerization of the corresponding blocks as calculated from the respective number-average molecular weights,  $M_n$ . <sup>b</sup>The number average molecular weight  $M_n$  was determined by SEC for the PtBMA and PS homopolymers, applying the respective calibrations. For the diblock copolymers the molecular weight was calculated from <sup>1</sup>H NMR using the molecular weight of the PB or PS precursor as reference. This was measured directly *via* MALDI-ToF MS in case of PB and SEC in case of PS. For the ABC miktoarm star terpolymers the overall molecular weight was calculated from the corresponding precursor polymers. <sup>c</sup>Determined by SEC in THF calibrated with PS standards. For the PtBMA homopolymer SEC with the corresponding standards was used. <sup>d</sup>This polymer was investigated in Ref. <sup>31</sup>

## 5.3.2 Hierarchical Self-Assembly of Miktoarm Star Terpolymers of Different Composition and Chemistry

### 5.3.2.1 Hydrophilic/Hydrophobic Balance

According to the mechanism we presented for a  $\mu$ -BVT miktoarm star terpolymer<sup>31</sup> (included as  $\mu$ -BV2T in Table 5-1), we hypothesized that such hierarchical processes should generally be applicable to all miktoarm star systems containing P2VPq segments. It is well-established that the molecular composition drastically affects the solution behavior of amphiphilic block copolymers, *i.e.* that spherical micelles, cylindrical micelles and vesicles are formed with decreasing fraction of the corona block.<sup>7,11,36</sup> Here, three polybutadiene-*b*-poly(2-vinylpyridine) diblock copolymers having an alkyne-function between the blocks and with comparable molecular weights but decreasing P2VP fraction (BV1, BV2 and BV3) were conjugated with the same azido-functionalized polystyrene homopolymer PS-N<sub>3</sub>. In that way,  $\mu$ -BVS miktoarm star terpolymers with different weight fractions of the hydrophilic block ( $w_{\text{hydrophilic}}$ ) were synthesized, the details of which are given in Table 5-1.

The P2VP segments of all three  $\mu$ -BVS miktoarm star terpolymers were first quaternized with methyl iodide resulting in  $\mu$ -BVqS with a permanently charged and hydrophilic P2VPq arm. After dialysis from dioxane into water (without added iodine), different micellar structures were visualized by TEM (Figure 5-1). The contrast primarily derives from the P2VPq phase, which is inherently stained with iodide. The PB and PS phases exhibit only low contrast and cannot be distinguished. Spherical micelles were observed for  $\mu$ -BVq1S ( $d_{\text{micelle}} \sim 20.5 \pm 2.0$  nm, Figure 5-1A) and  $\mu$ -BVq2S ( $d_{\text{micelle}} \sim 27.0 \pm 1.5$  nm, Figure 5-1B), whereas in the latter case also some linear assemblies could be seen (inset in Figure 5-1B). Due to the shorter P2VPq block these micelles are slightly larger than those of  $\mu$ -BVq1S. In contrast,  $\mu$ -BVq3S with only 23 wt-% hydrophilic segments mainly yielded vesicular aggregates with some cylindrical micelles (Figure 5-1C) being present as well. This was supported by cryo-TEM investigations (inset in Figure 5-1C and Figure 5-S5A). As expected for vesicles; the size-distribution was rather broad ( $\sim 50$  to 200 nm in diameter from cryo-TEM). The dimensions of the vesicles were further confirmed by DLS ( $R_{\text{h,app}} = 117$  nm, D.I. = 0.14 Figure 5-S6). Both in TEM and cryo-TEM

some spherical structures were also detected, mostly at the end or kinks of cylindrical micelles, indicating fusion/fission processes during vesicle formation.<sup>37</sup> Thus, reducing the fraction of the solubilizing block expectedly induces a transition from spherical micelles ( $\mu$ -BVq1S,  $\mu$ -BVq2S) to vesicles coexisting with cylinders ( $\mu$ -BVq3S).

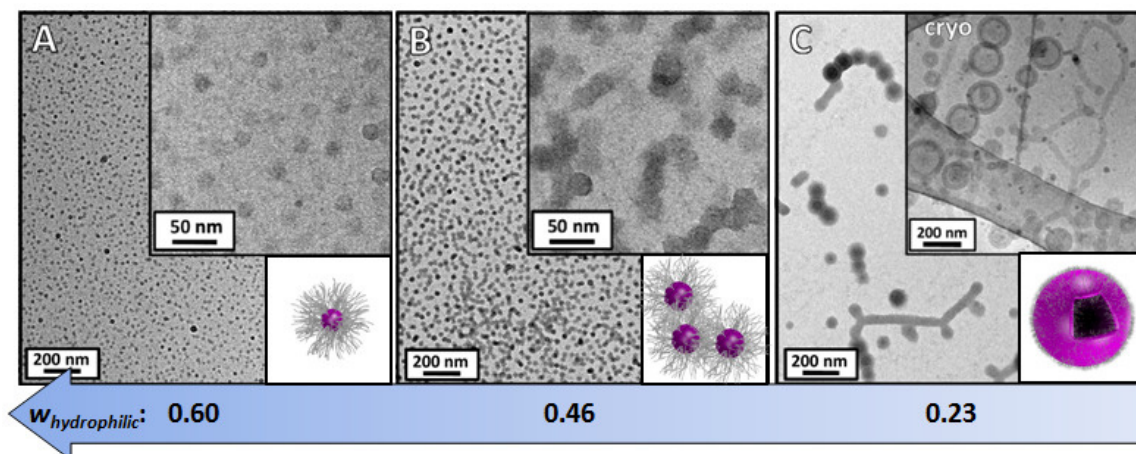


**Figure 5-1.** TEM micrographs of micellar aggregates of  $\mu$ -BVq1S (A),  $\mu$ -BVq2S (B), and  $\mu$ -BVq3S (C) in water. No staining was performed. The inset in (C) displays a cryo-TEM micrograph of the same sample. The concentration was 0.2 g/L for TEM and 0.41 g/L for the cryo-TEM in (C). The schematic illustrations represent the main aggregation form.

When iodine (0.25 equiv with respect to P2VPq) was added to the  $\mu$ -BVqS dioxane solutions prior to dialysis into water, drastic changes regarding micellar morphology are observed (Figure 5-2). Visual inspection showed an increase of the turbidity, clearly indicating the formation of larger structures. For  $\mu$ -BVq1S, mainly spherical micelles and a small fraction of cylinders were present, but also large superstructures with a periodic lamellar fine structure (Figure 5-2A). These structures are analogous to our previous findings for  $\mu$ -BVqT and the observations are confirmed by cryo-TEM (Figures 5-2D, 5-S7A). Here, superstructures of up to several  $\mu\text{m}$  in length were found and the P2VPq segments are only visible at the sheet edges, probably due to an increased segmental density directly at the surface (see gray scale analysis in the inset in Figure 5-2D). In contrast to the “woodlouse” structure reported earlier,<sup>31</sup> the superstructures consist of rather stacked lamellae instead of back-folded and bent lamellae. This is most probably caused by the higher hydrophilic weight fraction  $w_{\text{hydrophilic}}$  (0.60 for  $\mu$ -BVq1S as compared to 0.38 for  $\mu$ -BVqT) which enables sufficient shielding of the hydrophobic edges. Comparably stacked/segmented structures were also reported for triblock terpolymer systems

where attractive interactions of the terminal stabilizing block were induced by interaction with divalent counterions<sup>29</sup> or decreased solvent quality.<sup>38</sup> In case of  $\mu$ -BVq2S, again a mixture of spherical micelles (smaller fraction) and cylinders or superstructures of disk-like aggregates (majority fraction) was found. In some cases, also multilamellar vesicles were observed and cryo-TEM confirms the coexistence of all these morphologies (Figure 5-2B, 5-2E and Figure 5-S7B). In contrast to  $\mu$ -BVq1S, the periodicity of the inner segmented fine structure is not as pronounced.

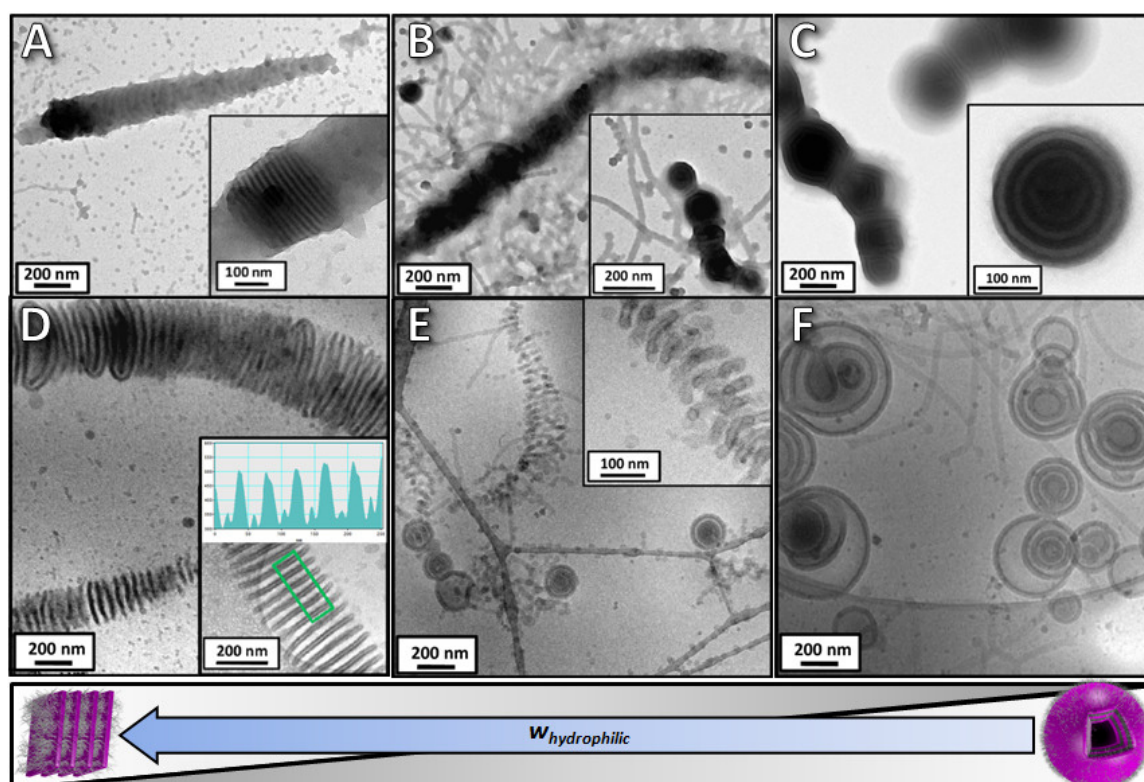


**Figure 5-2.** TEM (A, B, C) and cryo-TEM micrographs (D, E, F) of micellar aggregates obtained from dialysis of  $\mu$ -BVq1S (A, D),  $\mu$ -BVq2S (B, E) and  $\mu$ -BVq3S (C, F) to water in the presence of 0.25 equiv  $I_2$  (with respect to P2VPq units). Except for the inset in (C), where  $OsO_4$  staining (selective for PB) was performed, the contrast results from the quaternized P2VP corona. The concentration was 0.2 g/L for TEM and 0.35 g/L for cryo-TEM. With decreasing length of the hydrophilic block a transition from lamellar structures to multilamellar vesicles is observed, as illustrated in the scheme at the bottom.

However, for  $\mu$ -BVq3S, the addition of iodine induced the formation of multilamellar vesicles with sizes up to 500 nm (Figure 5-2C). As a consequence of the low  $T_g$  of the PB block, which represents the majority phase of the wall, the structures are rather flattened on the substrate in the dried state. In contrast, cryo-TEM (Figure 5-2F, Figure 5-S5B to D) reveals intact multilamellar vesicles with up to 5 lamellae and, additionally, the presence of cylindrical micelles. In some cases also fusion/fission processes during vesi-

cle formation can be visualized (Figure 5-S5B). The fusion-induced increased size and high dispersity of the vesicles with diameters of 200 to over 500 nm (as observed from cryo-TEM) is corroborated by DLS studies ( $R_{h,app} = 236$  nm, D.I. = 0.60, DLS in Figure 5-S6).

When higher amounts of iodine (0.40 equiv) were added before dialysis, precipitation occurred for  $\mu$ -BVq1S and  $\mu$ -BVq2S, most probably due to insufficient coronal stabilization of the disk-like building units, whereas  $\mu$ -BVq3S yielded colloiddally stable solutions. TEM revealed huge, disperse aggregates of vesicles larger than 500 nm in diameter, which sometimes appear in a stacked manner (Figure 5-3A). For some features a lamellar inner structure, similar to the “woodlice” was visible as indicated by the white arrow in Figure 5-3A. Cryo-TEM confirms the coexistence of multilamellar vesicles and elongated structures with an internal lamellar arrangement perpendicular to the longitudinal axis (Figure 5-3B). DLS measurements support the increased dimensions ( $R_{h,app} = 391$  nm, D.I. = 0.12, DLS in Figure 5-S6). Since we did not observe any huge aggregates of several micrometers in length in cryo-TEM, we attribute their presence in the dried state to drying effects. Overall, the multilamellar constitution of the vesicles is much more pronounced than for the sample with 0.25 equiv of  $I_2$  (Figure 5-2F). The increased amount of triiodide accordingly favors fusion into vesicles filled with deformed vesicles due to decreased coronal solubility (lower inset in Figure 5-3B). At a certain threshold value we assume the internal crowding of the vesicles to force rearrangement into elongated structures with a parallel aligned interior to decrease surface curvature (upper inset in Figure 5-3B). These structures are quite similar to the “woodlouse” structures reported for  $\mu$ -BVq2T.<sup>31</sup>

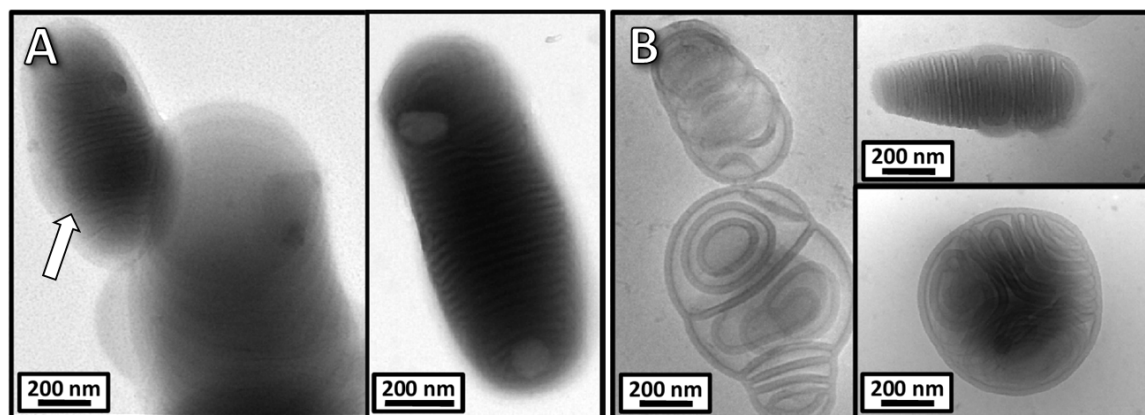


**Figure 5-3.** TEM (A) and cryo-TEM (B) micrographs of vesicular structures obtained from the dialysis of  $\mu$ -BVq3S with 0.40 equiv  $I_2$  to water. For the micrograph at the right side of (A) the polybutadiene phase of the core was selectively stained with  $OsO_4$ . In case of TEM the concentration was 0.2 g/L and for cryo-TEM 0.50 g/L, respectively.

The composition of the core segment for superstructures formed by  $\mu$ -BVq3S will be shortly discussed according to TEM data. Although the phase segregation parameter,  $\chi N = 15.8$ , would suggest the PS and PB arms to be within the strong segregation regime,<sup>39,40</sup> no compartmentalization of the vesicle walls was observed after selective staining of the PB phase with  $OsO_4$  (inset in Figure 5-2C and 5-3A). Additionally, even despite a lower  $\chi N$  of 8.8, differential scanning calorimetry (DSC) of  $\mu$ -BV2S implies phase segregation between PS and PB as the glass transition of PB at  $-2$  °C is detected (Figure 5-S8). We hypothesize that compartmentalization is not visible in the insets in Figure 5-2C and 5-3A, because the shorter PS block (DP = 36) is shielding the PB phase (DP = 223) from the P2VPq by the formation of a thin continuous PS lamella. This situation is hard to visualize in TEM as staining with  $RuO_4$  simultaneously enhances the contrast in the P2VPq phase. Similar findings were made by Hückstädt *et al.* for bulk morphologies of SBV miktoarm star terpolymers with larger volume fractions of PB than PS.<sup>41</sup>

Nevertheless, for all three miktoarm stars different hierarchical superstructures were observed when iodine was added prior to dialysis to water. Whereas for  $\mu$ -BVq1S and  $\mu$ -BVq1S similar processes seem to operate as identified for  $\mu$ -BVqT earlier (aggregation of spherical micelles into cylinders or disks and superstructures thereof),<sup>31</sup> in case of  $\mu$ -BVq3S (displaying the lowest fraction of P2Vq) the fusion of vesicles into multilamellar structures with up to 500 nm in diameter took place, followed by partial rearrangement

into “woodlouse”-like structures upon increasing the triiodide content. Even though in all cases discussed rather non-ergodic structures or, more precisely, mixtures of different morphologies were found, our methodology of counterion-mediated hierarchical self-assembly is clearly applicable to  $\mu$ -BVqS miktoarm star terpolymers of different composition.

The P2VP/P2VPq segments have the added advantage that they are capable to coordinate metal ions.<sup>42,43</sup> We exploited this to directly visualize the P2VPq domains within segmented disk-like structures formed by  $\mu$ -BVq1S. Therefore, H<sub>2</sub>AuCl<sub>4</sub> was added to a micellar solution obtained by dialysis with 0.25 equiv I<sub>2</sub> and subsequently reduced with NaBH<sub>4</sub>. The resulting hybrid superstructures are seen in the cryo-TEM micrograph in Figure 5-4A, with the majority of the Au nanoparticles being located within alternating compartments. Further, a preferential location of the Au nanoparticles at the edges of the sheets is seen. The size distribution of the nanoparticles is quite broad, with diameters between 2-14 nm (see inset in Figure 5-4A). Besides the visualization in TEM the successful nanoparticle generation was also proven by UV-vis measurements (Figure 5-4B). The observed surface plasmon resonance band at 546 nm is blue-shifted as compared to the ~525 nm expected from the size range of the nanoparticles.<sup>44</sup> This might be explained by the dense NP population at the surface of the individual sheets and the decreased interparticle distance, which influences the position of the surface plasmon resonance band.<sup>45</sup>

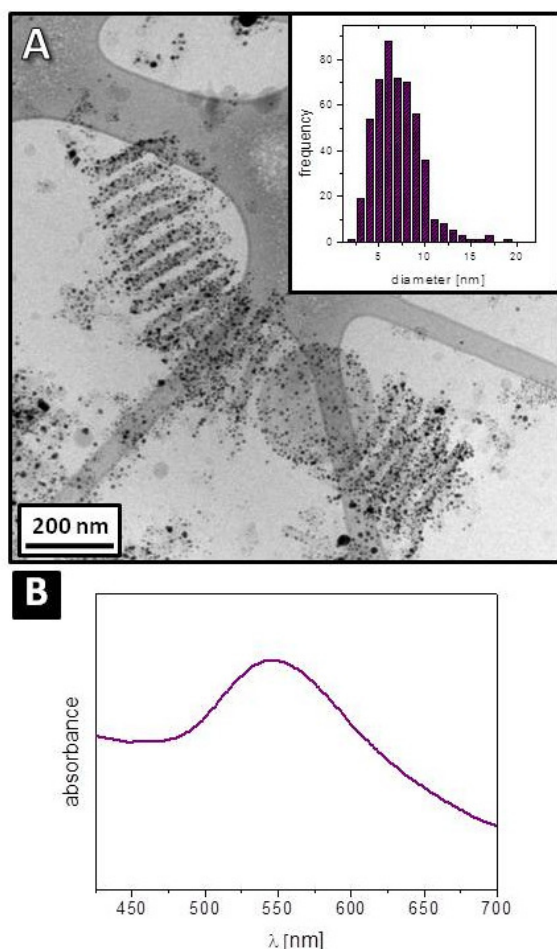


**Figure 5-4.** (A) Cryo-TEM micrograph of micellar aggregates from  $\mu$ -BVq1S ( $c \sim 0.35$  g/L) with *in-situ* formed Au nanoparticles and (B) UV-vis spectrum of the aqueous micellar solution.

### 5.3.2.2 Effect of a High- $T_g$ Core-Forming Block

We further substituted the low- $T_g$  PB block ( $T_g \sim -10$  °C for 1,2-PB homopolymer)<sup>46</sup> with a glassy PS block ( $T_g \sim 80$  °C for a comparable molecular weight of  $\sim 4000$  g/mol)<sup>47</sup> to obtain a  $\mu$ -SVS' miktoarm star copolymer. The arms of this star have comparable molecular weights as those of  $\mu$ -BV2S. This substitution simplifies the system and allows evaluating whether a dynamic segment is necessary for the rearrangement processes during hierarchical self-assembly. Compared to linear PS-*b*-P2VP diblock copolymers, the presence of two polystyrene segments at the block junction leads to a higher segmental density of the hydrophobic block and, hence, influences surface curvature as already shown for comparative studies of  $A_2B$  miktoarm star and AB diblock copolymer systems.<sup>48,49</sup> Most recently, experimental data and theoretical investigations confirmed that this favors the formation of wormlike and vesicular structures compared to linear diblock copolymers

of the same composition.<sup>50,51</sup> Additionally, for  $\mu$ -SVS' the reduced dynamics might enable the isolation of intermediate structures, allowing further insight into the underlying mechanism.

Solutions of the  $\mu$ -SVS' miktoarm star terpolymer were treated using the same quaternization/dialysis procedure, as applied for the other systems. For the dialysis without added iodine, mostly wormlike micelles and completely collapsed vesicles with sizes up to 300 nm were found (Figure 5-5A). As a consequence of this collapse the vesicle walls exhibit a bilayered structure, as shown in the inset in Figure 5-5A and Figure 5-S9A. However, cryo-TEM investigations revealed that this deformation is a consequence of the drying process (Figure 5-5B). Similarly deformed structures were already reported by the group of Eisenberg for poly(acrylic acid)-*b*-polystyrene diblock copolymers under special drying conditions and termed "kippah" structures.<sup>52</sup> Besides that, cryo-TEM also confirmed the presence of cylindrical micelles, which aligned parallel to the vesicle walls (indicated by the arrows in Figure 5-5B) and multilamellar vesicles. Similarly, the vesicles were aligned in a string-like fashion, presumably due to attractive inter-corona interactions originating from minute amounts of triiodide formed during the quaternization process (Figure 5-S10A). We assume that this slight attraction in between different P2VPq coronae is the reason for the complete collapse of the vesicle walls during sample preparation in TEM. During drying of the samples the water outside the vesicles will evaporate faster than inside. The decreasing internal volume in combination with the attractive interactions of the hydrated and therefore flexible inner P2VPq wall might consequently slowly lead to a complete collapse of the vesicle walls into the "kippah" structure (Figure 5-5C). This is supported by another way of sample preparation for TEM measurements. If the sample was directly freeze-dried on the grid the vesicles have no time to completely collapse, only show slight indentations, and no bilayered vesicle walls were present (Figure 5-S9B). Only quite rarely "kippah" structures were observed in contrast to the sample which was dried under ambient temperature.

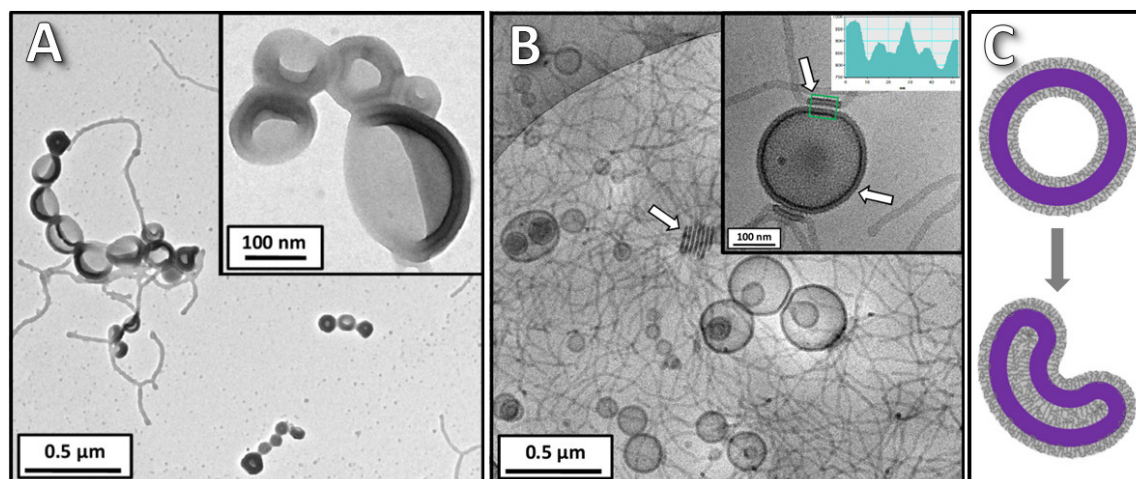


**Figure 5-5.** TEM (A) and cryo-TEM (B) micrographs of  $\mu$ -SVqS' structures obtained *via* dialysis from dioxane solutions to water without supplementary iodine. The P2VPq phase appears dark due to iodide ions and the PS phase is grey. The concentration was 0.2 g/L (A) and  $\sim$ 0.4 g/L (B). The insets in (A) show a higher magnification of the “kippah” vesicles and (B) also includes the gray-scale analysis of the marked area. The white arrows in (B) highlight the areas where stacking of cylinders/vesicle walls into superstructures starts to take place. (C) shows the schematic illustration of the collapse of the vesicles during drying, leading to the “kippah” structure.

When 0.05 equiv of iodine were added before dialysis, comparable structures, but an increased amount of deformed vesicles were observed (Figure 5-6A). For 0.08 equiv  $I_2$  a transition state is reached, where the vesicles show a strong tendency to aggregate into larger clusters (Figure 5-6B). In some cases, structures with beginning internal lamellar periodicity were observed (upper left inset in Figure 5-6B). Interestingly, less individual cylindrical micelles are present, rather a merging into flattened unilamellar sheets is found (upper right inset in Figure 5-6B). As in cryo-TEM (Figure 5-7A and 5-S10B) the same morphological features are present, we attribute the two-dimensional structures to pre-stages of vesicles. Also here, flat sheets (left inset in Figure 5-7A) and curved bilayered structures (right inset in Figure 5-7A) were observed, which have already been identified and named “octopi” and “jellyfish” in the literature.<sup>11</sup> This mixture of different frozen structures is most likely attributed to the glassy nature of the PS segments.<sup>53</sup> Figure 5-6E gives a schematic illustration of the formation of the different structures.

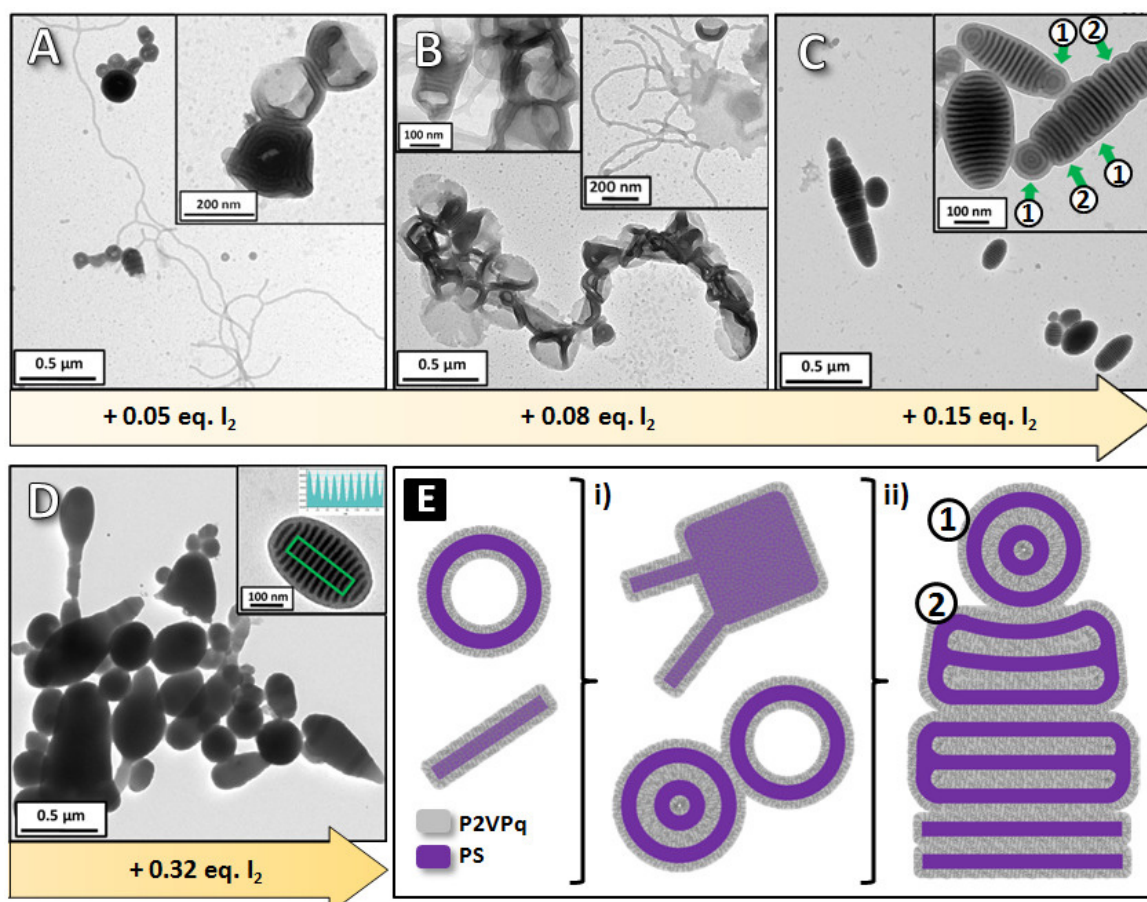


**Figure 5-6.** TEM micrographs of  $\mu$ -SVqS' structures obtained *via* dialysis from dioxane solutions to water with 0.05 (A), 0.08 (B), 0.15 (C) and 0.32 equiv (D) of supplementary iodine. The P2VPq phase appears dark and the PS phase is gray. The concentration was 0.2 g/L. The green arrows in the inset in (C) highlight the individual substructures within the aggregate. The inset in (D) displays a gray scale analysis of the lamellar structure. In (E) a schematic representation of the hierarchical self-assembly process is illustrated: (i) the addition of iodine induces aggregation of vesicles and the formation of nascent bilayers from cylindrical micelles; (ii) formation of well-defined hierarchical lamellar superstructures.

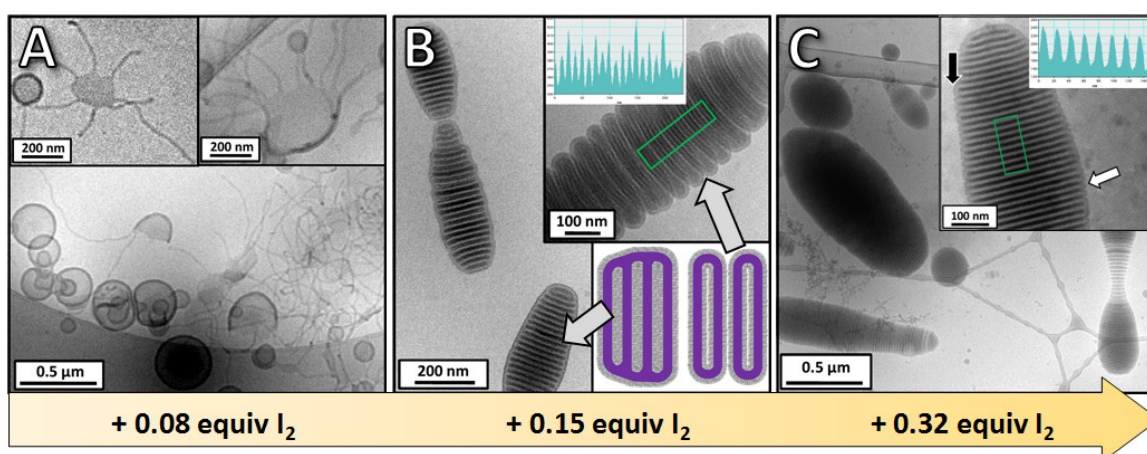


**Figure 5-7.** Cryo-TEM micrographs of  $\mu$ -SVqS' after dialysis to water with 0.08 (A), 0.15 (B) and 0.32 equiv (C) of supplementary iodine. The polymer concentration was  $\sim$ 0.4 g/L and in the corresponding insets gray scale analyses are shown (P2VPq black, PS gray). In (B) a cartoon of the different stages of fused or stacked vesicles is shown. Here, the gray illustrated P2VPq corona appears dark in cryo-TEM, whereas the violet depicted PS core appears gray. The black arrow in (C) accentuates a region where the individual lamellae are back-folded, whereas the white arrow points out an area where the lamellae are stacked.

When 0.15 equiv  $I_2$  were added, huge superstructures ( $\sim 240 \pm 180$  nm for longitudinal axis) with a well-defined internal fine structure were formed (Figure 5-6C). Similar to the “woodlouse” structures observed for  $\mu$ -BVqT, the particles are elongated and ellipsoidal in shape. The presence of trapped multilamellar (1) and deformed vesicles (2) within the compartmentalized particles indicates that these served as intermediate building blocks (inset in Figure 5-6C). These observations are confirmed by cryo-TEM (Figure 5-7B). Interestingly, two populations of the objects were present. Some objects were rather tightly packed, with a dark corona of P2VPq surrounding the complete aggregate (left side of Figure 5-7B), presumably due to slight differences in corona hydrophobicity. In other cases the packing was less dense with associated subunits emerging from fused and deformed aggregated vesicles (upper inset in Figure 5-7-B). The two packing motifs are illustrated in Figure 5-7B. Additionally, cryo-TEM tilt images series (video 5-S1) clearly reveal that the less densely packed structures consist of stacks of laterally compressed vesicles.

Supplementary video related to this article can be found at <http://dx.doi.org/10.1016/j.polymer.2013.05.071>.

For 0.32 equiv of  $I_2$  similar multilamellar and elongated structures were found, but larger in size ( $\sim 370 \pm 250$  nm for the longitudinal axis, Figure 5-6D). This increased size is attributed to surface minimization in order to decrease the unfavorable corona/solvent interface triggered by the higher concentration of triiodide counterions. The inner compartments feature alternating stripes with high periodicity ( $d_{\text{dark}} = 9.0 \pm 1.0$  nm,  $d_{\text{bright}} = 7.5 \pm 1.0$  nm, see inset in Figure 5-6D). However, the individual vesicular building blocks are not as pronounced as in the case of 0.15 equiv  $I_2$  and the presence of terminal (multi)vesicular features was not observed at all. The lamellar periodicity was confirmed by cryo-TEM (Figure 5-7C and 5-S10C), where different stacking arrangements of these lamellae are visible. Either, the lamellae were connected at the particle edges (black arrow in Figure 5-7C), or consisted of stacks of individual sheets (white arrow in Figure 5-7C), which might evolve from rearrangements of intermediate vesicular building blocks. Overall, the aggregates were more tightly packed, as compared to the dialysis with 0.15 equiv  $I_2$ . Again, in cryo-TEM varying lamellae thicknesses could be found (Figure 5-S10C), depending whether structure formation from stacked/deformed or fused vesicular sub-

units occurred as illustrated in the inset in Figure 5-7B. All the intermediate stages on the way to the substructured particles were also investigated by dynamic light scattering (Figure 5-S11), where a continuous shift of the peak maxima is clearly observed with increasing amount of iodine added. The dispersity indices were quite high (0.36-0.87), which we attribute to the low mobility of the core-forming block, resulting in the presence of different aggregation forms. For the transition state at 0.08 equiv increased dimensions and a broader size distribution were detected, reflecting the presence of nascent bilayer sheets.

We furthermore confirmed the lamellar compartmentalization of the particles shown in Figure 5-6C and 5-6D by small angle X-ray scattering (SAXS). For this, the particles were freeze-dried and mounted on a metal rack using tape. For both samples (dialysis with 0.15 and 0.32 equiv of I<sub>2</sub>) identical scattering patterns were observed (Figure 5-8), corresponding to the [100], [200] and [300] reflexes at  $q = 0.384, 0.782$  and  $1.152 \text{ nm}^{-1}$  for a lamellar morphology with a long period  $d_{\text{lam}} = 16.5 \pm 1.0 \text{ nm}$ . This is in perfect agreement with the value observed by TEM as depicted in Figure 5-6D ( $d_{\text{lam}} = 16.5 \pm 1.0 \text{ nm}$ ).

Further, the freeze-dried sample with 0.15 equiv was embedded into a resin and investigated by TEM after microtome cuts were prepared (Figure 5-S12). The presence of the lamellar structure within the centers of the particles supports the assumption of compact, non-hollow structures.

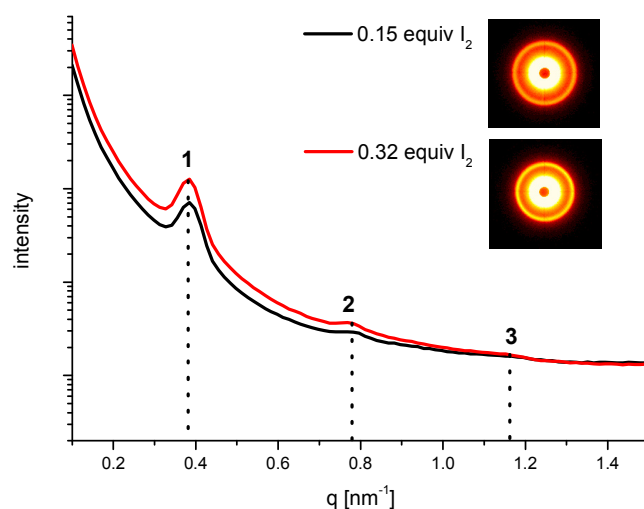


**Figure 5-8.** SAXS patterns of freeze-dried powders of the “woodlouse” aggregates obtained by dialysis of  $\mu$ -SVqS’ with 0.15 (black curve) and 0.32 equiv I<sub>2</sub> to water. The integer numbers indicate the relative reflex positions and the insets depict the corresponding 2D scattering patterns.

As compared to the structures from  $\mu$ -BVqT,<sup>31</sup> similar “woodlouse” morphologies were observed for  $\mu$ -SVqS’, although the hierarchical self-assembly seems to occur *via* a completely different mechanism, starting from vesicles instead of spherical micelles. This behavior is quite unexpected as the hydrophilic weight fraction,  $w_{\text{hydrophilic}}$ , of the respective unquaternized precursor star polymer is even lower for  $\mu$ -BVT (0.37) than for  $\mu$ -SVS’ (0.41). A possible explanation might be the different solubilities during the dialysis from dioxane to water. Whereas we have shown for  $\mu$ -BVqT that first PB collapses during the increase of water content, followed by PtBMA,<sup>31</sup> in case of  $\mu$ -SVqS’, both PS segments collapse simultaneously, leading to a higher weight fraction of insoluble block(s) already at the initial stages. The structures obtained from the  $\mu$ -BVqS system support this assumption. The PB and PS block are both nonpolar and are therefore supposed to also collapse simultaneously during dialysis to water. Even though for  $\mu$ -BVq2S ( $w_{\text{hydrophilic}} = 0.43$  for the unquaternized precursor) spherical micelles serve as initial building blocks, already a slight tendency for further agglomeration was observed (Figure 5-1B) and after addition of iodine a certain fraction of vesicles is present (Figure 5-2B and E). In contrast,  $\mu$ -BV3qS ( $w_{\text{hydrophilic}} = 0.21$  for the unquaternized precursor) predominantly formed vesicles. Interestingly, the influence of the low  $T_g$  PB induces the fusion into tightly packed multilamellar vesicles (Figure 5-2F) instead of deformed and aggregated vesicles for  $\mu$ -SVqS’ (Figure 5-7B and C).

For the initial levels of aggregation of  $\mu$ -SVqS', a mixture of different morphologies was found, which we also attribute to the absence of a soft PB block. In general, block copolymers containing segments with a high  $T_g$ , as *e.g.* PS or PtBMA, lead to frozen micelles in water, without detectable unimer mobility, whereas soft core-forming blocks like PB lead to partially dynamic structures.<sup>53-55</sup> Remarkably, our approach seems to be applicable even to systems with glassy PS vesicle walls, as the crucial steps of self-organization take place during dialysis, where the presence of the organic co-solvent dioxane sufficiently swells the PS segments and drastically enhances mobility. Further increase of the water content finally leads to frozen structures, which are discernible, like *e.g.* as "jellyfish" or the building units of the "woodlouse" structured aggregates. In contrast to the "woodlouse" structures reported for  $\mu$ -BV2qT, which formed *via* cylindrical intermediate stages, for  $\mu$ -SVqS' defects in periodicity and branching are by far less pronounced as a consequence of vesicles acting as primary building units.

## 5.4 Conclusions

We have demonstrated the universal applicability of triiodide-mediated hierarchical self-assembly for different miktoarm star terpolymer and copolymer systems. In analogy to diblock copolymer systems, adjusting the hydrophilic/hydrophobic balance of the respective system allows to control the resulting morphologies. With decreasing length of the stabilizing coronal block, a transition from spherical micelles to cylindrical micelles and vesicles as initial building blocks was detected. Starting from these, segmented wormlike superstructures, multilamellar vesicles, and superstructures thereof were formed by hierarchical self-assembly.

The successful use of an ABA' miktoarm star copolymer with two glassy PS blocks as hydrophobic segments revealed that this approach is not limited to systems comprising a soft core-forming block like PB. Crucial intermediates are formed during early stages of the dialysis procedure, where the PS segments are still swollen with organic co-solvent and exhibit sufficient chain mobility. However, the overall mobility of the system is lower, resulting in the formation of less uniformly packed superstructures. Interestingly, similar superstructures to the already reported "woodlouse" aggregates were obtained for this system despite vesicles acting as the primary building units. For some samples these vesicular building blocks were distinguishable in the "woodlouse" particles. The anisotropic stacking of these deformed vesicular primary building units resulted in primarily elongated aggregates with only a marginal fraction of branched features.

As vesicles act as adequate primary building blocks for the hierarchical self-assembly process into "woodlouse" aggregates, encapsulation processes are theoretically possible. In combination with the possibility of post-functionalization, the domain-selective generation of metal nanoparticles, and the wide applicability of our synthetic strategy, this triiodide-mediated hierarchical self-assembly is of possible interest in the design of novel stimuli-responsive substructured materials.

**Acknowledgements.** This work was supported by the Deutsche Forschungsgesellschaft within SPP 1165 (Mu896/22). FHS is grateful for a fellowship from the Verband der Chemischen Industrie (VCI) and to the Thuringian Ministry for Education, Science and Culture (TMBWK, Grant No. B514-09051, NanoConSens, and Grant No. B515-11028, SWAXS-JCSM) for financial support.

**Supplementary Data.** Supplementary data related to this article can be found at <http://dx.doi.org/10.1016/j.polymer.2013.05.071>.

## 5.5 References

- (1) Matsen, M. W.; Bates, F. S. Unifying Weak- and Strong-Segregation Block Copolymer Theories. *Macromolecules* **1996**, *29*, 1091-1098.
- (2) Khandpur, A. K.; Foerster, S.; Bates, F. S.; Hamley, I. W.; Ryan, A. J.; Bras, W.; Almdal, K.; Mortensen, K. Polyisoprene-Polystyrene Diblock Copolymer Phase Diagram Near the Order-Disorder Transition. *Macromolecules* **1995**, *28*, 8796-8806.
- (3) Lorenzo, A. T.; Arnal, M. L.; Müller, A. J.; Boschetti de Fierro, A.; Abetz, V. Confinement Effects on The Crystallization and SSA Thermal Fractionation of the PE Block within PE-*b*-PS Diblock Copolymers. *Eur. Polym. J.* **2006**, *42*, 516-533.
- (4) Schacher, F. H.; Rupar, P. A.; Manners, I. Functional Block Copolymers: Nanostructured Materials with Emerging Applications. *Angew. Chem., Int. Ed.* **2012**, *51*, 7898-7921.
- (5) Zhang, L.; Eisenberg, A. Multiple Morphologies of "Crew-Cut" Aggregates of Polystyrene-*b*-poly(acrylic acid) Block Copolymers. *Science* **1995**, *268*, 1728-1731.
- (6) Won, Y.-Y.; Davis, H. T.; Bates, F. S. Giant Wormlike Rubber Micelles. *Science* **1999**, *283*, 960-963.
- (7) Jain, S.; Bates, F. S. On the Origins of Morphological Complexity in Block Copolymer Surfactants. *Science* **2003**, *300*, 460-464.
- (8) Savić, R.; Luo, L.; Eisenberg, A.; Maysinger, D. Micellar Nanocontainers Distribute to Defined Cytoplasmic Organelles. *Science* **2003**, *300*, 615-618.
- (9) Mai, Y.; Eisenberg, A. Self-Assembly of Block Copolymers. *Chem. Soc. Rev.* **2012**, *41*, 5969-5985.
- (10) Pietsch, C.; Mansfeld, U.; Guerrero-Sanchez, C.; Hoepfner, S.; Vollrath, A.; Wagner, M.; Hoogenboom, R.; Saubern, S.; Thang, S. H.; Becer, C. R.; Chiefari, J.; Schubert, U. S. Thermo-Induced Self-Assembly of Responsive Poly(DMAEMA-*b*-DEGMA) Block Copolymers into Multi- and Unilamellar Vesicles. *Macromolecules* **2012**.
- (11) Blanz, A.; Madsen, J.; Battaglia, G.; Ryan, A. J.; Armes, S. P. Mechanistic Insights for Block Copolymer Morphologies: How Do Worms Form Vesicles? *J. Am. Chem. Soc.* **2011**, *133*, 16581-16587.
- (12) Philp, D.; Stoddart, J. F. Self-Assembly in Natural and Unnatural Systems. *Angew. Chem., Int. Ed.* **1996**, *35*, 1154-1196.
- (13) Klug, A. From Macromolecules to Biological Assemblies (Nobel Lecture). *Angew. Chem., Int. Ed.* **1983**, *22*, 565-582.
- (14) Grantcharova, V.; Alm, E. J.; Baker, D.; Horwich, A. L. Mechanisms of Protein Folding. *Curr. Opin. Struct. Biol.* **2001**, *11*, 70-82.
- (15) Klug, A. The Tobacco Mosaic Virus Particle: Structure and Assembly. *Philos. Trans. R. Soc. London B* **1999**, *354*, 531-535.
- (16) Moughton, A. O.; Hillmyer, M. A.; Lodge, T. P. Multicompartment Block Polymer Micelles. *Macromolecules* **2012**, *45*, 2-19.
- (17) Gohy, J.-F.; Willet, N.; Varshney, S.; Zhang, J.-X.; Jérôme, R. Core-Shell-Corona Micelles with a Responsive Shell. *Angew. Chem., Int. Ed.* **2001**, *40*, 3214-3216.
- (18) Berlepsch, H. v.; Bottcher, C.; Skrabania, K.; Laschewsky, A. Complex Domain Architecture of Multicompartment Micelles from a Linear ABC Triblock Copolymer Revealed by Cryogenic Electron Tomography. *Chem. Commun.* **2009**, 2290-2292.
- (19) Wang, L.; Lin, J. Discovering Multicore Micelles: Insights into the Self-Assembly of Linear ABC Terpolymers in Midblock-selective Solvents. *Soft Matter* **2011**, *7*, 3383-3391.
- (20) Li, Z.; Hillmyer, M. A.; Lodge, T. P. Morphologies of Multicompartment Micelles Formed by ABC Miktoarm Star Terpolymers. *Langmuir* **2006**, *22*, 9409-9417.
- (21) Saito, N.; Liu, C.; Lodge, T. P.; Hillmyer, M. A. Multicompartment Micelles from Polyester-Containing ABC Miktoarm Star Terpolymers. *Macromolecules* **2008**, *41*, 8815-8822.
- (22) Liu, C.; Hillmyer, M. A.; Lodge, T. P. Multicompartment Micelles from pH-Responsive Miktoarm Star Block Terpolymers *Langmuir* **2009**, *25*, 13718-13725.
- (23) Liu, C.; Zhang, K.; Chen, D.; Jiang, M.; Liu, S. Transforming Spherical Block Polyelectrolyte Micelles into Free-suspending Films *via* DNA Complexation-induced Structural Anisotropy. *Chem. Commun.* **2010**, *46*, 6135-6137.
- (24) Dupont, J.; Liu, G. ABC Triblock Copolymer Hamburger-like Micelles, Segmented Cylinders, and Janus Particles. *Soft Matter* **2010**, *6*, 3654-3661.

- (25) Cui, H.; Chen, Z.; Wooley, K. L.; Pochan, D. J. Controlling Micellar Structure of Amphiphilic Charged Triblock Copolymers in Dilute Solution *via* Coassembly with Organic Counterions of Different Spacer Lengths. *Macromolecules* **2006**, *39*, 6599-6607.
- (26) Pochan, D. J.; Chen, Z.; Cui, H.; Hales, K.; Qi, K.; Wooley, K. L. Toroidal Triblock Copolymer Assemblies. *Science* **2004**, *306*, 94-97.
- (27) Chen, Z.; Cui, H.; Hales, K.; Li, Z.; Qi, K.; Pochan, D. J.; Wooley, K. L. Unique Toroidal Morphology from Composition and Sequence Control of Triblock Copolymers. *J. Am. Chem. Soc.* **2005**, *127*, 8592-8593.
- (28) Cui, H.; Chen, Z.; Zhong, S.; Wooley, K. L.; Pochan, D. J. Block Copolymer Assembly *via* Kinetic Control. *Science* **2007**, *317*, 647-650.
- (29) Li, Z.; Chen, Z.; Cui, H.; Hales, K.; Wooley, K. L.; Pochan, D. J. Controlled Stacking of Charged Block Copolymer Micelles. *Langmuir* **2007**, *23*, 4689-4694.
- (30) Cui, H.; Chen, Z.; Wooley, K. L.; Pochan, D. J. Origins of Toroidal Micelle Formation Through Charged Triblock Copolymer Self-Assembly. *Soft Matter* **2009**, *5*, 1269-1278.
- (31) Hanisch, A.; Gröschel, A. H.; Förtsch, M.; Drechsler, M.; Jinnai, H.; Ruhland, T. M.; Schacher, F.; Müller, A. H. E. Counterion-Mediated Hierarchical Self-Assembly of an ABC Miktoarm Star Terpolymer. *ACS Nano* **2013**, *3*, 4030-4041.
- (32) Hanisch, A.; Schmalz, H.; Müller, A. H. E. A Modular Route for the Synthesis of ABC Miktoarm Star Terpolymers *via* a New Alkyne-Substituted Diphenylethylene Derivative. *Macromolecules* **2012**, *45*, 8300-8309.
- (33) Binder, W. H.; Sachsenhofer, R. 'Click' Chemistry in Polymer and Materials Science. *Macromol. Rapid Commun.* **2007**, *28*, 15-54.
- (34) Mark, J. E. In *Physical Properties of Polymers Handbook*; American Institute of Physics Press: Woodbury, 1996.
- (35) Schacher, F.; Yuan, J.; Schoberth, H. G.; Müller, A. H. E. Synthesis, Characterization, and Bulk Crosslinking of Polybutadiene-*block*-poly(2-vinyl pyridine)-*block*-poly(*tert*-butyl methacrylate) Block Terpolymers. *Polymer* **2010**, *51*, 2021-2032.
- (36) Zehm, D.; Ratcliffe, L. P. D.; Armes, S. P. Synthesis of Diblock Copolymer Nanoparticles via RAFT Alcoholic Dispersion Polymerization: Effect of Block Copolymer Composition, Molecular Weight, Copolymer Concentration, and Solvent Type on the Final Particle Morphology. *Macromolecules* **2012**.
- (37) Antonietti, M.; Förster, S. Vesicles and Liposomes: A Self-Assembly Principle Beyond Lipids. *Adv. Mater.* **2003**, *15*, 1323-1333.
- (38) Zhu, J.; Jiang, W. Self-Assembly of ABC Triblock Copolymer into Giant Segmented Wormlike Micelles in Dilute Solution. *Macromolecules* **2005**, *38*, 9315-9323.
- (39) Leibler, L. Theory of Microphase Separation in Block Copolymers. *Macromolecules* **1980**, *13*, 1602-1617.
- (40) Bates, F. S.; Fredrickson, G. H. Block Copolymer Thermodynamics: Theory and Experiment. *Annu. Rev. of Phys. Chem.* **1990**, *41*, 525-557.
- (41) Hückstädt, H.; Göpfert, A.; Abetz, V. Synthesis and Morphology of ABC Heteroarm Star Terpolymers of Polystyrene, Polybutadiene and Poly(2-vinylpyridine). *Macromol. Chem. Phys.* **2000**, *201*, 296-307.
- (42) Schacher, F.; Betthausen, E.; Walther, A.; Schmalz, H.; Pergushov, D. V.; Müller, A. H. E. Interpolyelectrolyte Complexes of Dynamic Multicompartment Micelles. *ACS Nano* **2009**, *3*, 2095-2102.
- (43) Walther, A.; Yuan, J.; Abetz, V.; Müller, A. H. E. Structure-Tunable Bidirectional Hybrid Nanowires *via* Multicompartment Cylinders. *Nano Lett.* **2009**, *9*, 2026-2030.
- (44) Haiss, W.; Thanh, N. T. K.; Aveyard, J.; Fernig, D. G. Determination of Size and Concentration of Gold Nanoparticles from UV-Vis Spectra. *Anal. Chem.* **2007**, *79*, 4215-4221.
- (45) Storhoff, J. J.; Lazarides, A. A.; Mucic, R. C.; Mirkin, C. A.; Letsinger, R. L.; Schatz, G. C. What Controls the Optical Properties of DNA-Linked Gold Nanoparticle Assemblies? *J. Am. Chem. Soc.* **2000**, *122*, 4640-4650.
- (46) Brandrup, J.; Immergut, E. H.; Grulke, E. A. In *Polymer Handbook*; Fourth Edition ed.; Wiley: New York, 1999.
- (47) Gan, Y.; Dong, D.; Hogen-Esch, T. E. Effects of Lithium Bromide on the Glass Transition Temperatures of Linear and Macrocylic Poly(2-vinylpyridine) and Polystyrene. *Macromolecules* **1995**, *28*, 383-385.

- (48) Pispas, S.; Hadjichristidis, N.; Potemkin, I.; Khokhlov, A. Effect of Architecture on the Micellization Properties of Block Copolymers: A<sub>2</sub>B Miktoarm Stars vs AB Diblocks. *Macromolecules* **2000**, *33*, 1741-1746.
- (49) Aliferis, T.; Iatrou, H. Aggregation Phenomena of Linear and Miktoarm Star Copolymers of Styrene and Dimethylsiloxane: Influence of the Architecture. *Eur. Polym. J.* **2008**, *44*, 2412-2417.
- (50) Plamper, F. A.; Gelissen, A. P.; Timper, J.; Wolf, A.; Zevin, A. B.; Richtering, W.; Tenhu, H.; Simon, U.; Mayer, J.; Borisov, O. V.; Pergushov, D. V. Spontaneous Assembly of Miktoarm Stars into Vesicular Interpolyelectrolyte Complexes. *Macromolecul. Rapid Commun.* **2013**, *34*, 855-860.
- (51) Zhulina, E. B.; Borisov, O. V. *ACS Macro Lett.* **2013**, *2*, 292-295.
- (52) Azzam, T.; Eisenberg, A. Fully Collapsed (Kippah) Vesicles: Preparation and Characterization. *Langmuir* **2010**, *26*, 10513-10523.
- (53) Nicolai, T.; Colombani, O.; Chassenieux, C. Dynamic Polymeric Micelles versus Frozen Nanoparticles Formed by Block Copolymers. *Soft Matter* **2010**, *6*, 3111-3118.
- (54) Riess, G. Micellization of block copolymers. *Prog. Polym. Sci.* **2003**, *28*, 1107-1170.
- (55) Betthausen, E.; Drechsler, M.; Fortsch, M.; Pergushov, D. V.; Schacher, F. H.; Müller, A. H. E. Stimuli-responsive Micellar Interpolyelectrolyte Complexes - Control of Micelle Dynamics via Core Crosslinking. *Soft Matter* **2012**, *8*, 10167-10177.

## 5.6 Supporting Information

### 5.6.1 Additional Experimental Section

#### Size Exclusion Chromatography (SEC)

SEC measurements were performed on a set of 30 cm SDV-gel columns (5  $\mu\text{m}$  bead size, with pore sizes of  $10^5$ ,  $10^4$ ,  $10^3$  and  $10^2$  Å) using refractive index and UV ( $\lambda = 254$  nm) detection. THF was used as eluent at a flow rate of  $1 \text{ ml min}^{-1}$ . Toluene was used as internal standard and the system was calibrated with PS and 1,4-PB standards

#### $^1\text{H}$ NMR Spectroscopy

$^1\text{H}$  NMR spectra were recorded on a Bruker Ultrashield 300 spectrometer at an operating frequency of 300 MHz.  $\text{CDCl}_3$  was used as solvent and tetramethylsilane as internal standard.

#### Matrix-Assisted Laser Desorption Ionization Time-of-Flight Mass Spectrometry (MALDI-ToF MS)

MALDI-ToF MS analysis was performed on a Bruker-Reflex III apparatus equipped with a  $\text{N}_2$  laser ( $\lambda = 337$  nm) at an acceleration voltage of 20 kV. *trans*-2-[3-(4-*tert*-Butylphenyl)-2-methyl-2-propenylidene]malonitrile (DCTB, Fluka, 99,0 %) was used as matrix and silver trifluoroacetate ( $\text{AgTFA}$ , Sigma-Aldrich, 99.99%) as ionization agent. Samples were prepared from THF solution by mixing matrix, polymer and salt in a ratio of 20/5/1 (v/v).

## 5.6.2 Miktoarm Star Ter- and Copolymer Synthesis

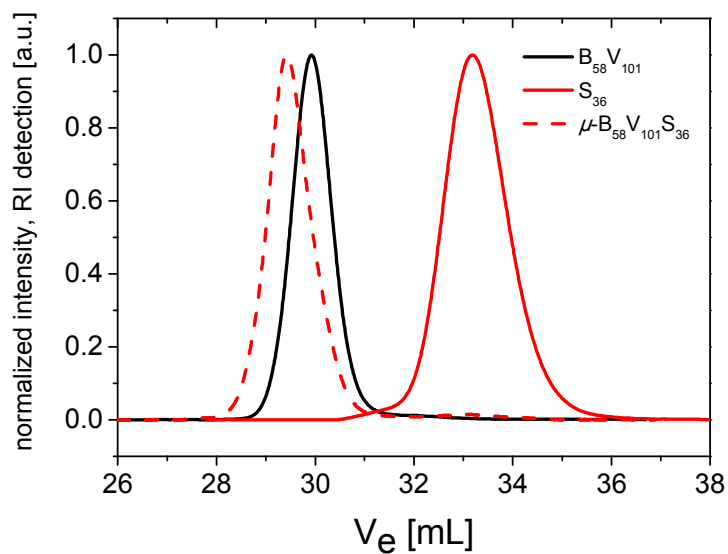


**Figure 5-S1.** SEC eluograms of  $\mu$ -BV1S miktoarm star terpolymer and the corresponding precursor PB-*b*-P2VP diblock copolymer (BV1) and PS homopolymer. In all cases the RI signal is shown.

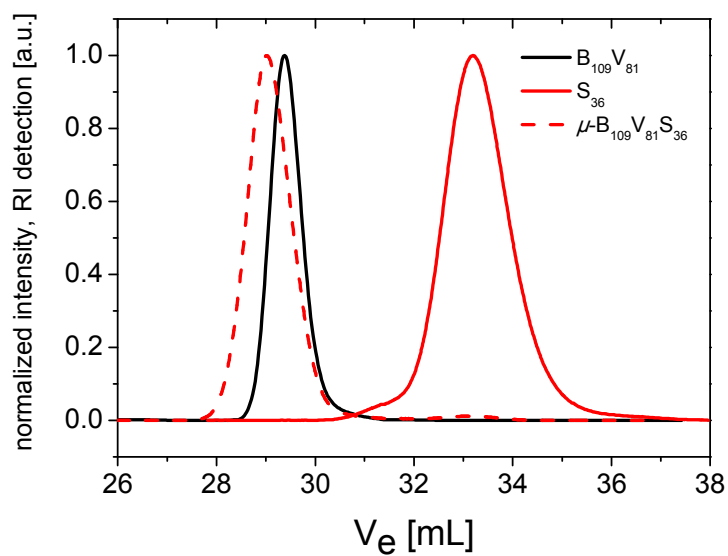


**Figure 5-S2.** SEC eluograms of  $\mu$ -BV2S miktoarm star terpolymer and the respective precursor PB-*b*-P2VP diblock copolymer (BV2) and PS homopolymer. In all cases the RI signal is shown.

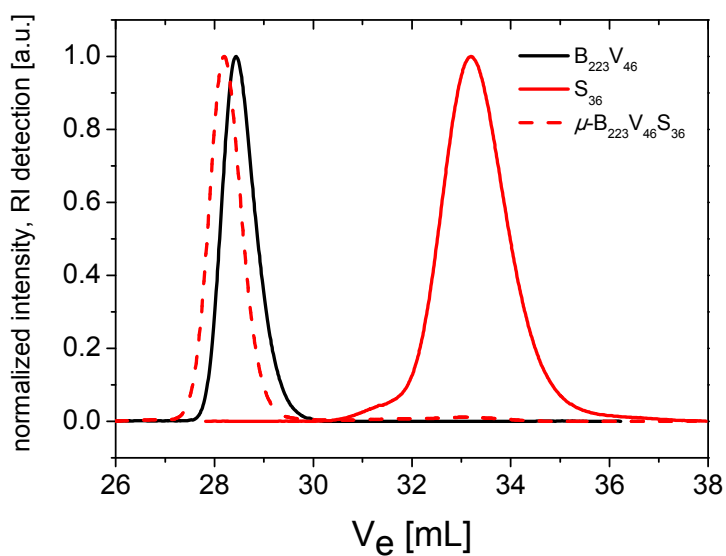


**Figure 5-S3.** SEC eluograms of  $\mu$ -BV3S miktoarm star terpolymer and the respective precursor PB-*b*-P2VP diblock copolymer (BV3) and PS homopolymer. In all cases the RI signal is shown.

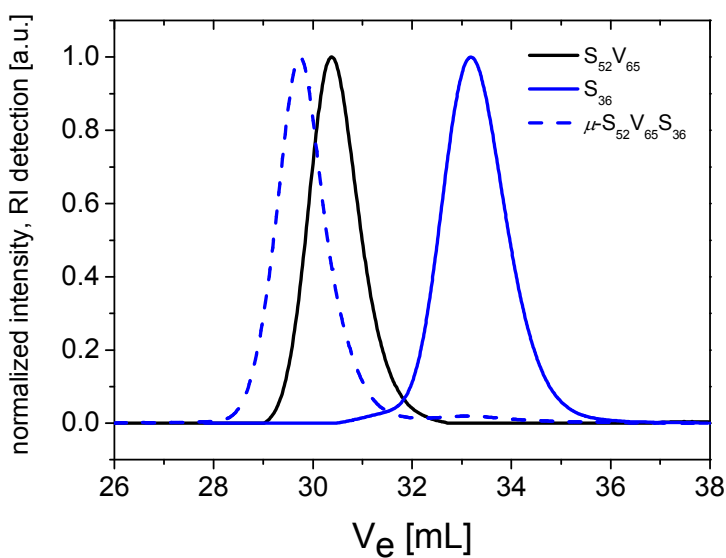


**Figure 5-S4.** SEC eluograms of  $\mu$ -SVS' miktoarm star terpolymer and the respective precursor PS-*b*-P2VP diblock copolymer and PS homopolymer. In all cases the RI signal is shown.

### 5.6.3 Hierarchical Self-Assembly of Miktoarm Star Terpolymers of Different Composition and Chemistry

#### 5.6.3.1 Hydrophilic/Hydrophobic Balance

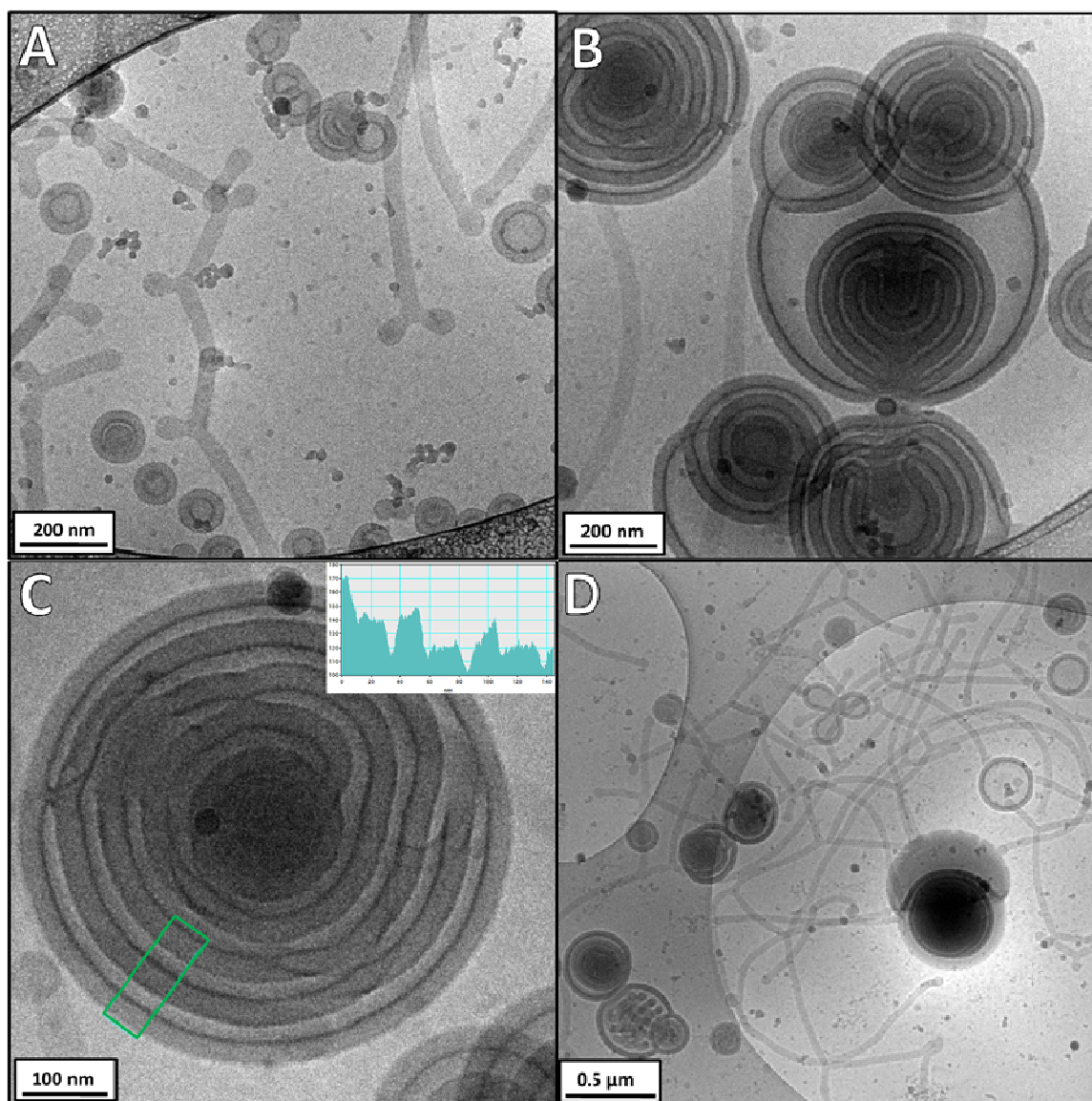


**Figure 5-S5.** cryo-TEM micrographs of vesicular aggregates obtained from dialysis of  $\mu$ -BVq3S dioxane solution to water, without (A) and with additional 0.25 equiv of supplementary iodine regarding 2VPq units (B, C, D). The concentrations were approximately 0.35 g/L.

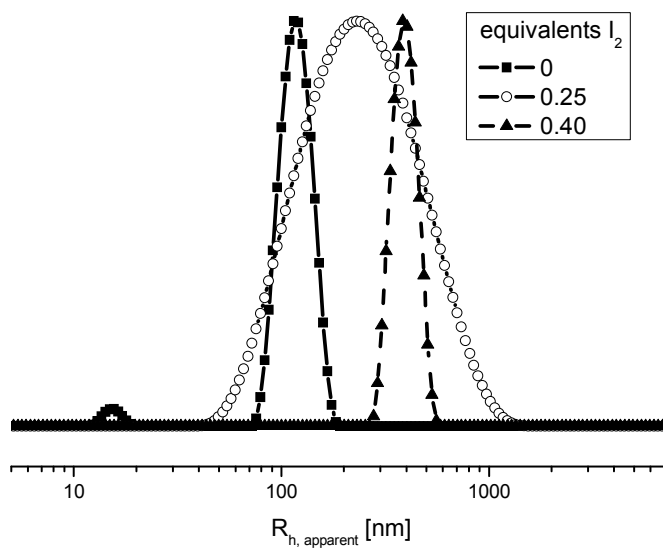


**Figure 5-S6.** Intensity-weighted DLS CONTIN plot of  $\mu$ -BVq3S after dialysis to water without (-■-,  $R_{h,app}$  = 117 nm, D.I. = 0.14) and with 0.25 (-○-,  $R_{h,app}$  = 236 nm, D.I. = 0.60) or 0.40 equiv  $I_2$  (-▲-,  $R_{h,app}$  = 391 nm, D.I. = 0.12). The concentrations were approximately 0.4 g/L.

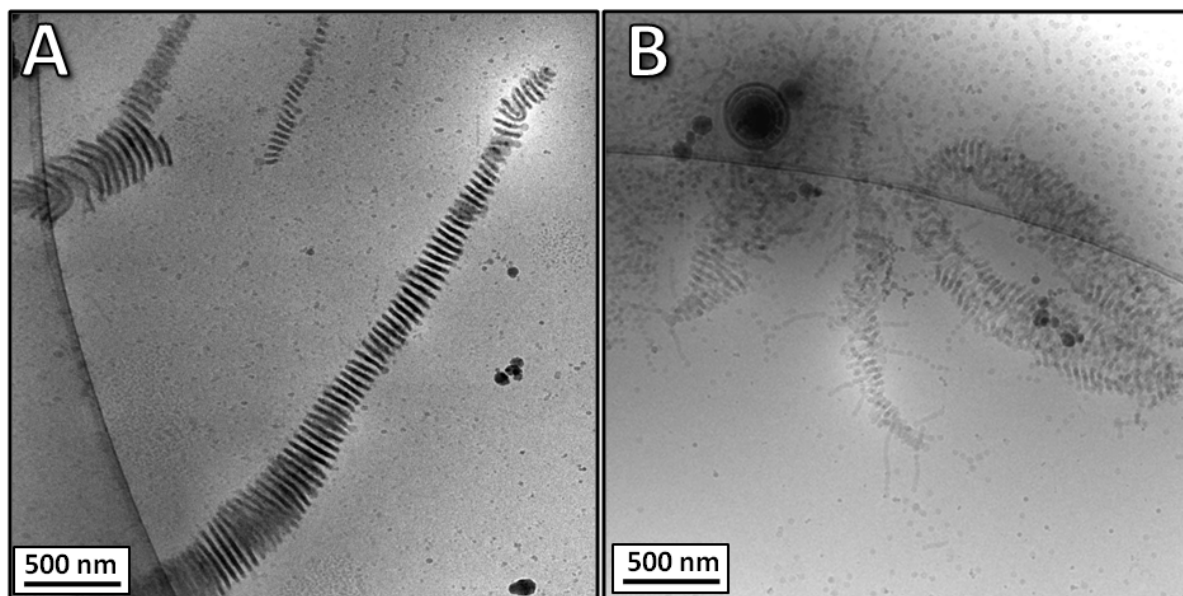


**Figure 5-S7.** cryo-TEM micrograph of aqueous solutions of superstructures obtained from dialysis of  $\mu$ -BVq1S (A) and  $\mu$ -BVq2S (B) with additional 0.25 equiv of free iodine regarding 2VPq units. The concentrations were approximately 0.35 g/L.

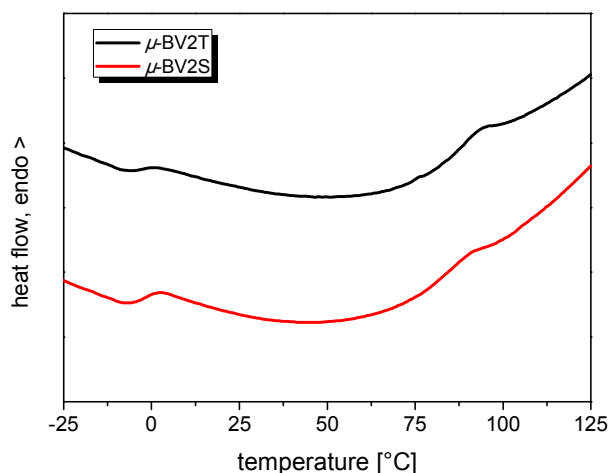


**Figure 5-S8.** DSC plots for the second heating scans of  $\mu$ -BV2T (solid black line) and the corresponding  $\mu$ -BV2S (solid red line). For both star terpolymers the transition at  $-2$  °C corresponds to the  $T_g$  of the polybutadiene phase.<sup>1</sup> The transitions in the range from 80 to 100°C clearly resemble the glass transition temperatures of P2VP and PtBMA or PS, respectively. Similar to literature we attribute this to consist of two non-resolved peaks.<sup>2</sup>

### 5.6.3.2 Effect of a High- $T_g$ Core-Forming Block

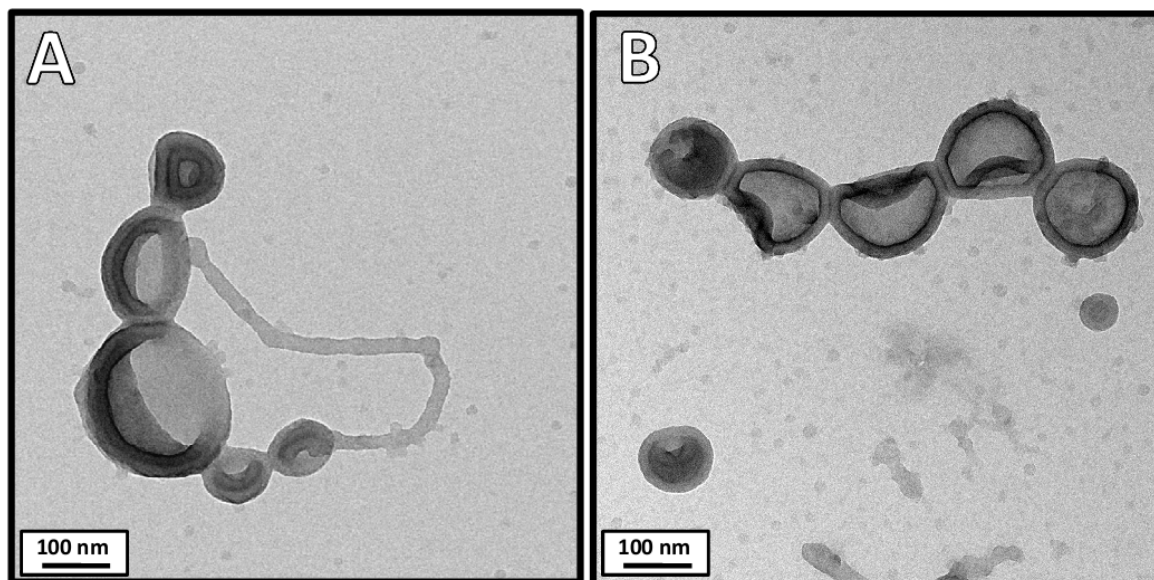


**Figure 5-S9.** TEM micrographs of vesicles obtained from dialysis of  $\mu$ -SVqS' dioxane solutions to water. The concentrations were 0.2 g/L. For (A) the sample was prepared by slow evaporation of the solvent in contrast to (B), where the solution was directly freeze-dried on the grid.

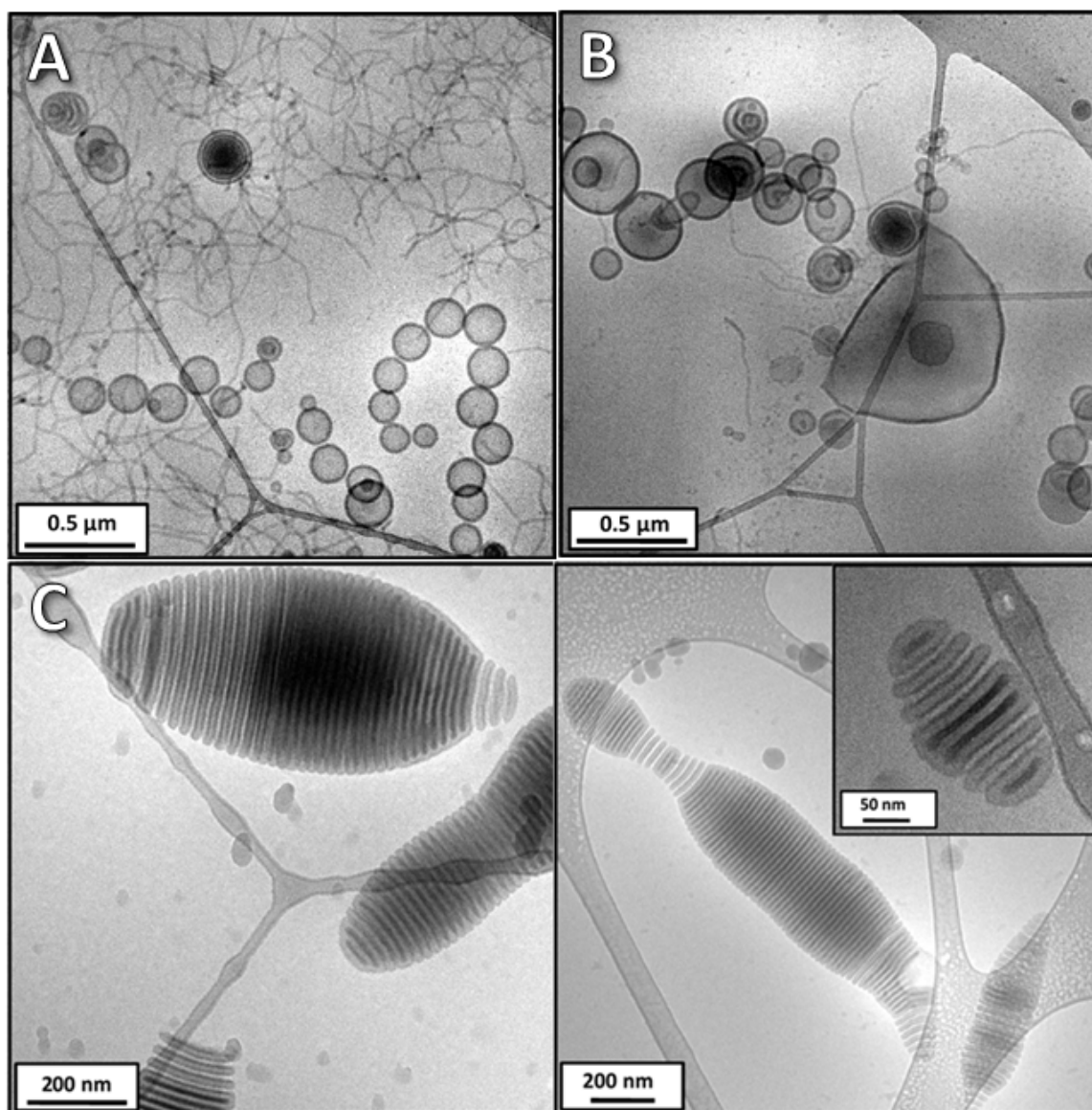


**Figure 5-S10.** cryo-TEM micrographs of self assembled structures obtained from dialysis of dioxane solutions of  $\mu$ -SVqS' without (A) and with 0.08 (B) and 0.32 equiv  $I_2$  (C) regarding P2VPq units to water. The concentration was 0.4 g/L. From the aggregates in (C) the non-uniformity of the distances of the individual sheets is clearly visible.

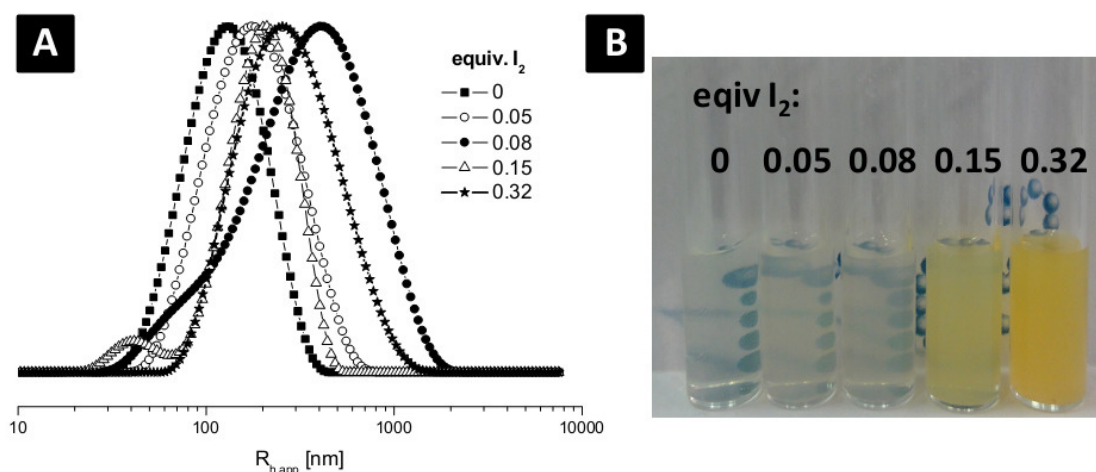


**Figure 5-S11.** (A) DLS CONTIN plots of the different aqueous solutions obtained from dialysis of  $\mu$ -SVqS' with different amounts of supplementary iodine. A continuous shift of the peak maxima is clearly observed with increasing amount of iodine added. For the intermediate structures including nascent bilayers and aggregated vesicles (Figure 5-7A) a broader size distribution was observed, whereas this decreases again above 0.08 equiv iodine due to the formation of more compact particles. The concentrations were between 0.35 and 0.50 g/L and the apparent hydrodynamic radii  $R_{h,app}$  (and dispersity indices D.I.) are 125 nm (0.46), 176 nm (0.51), 328 nm (0.87), 179 nm (0.36) and 272 nm (0.57) for the different samples with 0 - 0.32 equiv  $I_2$ . In (B) the photograph of the corresponding solutions is shown.

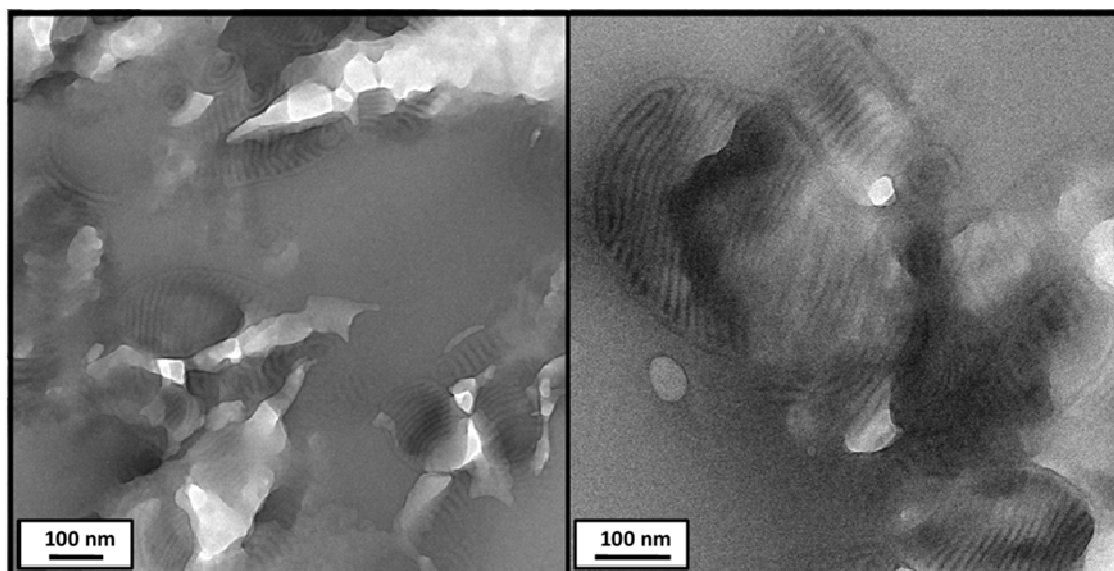


**Figure 5-S12.** TEM micrographs of 50 nm thick cuts from freeze-dried and embedded sample of  $\mu$ -SVqS' aggregates obtained by dialysis with 0.15 equiv  $I_2$ . Due to the high electron contrast of iodide/triodide the quaternized P2VP phase appears dark.

## 5.6.4 References

- (1) Hanisch, A.; Gröschel, A. H.; Förtsch, M.; Drechsler, M.; Jinnai, H.; Ruhland, T. M.; Schacher, F.; Müller, A. H. E. Counterion-Mediated Hierarchical Self-Assembly of an ABC Miktoarm Star Terpolymer. *ACS Nano* **2013**, *3*, 4030-4041.
- (2) du Sart, G. G.; Rachmawati, R.; Voet, V.; van Ekenstein, G. A.; Polushkin, E.; ten Brinke, G.; Loos, K. Poly(*tert*-butyl methacrylate-*b*-styrene-*b*-4-vinylpyridine) Triblock Copolymers: Synthesis, Interactions, and Self-Assembly. *Macromolecules* **2008**, *41*, 6393-6399.

---

## 6 Appendix

### 6.1 Triiodide-Directed Self-Assembly: Polycation Nature and Reversibility

From the results presented in Chapter 4 and 5, the presence of iodide as counterion was determined to be crucial for the formation of triiodide as external stimulus. Also other polymers with quaternized amino-functions are able to serve as polycation for triiodide. To determine whether the quaternized poly(2-vinylpyridine) segment is necessary for superstructure formation, another miktoarm star terpolymer ( $\mu$ -B<sub>111</sub>T<sub>42</sub>D<sub>34</sub>, the subscripts denote the degrees of polymerization and the detailed molecular characterization is listed in Table 3-3), where the P2VP segment was exchanged by PDMAEMA was subjected to the same quaternization procedure with methyl iodide and subsequent dialysis to water. Polydisperse structures of mainly spherical micelles were obtained in aqueous solution. Here, in contrast to the miktoarm star terpolymers with the P2VP block, which were treated with the same procedure, no significant changes in micellar morphology were found when 0.25 equiv of iodine were added before dialysis (Figure 6-1). Already in the unquaternized form the PDMAEMA homopolymer is more hydrophilic than P2VP due to its more polar composition in addition to the amino-function. Therefore, in case of the quaternized PDMAEMA the presence of triiodide as counterion is insufficient to decrease the hydrophilicity of the polymer to such an extent that aggregation occurs. As a consequence of the absence of superstructure formation after addition of iodine, the quaternized P2VP block is essential for triggering the hierarchical aggregation. Additionally, iodine is known to strongly interact with pyridine *via* the formation of charge-transfer complexes.<sup>1</sup>

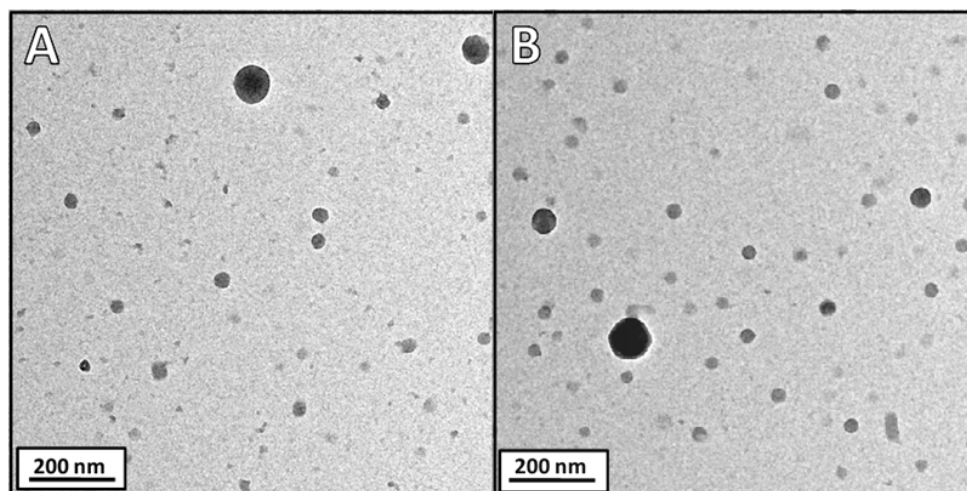


**Figure 6-1.** TEM micrographs of micelles obtained from dialysis of dioxane solutions of  $\mu$ -B<sub>111</sub>T<sub>42</sub>D<sub>34</sub>q without (A) and with 0.25 equiv I<sub>2</sub> (B) regarding the quaternized DMAEMA units to water. The concentrations were 0.2 g/L.

Due to its frozen character, the “woodlouse” aggregates obtained from  $\mu$ -SVqS’ (Chapter 5) were further chosen to test the sensitivity of the iodide/triiodide system toward reductive conditions. Upon exposure to sodium thiosulfate, triiodide is reduced to iodide.<sup>2</sup> Under this reductive environment disintegration into the deformed vesicular building units was initially expected, due to their glassy core. Therefore, 10 equiv of Na<sub>2</sub>S<sub>2</sub>O<sub>3</sub> with respect to P2VPq units was added to the preformed “woodlouse” structures from  $\mu$ -SVqS’ with 0.32 equiv I<sub>2</sub>. After 1 week of stirring huge ill-defined aggregates were found and the lamellar periodicity was only partially retained (Figure 6-2A). After stirring for additional 10 days, merely ill-defined structures without any internal periodicity were observed (Figure 6-2B). To exclude the influence of stirring as mechanical stress, the same sample was only slowly agitated for 3 weeks. Interestingly, the aggregates retained their overall shape whereas to some extent dissolution of the surface was observed (Figure 6-2C). Consequently, the “woodlouse” aggregates clearly respond to reductive environment. However, reversibility of the system was not achieved and only slight dissolution effects or complete disruption upon stirring were obtained.

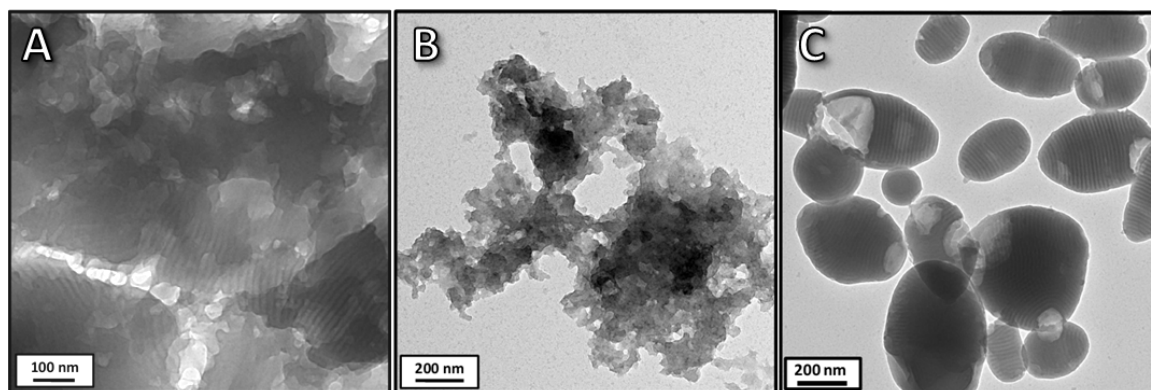


**Figure 6-2.** TEM micrographs of “woodlouse” structures from  $\mu$ -SVqS' (0.32 equiv  $I_2$ ) treated with 10 equiv of  $Na_2S_2O_3$  regarding P2VPq units. The aqueous solutions were stirred for 7 (A) or 17 days (B) or slightly agitated for 21 days (C). The concentrations were 0.2 g/L.

## 6.2 References

- (1) Haque, I.; Wood, J. L. The infra-red spectra of pyridine-halogen complexes. *Spectrochim. Acta, Part A* **1967**, *23*, 959-967.
- (2) Scheper, W. M.; Margerum, D. W. Non-metal Redox Kinetics: Reactions of Iodine and Triiodide with Thiosulfate via  $I_2S_2O_3^{2-}$  and  $IS_2O_3^-$  Intermediates. *Inorg. Chem.* **1992**, *31*, 5466-5473.



---

**List of Publications**

- (8) **Hanisch, A.**, Gröschel, A.H., Förtsch, M., Löbbling, T.I., Schacher, F.H., Müller, A.H.E.: „Hierarchical Self-Assembly of Miktoarm Star Polymer Systems Containing a Polycationic Segment: A General Concept”, *Polymer* **2013**, *54*, 4528-4537
- (7) **Hanisch, A.**, Gröschel, A.H., Förtsch, M., Drechsler, M., Jinnai, H., Schacher, F.H., Müller, A.H.E.: “Counterion-Mediated Hierarchical Self-Assembly of an ABC Miktoarm Star Terpolymer”, *ACS Nano* **2013**, *7*, 4030-4041
- (6) Kuttner, C., **Hanisch, A.**, Schmalz, H., Eder, M., Schlaad, H., Burgert, I., Fery, A.: “Influence of the Polymeric Interphase Design on the Interfacial Properties of (Fiber-Reinforced) Composites”, *ACS Appl. Mater. Interfaces* **2013**, *5*, 2469-2478
- (5) Rettler, E., Rudolph, T., **Hanisch, A.**, Höppener, S., Retsch, M., Schubert, U.S., Schacher, F.H.: “UV-Induced Crosslinking of the Polybutadiene Domains in Polystyrene-block-polybutadiene Block Copolymer Films – An In-Depth Study”, *Polymer* **2012**, 5641-5648
- (4) **Hanisch, A.**, Schmalz, H., Müller, A.H.E.: “A Modular Route for the Synthesis of ABC Miktoarm Star Terpolymers via a New Alkyne-Substituted DPE-Derivative”, *Macromolecules* **2012**, *45*, 8300-8309
- (3) Gröschel, A.H., Walther, A., Löbbling, T.I., Schmelz, J., **Hanisch, A.**, Schmalz, H., Müller, A.H.E.: *Facile*, “Solution-Based Synthesis of Soft, Nanoscale Janus Particles with Tunable Janus Balance”, *J. Am. Chem. Soc.* **2012**, *134*, 13850-13860
- (2) **Hanisch, A.**, Gröschel, A.H., Schacher, F.H., Förtsch, M., Drechsler, M., Müller, A.H.E.: “Worms, Beehives and Woodlice – Evolution of Multicompartment Micelles from New ABC Miktoarm-Star-Terpolymers”, *Polym. Mat. Sci. Eng.* **2012**, *106*, 203-204
- (1) Yuan, J., Schacher, F.H., Drechsler, M., **Hanisch, A.**, Lu, Y., Ballauff, M., Müller, A.H.E.: “Stimuli-Responsive Organosilica Hybrid Nanowires Decorated with Metal Nanoparticles”, *Chem. Mater.* **2010**, *22*, 2626-2634



## Danksagung

Zuallererst möchte ich mich bei meinem Doktorvater Prof. Axel Müller für die Möglichkeit bedanken, eine Doktorarbeit an seinem Lehrstuhl anzufertigen. Nachdem ich zuvor bereits eine Facharbeit und meine Diplomarbeit am Lehrstuhl MC2 bearbeitet habe, hat er mich somit für insgesamt etwas über ein Jahrzehnt in meiner wissenschaftlichen Ausbildung vom Abitur über das Diplom bis hin zur Doktorarbeit begleitet. Das entgegengebrachte Vertrauen und die Freiheit bei der wissenschaftlichen Arbeit zu entscheiden, wo der Weg hingehen soll, weiß ich sehr zu schätzen, genauso die Möglichkeit zu jeder möglichen und unmöglichen Tageszeit (egal ob an einem Werktag oder am Wochenende) einen Ratschlag, Anregungen und Unterstützung zu bekommen. Seine Freude an der Chemie und der Arbeit gegenüber ist eine wirklich bewundernswerte Eigenschaft und hat zudem einen großen Einfluss auf die eigene Motivation. Für die Möglichkeit, meinen wissenschaftlichen Horizont auf diversen Tagungen zu erweitern, dort interessante Vorträge zu hören und interessante Personen zu treffen und dabei noch fremde Länder zu bereisen bin ich natürlich sehr dankbar.

Bei meinen BayNAT-Mentoren Prof. Stephan Förster und Holger Schmalz möchte ich mich für die Hilfe und Anregungen bedanken. Zudem bedanke ich mich auch bei Jun. Prof. Felix Schacher für seine stete Unterstützung und Kommentare hinsichtlich der Untersuchung der „Kellerasseln“.

Auf die insgesamt 5½ Jahre (Praktika, Diplomarbeit und Doktorarbeit), die ich mit der MC<sup>2</sup> „verheiratet“ war, blicke ich gerne zurück, und besser als mit diesem Haufen hätte man es wirklich nicht erwischen können, und die Arbeitsatmosphäre, Zusammenarbeit, Zusammenhalt... sind definitiv einmalig. Neben den Leuten die direkt zum Gelingen der Arbeit beigetragen haben und somit bereits in den vorherigen Kapiteln persönlich aufgeführt wurden, danke ich im Folgenden (ungefähr alphabetisch sortiert nach dem letzten Buchstaben des Nachnamen) für die großartige Atmosphäre: Shohei Ida, Sandrine Tea, Girish Behera, Ramon Novoa, Larisa Sigolaeva, Marina Krekhova, Thomas Ruhland, Pierre-Eric Millard, Stefan Reinecke, Christopher Synatschke, Anthony Granville, Ainhoa Tolentino Chivite, André Pfaff, Andrea Wolf, Evis Penott-Chang, Zhicheng Zheng, Tina Löbbling, Adi Eisenberg, Weian Zhang, Jie Kong, Markus Retsch, Melanie Förtsch, Tobias Rudolph, Alexander Majewski, André Gröschel, Daniel Alexander, Annette Krökel, Marietta Böhm, Hülya Arslan, Jiayin Yuan, Eva Betthausen, Anja Goldmann, Tomohiro Hirano, Yuri Matsuo, Hansi Voigtländer, Sabine Wunder, Annika Pfaffenberger, Felix Schacher, Manuela Schumacher, Andreas Walther, Stefan Döhler, Markus Drechsler, Müllner's Markus, Daniela Pirner, Felix Plamper, Jeannine Rockser, Dale Blasser, Gaby Oliver, Stephan Weiß, Annika Eckhardt, Sylvain Catrouillet, Francesca Bennet, Kerstin Küspert, Meirav Ben-Lulu, Youyong Xu, Dima V. Pergushov, Christo Tsvetanov, Petar Petrov, Oleg Borisov Sergey Nosov, Matt Hunley, Sascha Yakimansky, Lourdes Pastor-Pérez, Alexander Schmalz, Holger Schmalz, Joachim Schmelz...

Gaby Oliver möchte ich nochmals ganz herzlich für die Hilfe bei diversen bürokratischen Angelegenheiten und ein stets offenes Ohr danken.

Ich hoffe meine Praktikanten Christian Probst, Moritz Tebbe, Janina Lauer, Julia Ewert und Daniel Kremer können aus ihren Forschungspraktika etwas mitnehmen und hatten Spaß, auch wenn aus meinen teils konfuse Ideen letztlich keine Paper resultiert sind. Ich bedanke mich bei euch für euren Einsatz.

Den Exilanten Thomas Ruhland, Andrea Wolf und Stephan Weiß danke ich für die unterhaltsame Begleitung auf dem Weg aus der MC<sup>2</sup> hin zur Abgabe und der gesamten MC1 für die nette Aufnahme einen Stockwerk tiefer. Hierbei geht jeweils persönlich ein „Gratias“ an Andreas Ringk und Florian Wieberger. Klaus Kreger, Robin Pettau, Katharina Neumann und Andreas Lang danke ich für die diversen und teilweise sehr kurzfristigen Salz-GPC Messungen. Ganz besonderer Dank gilt natürlich Prof. Hans-Werner Schmidt und Prof. Stephan Kümmel für die Bereitstellung eines Arbeitsplatzes in der Endphase des Schreibens und natürlich auch deren Sekretärinnen Petra Weiß und Monika Birkelbach für die Organisation.

Für eine geniale Zeit während der an wissenschaftliche Tagungen angeschlossenen Roadtrips in Israel und Kalifornien, die ein gelungener, entspannter Ausgleich zum Doktorandenalltag waren, danke ich André Gröschel, Stephan Weiß, Alexander Majewski und Thomas Ruhland, v.a. auch weil dabei mal mehrere Wochen nicht nur über Chemie geredet wurde. Alle anderen, die sonst in Bayreuth noch für Ablenkung gesorgt haben aufzuzählen, wäre wohl zu viel, deshalb möchte ich mich bei all denjenigen bedanken, die sich im und um den Dunstkreis der CSG bewegen und bewegt haben und mit denen ich eine schöne Zeit verbringen konnte. Nichtsdestotrotz möchte ich mich noch namentlich bei Matthias Turtle, Kathi Inzenhofer, Andy Lang, Sabine Simon, Joe-Achim Schmelz, Eva Gareis und Cornelius Friedrichs als Begleiter der ersten (Chemie-)Stunde bedanken, mit denen ich auch nach fast einem Jahrzehnt Bayreuth immer noch im Kontakt stehe und hoffe doch, das bleibt auch so.

Der Bayreuther Graduiertenschule BayNAT danke ich für die Aufnahme im Graduiertenprogramm *Polymer Science* und der DFG innerhalb des SPP 1165 und SFB 481 und 840 für die finanzielle Unterstützung.

Nachdem bis hierher keine Ausrufezeichen verwendet wurden, müssen diese jetzt endlich herausgeholt werden: Tausend Dank an meine Eltern Monika und Manfred für die permanente Unterstützung in jeglicher Art!!!!!!! Danke, dass ihr nie an mir gezweifelt habt!!!! Auch der Rest des Hanisch Clan's hat mir immer die nötige Ablenkung gegeben und mich ständig motiviert!!! DANKE Martin, Thomas, Nicol und natürlich Greta und kleiner Oskar!!! Spitze!!

## **Erklärung**

Die vorliegende Arbeit wurde von mir selbständig verfasst und ich habe dabei keine anderen als die von mir angegebenen Quellen benutzt.

Ferner habe ich nicht versucht, anderweitig mit oder ohne Erfolg eine Dissertation einzureichen oder mich der Doktorprüfung zu unterziehen.

Bayreuth, den 25.01.2013

Andreas Hanisch

